Group 14 Complexes for Thin Film Deposition: Studies in Stabilization and Reactivity

by

Jocelyn Sinclair

A thesis submitted in partial fulfillment of the requirements for the degree of

Doctor of Philosophy

Department of Chemistry

University of Alberta

© Jocelyn Sinclair, 2022

Abstract

The work in this Thesis strives to form a bridge in the understanding between the thriving field of Main Group element stabilization with *N*-heterocyclic carbenes and developments in thin film deposition for technological applications. Previous work in the Rivard group has excelled at applying Lewis acid-base stabilization to isolate reactive intermediates of Group 14 hydrides, and the work in this Thesis builds upon these established synthetic methods and framework to controllably liberate germanium and tin hydride moieties for pure element thin film deposition at low temperatures in solution.

The first research Chapter in this Thesis presents a synthetic method for the isolation of a high wt% germanium complex using an *N*-heterocyclic carbene. This germanium complex undergoes thermolysis at 100 °C to deposit amorphous Ge thin films on a variety of substrates, most notably silicon wafers. The germanium complex and similar derivatives were investigated experimentally and computationally, with decomposition occuring through direct cleavage of dative bonds to release Ge and soluble by-products. In the following Chapter, *N*-heterocyclic carbenes prove to be a hinderance in the hydrogermylation of germanium alkoxides *en route* to semi-crystalline germanium thin films. The germanium alkoxide studied is able to produce two interesting materials when combined with a mild hydride source: 1) a branched oligogermane is obtained with a remarkable degree of hydride substitution at germanium and 2) thin microcrystalline Ge^0 films which can be controllably deposited at low temperatures. Finally, an analogous tin alkoxide species is shown to undergo rapid hydrostannylation at room temperature to give crystalline Sn.

Preface

Sections of the work in this Thesis were completed with the assistance and collaboration of researchers within the group of Prof. Eric Rivard and with other researchers in the University of Alberta, Department of Chemistry. Additionally, some analyses were conducted at the Technische Universität München with the support of Prof. Dr. Thomas Fässler.

The work in this Thesis was supported by Natural Sciences and Engineering Research Council of Canada (NSERC), the Faculty of Science at the University of Alberta, the Ontario Research Fund, the JSPS Fellowship for Young Scientists program and the Alberta/Technical University of Munich International Graduate School for Hybrid Functional Material (NSERC CREATE grant).

Single-crystal X-ray crystallography was conducted by Dr. Robert McDonald and Dr. Michael J. Ferguson at the University of Alberta, including the selection and mounting of crystals, instrument operation and data collection, and full structural refinement. Elemental analysis, thermogravimetric analysis, and differential scanning calorimetry were performed at the Department of Chemistry Analytical Instrumentation Lab by Jennifer Jones, Wayne Moffat, or one of their trained student staff members. Variable temperature NMR, ^{2}H NMR, and DOSY NMR experiments were conducted by Mark Miskolzie at the University of Alberta Nuclear Magnetic Resonance Facility.

The computational studies were made possible with the support of the Shared Hierarchical Academic Computing Network (SHARCNET: www.sharcnet.ca), Westgrid (www.westgrid.ca), and Compute Canada (www.computecanada.ca). My understanding of computational studies was made possible by Dr. Emanuel Hupf and Dr. Meagan Oakley.

In Chapter 2, Dr. Guoliang Dai and Prof. Alex Brown contributed computational investigations related to adduct decomposition and rearrangement pathways (exclusive of the Raman modelling and energy barrier studies performed by myself); further credit belongs to Tyler Ries and Hanseul Kim for carrying out the exploratory computational studies on the decomposition of IPr•GeH_2•BH_3. Dr. Haoyang Yu conducted secondary electron microscopy, and Dr. Christoph Wallach (TUM) and Dr. Mustafa Supur collected Raman data. Lorenzo Garcia conducted initial work on the synthesis of Im^{i}Pr$_2$Me$_2$•GeH_2•BH_3.

In Chapter 3, William Medroa del Pino conducted synthesis and reactivity studies of oligomeric $[GeH_x(O^tBu)_{(2-x)}]_n$. Kwami Aku-Dominguez carried out synthetic and computational explorations of *N*-heterocyclic carbene $Ge(OR_2)$ complexes as part of his CHEM 399/401/403 research. Dr. Yohei Minami undertook the catalysis studies involving the Ge pre-catalysts. Anagha Kiran performed structural optimizations with guidance from myself for the computed Ge_xH_{2x} conformers. Yingjie (Jay) He collected and processed EDX and SEM data, Huijin Mao collected Raman data, and Alvaro Omaña provided a sample of the ligand **PB** for trapping studies and performed analysis of the reaction products. Dr. Shihong Xu at nanoFab (University of Alberta) collected air-free XPS data collection.

In Chapter 5, the graphene aerogels discussed were synthesized by Yingjie (Jay) He.

In the Appendix, the work discussed was carried out by the entirety of the UAlberta Working for Inclusivity in Chemistry team, with special thanks to Dr. Meagan

Oakley, Dr. Sorina Chiorean, Dr. Rochelin Danlangin, Dr. Regina Sinelnikov, and Kleinberg Fernandez, as well as Prof. Florence Williams.

Following standard procedure in the Rivard Group, each Chapter presented in this Thesis is essentially a self-contained research paper intended for peer-reviewed publication. Accordingly, portions of this Thesis have been published elsewhere, and these publications are listed below:

Chapter 2: J. Sinclair, G. Dai, R. McDonald, M. J. Ferguson, A. Brown and E. Rivard, *Inorg. Chem.*, 2020, **59**, 10996.

Chapter 3: J. Sinclair, W. Medroa del Pino, K. Aku-Dominguez, Y. Minami, A. Kiran, M. J. Ferguson, M. Yasuda and E. Rivard, *Dalton Trans.*, 2021, **50**, 17688.

Appendix: S. Chiorean, M. A. Oakley and J. Sinclair, *Can. J. Chem.*, 2021, **99**, 679.

This Thesis is dedicated to my family, and those I have adopted into it.

If you are reading this Thesis, and it's not your job to do so, you count.

"What we think we'll do is often not what we'll end up doing. It isn't always in our own control…"

- Guy Gavriel Kay

Acknowledgements

It is a truth universally acknowledged that a person in pursuit of a Doctorate must be in want of support.

My thanks, first and foremost, to my Supervisor Prof. Eric Rivard. In addition to chemistry expertise and formal support through all requirements of the Doctoral program, he has provided moral and career support, and a good kick in the pants when needed. My thanks also to my core committee, Prof. Jonathan Veinot and Prof. Vladimir Michaelis for numerous office chats – troubleshooting and checking in. Thank you also to my External and Internal Doctoral examination committee members, for participating in and supporting me through the final stage of this program.

The Facilities Staff in the Department are unparalleled (probably, I haven't actually tried to do a Doctorate anywhere else). I am thankful for Dr. Mike Ferguson, Wayne Moffat, Jennifer Jones, and Mark Miskolzie, who were always willing to sit down and hash out a plan and an experiment to get the answer I needed. Thanks also to the guys in the Machine, Glass and Electrical Shops, as well as and Distribution Services for keeping us well-supplied and informed.

To all members of the Rivard group, past and present, my eternal thanks for the outstanding environment of mutual support, commiseration, glovebox banter, morning coffees, afternoon coffees, and evening beers that made this whole degree doable in the day-to-day grind. The pandemic truly highlighted how important our comradery is to my success and joy in this process. You are all my family now (even if you don't read this thesis), and I can't wait to see where everyone ends up. Outside of our more permanent

members, I have been lucky to work closely with two undergraduate students (Fuwei Wen, Kwami Aku-Dominguez), a volunteer (Anagha Kiran), and visitors (including Yohei Minami and Michael Giebel). The international collaborations (and socializations) facilitated by the ATUMS program and in hosting individual visiting students were also a huge part of the beginning of my program, and I am thankful to have friends in Germany, Japan, and America upon whom to call.

This Doctorate has not only been a gargantuan academic effort, but an effort of community-building as well. I am so thankful for the time I spent working with other passionate graduate students in the Chemistry Graduate Students' Society, Working for Inclusivity in Chemistry, and the Science Graduate Students' Association Council (I'm aware that name sounds fake). It has been a joy to seek out and find people who share my passions, and who are willing to put in the work to advocate for changes, run events, and provide ongoing support to our peers. My parents taught me to always return something in better condition than it was lent to you – I hope the University of Alberta is a little better with our contributions.

My constant rocks through the past five (and a bit) years have been my friends, near and far, and I am heart-swellingly thankful for each of them. In particular, and in no real order: Meagan, my designated pandemic buddy, mutually bribed into deep friendship by baked goods and crafts, kept me afloat through the past couple years and I am so, so grateful; Andrew, fellow Athenian, who bolstered my writing and self-confidence in academia and in advocacy; Caley and Michelle, deeply engaged in each others' happiness and the consumption of the mushiest movies in existence; Emily, for unfiltered honesty,

outdoor adventures, and sleepovers; and my Henry House friends, who are my yearly tie to my best self. Carmen, for deep chats whenever needed, even when I didn't know they were needed (and thanks for letting me adopt all your hobbies); Emma, for warmth and unbridled love; Gill, for energy and joy and long walks talking nonsense. I hope you all come to live in my pottery-throwing/sewing/hiking/vegetable-growing/science-doing commune someday.

Thank you to Dr. Ian C. Watson, my partner in life (but hopefully not crime), dinner buddy, and adventure companion. Thank you for sharing love and support and distraction, and for demonstrating only the mildest of bemusement during my rabid crafting sprees. I will continue to drown you in not-great presents for as long as you will let me. I think you're pretty cool. Acknowledgement also to my cat Jake, who hates cuddles but gets them anyways.

Lastly, an acknowledgement of my family, though words will never be enough. Thank you to all the family, here and gone, who have provided tacit encouragement and support for my entire life. Thank you to Nana, who calls whenever she can to tell me she is proud of me and to make sure I am happy. My parents are an ever-present force of good in my life. They have taught me everything they can to help me succeed and are always there to pick me up when I fail. Mom is the best listener I know. Dad, the best problem solver. I could not be more thankful to be their daughter. My brother Mark has been my constant, daily companion, through thick and thin and thinner. Thank you for your unwavering faith, support, and deep sass and wit.

This was really, really hard. It is thanks to all of you that I made it through.

Table of Contents

List of Figures

List of Tables

List of Schemes

List of Charts

List of Symbols, Nomenclature, and Abbreviations

Å	Angstrom, 1×10^{-10} m
AACVD	Aerosol-assisted chemical vapour deposition
acac	acetylacetonate
ALD	Atomic layer deposition
Ar, Ar*	Aryl substituent
at%, atom%	Atom percent
ATR	Attenuated total reflectance
Bcat	Catecholboryl
Bpin	Pinacolboryl
cm	Centimetre
Cp	Cyclopentadienyl
CSD	Chemical solution deposition
°C	Degrees Celsius
Cy	Cyclohexyl
°	Degrees
D	Diffusion contant
DFBP	difluorobiphenyl
DFT	Density functional theory
DIBAL-H	Diisobutylaluminum hydride
Dipp	Diisopropylphenyl, 2,6-$^{i}Pr_2C_6H_3$
DLS	Dynamic light scattering

DOSY	Diffusion-ordered spectroscopy
DRA	Diffuse reflection accessory
DSC	Differential scanning calorimetry
E	Energy
EDX	Energy dispersive X-ray analysis
E_g	Optical band gap energy
EI-MS	Electron impact mass spectrometry
Et	Ethyl substituent
FinFET	Fin field effect transistor
FLP	Frustrated Lewis pair
g	Gram
(g)	Gas phase
G	Gibbs' free energy or Gauss (as unit)
GeNC	Germanium nanocrystal
GST225	$Ge_2Sb_2Te_5$
h	Plank's constant
HMBC	Heteronuclear multiple bond correlation
HOMO	Highest occupied molecular orbital
hr/hrs	Hour/hours
HSQC	Heteronuclear single quantum coherence
IEF-PCM	integral equation formalism polarizable continuum model
IM	intermediate
Im	$(HCNH)_2C$:

$ImMe_2$	$(HCNMe)_2C$:
$ImMe_4$	$(MeCNMe)_2C$:
$Im^iPr_2Me_2$	$(MeCN^iPr)_2C$:
^{i}Bu	*Iso*-butyl substituent
^{i}Pr	*Iso*-propyl substituent
IR	Infrared
ITO	Indium tin oxide
K	Degrees Kelvin
kg	Kilogram
k	Rate constant
kHz	Kilohertz
KIE	Kinetic isotope effect
kJ	Kilojoule
kV	Kilovolt
L	Ligand
LA	Lewis acid
LB	Lewis base
ln	Natural logarithm
LUMO	Lowest unoccupied molecular orbital
m	metre
M	Metal element or moles per litre (as a unit)
mA	Milliamp
Me	Methyl substituent

Mes	Mesityl, 2,4,6-$Me_3C_6H_2$
Mes*	2,4,6-$^tBu_3C_6H_2$
mbar	millibar
MBE	Molecular beam epitaxy
MHz	Megahertz
min	minute
mol	Mole
MOSFET	Metal oxide semiconductor field effect transistors
Mp	Melting point
mTorr	Millitorr
mW	Milliwatt
NBO	Natural bond orbital
^{n}Bu	*Normal*-butyl substituent
NHC	*N*-heterocyclic carbene
NIR	Near infrared
nm	Nanometre, 1×10^{-9} m
NMR	Nuclear magnetic resonance
NP	Nanoparticle
ORTEP	Oak Ridge Thermal Ellipsoid Plot
Pa	Pascal
PCM	Polarizable continuum model
PDI	Polydispersity index
PET	Polyethylene terephthalate

Ph	Phenyl substituent
PMT	Photomultiplier tube
ppm	parts per million
PRAM	Phase-change random access memory
pXRD	Powder X-ray diffraction
RDS	Rate determining step
rt	Room temperature
s	Seconds
(s)	Solid phase
^{s}Bu	*Sec*-butyl
SEM	Scanning electron microscopy
$SImMe_2$	$(H_2CNMe)_2C$:
X	Halide
XRD	X-ray diffraction
XP	X-ray photoelectron
XPS	X-ray photoelectron spectroscopy
^{t}Bu	*tert*-butyl
TD-DFT	Time-dependent density functional theory
T	Temperature
Tf	Triflate, SO_2CF_3
TGA	Thermogravimetric analysis
THF	Tetrahydrofuran
TS	Transition state

UV-Vis	Ultraviolet-visible
VT	Variable temperature
‡	Transition state
wt%	Weight percent
δ	Partial charge or chemical shift from standard in ppm
Δ	Partial change
λ	Wavelength
η	Hapticity
Ω	Ohm
Σ	Sum
θ	Incident angle, degrees
u	Component of kinetic energy, $h\nu/kT$
ν	Vibrational frequency

Chapter 1: Introduction

1.1 Synthesis and reactivity of relevant low oxidation state Group 14 hydrides

1.1.1 Relative stability of the parent tetrelenanes (EH_4) and tetrelenes (EH_2, E = Group 14 element)

The decomposition of Group 14 hydrides (EH_4; E = Si, Ge, Sn and Pb) into hydrogen gas and the corresponding pure (bulk) element is a matter of fundamental/mechanistic and applied interest.[1] While the tetrel elements contain four valence electrons, their bonding environments in compounds can differ substantially, especially amongst hydrides.[1,2] As the degree of orbital overlap within the E-H bonds decreases upon descending Group 14 of the Periodic Table, the corresponding element hydrides undergo a significant lowering in thermal stability from CH_4 to SnH_4; PbH_4 is not even stable at -78 °C and can only be generated and intercepted under matrix isolation conditions.[3] This effect is quite dramatic as the lightest congener, methane, CH_4, is an environmentally stable gas which must be heated to 600 °C before releasing H_2 and ethane.[4] Silane gas, SiH_4, is generally heated to greater than 600 °C to deposit pure Si and release H_2, and this procedure is used widely in industrial applications to deposit thin crystalline films,[5] despite the risk of explosive decomposition when silane comes into contact with atmospheric oxygen. Germane (GeH_4) deposits metal upon heating to 327 °C, while stannane (SnH_4) decomposes slowly at room temperature into Sn and H_2.[6] The

formation of the dihydrotetrelenes :SiH_2 and :GeH_2 are observed during the pyrolysis of parent silane and germane[5,7] and their stabilities will be discussed in greater detail below.

While methylene (CH_2) adopts a triplet ground state,[8] with two unpaired non-bonding electrons, the heavy element tetrelenes share a common singlet ground state (:EH_2) and substantial hydridic ($H^{\delta-}$) character of their associated hydrogens, due to the higher electronegativity of hydrogen in relation to the heavier tetrels Si, Ge, Sn and Pb.[1,9] The lone pair in these heavier :EH_2 analogues adopt increased s-orbital character and decreased electron-electron repulsion within the more diffuse orbital that houses the lone pair, leading to a larger promotion energy between the ground state singlet and excited state triplet states.[1,9] Commonly attributed to the Inert Pair Effect,[10] the increase in lone pair s-character in the EH_2 species as Group 14 is descended also impacts the ligand geometry around the E centre: specifically, the remaining orbitals at the tetrel E possess increasing p-character, leading to H-E-H bond angles that approach 90° as the element (E) becomes heavier.[1,2] The expected dual Lewis base/acid character of these heavy element EH_2 species, due to the concurrent presence of a lone pair and an unoccupied p-orbital present on the E centre, makes them prone to oligomerization.[1] Free :EH_2 species can be isolated in frozen inert matrices (*e.g.*, in solid Ar) at low temperatures or detected *in situ* in the solution or gas phases, and are often accompanied by polyhydride co-products.[8,11] Laser ablation of elemental targets in the presence of H_2 at 4 K allows for the identification of the Ge-Pb series of tetrelenes by infrared spectroscopy (IR),[11a] while other preparations involve D_2, Ne, or Ar matrices.[11b-d]

1.1.2 Lewis acid/base stabilization of tetrelenes (ER_2)

The ambiphilic character of tetrelenes (ER_2) has been leveraged to stabilize these transient species via Lewis acid and Lewis base coordination. The small HOMO-LUMO gaps of these species allows for the dual coordination of electron-donating (Lewis base, LB) and electron-accepting (Lewis acid, LA) ligands (see Figure 1.1).[12] The coordination of a Lewis acid to the lone pair of the element centre (E) lowers the energy of the adjacent empty p orbital, allowing for a stronger LB-E dative interaction to form,[12,13] assuming that the LB and LA are chosen appropriately.[12-14] Stable complexes can thus be isolated of moieties that would otherwise undergo self-oligomerization, as demonstrated by Marks who isolated $SnMe_2$ in the form of the LA/LB adduct $THF{\bullet}SnMe_2{\bullet}Fe(CO)_4$.[15] The Baines Group has worked extensively with $LB{\bullet}GeR_2$ complexes and used the stability gained by the Lewis adduct formation to induce a wide range of substitution chemistry at the germanium centre.[16] The Scheer Group has employed donor-acceptor stabilization to isolate a wide range of Group 13 and 15 element hydrides, often using the strongly Lewis acidic unit $W(CO)_5$ (*e.g.*, to intercept $H_2Al\text{-}PH_2$ complexes).[17]

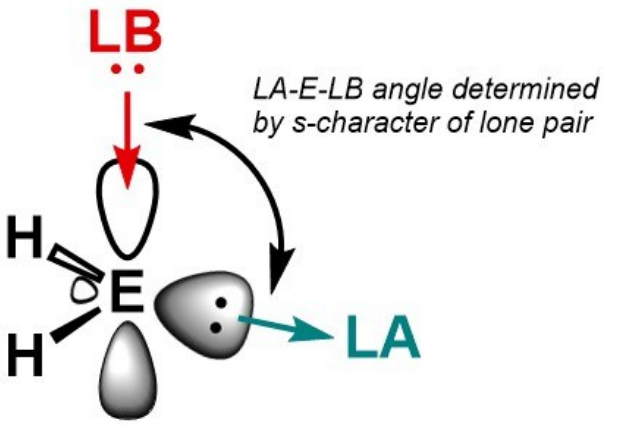

Figure 1.1. The orbitals involved in Lewis acid/base stabilization of the parent EH_2 tetrelenes (E = Si, Ge, Sn, and Pb)

N-Heterocyclic carbenes (NHCs), originally prepared as isolated species by Arduengo in 1991,[17] are highly tunable Lewis bases that are used often to stabilize reactive Main Group moieties.[19] The cyclic framework within these carbenes allows for the stabilization of a singlet carbene electronic state via the σ-electron withdrawing and π-electron donating nature of the neighbouring nitrogen atoms (see Figure 1.2). These electronic interactions lower the energy of the carbene carbon's HOMO (sp^2 lone pair) and increases the energy of its LUMO (of C-N π* character), resulting in a strongly σ-donating ligand.[19,20,] NHCs commonly adopt formally dative single bonds when adducted with main group species, but the unoccupied C-N π*-type "p_z orbital" at carbon also allows for π-backbonding in some instances.[13,19] Of note, *N*-heterocyclic carbenes have been used to stabilize ambiphilic and paramagnetic species,[21] and light Main Group complexes (C, O, N).[22]

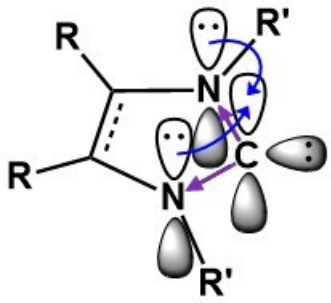

Figure 1.2. Electronic stabilization of a singlet carbene by neighbouring nitrogen atoms in *N*-heterocyclic carbenes. The nitrogen atoms withdraw σ-electron density from the carbene carbon (purple arrows) and donate to the formally empty "p_z orbital" at carbon (blue arrows).

1.1.3 Ligand-stabilized heavy tetrel(II) mono- and dihydrides

Germanium(II) halides are sufficiently Lewis acidic to be coordinated by a Lewis base alone. Perhaps the most relevant example of this form of complexation is in the bottleable complex Cl_2Ge•dioxane, a thermally stable white solid that is used as a germanium source in many syntheses.[2,23] Cl_2Ge•dioxane can be directly combined with NHCs to form NHC•$GeCl_2$ complexes (**1**) via the elimination of dioxane, and the resulting carbene adducts can be functionalized at the Ge centre to produce a wide range of new Ge(II) complexes (**2**-**7**), as outlined in Scheme 1.1.[1,12,16,23-30]

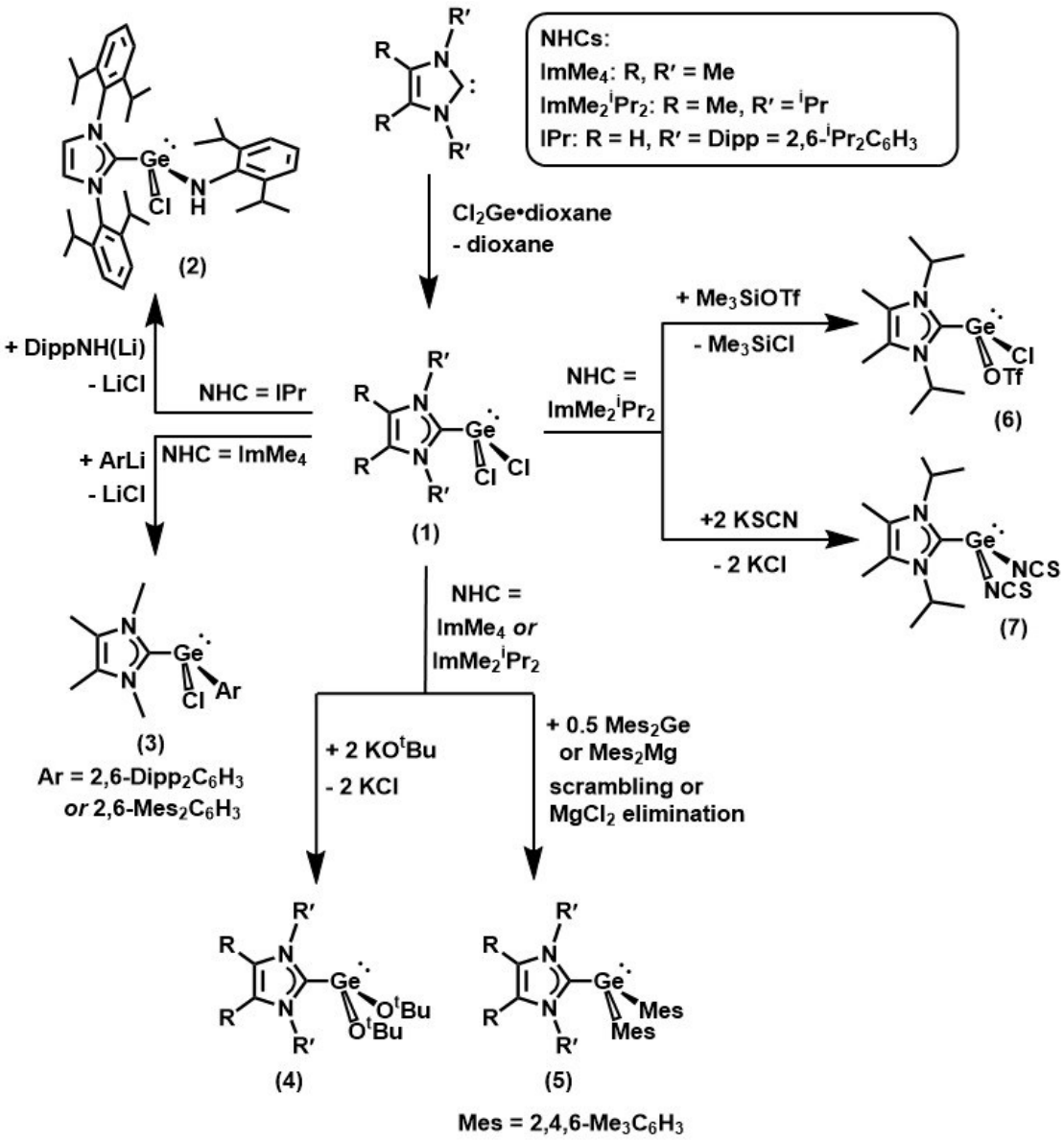

Scheme 1.1. NHC•$GeCl_2$ complexes as starting materials.[1,12,16,23-30]

Rivard and coworkers have reacted the Lewis acid-base pair of IPr•$GeCl_2$ (IPr = $[(HCNDipp)_2C:$, Dipp = 2,6-$^iPr_2C_6H_3$) (**9**) with the dual hydride/Lewis base source $Li[BH_4]$ to give IPr•GeH_2•BH_3 (**10**) (Scheme 1.2).[24] This complex was the first example of

an isolable complex of :GeH_2. The temperature-sensitive dative C_{NHC}-Ge and Ge-B bonds in **10** could also be exploited to release Ge, H_2, and IPr•BH_3 upon heating to 70 °C.[24] The lability of the BH_3 group in IPr•GeH_2•BH_3 (**10**) and in its silicon congener IPr•SiH_2•BH_3 (**11**) was confirmed by introducing a stronger Lewis acid, leading to Lewis acid exchange and the subsequent isolation of IPr•EH_2•$W(CO)_5$ (E = Si (**12**), Ge (**13**)) and removal of THF• BH_3 (Scheme 1.2).[30,31]

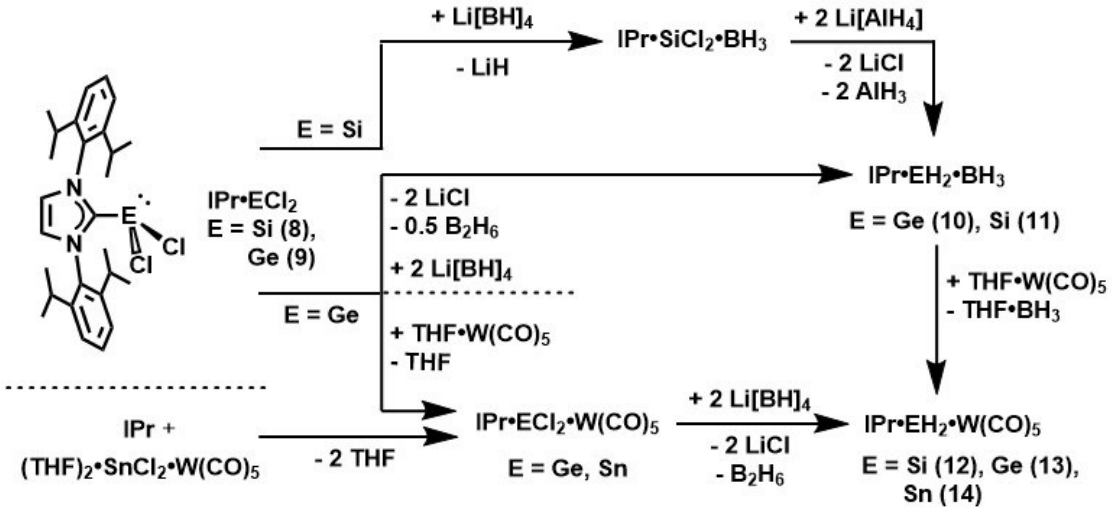

Scheme 1.2. Summary of LB•EH_2•LA (E = Si, Ge and Sn) synthesis by the Rivard Group.[24,30-32]

The Wittig reagent $Ph_3P{=}CMe_2$ can also be employed to stabilize Main Group hydrides for fundamental and application-based studies.[33] This Lewis base has a resonance form with a formal positive charge on the phosphorus centre and a lone pair/ negative charge on the carbon, leading to a carbene-type donation to :EH_2 moieties (see top inset, Scheme 1.3).[33,34] Specifically, $Ph_3P{=}CMe_2$ was used to stabilize :GeH_2 in a push-

pull LB/LA framework with BH_3 as the Lewis acid, and $W(CO)_5$ for germanium(II) and tin(II) dihydrides, (*i.e.*, $Ph_3PCMe_2{\bullet}EH_2{\bullet}W(CO)_5$, E = Ge and Sn).[34] $Ph_3PCMe_2{\bullet}GeH_2{\bullet}BH_3$ (**16**) was subsequently observed to decompose into elemental germanium and soluble by-products[34] upon heating to 100 °C in toluene. This low-temperature deposition of elemental Ge from a single-source precursor was immediately leveraged to form germanium nanocrystals (GeNCs) (see Scheme 1.3).[35] This method represented a new approach to the synthesis of GeNCs, which have been previously synthesized by solution-phase reduction of precursors including $GeX_{2\text{ or }4}$ (X = halide), thermal decomposition of organogermanes, or from metathesis reactions involving Ge Zintl phases.[36] $Ph_3PCMe_2{\bullet}GeH_2{\bullet}BH_3$ (**16**) decomposes in the presence of capping ligands upon heat injection or microwave irradiation to produce GeNCs of 5-10 nm. The microwave irradiation method (190 °C, 2 hours) proved to be more tunable in terms of size control and was applicable to a wider range of either hydrophobic or hydrophilic capping ligands.[35] The resultant GeNCs could be produced with consistent size distribution, and the elemental composition was consistent with the presence of desired surface capping ligand (with $Ph_3PCMe_2{\bullet}BH_3$ removed as a soluble by-product); the optical properties of the resulting nanoparticles were in line with those of GeNCs synthesized by other methods.[37]

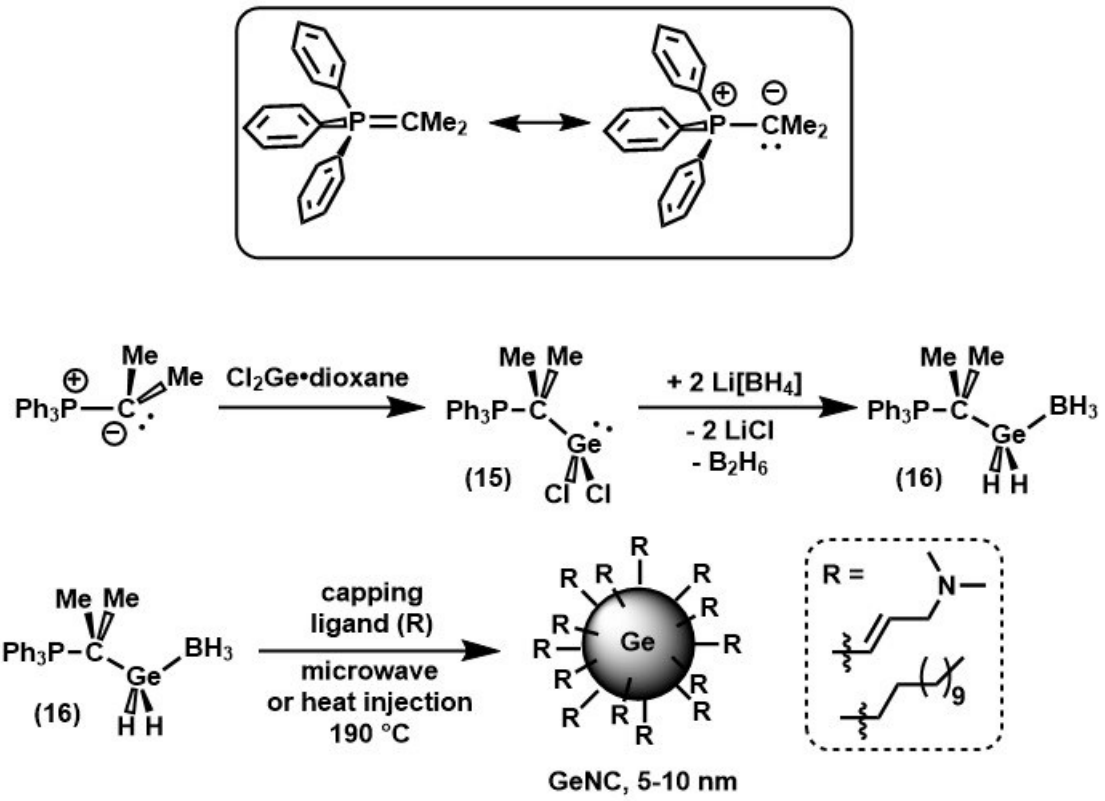

Scheme 1.3. A Wittig reagent as Lewis base for GeH_2 stabilization and subsequent decomposition of the Ph_3PCMe_2•GeH_2•BH_3 (**16**) adduct into GeNCs.

Rivard and coworkers also exploited NHC•EH_2•LA frameworks for the isolation of tin(II) hydrides. The tin analogue, IPr•SnH_2•BH_3, was unable to be isolated due to insufficient Lewis acidity and basicity of :SnH_2.[30] In this case, increasing the acidity of the coordinating Lewis acid was necessary, and tin(II) hydride IPr•SnH_2•$W(CO)_5$ (**14**) was synthesized from IPr•$SnCl_2$•$W(CO)_5$ and Li[BH_4] (see Scheme 1.2).[30] A similar approach was used to prepare Ph_3PCMe_2•SnH_2•$W(CO)_5$.[34]

Tetrel monohydrides are commonly synthesized either from hydride-containing precursors or by induced reactivity at the element centre of a complex;[2] some key advances in the field are summarized in Scheme 1.4. E(II) monohydrides can be coordinated to NHC ligands by the reductive elimination of functional groups from E(IV) centres, as demonstrated by the synthesis of **17**,[38] **18**,[40] and **22**.[41] Introducing steric bulk or strain in the E(IV) precursors provides a thermodynamic driving force for tetrelene coordination with the NHC, as shown by Müller's synthesis of $ImMe_4$•Si(H)Ar (**18**, Ar = C_6H_3-2,6-(2,4,6-$Mes)_2$).[39] Electronic and steric stabilization can be introduced in the remaining R substituent in the LB•E(H)R.[39,40] In extreme cases, large groups can also be incorporated to produce low-valent E(II) centres, as developed by the Jones Group, compound **20**.[41] This example, as well as those of the Roesky Group (compound **21**),[42] demonstrate post-complexation E-H bond formation.

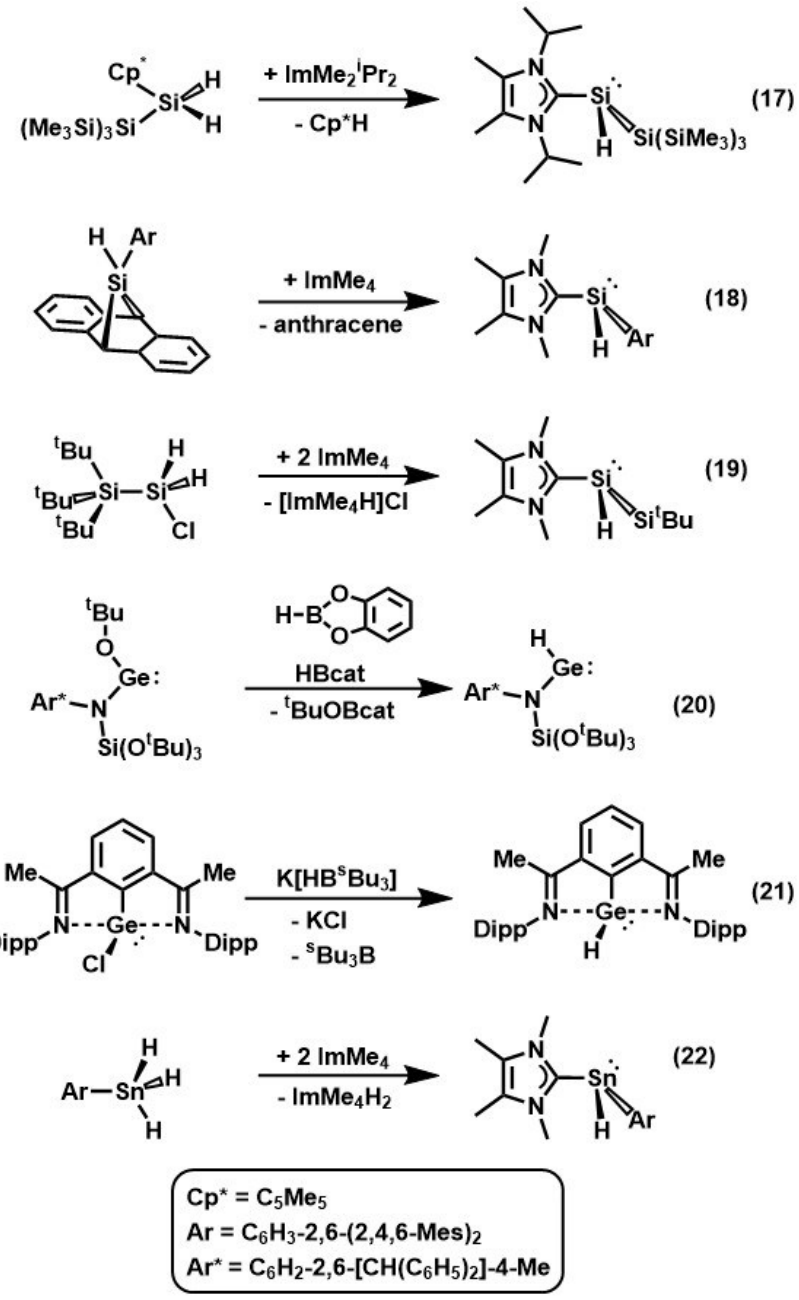

Scheme 1.4. Selected syntheses of Group 14 monohydrides.

1.2 Deposition and applications of Group 14 thin films in devices

Electrical devices now often contain electronically- and optically-active components that are in the sub-10 nm regime, hence there is a continual need for depositing very thin films of elements in a controlled fashion. Ideally such deposition processes should occur rapidly and without interfering contaminants and should be compatible with typical bottom-up device fabrication and patterning protocols.[43,44] To date, the central techniques for the deposition of thin solid films include chemical solution deposition (CSD), chemical vapour deposition (CVD), and atomic layer deposition (ALD); typically, volatile metallorganic complexes are utilized in the latter two methods. These methods will now be described in turn, with focus on the deposition of solid-state materials containing Group 14 (tetrel) elements.

1.2.1 Methods of deposition

CVD has been integral to many device fabrication protocols, due to its ability to deposit conformal layers of material onto rough and patterned/raised topographies. This methodology requires the substrate to be placed within a vacuum chamber, where gases can be introduced and the pressure within the reactor can be modified in a controlled manner. Volatile precursors (sometimes in the presence of carrier gases or co-reactants) are introduced to the reaction chamber, where they react with the substrate surface to deposit the target material as nanoscale films. Categorically, CVD must involve a chemical reaction, versus physical deposition methods such as the sputtering or evaporation of target materials.[44] CVD reactions are often driven by the thermal

decomposition of the precursor onto a heated substrate, but can be enhanced by additional processes.[45] For example, photosensitization and irradiation, and plasma-enhancement have been used extensively in industry for the deposition of thin Si and TiN films.[45] CVD has a long history, and the first patent for chemical vapour deposition (CVD) was filed in 1925 by van Arkel and de Boer for the deposition of Ti, Zr, Hf and Th.[46] Moreover, earlier evidence of a CVD-based process (in 1893) was noted in the deposition of W lamp filaments by the reduction of WCl_6 with H_2.[47]

The primary difference between CVD and atomic layer deposition (ALD) is the self-limiting behaviour of the deposition in ALD, enabling sub-monolayer thickness control on substrates; the term "sub-monolayer" refers to partial coverage of a substrate surface.[44] Rather than undergoing thermal decomposition upon contact with the substrate, the thin film precursors form a self-terminating layer/coating on the substrate. The chamber is then purged of excess precursor, and a co-reactant is introduced that reacts on the surface with the surface-adhered precursor to form the deposited layer.[48] The co-reactant may be a gas or a plasma (ionized gas), and the selection of co-reactant introduces another level of compositional control over the deposition.[43] The reactions used in ALD are designed to release volatile by-products, such that they can be removed from the chamber, and the substrate can undergo another exposure to the precursor without contaminating surface products. Typically, ALD substrate growth is an iterative process, since the self-limiting nature of precursor deposition necessitates multiple rounds of ALD material growth to obtain thicker films.

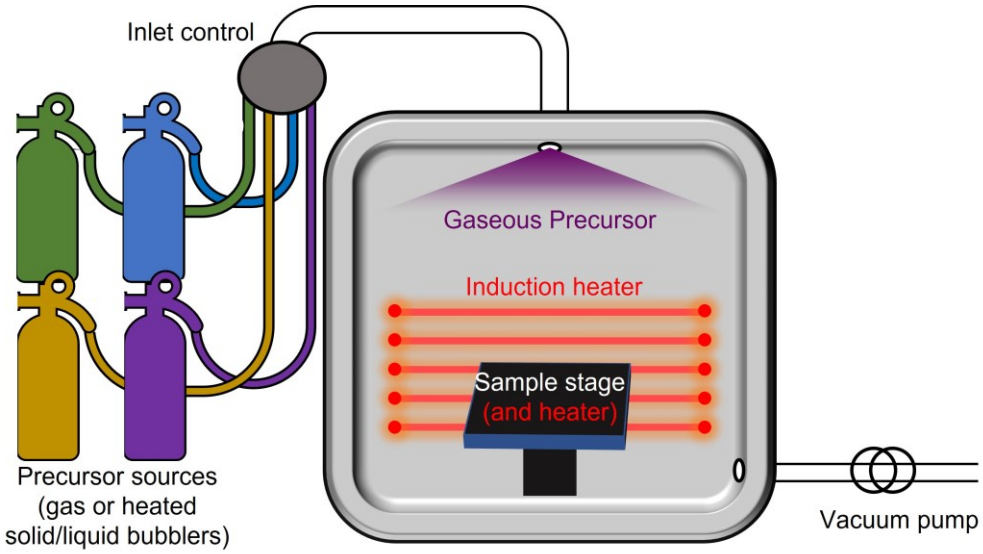

Figure 1.3. A simplified diagram of a CVD or ALD reactor.

Chemical solution deposition (CSD), as the name states, involves the deposition of a film of material from solution, either by a direct chemical reaction between two (or more) reactants or via the thermal or photolytic decomposition of a precursor.[49] Perhaps the most well-known example of CSD is that of the reaction of Tollen's reagent $[Ag(NH_3)_2(OH)]$ with aldehydes and ketones to give a silver mirror.[50] The first reported case of semiconductor thin film deposition is that of PbS from the reaction of lead tartrate and thiourea, first reported in the 1880s.[51] Most CSD methods used in industry continue to be in aqueous solution and involve the deposition of semiconducting bimetallic or insulating metal oxide layers[50] for device applications, such as in solar cells. Another application of solution-based deposition precursors is aerosol-assisted CVD (AACVD), wherein a highly soluble (but non-volatile) precursor in solution is ultrasonicated to produce solvent vapour droplets loaded with precursor which can then be introduced to the CVD chamber and react with the substrate for element and mixed-

element deposition.[49] CSD with air- or water-sensitive reagents is an active area of study, and can be used for the screening of deposition precursors for CVD and ALD applications.

Solution studies (that can be viewed as CSD) have been carried out to determine the mechanism of deposition within an ALD reaction, to expand the scope of species produced, and to analyze the relative reactivity of different co-reactants. In one example, bis(*N*-isopropylpyrrolylaldiminate)copper(II) (**23**)[52] was combined with $ZnEt_2$ under ALD conditions for the target deposition of high-purity Cu films (Scheme 1.5). Unfortunately, the resulting films always contained some Zn metal contamination. However, solution reactivity studies[52] identified step-wise ligand exchange at Cu and the thermal decomposition of the resulting organocopper intermediates as key steps in the mechanism, leading to the eventual discovery of optimal $AlMe_3$ and BEt_3 ALD co-reactants for the deposition of high-purity copper films.[52]

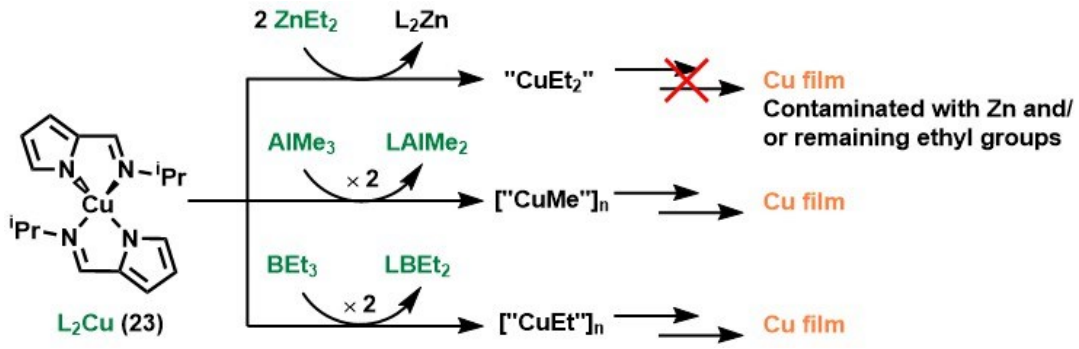

Scheme 1.5. Solution reactivity studies can be used to determine by products of an ALD reaction and to identify suitable conditions to achieve higher purity films, as was demonstrated by Britten and coworkers for bis(N-isopropylpyrrolyl-aldiminate)copper(II) (L_2Cu, **23**).[52] Green text indicates volatile species.

Alternatively, solution reactivity studies can be used to identify probable ALD precursor/co-reactant pairs, due to the ability to rapidly screen for the presence of deposited metal (or related solid-state films) at various temperatures under solution reaction conditions without the requirement of a sophisticated ALD apparatus. This process front-loads the reactivity studies and helps to eliminate co-reactants from the time- and resource-intensive ALD studies,[44] and has been used for the identification of Cu and Ni- depositing reactant pairs.[53] Precursors and co-reactants identified in this manner must be subjected to additional screening to determine their individual suitability for introduction to the ALD chamber and subsequent deposition of the desired films, as will be discussed further below.

1.2.2 Criteria for deposition precursors

A number of criteria exist for the design of deposition precursors, both in solution (CSD) and for gas phase CVD and ALD applications. Primary among them are criteria that ensure high-quality film deposition. The precursors (and their co-reactants) must have surface reactivity, such that adsorption to the initial substrate, as well as the growing film, facilitates deposition.[44,49] The by-products of the deposition must additionally be easily removed from the reaction vessel and substrate.[44,45,49] For this reason, salt elimination reactions between precursor and co-reactant are undesirable; salts often have low volatility and solubility, and thus are generally difficult to remove from a film. Precursors bearing a single element for deposition are most common, however, many bimetallic, metal oxide, and metal nitride precursors have been developed to deposit secondary, ternary, and quaternary component films.[44,45,49] Co-reactants can also be selected such that additional elements are incorporated into the film (*e.g.*, O_2 is often used as a co-reactant in the formation of element oxide films). Finally, the precursors must also have scalable syntheses, allowing their production at a large (multigram to kg) scale with reasonable yields.[44,45,49] Many precursor/co-reactant pairs used in ALD have parallels to compound synthesis or solution depositions of films and/or nanoparticles, provided that the ALD is not accomplished at temperatures outside of the reasonable range for solution reactivity (< 150 °C).[54] When translating deposition chemistry from the solution to the gas phase, the physical properties of the precursor must be taken into account, as well as any solvent interactions. Solvents can act as temporary ligands to stabilize intermediates during reactions, and can also be used to tune the dielectric environment of the reaction mixture.[45,49]

For ALD and CVD, additional criteria exist, specifically related to the gas phase delivery of the precursors. The temperature at which a precursor becomes sufficiently volatile is ideally below the substrate deposition temperature, to avoid condensation of the reactants prior to deposition.[44,45] The precursors also need to have long term stability at their delivery temperature and should become volatile/gaseous in the 0.1–10 Torr window for use in industrial instruments.[44] As mentioned previously, the by-products of CVD and ALD must be easily removable (*i.e.*, these by-products must be volatile at the same chamber temperature as the precursor and co-reactant) to allow them to be purged from the chamber between deposition cycles.[44,45]

Common reaction mechanisms for the association of precursors to the substrate surface include ligand displacement reactions,[55] thermal decomposition,[56] electron impact dissociation[57] and thermally-induced dissociative mechanisms.[58] Many of these methods are coupled with thermal decomposition of products formed on the surface following the initial substrate-precursor association, or after reductive elimination of volatile by-products following the introduction of a co-reactant gas such as H_2 or NH_3, thus facilitating self-limiting growth of the deposited layer (ALD).[44,58] Examples of each of these methods are given in Scheme 1.6. Precursor design and co-reactant selection allows for a wide range of deposition reactivity, depending upon precursor, substrate-precursor, and precursor-co-reactant stabilities and reactivities.

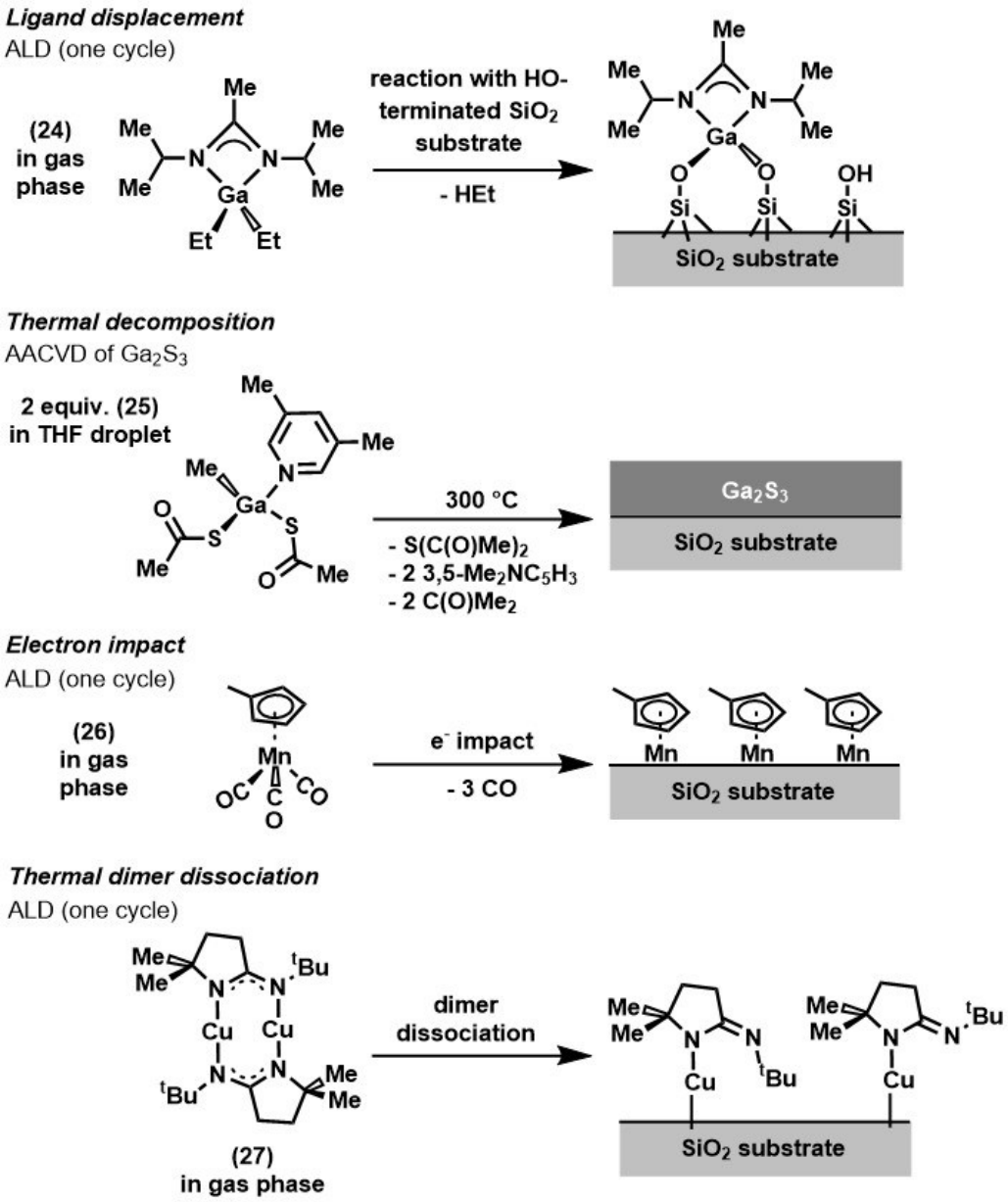

Scheme 1.6. Precursors for the deposition of element thin films and their methods of deposition.[44,55-58]

A common method of evaluating film deposition precursors is thermogravimetric analysis (TGA), which involves progressive heating of a sample at a consistent rate and recording the mass loss with increasing temperature. An ideal precursor for ALD and

CVD will show a single volatilization event (within a minute, assuming sample is suitably small – 3-8 mg) and a smooth and rapid mass loss to near 0 % residual mass (see Figure 1.4).[58] Compounds that show multiple mass loss events, or which do not reach 0 % mass, are likely experiencing decomposition rather than clean volatilization. With respect to CSD, one can also use TGA to determine the temperature at which a single-source film precursor begins to decompose, which can guide the solution-phase deposition temperatures used.[49] Differential scanning calorimetry (DSC) can be used in parallel to TGA to determine the temperatures at which thermal events, such as sample melting and/or decomposition, occur.[44,45,49,58]

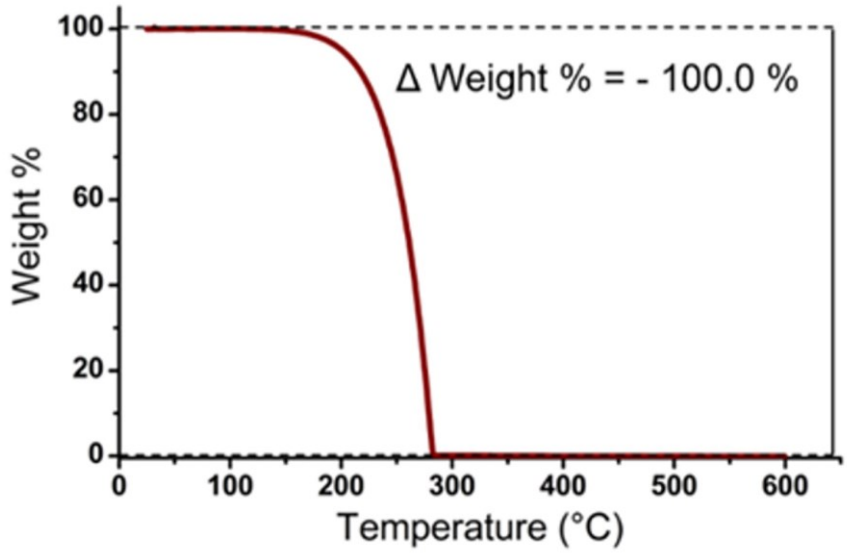

Figure 1.4. Exemplary TGA for a suitable CVD/ALD precursor.

1.2.1 Device applications for Group 14 thin films

Group 14 elements have a long history of application within the technology sector. The first point-contact transistors developed in the 1940s by Bell Laboratories[59a] (and simultaneously through the work of H. F. Mataré and H. Welker in France[59b]) were composed of pure germanium semiconducting crystals and two gold foil contacts covering a plastic wedge.[50,59] Upon pressure contact, current could pass from one gold contact through the germanium crystal and into the other gold contact, completing the circuit and amplifying the initial signal. These systems relied on the high carrier mobility of germanium, but were limited by operational temperature range and the difficulty of growing pure germanium crystals on industrial scales.[60] Nevertheless, germanium was the dominant semiconductor material in transistors until the late 1950s and three Bell Laboratories scientists (Bardeen, Shockley, and Brattain) were awarded the Nobel Prize in Physics in 1956 for their research on semiconductors and their discovery of the transistor effect. Shockley moved to Paulo Alto, California, started a research group, and founded what was to become the "Silicon Valley;" silicon replaced germanium as the major element in semiconducting devices due to its abundance and improved conductivity following surface passivation treatments.[61] Germanium and silicon single crystal wafers are manufactured by the growth of single crystal ingots from a melt and a seed crystal (called the Czochralski method). Wafers are cleaved, passivated as necessary, then processed to create multi-layered or doped systems for circuits.[60,61]

One of the primary uses of germanium deposition in emerging technologies is in the formation of GeTe and $Ge_2Sb_2Te_5$ (GST225) for nano-scale phase-change random

access memory devices (PRAM), which have rapid read-write speeds and non-volatile data retention.[62] Leskelä and coworkers at the University of Helsinki[63] have demonstrated ALD of these desirable alloys by employing a Lewis acid/base reaction between two metal-containing precursors. In this protocol, Cl_2Ge•dioxane is first deposited, followed by the introduction of the tellurium precursor $Te(SiEt_3)_2$, which undergoes a double displacement reaction at 90 °C with Cl_2Ge•dioxane to release the volatile triethylsilyl chloride and deposits GeTe on the surface.[63] A subsequent ALD cycle introduces Sb via a similar elimination between the same tellurium precursor and $SbCl_3$. Alternation of these precursors provides semiconductor layers of tunable composition, as shown in Scheme 1.7. A similar pseudo-tertiary system can be achieved with $Te(SiEt_3)_2$, $Ge(OEt)_4$, and $Sb(OEt)_3$ via elimination of $EtOSiMe_3$.[62b,c] Additional work in this field has identified $Ge(OMe)_4$[62b] and $Ge(OEt)_4$[62a] as potential precursors, however, both compounds contain Ge^{4+} centres rather than the desired Ge^{2+} oxidation state found in GeTe and $Ge_2Sb_2Te_5$ films.[63] Cyclopentadienyl (Cp), amide, and amindinate Ge^{2+} precursors have also been investigated in ALD, which have reasonable deposition rates between 200–300 °C when co-reacted with H_2 or NH_3 gases.[64]

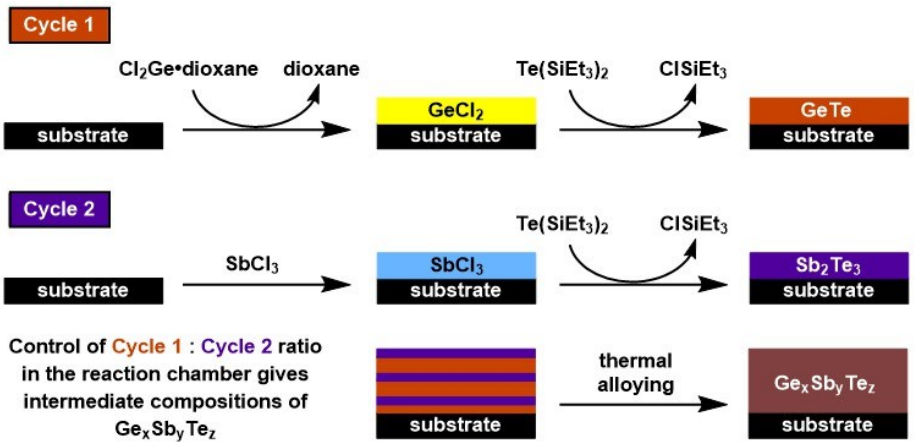

Scheme 1.7. Co-deposition ALD reactions to form GeTe and Ge-Sb-Te alloys for PRAM devices.[62]

Mixed Group 14 element layers are also under investigation for improving carrier and hole mobility in transistors, as well as in nanoscale optoelectronic devices. In the industrial drive for producing smaller and smaller processors (whose progress is predicted by Moore's law), barriers arise in using pure Si layers in transistors and other components. The high power densities in modern (nanodimensional) circuits result in leakage currents and carrier degradation, and eventual failure of the device.[62,65] One solution spearheaded by Intel in 2002 is the use of strained $Si_xGe_{(1-x)}$[65-66] or $Ge_xSn_{(1-x)}$ systems,[65,67] which improve carrier and hole mobility in MOSFET (metal oxide semiconductor field effect transistors) and FinFET transistors (fin field effect transistor, a multi-gate transistor), [65-67] allowing for lower pass voltages to be applied, thus decreasing leakage and allowing the devices to be smaller. The properties of these systems are highly tunable, with strain controlled by the ratio of Si or Sn to Ge. Remarkable improvements can be achieved with careful doping – just 3 at% tin in SnGe improves hole mobility by

20 % in a FinFET, as system reported by Saraswat and coworkers at Stanford University.[67] Ge and Si/Ge layers are also used in optoelectonic devices,[68] where Ge's transparency to infrared (IR) and near-IR wavelengths is leveraged to create integrated optical filters,[69] or to improve energy-harvesting.[70] The nanoscale $Si_xGe_{(1-x)}$ or $Ge_xSn_{(1-x)}$ films needed for both transistor and optoelectronic devices are commonly grown using molecular beam epitaxy (MBE, electron-beam evaporation of pure element targets) or CVD.

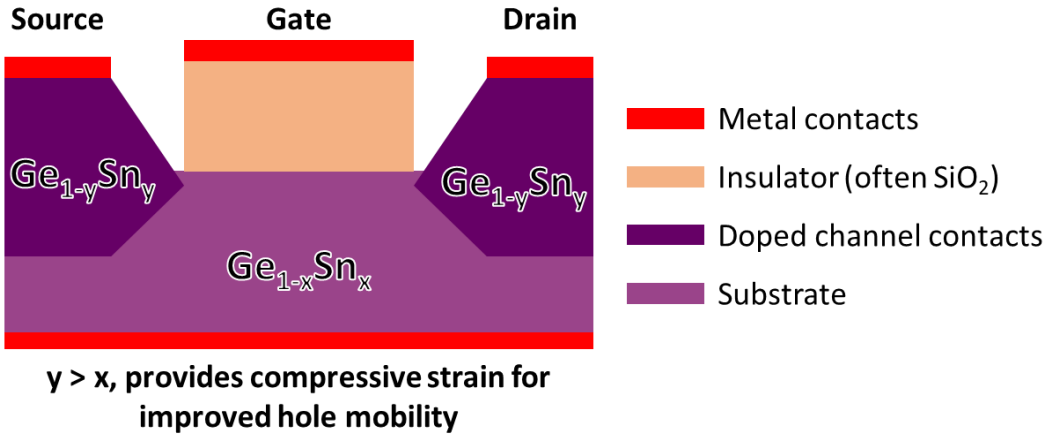

Figure 1.5. A schematic of a mixed-Group 14 element transistor (pMOSFET).

1.3 Inorganic polyethylene analogues

1.3.1 Properties of polyethylene and its inorganic Group 14 analogues

Polymeric inorganic methylenes, $[EH_2]_n$, are of fundamental interest due to their structural similarities to polyethylene, $[CH_2CH_2]_n$.[1] The catenation of ethylene into polyethylene has spurred initial fundamental inquiries that led to the development of

macromolecular theory,[71] as well as being the mainstay of the commodity plastics industry.[72] Polyethylene is most often produced via metal-catalyzed olefin polymerization reactions,[72] a process which cannot be applied to heavier Group 14 analogues due to the decreased stability of the E-E π-bonds in the requisite H_2EEH_2 ethylene analogues.[1] The accepted method of chain growth for the formation of $[EH_2]_n$ oligomers (E = Si and Ge) involves the formation of EH_2 species, followed by their oligomerization. As such, Si and Ge analogues ($[SiH_2]_n$ and $[GeH_2]_n$) can be synthesized, but the heavier Sn and Pb analogues are unknown in the bulk state.[1]

The properties of polysilanes and polygermanes, $[ER_2]_n$, follow expected trends regarding thermal properties and stability. Longer chains have higher melting and boiling points, and branched species have higher phase change (*e.g.*, melting) temperatures than their linear forms.[1,73] Due to the increased tendency of heavy element EH_2 units to insert into E-H or E-E bonds, inorganic $[EH_2]_n$ materials also have a strong thermodynamic preference for branched over linear structures.[1,2,74] Oligomerization of EH_4 can be achieved through radical pathways or hydrogen migration, with hydrogen migration pathways generally kinetically preferred until large molecular weight, highly branched systems allow for more stable radical formation.[1,75] Higher order ($[EH_2]_n$, $n > 10$) linear heavy polyethylene structures have not been reported from bottom-up synthetic methods (*i.e.*, the dehydrogenative oligomerization of silane or germane gas, *vide infra*) due to the thermodynamic preference for branched structures, but these species are predicted to have direct optical band gaps of *ca.* 3.9 and 3.3 eV for $[SiH_2]_n$ and $[GeH_2]_n$, respectively,[76]

making them interesting targets for devices that rely on light absorption in the IR and near-IR regions (*e.g.*, solar cells and detectors).[69]

1.3.2 Top-down and solid-state syntheses of $[EH_2]_n$, E = Si or Ge

Oligomeric hydridosilanes and -germanes where the backbone element chain contains ≤ 10 atoms are commonly synthesized from M_2E (M = Mg or Ca) salts or from the reductive (Wurtz) coupling of X_2EH_2 monomers (X = halide).[77] The treatment of Ca_2E (E = Si or Ge) with HCl results in the elimination of $CaCl_2$ and the formation of EH_4 as well as oligomers E_nH_{2n+n} (n < 10). These oligomeric hydrides are commonly separated by fractional distillation.[78] Poly(dihydrosilylene) $[SiH_2]_n$ has also been synthesized by the reaction of I_2SiH_2 with alkali metals.[79] Thermal disproportionation of SiH_4 and GeH_4 is also used academically to produce higher order tetrelane oligomers;[73] careful thermal control must be implemented here to avoid complete disproportionation to the elemental species and H_2 (*vide supra*). Applications of these isolated Group 14 oligomers include film deposition and patterning; for example, the liquid Ge_3H_8 has been shown to have improved Ge CVD characteristics over GeH_4[73a] and cyclo-Si_5H_{10} can be spin coated and heated to deposit amorphous Si films.[80]

In order to target linear chains of Si or Ge rather than the thermodynamically preferred branched structures, it is beneficial for the E-E bonds to be in place prior to the formation of the H-substituted polymer. This configuration can be achieved by solid-state exfoliation reactions of alkaline earth metal-tetrel salts, which contain long range

order and E-E bonds.[81-83] Exfoliations of Ca_2Ge or CaGe with HCl to release $CaCl_2$ and hydride-rich E-H solids have been known since the 1930s;[81,83] the analogous CaSi salt is also known.[84] Both $[SiH_2]_n$ and $[GeH_2]_n$ obtained from this top-down method are highly air-sensitive orange solids, and have been broadly identified as hydride-rich amorphous solids.[81-83] Early studies on the conductivity of pressed pellets of $[SiH_2]_n$ indicated that it possessed a conductivity less than that of polyacetylene (10^{-7}–10^{-11} Ω^{-1} cm^{-1} vs. 10^{-5}–10^{-9} Ω^{-1} cm^{-1}) at room temperature.[79b] A recent study by the Veinot group at the University of Alberta characterized a crystalline $[GeH_2]_n$ product (Figure 1.6) obtained from the controlled exfoliation of CaGe with HCl, and measured an optical band gap of 2.70 eV.[83]

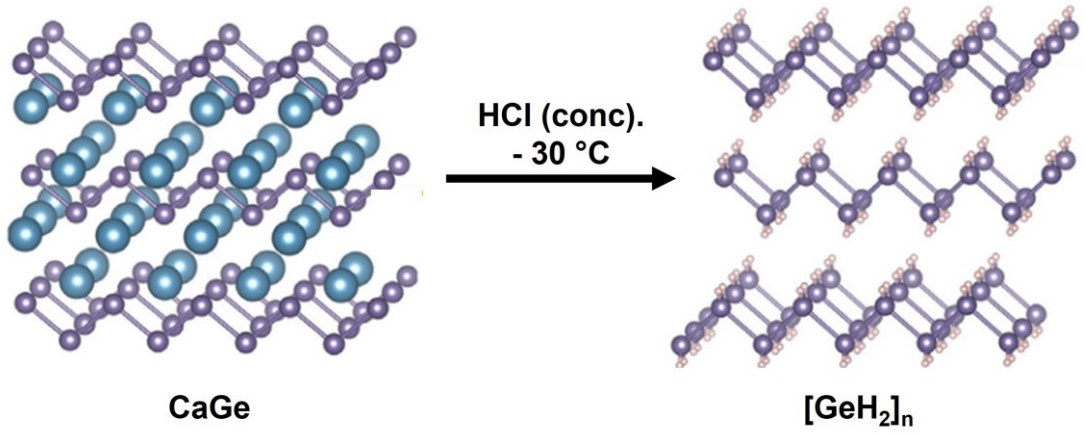

Figure 1.6. Crystal structure of CaGe, showing the Ge-Ge interactions with intercalated Ca^{2+}, adapted from the work of Veinot and coworkers.[83]

1.4 Thesis objectives

As examples of Lewis acid/base stabilization of tetrel dihydrides for deposition applications remain few, this Thesis aims to investigate this promising class of precursors. While some LB•GeH_2•LA examples have been shown previously by the Rivard Group,[1,2,12,24,28,30,31,35] they have not previously been applied to thin film deposition (CSD), and their mechanism of decomposition to elemental germanium remains unstudied. This Thesis will investigate the optimization of precursor syntheses for NHC-adducts of germanium and their solution deposition conditions via the formation of GeH_2 intermediates. In Chapter 2, a high Ge wt% $ImMe_2$•GeH_2•BH_3 is synthesized and applied to thin film deposition, resulting in amorphous Ge^0 films with 17(2) to 29(4) nm thicknesses on crystalline Si wafers. The mechanism of this deposition is explored experimentally and computationally, determining that the deposition proceeds via monomeric thermal dissociation of the Lewis acid-base complex, resulting in the release of Ge and $ImMe_2$•BH_3. Additional contributions from computational collaborators indicated that this is the energetically preferred decomposition pathway (vs. hydride migration and ring expansion pathways) for NHC•EH_2•BH_3 (E = Ge or Sn, NHC = Im, $ImMe_2$, IPr) with few exceptions. In Chapter 3, a route to polytetrelenes and elemental thin films from germanium *bis*-alkoxides via *in situ* production of EH_2 is investigated, and the impact of the addition of Lewis basic NHCs to these precursors studied. $[Ge(O^tBu)_2]_2$ is determined to be a highly soluble germanium(0) and oligogermanium hydride precursor; with strong hydride sources, thin films of semicrystalline germanium(0) can be deposited on a number of substrates, while reaction with organoboranes resulted in the isolation of a highly substituted $[GeH_{1.92}(O^tBu)_{0.08}]_n$ solid. Attempts for the analogous tin

system are explored in Chapter 4, and reactions of $[Sn(O^tBu)_2]_2$ with hydride sources result in the rapid deposition of crystalline tin(0).

1.5 References

1. E. Rivard, *Chem. Soc. Rev.*, 2016, **45**, 989.
2. M. M. D. Roy, A. A. Omaña, A. S. S. Wilson, M. S. Hill, S. Aldridge and E. Rivard, *Chem. Rev.*, 2021, **121**, 12784.
3. D. Ugur, A. J. Storm, R. Verberk, J. C. Brouwer and W. G. Sloof, *Appl. Surf. Sci.*, 2014, **288**, 673.
4. C.-J. Chem, M. H. Back and R. A. Back, *Can. J. Chem.*, **1976**, *54*, 3175.
5. (a) W. Simmler, in *Ullman's Encyclopedia of Industrial Chemistry*, Wiley-VCH Verlag GmbH & Co. KGaA, Weinheim, 7th edn., vol. 32, 2012; (b) W. O. Filtvedt, A. Holt, P. A. Ramachandran and M. C. Melaaen, *Sol. Energy Mater. Sol. Cells*, 2012, **107**, 188 and references therein.
6. (a) V. H. Nguyen, A. Dobbie, M. Myronov, D. J. Norris, T. Walther and D. R. Leadley, *Thin Solid Films,* 2012, **520**, 3222; (b) R. Venkatasubramanian, R. T. Pickett and M. L. Timmons, *J. Appl. Phys.*, **1989**, *66*, 5662.
7. (a) J. M. Jasinski and S. M. Gates, *Acc. Chem. Res.*, 1991, **24**, 9; (b) W. L. M. Weerts, M. H. J. M. de Croon and G. B. Marin, *J. Electrochem. Soc.*, 1998, **145**, 1318; (c) J. Dzarnoski, H. E. O'Neal and M. A. Ring, *J. Am. Chem. Soc.*, 1981, **103**, 5740 and references therein.
8. Y. Apeloig, R. Pauncz, M. Karni, R. West, W. Steiner and D. Chapman, *Organometallics*, 2003, **22**, 3250 and references therein.

9. D. F. Shriver, M. Weller, T. Overton, J. Rourke and F. Armstrong, *Inorganic Chemistry*, W. H. Freemen and Co., New York, 6th edn, 2014, p. 301.

10. P. P. Power, *J. Chem. Soc., Dalton Trans.*, 1998, 2939.

11. (a) X. Wang and L. Andrews, *J. Am. Chem. Soc.*, 2003, **125**, 6581; (b) S. Aldridge and A. J. Downs, *Chem. Rev.*, 2001, **101**, 3305; (c) E. Hirota and H. Ishikawa, *J. Chem. Phys.*, 1999, **110**, 4254; (d) X. Wang, L. Andrews and G. P. Kushto, *J. Phys. Chem. A*, 2002, **106**, 5809; (e) P. S. Billone, K. Beleznay, C. R. Harrington, L. A. Huck, and W. J. Leigh, *J. Am. Chem. Soc.*, 2011, **133**, 10523.

12. E. Rivard, *Dalton Trans.*, 2014, **43**, 8577.

13. (a) A. Haaland, *Angew. Chem., Int. Ed. Engl.*, 1989, **28**, 992; (b) D. Himmel, I. Krossing and A. Schnepf, *Angew. Chem., Int. Ed.*, 2014, **53**, 370.

14. (a) W. Petz, *Chem. Rev.*, 1986, **86**, 1019; (b) M. S. Holt, W. L. Wilson and J. H. Nelson, *Chem. Rev.*, 1989, **89**, 11.

15. (a) T. J. Marks and A. R. Newman, *J. Am. Chem. Soc.*, 1973, **95**, 769; (b) G. W. Grynkewich, B. Y. K. Ho, T. J. Marks, D. J. Tomaja and J. J. Zuckerman, *Inorg. Chem.*, 1973, **12**, 2522.

16. (a) P. A. Rupar, V. N. Staroverov, P. J. Ragogna and K. M. Baines, *J. Am. Chem. Soc.*, 2007, 129. 15138; (b) M. J. Ward, P. A. Rupar, M. W. Murphy, Y.-M. Yiu, K. M. Baines and T. K. Sham, *Chem. Commun.*, 2010, **46**, 7016; (c) P. A. Rupar, M. C. Jennings and K. M. Baines, *Organometallics*, 2008, **27**, 5043; (d) P. A. Rupar, V. N. Staroverov and K. M. Baines, *Science*, 2008, **322**, 1360; (e) P. A. Rupar, M. C. Jennings, P. J. Ragogna and K. M. Baines, *Organometallics*, 2007, **26**, 4109.

17. (a) U. Vogel, A. Y. Timoshkin and M. Scheer, *Angew. Chem., Int. Ed.*, 2001, **40**, 4409; (b) M. Bodensteiner, U. Vogel, A. Y. Timoshkin and M. Scheer, *Angew. Chem., Int. Ed.*, 2009, **48**, 4629; (c) M. Bodensteiner, A. Y. Timoshkin, E. V. Peresypkina, U. Vogel and M. Scheer, *Chem. Eur. J.*, 2013, **19**, 957; (d) C. Marquardt, A. Adolf, A. Stauber, M. Bodensteiner, A. V. Virovets, A. Y. Timoshkin and M. Scheer, *Chem. Eur. J.*, 2013, **19**, 11887; (e) C. Marquardt, C. Thoms, A. Stauber, G. Balázs, M. Bodensteiner and M. Scheer, *Angew. Chem., Int. Ed.*, 2014, **53**, 3727.

18. A. J. Arduengo III, R. L. Harlow and M. Kline, *J. Am. Chem. Soc.*, 1991, **113**, 361.

19. V. Nesterov, D. Reiter, P. Bag, P. Frisch, R. Holzner, A. Porzelt and S. Inoue, *Chem. Rev.*, 2018, **118**, 9678.

20. (a) D. J. Nelson and S. P. Nolan, *N-Heterocyclic Carbenes*, Wiley-VCH Verlag GmbH & Co. KGaA, New York, 2014, pp. 1−24; (b) D. J. Nelson and S. P. Nolan, *Chem. Soc. Rev.* 2013, **42**, 6723; (c) J. P Moerdyk and C. W. Bielawski, *Contemporary Carbene Chemistry*, John Wiley & Sons, Inc., New York, 2013, pp. 40−74; (d) G. Bertrand, *Reactive Intermediate Chemistry*; John Wiley & Sons, Inc., New York, 2005, pp. 329−373; (e) M. C. Jahnke and F. E. Hahn, *N-Heterocyclic Carbenes: From Laboratory Curiosities to Efficient Synthetic Tools*, The Royal Society of Chemistry, UK, 2017, pp. 1−45.

21. (a) C. D. Martin, M. Soleilhavoup and G. Bertrand, *Chem. Sci.*, 2013, **4**, 3020; (b) K. C. Mondal, S. Roy and H. W. Roesky, *Chem. Soc. Rev.*, 2016, **45**, 1080.

22. (a) M. W. Lui, C. Merten, M. J. Ferguson, R. McDonald, Y. Xu and E. Rivard, *Inorg. Chem.*, 2015, **54**, 2040; (b) H. W. Wanzlick, *Angew. Chem., Int. Ed. Engl.*,

1962, **1**, 75; (c) H. W. Wanzlick, and H. J. Schönherr, *Angew. Chem., Int. Ed. Engl.,* 1968, **7**, 141; (d) H. W. Wanzlick, B. Lachmann and E. Schikora, *Chem. Ber.*, 1965, **98**, 3170.

23. G. Prabusankar, A. Sathyanarayana, P. Suresh, C. N. Babu, K. Srinivas and B. P. R Metla, *Coord. Chem. Rev.*, 2014, **269**, 96.

24. K. C. Thimer, S. M. I. Al-Rafia, M. J. Ferguson, R. McDonald and E. Rivard, *Chem. Commun.*, 2009, 7119.

25. A. Sidiropoulos, C. Jones, A. Stasch, S. Klein and G. Frenking, *Angew. Chem., Int. Ed.*, 2009, **48**, 9701.

26. A. J. Ruddy, P. A. Rupar, K. J. Bladek, C. J. Allan, J. C. Avery and K. M. Baines, *Organometallics*, 2010, **29**, 1362.

27. A. C. Filippou, O. Chernov, B. Blom, K. W. Stumpf and G. Schnakenburg, *Chem. Eur. J.*, 2010, **16**, 2866.

28. S. M. I. Al-Rafia, R. McDonald, M. J. Ferguson and E. Rivard, *Chem. Eur. J.*, 2012, **18**, 13810.

29. M. Y. Abrahim, Y. Wang, Y. Xie, P. Wei, H. F. Schaefer III, P. v. R. Schleyer and G. H. Robinson, *J. Am. Chem. Soc.*, 2011, **133**, 8874.

30. S. M. I. Al-Rafia, A. C. Malcolm, S. K. Liew, M. J. Ferguson and E. Rivard, *J. Am. Chem. Soc.*, 2011, **133**, 777.

31. S. M. I. Al-Rafia, A. C. Malcolm, R. McDonald, M. J. Ferguson and E. Rivard, *Chem. Commun*., 2012, **48**, 1308.

32. R. S. Ghadwal, H. W. Roesky, S. Merkel, J. Henn and D. Stalke, *Angew. Chem., Int. Ed.*, 2009, **48**, 5683.

33. (a) H. J. Bestmann and O. Kratzer, *Chem. Ber.*, 1963, **96**, 1899; (b) H. J. Bestmann, K. Sühs and T. Röder, *Angew. Chem., Int. Ed. Engl.*, 1981, **20**, 1038; (c) I. V. Borisova, N. N. Zemlyansky, V. K. Belsky, N. D. Kolosova, A. N. Sobolev, Y. N. Luzikov, Y. A. Ustynyuk and I. P. Beletskaya, *J. Chem. Soc., Chem. Commun.*, 1982, 1090; (d) H. J. Bestmann, T. Röder and K. Sühs, *Chem. Ber.*, 1988, **121**, 1509; (e) F. Breitsameter, H.-P. Schrödel, A. Schmidpeter, H. Nöth and S. Rojas-Lima, *Z. Anorg. Allg. Chem.*, 1999, **625**, 1293.

34. A. K. Swarnakar, S. M. McDonald, K. C. Deutsch, P. Choi, M. J. Ferguson, R. McDonald and E. Rivard, *Inorg. Chem.*, 2014, **53**, 8662.

35. T. K. Purkait, A. K. Swarnakar, G. B. De Los Reyes, F. A. Hegmann, E. Rivard and J. G. C. Veinot, *Nanoscale*, 2015, **7**, 2241.

36. For a review on nanoscale colloidal germanium, see: D. D. Vaughn II and R. E. Schaak, *Chem. Soc. Rev.*, 2013, **42**, 2861 and references therein.

37. (a) S. Prabakar, A. Shiohara, S. Hanada, K. Fujioka, K. Yamamoto and R. D. Tilley, *Chem. Mater.*, 2010, **22**, 482; (b) N. Shirahata, D. Hirakawa, Y. Masuda and Y. Sakka, *Langmuir*, 2013, **29**, 7401.

38. K. I. Lesczyńska, P. Deglmann, C. Präsang, V. Huch, M. Zimmer, D. Schweinfurth and D. Scheschkewitz, *Dalton. Trans.*, 2020, **49**, 13218.

39. D. Lutters, C. Severin, M. Schmidtmann and T. Müller, *J. Am. Chem. Soc.*, 2016, **138**, 6061.

40. C. P. Sindlinger, W. Grahneis, F. S. W. Archer and L. Wesemann, *Chem. Eur. J.*, 2016, **22**, 7554.

41. T. J. Haddlington, B. Schwartze, E. I. Izgorodina and C. Jones, *Chem. Commun.*, 2015, **51**, 6854.

42. S. Kahn, P. P. Samuel, R. Michel, J. M. Deiterich, R. Mata, J. P. Demers, A. Lange, H. W. Roesky and D. Stalke, *Chem. Commun.*, 2012, **48**, 4890.

43. S. E. Koponen, P. G. Gordon and S. T. Barry, *Polyhedron*, 2016, **108**, 59.

44. D. J. H. Emslie, P. Chadha and J. S. Price, *Coord. Chem. Rev.*, 2013, **257**, 3282.

45. A. C. Jones and M. L. Hitchman, *Chemical Vapour Deposition: Precursors Processes and Applications*, RSC Publishing, Cambridge, 2009.

46. A. E. Van Arkel and J. H. De Boer, *Z. Anorg, Allg. Chem.*, 1925, **148**, 345.

47. J. S. De Lodyguine, U. S. Patent 575, 002, 1893.

48. For some examples of ALD precursors see: (a) H. Kim, *J. Vac. Sci. Technol., B*, 2003, **21**, 2231; (b) F. Zaera, *J. Phys. Chem. Lett.*, 2012, **3**, 1301; (c) N. Bahlawane, K. Kohse Höeinghaus, P. A. Premkumar and D. Lenoble, *Chem. Sci.*, 2012, **3**, 929; (d) M. Knez, K. Nielsch and L. Niinistö, *Adv. Mater.*, 2007, **19**, 3425; (e) S. M. George, *Chem. Rev.*, 2010, **110**, 111; (f) H. Kim, H.-B.-R. Lee and W.-J. Maeng, *Thin Solid Films*, 2009, **517**, 2563; (g) F. Zaera, *J. Mater. Chem.*, 2008, **18**, 3521; (h) R. L. Puurunen, *J. Appl. Phys.*, 2005, **97**, 121301; (i) M. Leskelä and M. Ritala, *Angew. Chem., Int. Ed.*, 2003, **42**, 5548.

49. C. E. Knapp and C. J. Carmalt, *Chem. Soc. Rev.*, 2016, **45**, 1036.

50. G. Hodes, *Chemical Solution Deposition of Semiconductor Films*, CRC Press, New York, 2002.

51. (a) C. Puscher. *Dingl. J.*, 1869, **190**, 421; (b) J. Emerson-Reynolds. *J. Chem. Soc.*, 1884, **45**, 162.

52. B. Vidjayacoumar, D. J. H. Emslie, J. M. Blackwell, S. B. Clendenning and J. F. Britten, *Chem. Mater.*, 2010, **22**, 4854.

53. A. Vidjayacoumar, V. Ramalingam, D. J. H. Emslie, J. M. Blackwell and S. B. Clendenning, *ECS Trans.*, 2012, **50**, 53.

54. A. Ludviksson, R. Zhang, C. T. Campbell and K. Griffiths, *Surf. Sci.*, 1994, **313**, 64, and references therein.

55. P. J. Pallister, S. C. Buttera and S. T. Barry, *J. Phys. Chem. C*, 2014, **118**, 1618.

56. G. Shang, M. J. Hampden-Smith and E. N. Duelser, *Chem. Commun.*, 1996, 1733.

57. H. Sun, X. Qin and F. Zaera, *J. Phys. Chem. Lett.*, 2012, **17**, 2523.

58. J. P. Coyle, W. H. Monillas, G. P. A. Yap and S. T. Barry, *Inorg. Chem.*, 2008, **47**, 683.

59. (a) J. Bardeen, B. H. Walter and Bell Telephone Lab Inc, U. S. Patent 2524035A, 1948; (b) H. F. Mataré and H. Welker, U.S. Patent 2673948A, 1948.

60. P. A. Gargini, in *Nanoelectronics: Materials, Devices, Applications*, eds. R. Puers, L. Baldi, M. van de Voorde and S. E. van Nooten, Wiley-VCH Verlag GmbH & Co. KGaA, Weinheim, 1st edn, 2012, ch. 1, pp. 3-54.

61. H.-J. Mussig and J. Dabrowski, *Silicon Surfaces and Formation of Interfaces*, World Scientific Publishing Company, London, 2000.

62. (a) T. Eom, T. Gwon, S. Yoo, B. J. Choi, M.-S. Kim, I. Buchanan, M. Xiao and C. S. Hwang, *Chem. Mater.*, 2014, **26**, 1583; (b) T. Eom, S. Choi, B. J. Choi, M. H. Lee, T. Gwon, S. H. Rha, W. Lee, M.-S. Kim, M. Xiao, I. Buchanan, D.-Y.Cho and C. S. Hwang, *Chem. Mater.*, 2012, **24**, 2099; (c) S. Yoo, C. Yoo, E.-S. Park, W. Kim, Y. K. Lee and C. S. Hwang, *J. Mater. Chem. C*, 2018, **6**, 5025.

63. (a) K. Knapas, T. Hatanpää, M. Ritala and M. Leskelä, *Chem. Mater.*, 2010, **22**, 1386; (b) V. Pore, T. Hatanpää, M. Ritala and M. Leskelä, *J. Am. Chem. Soc.*, 2009, **131**, 3478; (c) M. Ritala, V. Pore, T. Hatanpää, M. Heikkilä, M. Leskelä, K. Mizohata, A. Schrott, S. Raoux and S. M. Rossnagel, *Microelectron. Eng.*, 2009, **86**, 1946; (d) T. Sarnet, V. Pore, T. Hatanpää, M. Ritala, M. Leskelä, A. Schrott, Y. Zhu, S. Raoux and H.-Y. Cheng, *J. Electrochem. Soc.* 2011, **158**, D694.

64. W. Hunks, P. S. Chen, T. Chen, M. Stender, G. T. Stauf, L. Maylott, C. Xu and J. F. Roeder *Mater. Res. Soc. Symp. Proc.*, 2008, vol. 1071, Materials Research Society.

65. G. Wang, M. Kolahdouz, J. Luo, C. Qin, S. Gu, Z. Kong, X. Yin, W. Xiong, X. Zhao, J. Liu, T. Yang, J. Li, H. Yin, H. Zhu, W. Wang, C. Zhao, T. Ye and H. H. Radamson, *J. Mater. Sci. Mater. Electron.*, 2020, **31**, 26.

66. T. David, J.-N. Aqua, K. Liu, L. Favre, A. Ronda, M. Abbarchi, J.-B. Claude and I. Berbezier, *Sci. Rep.*, 2018, **8**, 289.

67. S. Gupta, X. Gong, R. Zhang, Y.-C. Yeo, S. Takagi and K. C. Saraswat, *MRS Bull.*, 2014, **39**, 678.

68. Z. Xia, H. Song, M. Kim, M. Zhou, T.-H. Chang, D. Liu, X. Yin, K. Xiong, H. Mi, X. Wang, F. Xia, Z. Yu, Z. (J.) Ma and Q. Gan, *Sci. Adv.*, 2017, **3**, e1602783.

69. (a) K.-T. Lee, S. Seo, J. Y. Lee and L. J. Guo, *Adv. Mater.*, 2014, **26**, 6324; (b) K.-T. Lee, S. Seo, J. Y. Lee and L. J. Guo, *Appl. Phys. Lett.*, 2014, **104**, 231112.

70. (a) V. Steenhoff, M. Theuring, M. Vehse, K. von Maydell and C. Agert, *Adv. Opt. Mater.*, 2015, **3**, 182; (b) D. O. Sigle, L. Zhang, S. Ithurria, B. Dubertret and J. J. Baumberg, *J. Phys. Chem. Lett.*, 2016, **6**, 1099; (c) Y. Xin, L. Wu, L. Ge, C. Han, Y. Li and S. Fang, *J. Mater. Chem. A*, 2015, **3**, 8659.

71. For a review, see: (a) R. Mülhaupt, *Angew. Chem., Int. Ed.*, 2004, **43**, 1054; (b) H. Staudinger, *Ber. Dtsch. Chem. Ges.*, 1924, **57**, 1203; (c) Original reports of polyethylene termed it as polymethylene: H. von Pechmann, *Ber. Dtsch. Chem. Ges.*, 1899, **31**, 2640.

72. (a) K. Ziegler, E. Holzkamp, H. Breil and H. Martin, *Angew. Chem.*, 1955, **67**, 426; (b) G. Natta, *Makromol. Chem.*, 1960, **35**, 94; (c) S. D. Ittel, L. K. Johnson and M. Brookhart, *Chem. Rev.*, 2000, **100**, 1169; (d) F. di Lena and K. Matyjaszewski, *Prog. Polym. Sci.*, 2010, **35**, 959.

73. (a) G. Grzybowski, A. V. G. Chizmeshya, C. Senaratne, J. Menendez and J. Kouvetakis, *J. Mater. Chem. C*, 2013, **1**, 5223; (b) F. Fehér and I. Fischer, *Z. Anorg. Allg. Chem.*, 1976, **421**, 9; (c) A. F. Clifford and G. R. Zeilenga, *Inorg. Chem.*, 1969, **8**, 1789; (d) S. D. Gokhale, J. E. Drake and W. L. Jolly, *J. Inorg. Nucl. Chem.*, 1965, **27**, 1911; (e) M. Akhtar, *Synth. React. Inorg. Met.-Org. Chem.*, 1986, **16**, 729; (f) Photolysis has also been used to generate higher silane oligomers: G. G. A. Perkins and F. W. Lampe, *J. Am. Chem. Soc.*, 1980, **102**, 3764; (g) G. Olbrich, P. Potzinger, B. Reimann and R. Walsh, *Organometallics*, 1984, **3**, 1267.

74. (a) J. Ma and S. Inagaki, *J. Am. Chem. Soc.*, 2001, **123**, 1193; (b) For the relative stability of branched and linear $(GeCl_2)_x$ oligomers, see: S. M. I. Al-Rafia, M. R. Momeni, R. McDonald, M. J. Ferguson, A. Brown and E. Rivard, *Angew. Chem., Int. Ed.*, 2013, **52**, 6390.

75. W. A. Eger, A. Genest and N. Rösch, *Chem. Eur. J.*, 2012, **18**, 9106.

76. (a) J. R. Damewood Jr. and R. West, *Macromolecules*, 1985, **18**, 159; (b) K. Takeda, K. Shiraishi and N. Matsumoto, *J. Am. Chem. Soc.*, 1990, **112**, 5043.

77. (a) C.-A. Wurtz, *Chim. Phys.*, 1855, **44**, 275; (b) A. D. Craig and A. G. MacDiarmid, *J. Inorg. Nucl. Chem.*, 1962, **24**, 161.

78. (a) A. Stock and C. Somieski, *Ber. Dtsch. Chem. Ges.*, 1916, **49**, 111; (b) F. Fehér, H. Baier, B. Enders, M. Krancher, J. Laakmann, F. J. Ocklenburg and D. Skrodski, *Z. Anorg. Allg. Chem.*, 1985, **530**, 191; (c) C. J. Ritter, WO 2012/021634 A2, **2012**; (d) W. C. Johnson and S. Isenberg, *J. Am. Chem. Soc.*, 1935, **57**, 1349; (e) P. L. Timms and C. S. G. Phillips, *Inorg. Chem.*, 1964, **3**, 606.

79. (a) T. Masuda, Y. Matsuki and T. Shimoda, *Thin Solid Films*, 2012, **520**, 6603; (b) P. John, I. M. Odeh and J. Wood, *J. Chem. Soc., Chem. Commun.*, 1983, 1496.

80. T. Shimoda, Y. Matsuki, M. Furusawa, T. Aoki, I. Yudasaka, H. Tanaka, H. Iwasawa, D. Wang, M. Miyasaka and Y. Takeuchi, *Nature*, 2006, **440**, 783.

81. (a) P. Royen and R. Schwartz, *Z. Anorg. Allg. Chem.*, 1933, **215**, 295; (b) L. M. Dennis and N. A. Skow, *J. Am. Chem. Soc.*, 1930, **52**, 2369; (c) For a related approach to $[GeH]_n$, see: T. Giousis, G. Potsi, A. Kouloumpis, K. Spyrou, Y. Georgantas, N. Chalmpes, K. Dimos, M.-K. Antoniou, G. Papavassiliou, A. B. Bourlinos, H. J. Kim, V. K. S. Wadi, S. Alhassan, M. Ahmadi, B. J. Kooi, G. Blake, D. M. Balazs, M. A. Loi, D. Gournis and P. Rudolf, *Angew. Chem., Int. Ed.*, 2021, **60**, 360.

82. P. Royen and C. Rocktäschel, *Z. Anorg. Allg. Chem.*, 1966, **346**, 279.

83. H. Yu, C. Ni, A. N. Thiessen, Z. Li and J. G. C. Veinot, *ACS Nano*, 2021, **15**, 9368.

Chapter 2: Insight into the Decomposition Mechanism of Donor-Acceptor Complexes of EH_2 (E = Ge and Sn) and Access to Germanium Thin Films from Solution

2.1 Introduction

Inorganic tetrelenes EH_2 (E = Si, Ge, Sn, and Pb) are highly reactive species that can be generated and trapped with sophisticated low temperature matrix techniques (often < -200 °C).[1] As shown in Chart 2.1, these main group species adopt singlet electronic ground states, leading to dual electron-accepting and -donating character. Group 14 element dihydrides are of considerable fundamental interest,[2] due in part to the role of SiH_2 and GeH_2 as key intermediates in the chemical vapour deposition (CVD) of bulk Si and Ge from gaseous tetrelanes EH_4.[3] While methylene-type (CH_2) reactivity can be coaxed from both metal (L_nMCH_2)[4] and non-metal (H_2CN_2)[5] precursors, compounds bearing heavier element EH_2 reactivity are much more scarce.[6] In 2009, the Rivard Group prepared the first isolable complex of GeH_2, in the form of the Ge(II) adduct IPr•GeH_2•BH_3 (IPr = [(HCNDipp)$_2$C:]; Dipp = 2,6-^{i}Pr$_2$C$_6$H$_3$).[7] This donor-acceptor stabilization approach involves coordinating reactive Main Group fragments (such as :GeH_2) between Lewis basic (LB) and Lewis acidic (LA) entities (Chart 2.1).[8,9] Subsequently, this general donor-acceptor protocol provided access to various isolable complexes of inorganic tetrelenes EH_2 and ethylenes H_2EEH_2 (E = Si, Ge, and/or Sn).[10] Of added note, LB•GeH_2•LA complexes were shown to be precursors to luminescent Ge nanoparticles upon microwave heating of the complexes to 190 °C in organic solvents.[11]

For comparison, this element deposition procedure is much more mild than the widely used gas phase decomposition of toxic GeH_4 (> 450 °C) into elemental Ge and dihydrogen.[3c]

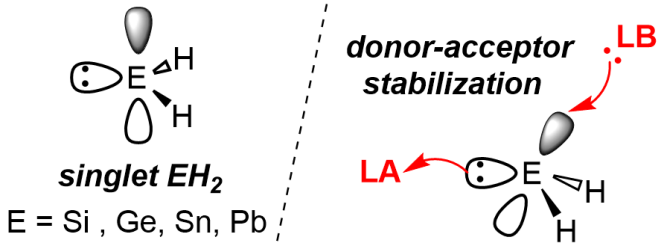

Chart 2.1. Depiction of the frontier orbitals in inorganic tetrelenes (EH_2; E = Si-Pb) and their stabilization via donor-acceptor (Lewis base/acid, LB/LA) coordination.

Herein, new germanium-rich NHC•GeH_2•BH_3 adducts (NHC = *N*-heterocyclic carbene) are introduced with nearly 40 wt.% of Ge. A number of different NHCs were investigated experimentally and computationally (Chart 2.2) *en route* to the isolation of the new reported complexes. Moreover, I show that $ImMe_2$•GeH_2•BH_3 ($ImMe_2$ = $(HCNMe)_2C$:) can cleanly deposit germanium as 20 to 70 nm thick films onto various substrates.[12,13] While $ImMe_2$•GeH_2•BH_3 complex does not have the required volatility to enable its use in CVD, the use of this complex to yield nanometer thick Ge coatings via an entirely solution-phase and low-temperature approach has distinct advantages over pre-existing routes to Ge films, including: the ability to deposit Ge onto thermally-sensitive and non-conducting substrates without the need for high vacuum chambers or electrochemical apparati.[13d-f] In addition to these promising new results, an important question remained unanswered: What is the mechanism of EH_2 release from the corresponding donor-acceptor complexes? Does the first step involve LB-E or E-LA

bond cleavage or does a competing process, such as a 1,2-hydrogen shift from the tetrel element (E) to an *N*-heterocyclic carbene carbon centre,[14] occur *en route* to element deposition? Due to the transient nature of EH_2 species,[15] a combined experimental (kinetics) and computational approach was used to evaluate possible decomposition pathways available to $ImMe_2{\bullet}GeH_2{\bullet}BH_3$. Computations were also used to evaluate the decomposition energetics associated with the E(II) dihydride adducts $NHC{\bullet}EH_2{\bullet}BH_3$ (NHC = IPr, $ImMe_2$, or $[(HCNH)_2C{:}]$ (Im); E = Ge or Sn).

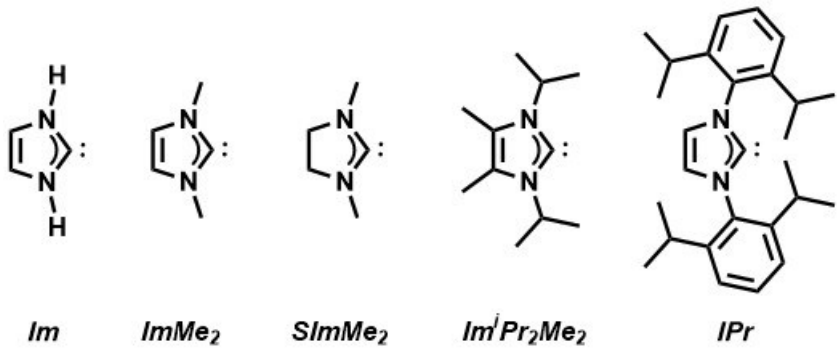

Chart 2.2. *N*-Heterocyclic carbenes investigated in this study.

2.2 Results and discussion

2.2.1 NHC•GeH_2•BH_3 adducts with increased germanium content

Given the successful preparation of $IPr{\bullet}GeH_2{\bullet}BH_3$,[7] and the subsequent application of similar donor-acceptor $LB{\bullet}GeH_2{\bullet}BH_3$ compounds for the deposition of bulk and nanodimensional germanium,[11] the functional group tunability of NHCs was leveraged to pursue higher germanium weight-content precursors. The first carbene

donor explored in this study, $Im^iPr_2Me_2$ ([(MeCN^{i}Pr)$_2$C:]), made an early debut in *N*-heterocyclic carbene chemistry[16] and is a ligand commonly employed for Group 14 element halides and alkoxides;[17] it also has half the molecular weight of IPr. Moreover, $Im^iPr_2Me_2$ is a useful supporting ligand for copper atomic layer deposition (ALD) as it helps impart good thermal stability and high volatility to the Cu complexes involved.[18]

The target Ge(II) dihydride complex $Im^iPr_2Me_2$•GeH_2•BH_3 (**2**) was prepared by combining the new Ge(IV) halide adduct $Im^iPr_2Me_2$•$GeCl_4$ (**1**, made from free $Im^iPr_2Me_2$ and $GeCl_4$) with excess Li[BH_4] (Scheme 2.1). A related *in situ* Ge(IV) to Ge(II) reduction/Ge-Cl to Ge-H metathesis procedure was used in the Rivard Group to generate IPr•GeH_2•BH_3.[19] Unlike its bulkier IPr congener, IPr•GeH_2•BH_3, the less hindered adduct $Im^iPr_2Me_2$•GeH_2•BH_3 (**2**) is prone to decomposition in solution, resulting in the formation of by-products containing the imidazolium cation $[Im^iPr_2Me_2H]^+$. As these charged by-products possess very similar solubility as the GeH_2 complex **2**, samples of $Im^iPr_2Me_2$•GeH_2•BH_3 (**2**) could only be obtained with a bulk purity of *ca.* 80 %. From a crude sample of **2**, crystals suitable for single-crystal X-ray crystallographic analysis were selected. The quality of the resulting crystallographic data was sufficient to allow for the full refinement of all boron- and germanium-bound hydrides (Figure 2.1)[20], leading to Ge-H [1.43(2) and 1.48(2) Å] bond lengths that are within the same range as those reported for IPr•GeH_2•BH_3.[7] The Ge-B distance [2.073(2) Å] in **2** is similar in length to the corresponding distance in IPr•GeH_2•BH_3 [2.053(3) Å].[7] The adjacent C_{NHC}-Ge bond length in $Im^iPr_2Me_2$•GeH_2•BH_3 (**2**) is 2.013(2) Å and is

shorter than the C_{NHC}-Ge interaction found in Baines' Ge(II) dichloride adduct $Im^iPr_2Me_2$•$GeCl_2$ [2.106(3) Å].[21]

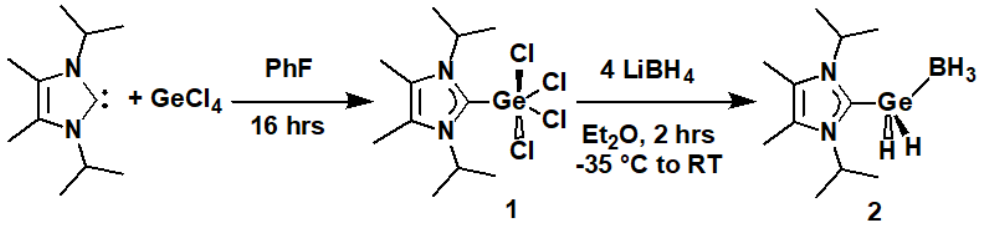

Scheme 2.1. Synthesis of $Im^iPr_2Me_2$•GeH_2•BH_3 (**2**).

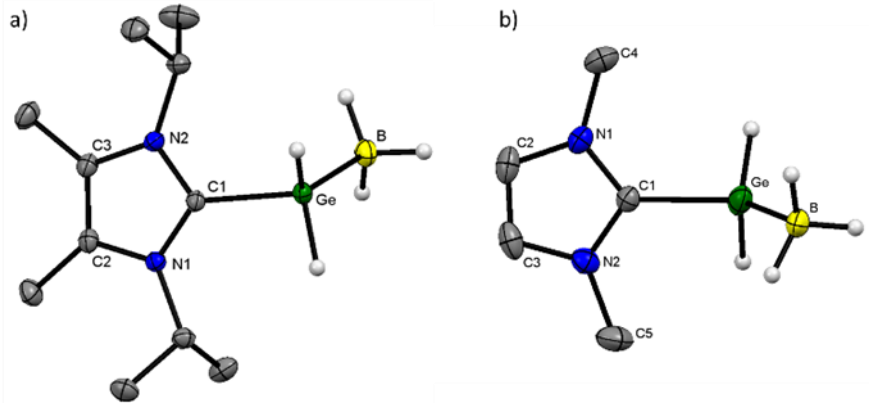

Figure 2.1. Crystal structures of: (a) $Im^iPr_2Me_2$•GeH_2•BH_3 (**2**, left) and (b) $ImMe_2$•GeH_2•BH_3 (**6**, right). Thermal ellipsoids plotted at 30 % probability level with all carbene-based hydrogen atoms omitted for clarity. Selected bond lengths [Å] and angles [°]: **2**: C1-Ge 2.013(2), Ge-B 2.073(2), Ge-H1 1.43(2), Ge-H2 1.48(2); N1-C1-N2 106.6(1), C1-Ge-B 110.21(7), H-Ge-H 101(1). **6**: C1-Ge 1.996(2), Ge-B 2.054(4), Ge-H1 1.46(3), Ge-H2 1.62(2); N1-C1-N2 106.0(2), C1-Ge-B 113.5(1), H-Ge-H: 101(1).[20]

Given the challenges in obtaining pure $Im^iPr_2Me_2$•GeH_2•BH_3 (**2**), I prepared the known saturated NHC complex $SImMe_2$•$GeCl_4$ (**3**)[22] [$SImMe_2$ = $(H_2CNMe)_2C$:] from a

C-Cl insertion reaction involving Cl_2Ge•dioxane, and then explored the reactivity of **3** with $Li[BH_4]$ (Scheme 2.2). Despite careful control of the reaction temperature (from -35 °C to room temperature), the main product isolated was invariably the known *trans*-isomer[23] of the dihydroaminal-bis(borane) adduct $[\{H_2CNMe(BH_3)\}_2CH_2]$ (**4**) (Scheme 2.2). The formation of **4** was accompanied by grey and white solids on the walls of the reaction vessel, consistent with the formation of bulk germanium and lithium chloride. Compound **4** was also isolated directly from the reaction between 2-chloro-1,3-dimethylimidazolinium chloride and $Li[BH_4]$ (Scheme 2.2).

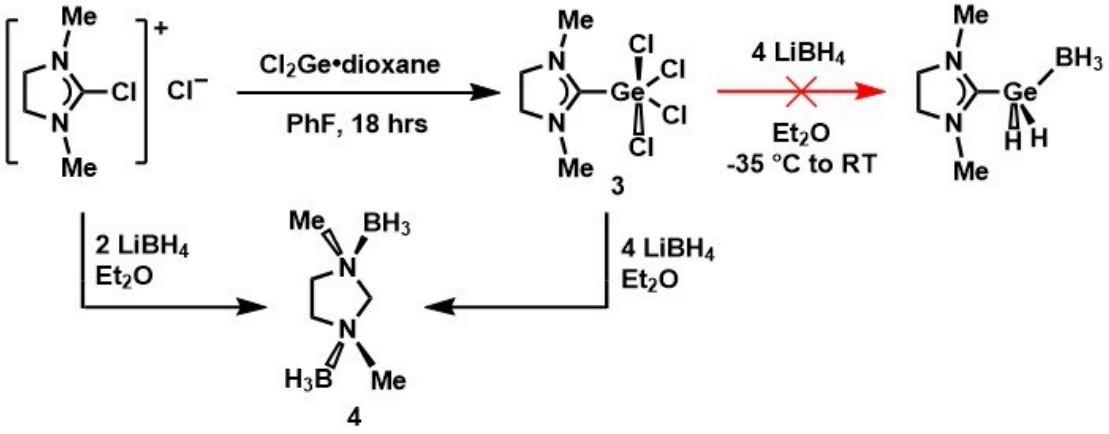

Scheme 2.2. Preparation of $SImMe_2$•$GeCl_4$ (**3**) and subsequent reactions with $Li[BH_4]$ to form 1,3-dimethyl-1,3-diazolidine bis(borane) (**4**).

The search for a new, stable, low-weight germanium-rich NHC•GeH_2•BH_3 complex ended successfully with the high yield preparation of $ImMe_2$•GeH_2•BH_3 ($ImMe_2$ = $[(HCNMe)_2C:]$). The route to this Ge(II) dihydride complex (Scheme 2.3) involves generation of the free carbene $ImMe_2$ *in situ*,[24] followed by the addition of a THF solution

of this carbene to Cl_2Ge•dioxane to afford the new adduct $ImMe_2$•$GeCl_2$ (**5**); notably, prior computational studies indicated that the precursor complex **5** should be stable.[25] Crystals of $ImMe_2$•$GeCl_2$ (**5**) suitable for X-ray crystallography (Figure 2.2)[19] were obtained by cooling a THF solution of this Ge(II) adduct to -35 °C. $ImMe_2$•GeH_2•BH_3 (**6**) was then prepared by combining slurries of $ImMe_2$•$GeCl_2$ and $Li[BH_4]$ in Et_2O, followed by vigorously stirring at room temperature for two hours (Scheme 2.3). After exchanging the solvent for fluorobenzene, X-ray quality crystals were subsequently grown at -35 °C, which conclusively identified the product as $ImMe_2$•GeH_2•BH_3 (**6**). As for $Im^iPr_2Me_2$•GeH_2•BH_3 (**2**), the quality of the data allowed for full refinement of the hydrogen atoms within the -GeH_2BH_3 unit (Figure 2.1). The observed Ge-B distance in $ImMe_2$•GeH_2•BH_3 (**6**) [2.054(4) Å] is similar in length as in the temperature-sensitive complex $Im^iPr_2Me_2$•GeH_2•BH_3 (**2**) [2.073(2) Å], while the adjacent Ge-C_{NHC} bond length in **6** [1.996(2) Å] is shorter than the Ge-C_{NHC} linkages found in both IPr•GeH_2•BH_3 [2.053(3) Å][7] and the precursor Ge(II) complex $ImMe_2$•$GeCl_2$ [2.069(4) to 2.085(3) Å; range from three different molecules in the asymmetric unit].[20]

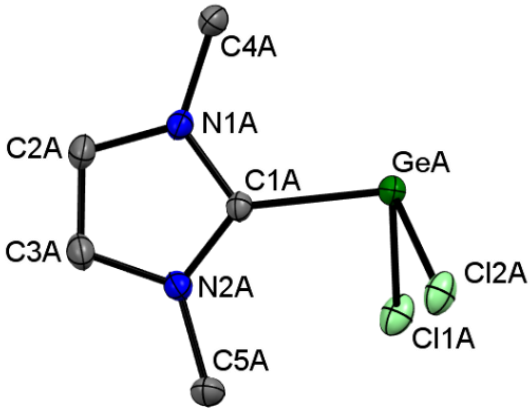

Figure 2.2. ORTEP of one of the three crystallographically independent molecules of $ImMe_2$•$GeCl_2$. Thermal ellipsoids are presented at a 30 % probability level, and all hydrogen atoms have been omitted for clarity. Selected bond lengths [Å] and angles [°] with values belonging to the second and third molecule in the asymmetric unit shown in square brackets: C1-Ge 2.067(4) [2.075(3), 2.081(3), Ge-Cl1 2.292(1) [2.2752(9), 2.3057(8)], Ge-Cl2 2.2987(9) [2.341(1), 2.3090(9)]; N1-C1-N2 106.0(3) [105.3(3), 104.7(3)], C1-Ge-Cl1 93.49(9) [96.83(9), 96.11(9)], C1-Ge-Cl2 95.66(9) [91.12(9), 89.65(9)], Cl1-Ge-Cl2 95.30(3) [97.62(3), 96.10(3)].[20]

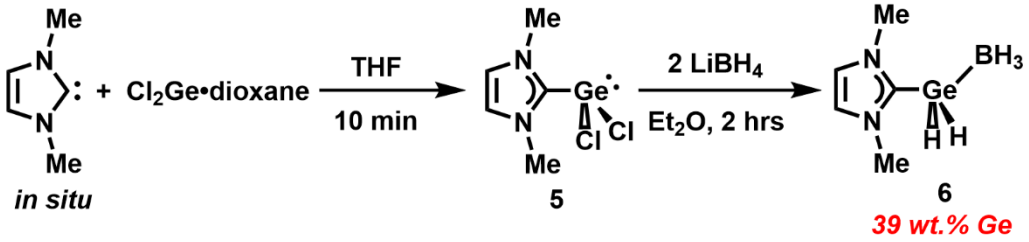

Scheme 2.3. Synthesis of $ImMe_2$•GeH_2•BH_3 (**6**).

*2.2.2 Controlled release of elemental germanium from $ImMe_2$•GeH_2•BH_3 (**6**)*

It was undertaken to determine if $ImMe_2$•GeH_2•BH_3 (**6**) could yield bulk Ge after heating in solution, and to identify the nature of the by-products formed in order to gain

insight into the mechanism of decomposition. To start, a sample of $ImMe_2•GeH_2•BH_3$ (**6**) was heated to 100 °C (2 hours) or 125 °C (3 days) under static vacuum (*ca.* 2×10^{-2} mbar), and the products were examined by Raman spectroscopy (Figure 2.3). Analysis of the products formed after heating **6** to 100 °C (Figure 2.3, left) showed the appearance of the expected Ge-Ge peak[26] at 280 cm^{-1} for amorphous Ge, coupled with a collective decrease in intensity of the Raman peaks associated with **6**. The consumption of **6** was accompanied by the formation of the carbene-borane adduct $ImMe_2•BH_3$. The photograph shown at the right of Figure 2.3 depicts the remaining sample after thermolysis of **6** at 125 °C under N_2 (for 18 hours) and illustrates the volatility of the decomposition by-product $ImMe_2•BH_3$, which crystallized on the walls of the upper (cooler) portion of the glass NMR tube; elemental Ge could be seen at the bottom of the tube. If the decomposition of **6** is repeated at 125 °C under a static vacuum of *ca.* 2×10^{-2} mbar for 3 days, the only non-volatile species that remains (according to Raman spectroscopy) is amorphous Ge (Figure 2.3, left). The clean conversion of $ImMe_2•GeH_2•BH_3$ (**6**) to Ge and volatile $ImMe_2•BH_3$ is promising, as the organic by-products formed can be removed either by sublimation or washing with organic solvent. Consistent with the Raman data in Figure 2.3, the deposited germanium from the solid-state thermolysis of **6** was confirmed to be amorphous by powder X-ray diffraction (Figure 2.4).

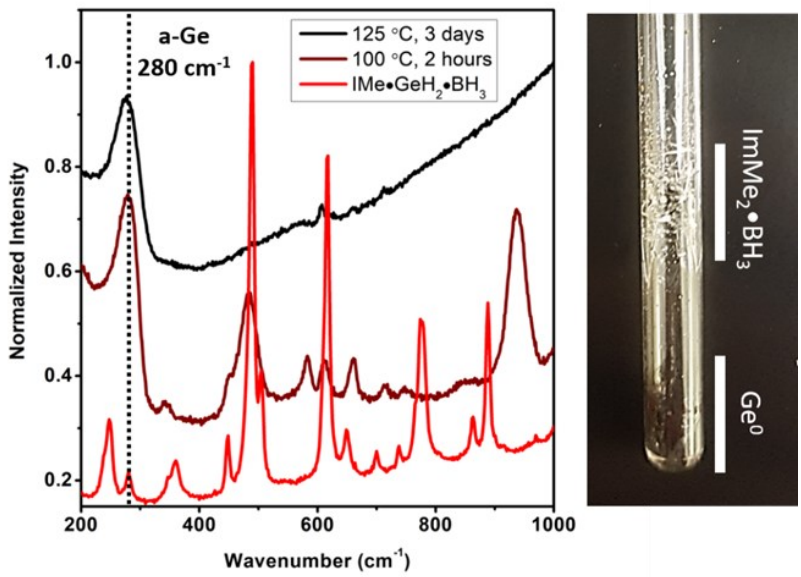

Figure 2.3. Left: Raman spectra associated with the decomposition of $ImMe_2•GeH_2•BH_3$ (**6**). Trials were conducted in the solid-state under static vacuum. Right: Photograph of a sealed glass NMR tube under N_2 after thermal decomposition of **6** at 125 °C (18 hours). Elemental Ge and crystalline $ImMe_2•BH_3$ (also confirmed by ^1H NMR analysis) can be seen in the lower and upper portions of the tube, respectively.

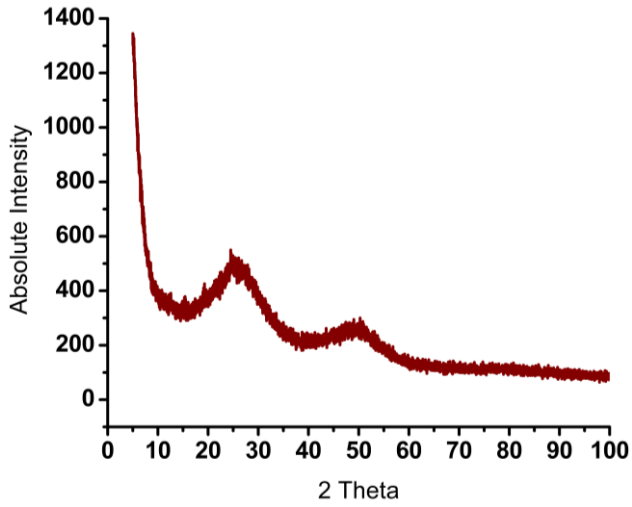

Figure 2.4. Powder XRD pattern of amorphous Ge deposited from $ImMe_2•GeH_2•BH_3$ via heating under static vacuum at 125 °C for 12 hours. Sample was lightly ground and mounted in a capillary tube. Broad resonances at 25° and 50° are typical of thin film amorphous Ge.[26]

To characterize the organic by-products from the above-mentioned decomposition of $ImMe_2•GeH_2•BH_3$ (**6**), a sample of this adduct was then heated to reflux in C_6D_6 (external bath temperature = 100 °C; **Caution! closed system**). ^1H and ^{11}B NMR spectroscopy after 48 hours indicated the clean conversion of **6** into the known compound $ImMe_2•BH_3$[27] (Figure 2.5). $ImMe_2•BH_3$ was also independently synthesized to confirm its identity and to determine its thermal properties (*vide infra*).

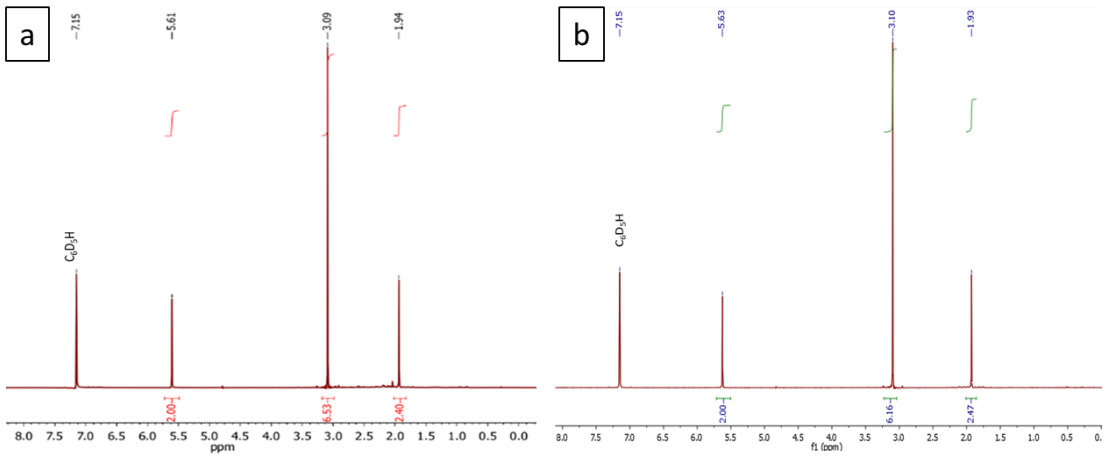

Figure 2.5. $^1H\{^{11}B\}$ NMR spectrum of (a) independently synthesized $ImMe_2•BH_3$ and (b) $ImMe_2•GeH_2•BH_3$ after heating to 100 °C for 48 hours in C_6D_6. Complete decomposition occurred, with only $ImMe_2•BH_3$ remaining.

The thermal properties of $ImMe_2•GeH_2•BH_3$ (**6**) were analyzed by differential scanning calorimetry (DSC) and thermogravimetric analysis (TGA), both conducted at heating rates of 10 °C/min under N_2. A representative DSC trace is shown in Figure 2.6a, and reveals the onset of an endothermic event at 108 °C, agreeing well with the visually determined melting point of **6** (103-105 °C). The subsequent exothermic event beginning

at 118 °C appears to be linked to the onset Ge deposition as thermal gravimetric analysis of $ImMe_2$•GeH_2•BH_3 (**6**) (Figure 2.6b) shows mass loss beginning at *ca.* 110 °C. TGA recorded another dip in mass near 150 °C, which corresponds with the tail end of the exothermic feature in the DSC of **6**. Continued heating of **6** up to 600 °C results in the sublimation of the decomposition product $ImMe_2$•BH_3 (*vide infra*) leading to a residual mass of 49.6 wt%, according to TGA. $ImMe_2$•BH_3 was independently subjected to TGA (Figure 2.6c) and the onset of its sublimation can be seen at 150 °C, aligning with features in the TGA trace of $ImMe_2$•GeH_2•BH_3 (**6**); for $ImMe_2$•BH_3, sublimation reaches completion (100 wt% loss) at 290 °C. Given that $ImMe_2$•GeH_2•BH_3 (**6**) initially contains 39 wt% Ge, there is unaccounted mass left in the residue after TGA. At this stage the reason for the mass difference is unclear, however oxidation of the deposited Ge by traces of atmospheric oxygen cannot be ruled out. It may be posited also that some $ImMe_2$ or organic contaminants remain adhered to the surface of the deposited germanium, leading to the higher final mass yield. Energy-dispersive X-ray (EDX) analyses of the residual samples of Ge after decomposition of **6** in solution (*vide infra*) do not indicate the presence of nitrogen, however the sensitivity of this technique to nitrogen is low.

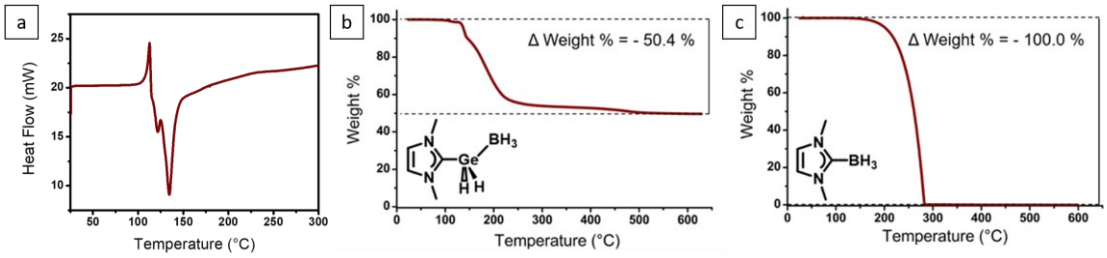

Figure 2.6. (a) DSC of $ImMe_2•GeH_2•BH_3$ (**6**) under a flow of N_2, with a heating rate of 10 °C/min (left). TGA of $ImMe_2•GeH_2•BH_3$ (**6**) (b) and $ImMe_2•BH_3$ (c) conducted under a gentle flow of N_2 at a heating rate of 10 °C/min.

The solution-phase deposition of Ge films was also carried out by immersion of various substrates into solutions of $ImMe_2•GeH_2•BH_3$ (**6**) in toluene, followed by controlled heating. The samples were heated at 100 °C for either 3 or 10 hours, after which time the substrates were then washed with benzene to remove the $ImMe_2•BH_3$ by-product. Gratifyingly, **6** was consistently able to deposit thin layers of elemental Ge onto a variety of substrates, including glass wool (Figure 2.7) and Si wafers (Figure 2.8). Deposition of thin films of germanium onto Si wafers yielded the best surface coverage, allowing for a reliable determination of the thickness of the deposited Ge by scratching the surface (post deposition, Figure 2.8a) and imaging the exposed Ge film edges at an angle of 54° (Figure 2.8b).[28] Energy-dispersive X-ray spectroscopy (EDX) analysis (Figure 2.7c and Figure 2.8c) illustrates the Ge deposited on the surface and lower Ge signal where the deposited layer has been removed.

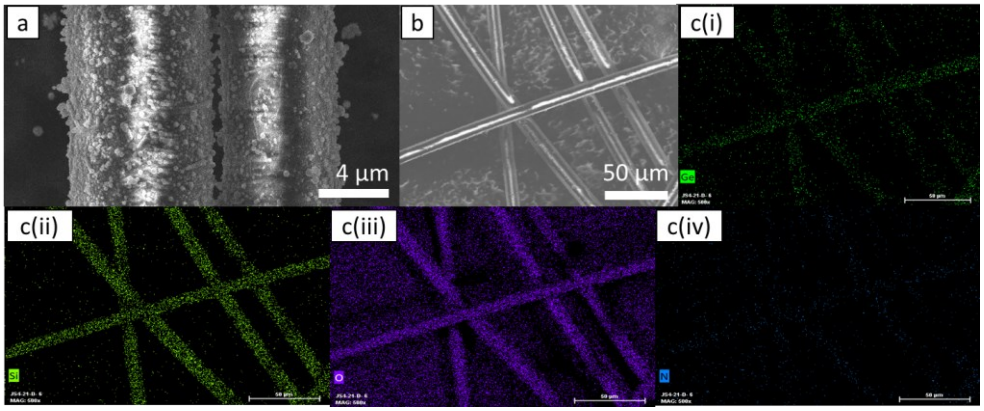

Figure 2.7. (a, b) Secondary electron SEM of Ge films deposited from 6.1 × 10^{-3} M solution of $ImMe_2$•GeH_2•BH_3 in toluene 100 °C over 3 hours onto glass (SiO_2) wool fibers. (c(i-iv)) show EDX maps of Ge, Si, O and N, respectively. Collected at 5.0 kV.

The thicknesses of the deposited layers after heating for 10 hours did not correlate with the concentration of **6** in solution (from 0.5-1.2 × 10^{-2} M); however all samples heated for this time period gave films with average thicknesses in the range of 17(2) to 29(4) nm (Table 2.1) with a similar morphology of overlapping hemispheroids. After samples of **6** were heated to 100 °C for a shorter period of 3 hours, deposition of Ge still transpired to yield thicker layers (up to 70 nm).

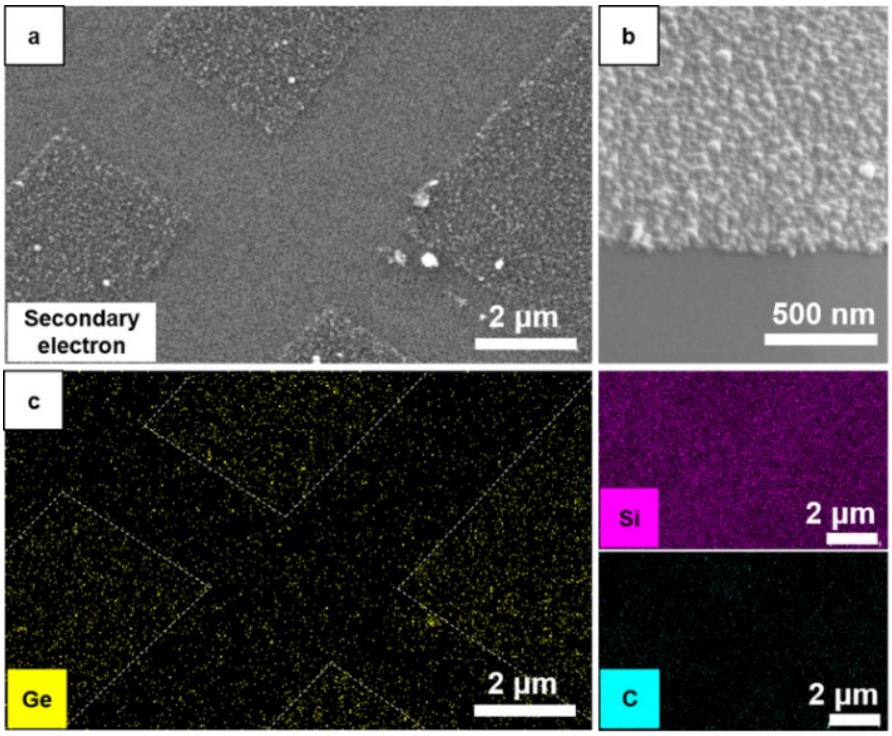

Figure 2.8. Ge layer deposited onto a Si wafer via decomposition of $ImMe_2$•GeH_2•BH_3 (**6**) in toluene (concentration = 6.3 × 10^{-3} M, 10 hours, 100 °C). (a) Secondary electron SEM of a Si wafer with Ge layer scratched off in a pattern using a stainless-steel needle. (b) Micrograph taken at a 54° with respect to the electron beam to determine layer thickness [17(2) Å] at the edge of the scratch. (c) EDX mapping of the imaged section in Figure 2.8a, showing a higher Ge signal in the unscratched areas, along with a strong background of Si; some background C was also detected. Micrographs and EDX measurements collected at 5 kV. Dotted lines on the Ge EDX map in Figure 2.8c provided as guides for the eye.

One possible explanation for the formation of thin films at longer deposition times (Table 2.1) is Ostwald ripening-type growth of remaining suspended Ge nanoparticles in toluene at the expense of surface-bound Ge.[29] Dynamic light scattering experiments reveal that the Ge particles in solution exhibit steady growth over time, from

a 187(28) nm solvodynamic radius after 30 minutes to 773(21) nm after 3 hours (Table 2.2), which provides support for the growth of Ge nanoparticles in solution over time. However, no direct evidence of migration from the surface germanium to suspended nanoparticles is observed, which would have supported the Ostwald ripening postulate mentioned above. The walls of the reaction vessel were coated with an orange/red precipitate after Ge film deposition onto Si, indicating that Ge deposition is not exclusive to the Si substrate. Although a number of equilibria are possible between solution, precipitate, and Ge film deposited on the substrate, it should be noted that the diameter of the hemispheroids deposited onto the Si wafer does not exceed ~150 nm (see Figure 2.9a), suggesting that larger particles of Ge are unstable on the Si surface, and may be rinsed off during substrate processing.

Table 2.1. Layer thickness measurements of amorphous Ge deposited from **6** onto Si wafers at 100 °C in toluene.

Deposition Time	[$ImMe_2$•GeH_2•BH_3] (M)	Layer Thickness (nm)
10 hrs	1.2×10^{-2}	20(4)
10 hrs	1.0×10^{-2}	22(4)
10 hrs	6.3×10^{-3}	17(2)
10 hrs	5.0×10^{-3}	29(4)
3 hrs	1.0×10^{-2}	73(12)
3 hrs	5.1×10^{-3}	40(7)

The Raman spectra of the deposited films consistently yield a characteristic broad peak for amorphous Ge, centered at 280 cm^{-1} (Figure 2.9b).[26] X-ray photoelectron spectroscopy (XPS) identified the major deposited species to be elemental Ge (61 %), with GeO and GeO_2 also present, likely due to unavoidable exposure of the sample to

oxygen before measurement. Surface oxidation is to be expected due to the intermittent exposure of the sample to air prior to XPS measurements, however, it should also be stated that XPS has a depth sensitivity of ~10 nm. Thus it is likely that the bulk sample contains a higher ratio of Ge than is detected on the surface by XPS. An extremely low amount of nitrogen (0.48 atom%) was detected by the survey XPS on the substrates after deposition, supporting the earlier supposition that very little carbene ($ImMe_2$) remains bound to the surface of the deposited germanium, even with the low deposition temperatures involved.

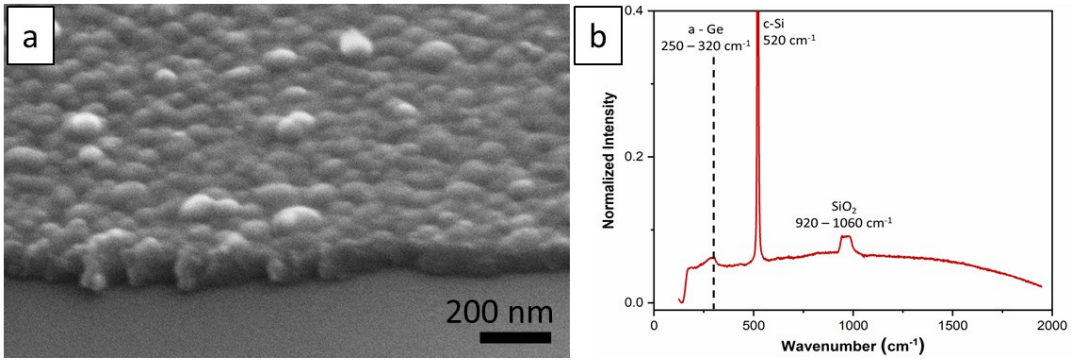

Figure 2.9. Characterization of Ge film deposited from 5.1 × 10^{-3} M solution of $ImMe_2$•GeH_2•BH_3 in toluene 100 °C over 3 hours onto a crystalline Si wafer. (a) Representative secondary electron micrograph held at 54° relative to the detector in order to determine layer thickness. (b) Representative Raman spectrum. Excitation wavelength: 532 nm. Spectrum shows a broad peak from 250–320 nm, indicating amorphous character.[26]

Table 2.2. Measured solvodynamic radii of Ge particulates in solution. Samples were heated at 100 °C for the time period indicated (6.1×10^{-3} M of **6** in toluene) in the presence of a Si wafer. All samples are direct aliquots of the toluene deposition solutions.

Time (min)	Average size (nm)	Average PDI
30	187(28)	0.5(1)
60	483(3)	0.12(1)
120	647(15)	0.32(2)
180	773(21)	0.34(2)

2.2.3 Computed structures for NHC•EH_2•BH_3 complexes (E = Ge and Sn)

To probe the electronic and steric effects associated with the decomposition of the Ge(II) dihydride complexes, computational collaborators Dr. Guoliang Dai and Prof. Alex Brown first optimized the structures of three adducts: NHC•GeH_2•BH_3, where NHC = $[(HCNR)_2C:]$ and R = Dipp (IPr), Me ($ImMe_2$), and H (Im), respectively (Chart 2.3, see Figure 2.17 for structures). The two most hindered complexes in the series IPr•GeH_2•BH_3[7] and $ImMe_2$•GeH_2•BH_3 (**6**) have been synthesized in the laboratory, while the parent system Im•GeH_2•BH_3 represents an experimentally unknown model complex. For comparison, the corresponding (unknown) Sn(II) dihydride complexes NHC•SnH_2•BH_3 were also studied computationally (Chart 2.3). Unless specified, all energies and geometrical parameters refer to those determined computationally with a THF polarizable continuum model (PCM); geometries for all structures are can be seen in Section 2.5 of this thesis. For all structures determined computationally in this work, the geometry optimizations were performed using density functional theory (DFT), using default convergence criteria, with the M06-2X functional.[30] In most computations, the cc-

pVDZ basis set[31] was used for all atoms except Sn, where, the cc-pVDZ-PP basis set and a corresponding effective core potential was used.[31] For Sn containing compounds, this combination of basis sets will be referred to as cc-pVDZ-(PP). For the largest IPr•GeH_2•BH_3 complex, the 6-311+G(d) basis set[31] was used.

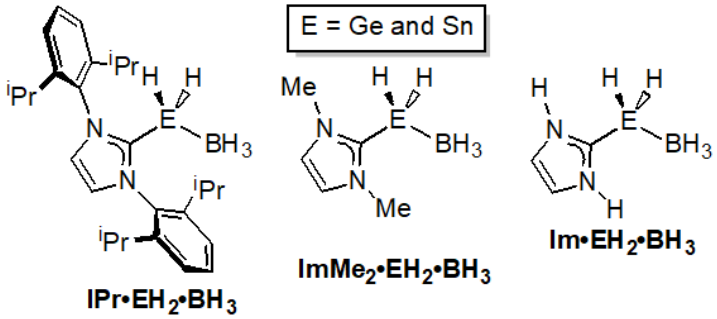

Chart 2.3. NHC•EH_2•BH_3 (E = Ge and Sn) donor-acceptor adducts examined computationally in this study.

These computations show that NHC substitution has only a modest impact on the proximal C_{NHC}-Ge bond length, with a *ca.* 0.04 Å bond elongation noted when the less hindered complex Im•GeH_2•BH_3 is compared to the Dipp-containing complex IPr•GeH_2•BH_3 [2.039 vs. 2.074 Å]. Notably, the C_{NHC}-Ge-B bond angle widens as the steric bulk of the NHC is increased: from 100.0° (NHC = Im) to 116.3° ($ImMe_2$) to 125.5° (IPr). Within the NHC•SnH_2•BH_3 series,[19] the computed C_{NHC}-Sn bond length in IPr•SnH_2•BH_3 (2.369 Å) is significantly longer than in Im•SnH_2•BH_3 (2.312 Å). The C_{NHC}-Sn-B bond angles also increase from 91.5° to 109.6° to 123.9° when the NHC is altered from Im to $ImMe_2$ to IPr, respectively. Lastly, the nature of N-bound substituents has minimal impact on the coordinative E-B bond lengths, with all values within 0.01 Å

of each other amongst the GeH_2 and SnH_2 adduct series. Natural Bond Orbital (NBO) analysis showed that the C_{NHC}-E linkages in the NHC•EH_2•BH_3 adducts are substantially polarized towards the ligating NHC carbon (C_{NHC}). For example, the C_{NHC}-Ge bond in IPr•GeH_2•BH_3 has single bond character with 76.3 % of electron density towards carbon, while the Ge-B bond in IPr•GeH_2•BH_3 shows a slight polarization of electron density towards the Ge atom (53.5 %).

2.2.4 Computational evaluation of possible decomposition mechanisms for NHC•GeH_2•BH_3 adducts

Given the abovementioned ability of $ImMe_2$•GeH_2•BH_2 to yield elemental germanium upon mild thermolysis in either THF or toluene, the mechanism by which this process happens is of significant interest. Herein, two possible decomposition routes were examined for the NHC•EH_2•BH_3 adducts (E = Ge or Sn): a) step-wise dissociation of E-B and C_{NHC}-E bonds (or in the reverse order) to liberate EH_2 to eventually afford bulk Ge (or Sn), NHC•BH_3 and H_2 gas (Paths **A** and **B** in Scheme 2.4); b) 1,2-hydride transfer (migration) routes that either involve carbene-ring expansion[14]/reductive elimination of Ge or Sn (Path **C** in Scheme 2.4), or the direct formation of a dihydroaminal $(NHC)H_2$ by sequential Ge (or Sn) to C hydride transfers (Path **D**). My collaborators also computed the Gibbs free energies associated with various intermediates and transition states along Paths **A-D**, both in the gas phase and with a THF polarizable continuum model (PCM). For the final E(g) to E(s) steps, the experimentally known $\Delta_{formation}G$ for the gaseous elements were used,[32] which are 335.9 kJ/mol and 267.3 kJ/mol for Ge(g) and Sn(g), respectively. The results determined at

298.15 K for Paths **A**/**B** and **C**/**D** for $ImMe_2$•GeH_2•BH_3 (**6**) are summarized in Figure 2.10 and Figure 2.12, respectively; corresponding results at 373.15 K (100 °C) in THF can be found in Section 2.5 (Figure 2.31 and Figure 2.32), and demonstrate that all reported free energy differences are reduced to a modest degree. The corresponding energy profiles for the decomposition of the structurally related Im•GeH_2•BH_3 and IPr•GeH_2•BH_3 adducts can be found as Figure 2.18 to Figure 2.21 (Section 2.5).

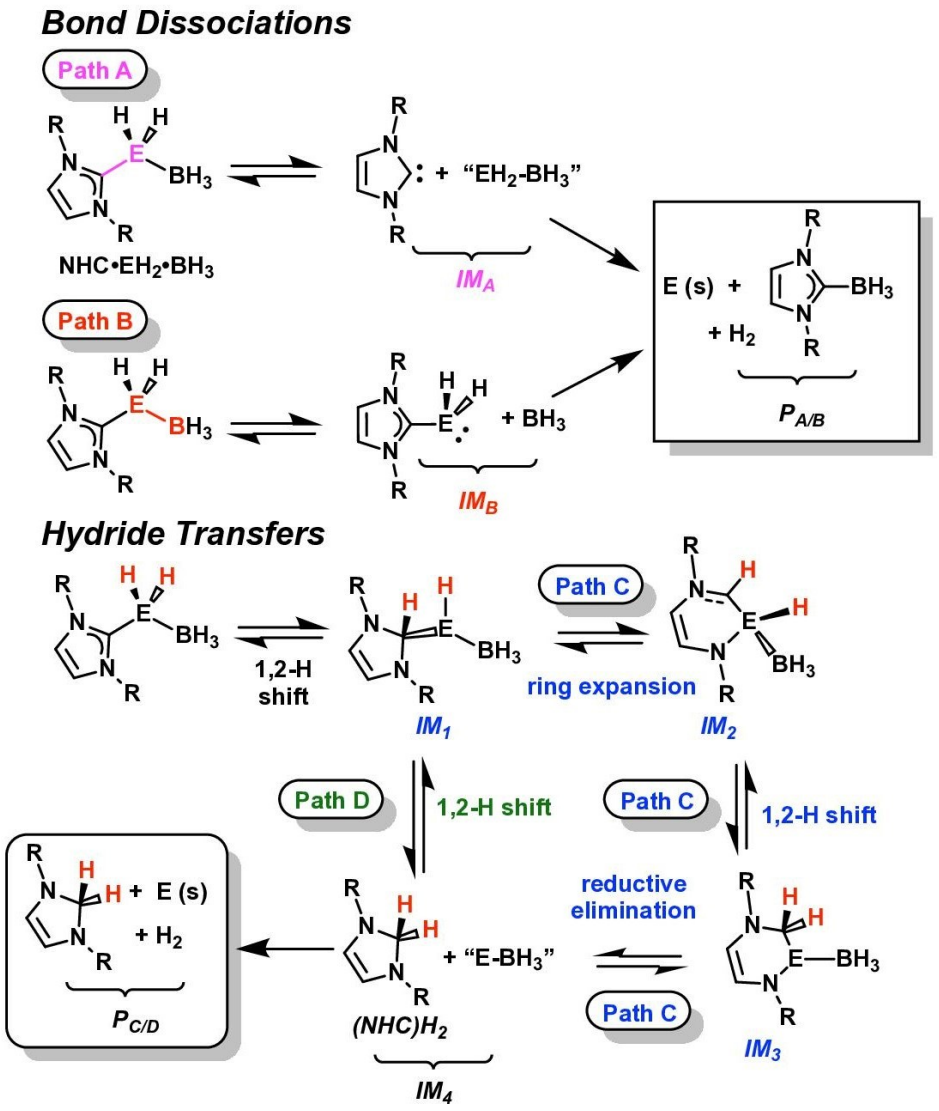

Scheme 2.4. Computationally investigated pathways for NHC•EH_2•BH_3 decomposition. Paths **A** and **B** represent heterolytic C_{NHC}-E and E-B bond cleavage, while Paths **C** and **D** follow an initial common 1,2-hydride shift to generate a putative (NHCH)E(H)•BH_3 intermediate (**IM_1**).

*2.2.5 Paths **A** and **B**: direct adduct cleavage*

The most direct route by which NHC•GeH_2•BH_3 adducts might decompose is via the initial heterolytic cleavage of a polar covalent (dative) C_{NHC}-Ge or Ge-B bond, with the eventual formation of NHC•BH_3, elemental Ge, and H_2. Path **A** (Scheme 2.4) involves initial C_{NHC}-Ge bond breakage, followed by the Ge-B bond dissociation; Path **B** (Scheme 2.4) begins with Ge-B bond dissociation, followed by C_{NHC}-Ge bond breakage. Both of these pathways then proceed by the coordination of BH_3 to NHC (yielding NHC•BH_3), and the concomitant decomposition of GeH_2 into Ge and H_2. As before, each mechanism was examined in the gas phase and in THF using a PCM. Path **A** involves the endoergic cleavage of a C_{NHC}-Ge bond in $ImMe_2$•GeH_2•BH_3 (Figure 2.10) at a Gibbs free energy penalty of 168.2 kJ/mol in THF, which is slightly less favourable in comparison to the free energy cost of 149.6 kJ/mol in the gas phase. Next, Ge-B cleavage in the putative intermediate H_2Ge-BH_3 is predicted to occur at a lower free energy change of 98.4 kJ/mol. Overall, the first step associated with Path **B** is slightly more energetically favourable, given the lower free energy associated with initial heterolytic Ge-B bond cleavage (ΔG = 122.7 kJ/mol) in THF, compared to initial C_{NHC}-Ge bond scission in Path **A** (*i.e.*, 168.2 kJ/mol). Once the BH_3 group is liberated, scission of the remaining coordinative C_{NHC}-Ge bond in the adduct $ImMe_2$•GeH_2 transpires with a free energy change of 143.9 kJ/mol (in THF); thus C_{NHC}-Ge bond cleavage becomes slightly more endoergic in $ImMe_2$•GeH_2•BH_3 versus in $ImMe_2$•GeH_2, which partially explains the inability to isolate NHC•GeH_2 complexes thus far in the Rivard Laboratory. As outlined in Figure 2.18 to Figure 2.21 in Section 2.5, similar energy trends for the

decomposition of IPr•GeH_2•BH_3 and Im•GeH_2•BH_3 are found, with a preference for Path **B** noted.

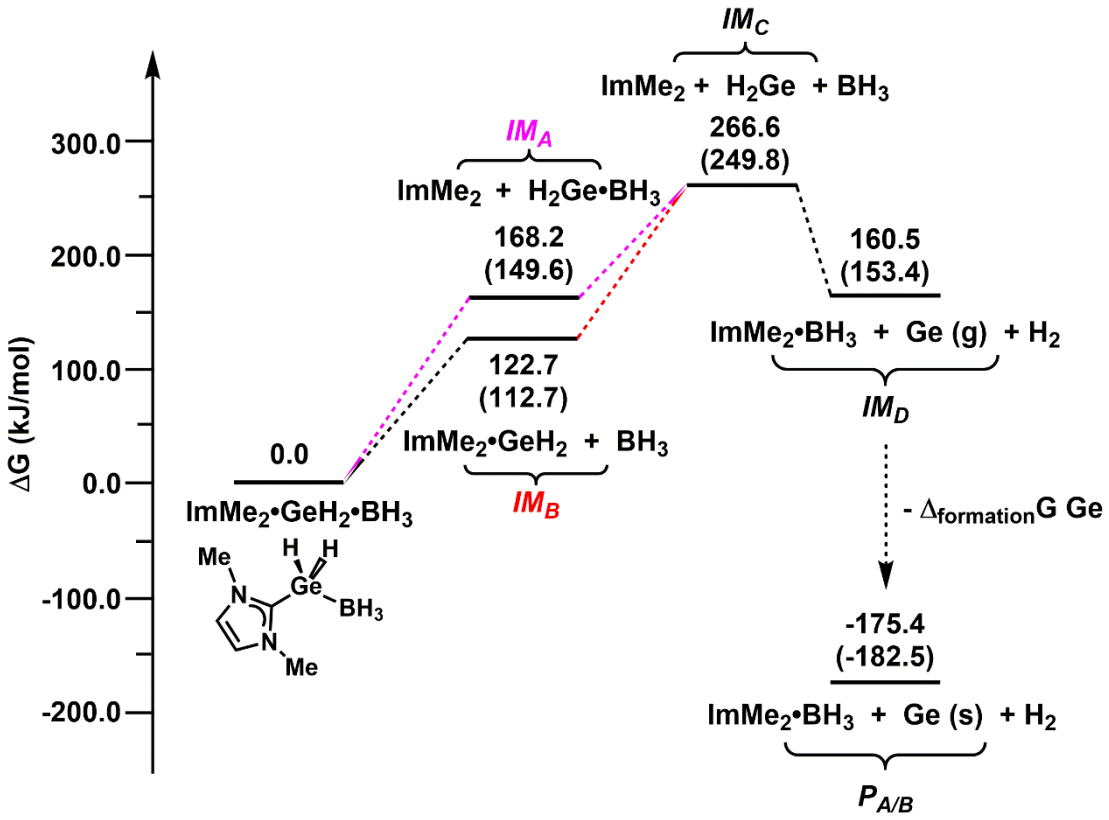

Figure 2.10. Computed Gibbs free energies in kJ/mol associated with the intermediates formed in the decomposition of ImMe$_2$•GeH_2•BH_3 via Path **A** (*e.g.,* $\mathbf{IM_A}$ and $\mathbf{P_{A/B}}$) and Path **B** (*e.g.*, $\mathbf{IM_B}$ and $\mathbf{P_{A/B}}$), with a THF PCM; values in parentheses refer to gas phase computations. Lowest energy states are plotted; in this case, $\mathbf{IM_C}$ contains H_2Ge in the singlet state, and $\mathbf{IM_D}$ is plotted containing Ge(g) (triplet) (see Table 2.3). Gibbs free energy of formation ($\Delta_{formation}G$) for Ge(g) taken as 335.9 kJ/mol.[32]

*2.2.6 Alternate decomposition routes for NHC•GeH_2•BH_3 adducts: ring-expansion (Path **C**) and direct H-transfer (Path **D**) mechanisms*

Path **C** is outlined in Scheme 2.4 and starts with a 1,2-hydride shift from germanium to the carbene carbon (C_{NHC}) to give (NHCH)GeH•BH_3 (**IM_1**), followed by a carbene ring-expansion to give eventually intermediate **IM_3**. Path **C** ends with the formal reductive elimination of the dihydroaminal (NHC)H_2 from the ring-expanded intermediate **IM_3**, releasing "Ge•BH_3" to later form elemental Ge and BH_3 as co-products (**$P_{C/D}$**, Scheme 2.4). For $ImMe_2$•GeH_2•BH_3 (Figure 2.12), the first step in Path **C**, hydride migration from Ge to C_{NHC}, involves a relatively high Gibbs free energy of activation of 218.8 kJ/mol; so at this stage Path **C** is already more unfavourable energetically for the decomposition of $ImMe_2$•GeH_2•BH_3 in relation to Paths **A** and **B**, by *ca.* 70-100 kJ/mol. The next step in path **C** involves carbene ring-expansion,[14] where a Ge atom inserts into a C-N bond to yield a GeN_2C_2 six-membered ring intermediate **IM_2** (Scheme 2.4 and Figure 2.12). This ring-expansion process is accompanied by a modest free energy of activation (via **TS_{1-2}**) of $\Delta G^{\ddagger}$ = 39.4 kJ/mol, which is energetically more favourable by about 180 kJ/mol in comparison to the initial 1,2-hydride shift. From **IM_2**, another 1,2-hydrogen shift (via **TS_{2-3}**) was modelled to transpire to yield the cyclic intermediate **IM_3** ($\Delta G^{\ddagger}$ = 106.8 kJ/mol). The last computed step in this mechanism involves the direct reductive elimination of the dihydroaminal ($ImMe_2$)H_2 from **IM_3**, producing the putative species "Ge•BH_3"; this step is the least favourable of Path **C** with a large free energy of activation of 230.3 kJ/mol (via **TS_{3-4}**).

A direct H-transfer mechanism (Path **D**) was also probed in which two direct Ge to C_{NHC} hydride transfer processes occur to release the dihydroaminal $(ImMe_2)H_2$, without carbene ligand ring-expansion. The first step in Path **D** is exactly the same as in Path **C**: a 1,2-H shift from Ge to C_{NHC} to form $(ImMe_2H)GeH{\bullet}BH_3$ (**IM**$_1$, Figure 2.12); to recap, this step has a large free energy of activation (in THF) of 218.8 kJ/mol. As summarized in Figure 2.12, Path **D** then involves a second direct 1,2-hydrogen migration between Ge and C_{NHC} in **IM**$_1$ to form $(ImMe_2)H_2$ and "$Ge{\bullet}BH_3$" (**IM**$_4$); this second 1,2-H shift has a computed free energy of activation of 78.4 kJ/mol (via **TS**$_{1\text{-}4}$). Once at the intermediates **IM**$_4$, Path **D** follows a similar route as Path **C** to eventually give the final decomposition products: $(ImMe_2)H_2$, Ge(s) and BH_3 (**P**$_{C/D}$ in Figure 2.12).

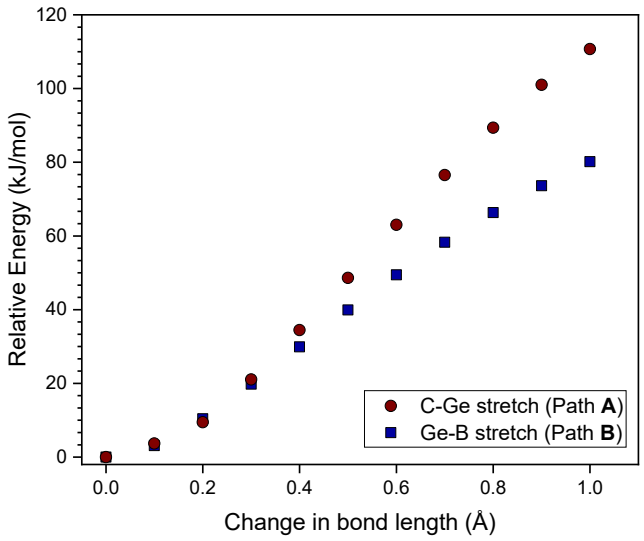

Figure 2.11. Energies (electronic energies only, no thermal contributions) for bond elongation relative to initial energy for $ImMe_2{\bullet}GeH_2{\bullet}BH_3$ for Paths **A** and **B**. No transition state is observed during this dissociation.

When rate-determining steps (RDSs) for Paths **A** to **D** (note: initial bond dissociations in Paths **A** and **B** are barrierless as determined by the author, see Figure 2.11), the decomposition of $ImMe_2$•GeH_2•BH_3 is predicted to go via path **B** (free energy of activation for RDS = 143.9 kJ/mol, Figure 2.10), with an associated barrier in the RDS for Path **A** of 168.2 kJ/mol (Figure 2.10). The initial cleavage of the Ge-B bond in Path **B** is the most energetically feasible initial step of the Paths explored (**A**-**D**), with a free energy penalty of 122.7 kJ/mol in THF; the RDSs for Paths **C** (230.3 kJ/mol) and **D** (218.8 kJ/mol) are energetically the highest of the series. In line with computations, the thermal decomposition of $ImMe_2$•GeH_2•BH_3 does not yield any dihydroaminal $(ImMe_2)H_2$, thus decomposition of the Ge(II) dihydride adducts via either Path **A** or **B** appears to be the most plausible.

The overall free energies associated with the formation of the $ImMe_2$•GeH_2•BH_3 decomposition products were estimated from Paths **A**/**B**: $ImMe_2$•BH_3, Ge(s), and H_2 ($\mathbf{P_{A/B}}$ in Scheme 2.4 and Figure 2.10). After taking the Gibbs free energy of formation for Ge(g) into consideration[32] an overall ΔG_{decomp} of -175.4 kJ/mol was estimated (-182.5 kJ/mol in the gas phase). For comparison, the free energy associated with $ImMe_2$•GeH_2•BH_3 decomposition via Paths **C**/**D** to give $(ImMe_2)H_2$, Ge(s) and BH_3 was found to be unfavourable in THF, with an estimated $\Delta_{decomp}G$ of +26.7 kJ/mol (-4.1 kJ/mol in the gas phase, Figure 2.12). Thus far, the computational and experimental data suggest that NHC•GeH_2•BH_3 adducts likely decompose either via Path **A** or **B** (Scheme 2.4).

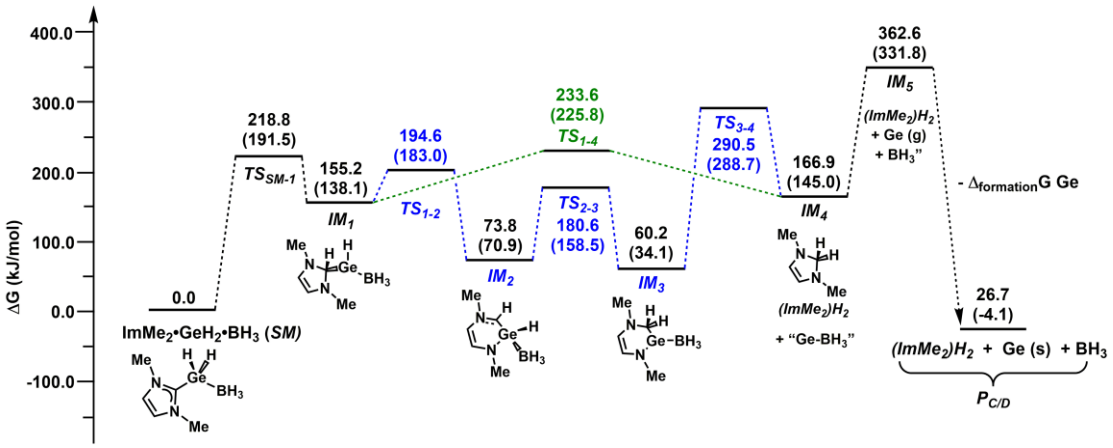

Figure 2.12. Computed Gibbs free energies in kJ/mol associated with the intermediates formed in the decomposition of $ImMe_2$•GeH_2•BH_3 via Path **C** (stepwise via $\mathbf{IM_1}$ through $\mathbf{IM_4}$) and Path **D** (via $\mathbf{TS_{1\text{-}4}}$) with THF PCM; values in parentheses refer to gas phase computations). Lowest energy states are plotted; in this case, $\mathbf{IM_5}$ is plotted containing Ge(g) (triplet) (see Table 2.3). Gibbs free energy of formation ($\Delta_{formation}G$) for Ge(g) taken as 335.9 kJ/mol.[32]

2.2.7 Computed mechanisms for NHC•SnH_2•BH_3 decomposition

My collaborators also computed the Gibbs free energies associated with the decomposition of the model Sn(II) dihydride complexes NHC•SnH_2•BH_3 (NHC = IPr, $ImMe_2$ and Im; Chart 2.2). It should be stated that previous attempts to prepare IPr•SnH_2•BH_3 afforded exclusively Sn metal, H_2 and IPr•BH_3,[7] while isolation of stable Sn(II) dihydride complexes required the presence of strongly Lewis acidic metal carbonyls, *e.g.*, IPr•SnH_2•$M(CO)_5$ (M = Cr and W).[10a,33] Overall similar trends are found with respect to the energetics of decomposition in the NHC•SnH_2•BH_3 models (see

Figure **2.24** to Figure 2.27 in Section 2.5) as in the abovementioned GeH_2 donor-acceptor complexes. When examining $ImMe_2$•SnH_2•BH_3, the biggest difference is the

more facile/favourable cleavage of the Sn-B linkage in Path **B** (90.3 kJ/mol in THF; 80.1 kJ/mol in the gas phase) in comparison to Ge-B bond breakage in $ImMe_2•GeH_2•BH_3$ (122.7 kJ/mol in THF). For $ImMe_2•SnH_2•BH_3$, the common Sn to C_{NHC} 1,2-hydride shift in Paths **C** and **D** (to give $(ImMe_2H)SnH•BH_3$) is substantially uphill energetically, with a free energy of activation of 192.8 kJ/mol in THF (see Figure 2.28 Figure 2.29). In addition, the overall decomposition reaction associated with Paths **A** and **B**: $ImMe_2•SnH_2•BH_3 \rightarrow ImMe_2•BH_3 + Sn(s) + H_2$ was estimated to have a $\Delta_{decomp}G$ value of -241.1 kJ/mol in THF (vs. -242.9 kJ/mol in the gas phase); as for the germanium analogues, similar overall trends were found in the computed Sn(II) dihydride complexes $Im•SnH_2•BH_3$ and $IPr•SnH_2•BH_3$.

*2.2.8 Kinetic analysis of the decomposition of $ImMe_2•GeH_2•BH_3$ (**6**) and link to computations*

Based on the computational work presented here, Paths **A** or **B** are viable routes by which germanium metal is extruded from $NHC•GeH_2•BH_3$ adducts. As THF was used as the solvent model, the decomposition of the Ge(II) hydride adduct $ImMe_2•GeH_2•BH_3$ (**6**) in refluxing THF-D_8 (18 hours) was explored to see if the dominant product was an $NHC•BH_3$ complex (arising from Paths **A** or **B**, Scheme 2.4) or a dihydroaminal $[(HCNMe)_2CH_2]$ (from Paths **C** or **D**, Scheme 2.4). After thermolysis of **6** in THF-D_8, $ImMe_2•BH_3$ was detected as a product by ^{1}H NMR spectroscopy (20 %, determined relative to 4,4′-difluorobiphenyl as an internal standard), however, other unidentified products were also present. Interestingly, $THF•BH_3$ was also detected by ^{11}B

NMR analysis of the end products, indicating that the coordinating solvent (THF) plays an added role in the thermal degradation of **6**, by trapping some BH_3 that is liberated.

To recap, when $ImMe_2$•GeH_2•BH_3 (**6**) was heated at 100 °C in either toluene-D_8 or C_6D_6, $ImMe_2$•BH_3 was found to be the only soluble decomposition product. Thus at this point, either Paths **A** or **B** were likely responsible for the decomposition of **6** in weakly coordinating solvents, due to the absence of the dihydroaminal degradation product [$(HCNMe)_2CH_2$]. To further investigate the mechanism by which $ImMe_2$•GeH_2•BH_3 (**6**) decomposes, a solution of **6**[34] in toluene-D_8 was heated in a sealed J-Young NMR tube to 100 °C, and the progress of the decomposition was monitored *in situ* using ^{1}H NMR spectroscopy (in the presence of 4,4′-difluorobiphenyl as an internal standard). As expected for unimolecular decomposition, a linear relationship of ln[**6**] with time was found (Figure 2.13), leading to a first-order rate constant of (k_H) $1.9(2) \times 10^{-4}$ s^{-1}. It should be stated that the observed first order decay in **6** could fit any of the computationally investigated Paths (**A**-**D**) in Scheme 2.4, as all paths are unimolecular-based decompositions. However, one might see different kinetic isotope effects (KIEs) amongst the proposed decomposition pathways, as Path **C** and **D** each start with a common Ge-H bond-breaking event as a rate determining step (*i.e.,* 1,2-hydrogen shift). As a result, the deuterium isotopologue $ImMe_2$•GeD_2•BD_3 (**6D**) was prepared from $ImMe_2$•$GeCl_2$ and Li[BD_4], and its decomposition in toluene-D_8 was examined.

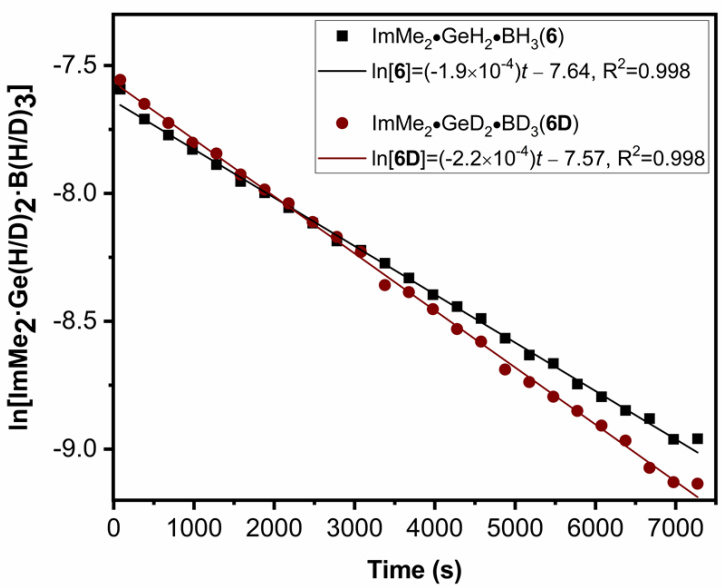

Figure 2.13. Decomposition rates of $ImMe_2$•GeH_2•BH_3 (**6**, black squares) and $ImMe_2$•GeD_2•BD_3 (**6D**, red circles). Each thermolysis run was conducted at 100 °C in toluene-D_8 with spectral integration relative to an internal standard of 4,4′-difluorobiphenyl. Average data points from three trials are plotted.

The thermolysis of **6D** in toluene-D_8 (100 °C) was carried out in triplicate, leading to a rate of decomposition of 2.2(2) × 10^{-4} s^{-1} (Figure 2.13), and a kinetic isotope effect (KIE = k_H/k_D) of 0.86(11). Rate determining hydride-transfer in Paths **C** or **D** would be expected to follow a normal primary KIE ($k_H/k_D >> 1$); thus, the observed kinetic data supports decomposition of **6** (and **6D**) via either Path **A** or **B**.[35] Moreover, Paths **A** and **B** might both yield a small inverse KIE ($k_H/k_D < 1$), as the H/D atoms are located in secondary positions in relation to the rate-determining bond cleavage (C-Ge or Ge-B) involved in decomposition.

Curious to further differentiate between Paths **A** and **B**, I decided to investigate computationally the KIE associated with each Path. Specifically, the aim was to determine whether an inverse KIE would be expected for these pathways due to secondary bond breakage effects. Before outlining my computational work, I would like to highlight equation 2.1, which links the dependence of KIE with changes in the kinetic energy during secondary bond breakage events:[36]

$$k_H/k_D = \exp\{-1/2 \times \Sigma[u^{\ddagger}_H - u^{\ddagger}_D - (u^{0}_H - u^{0}_D)]\} \qquad (2.1)$$

Given that u represents $h\nu/kT$ of the transition state (‡) and initial condition (^{0}), respectively, and the relationship between the vibrational frequencies of E-H/E-D bonds can be approximated as $\nu_{E\text{-}D} = \nu_{E\text{-}H}/1.35$, this expression can be simplified to equation 2.2, wherein the direct association of KIE to the sum of the E-H vibrational frequency changes becomes evident. When the overall change in E-H bond frequencies ($\Sigma\Delta\nu$, in cm^{-1}) becomes greater than zero ($\Sigma\Delta\nu > 0$) during complex dissociation, an *inverse* kinetic isotope can be expected (*i.e.* $k_H/k_D < 1$):[39]

$$k_H/k_D = \exp\{(-0.1865/T) \times \Sigma\Delta\nu\} \qquad (2.2)$$

Going back to the assumption that either Path **A** or **B** (Ge-C or Ge-B bond cleavage) is the most likely mechanism for the decomposition of $ImMe_2{\bullet}GeH_2{\bullet}BH_3$ (**6**) (*vide supra*), a computational study (B3LYP/cc-pVDZ) was carried out to investigate the change in Raman frequencies of the Ge-H and B-H bonds during adduct dissociation/bond cleavage.[37] As the simplified expression in equation 2.2 relies only on the change in vibrational frequency, and already accounts for the change in mass between H and D, calculations were carried out only on the hydrogen isotopologue $ImMe_2{\bullet}GeH_2{\bullet}BH_3$ (**6**). Although the default temperature for computed vibrational

frequencies is 298 K and experimental decomposition occurred at 373 K, Raman frequencies do not shift drastically with temperature,[38] therefore comparison can be made between computed and experimental KIE values.

For the calculations related to Path **A**, sequential C-Ge bond extensions in 0.1 Å increments were applied, starting from an optimized C-Ge bond length of 2.062 Å to a final distance of 3.062 Å (B3LYP/cc-pVDZ). After each bond elongation event, the new bond length was then frozen, and all other angles and bond lengths in the molecule were optimized. Figure 2.14 shows the changes in the Raman resonance frequency of the BH_3 and GeH_2 symmetric and asymmetric stretches during the $ImMe_2$ dissociation from $ImMe_2$•GeH_2•BH_3 (**6**). According to equation 2.2, the Raman frequencies should be modeled at the transition state of the bond-breaking step. However, the energies associated with this dissociation confirmed the earlier assumption that the bond is broken without an energy barrier in the form of a transition state, therefore the highest energy species (longest bond length) was examined for comparative purposes. The longest tested bond length has a C-Ge bond length of 3.062 Å. The sum changes in E-H frequencies at this C-Ge distance have values of -35 cm^{-1} and +99 cm^{-1} for the B-H and Ge-H stretches, respectively. Of particular note is the strong negative contribution of the BH_3 symmetric stretching frequency, which comprises the entirety of the negative frequency contributions.[37] Applying Equation 2.2 to this system ($k_H = 1.9 \times 10^{-4}$ s^{-1}, $\Sigma\Delta\nu = +64$ cm^{-1}, T = 373 K), a k_D of 2.0×10^{-4} s^{-1} is expected (KIE = 0.93).

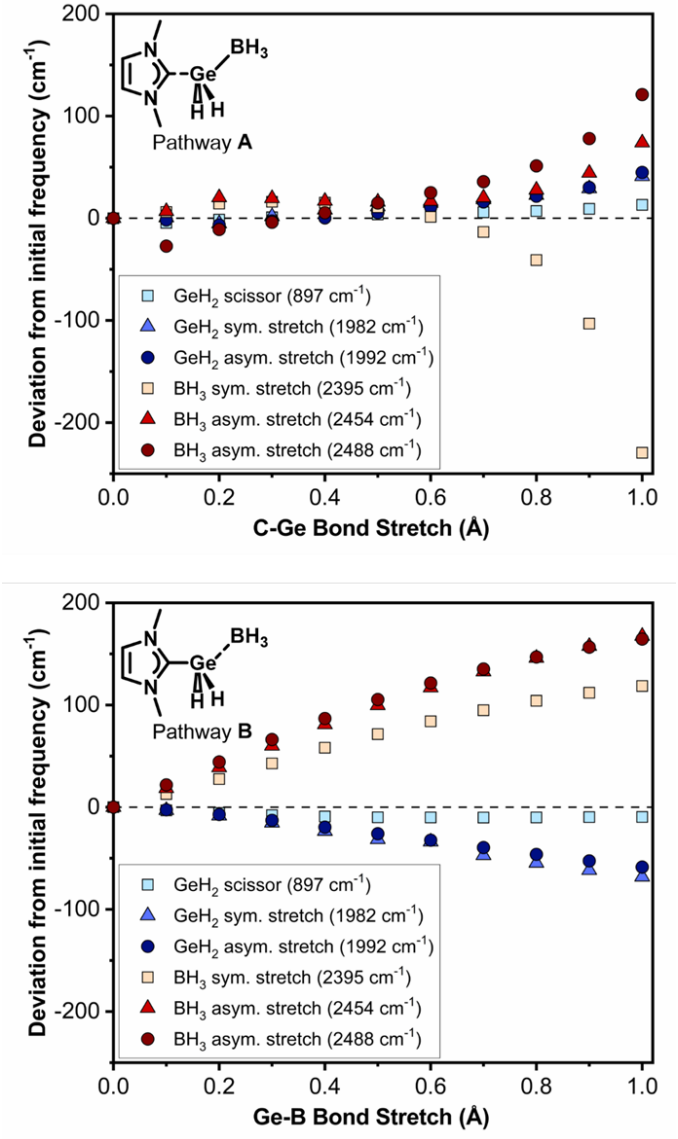

Figure 2.14. Deviations from initial calculated Raman frequencies (B3LYP/cc-pVDZ) of the BH_3 and GeH_2 resonance frequencies with increasing C-Ge (Pathway **A**, starting bond length 2.010 Å) and Ge-B (Pathway **B**, starting bond length 2.060 Å) bond length.

Path **B** was modelled in a similar fashion with sequential Ge-B bond extensions in 0.1 Å increments from a starting bond length of 2.010 Å to a final distance of 3.010 Å. As the BH_3 unit in this model begins to rehybridize from its starting four-coordinate sp^3-

environment in **6** to an approximately planar sp^2-arrangement as the B-Ge bond lengthens, the resulting increase in s-orbital character in the B-H bonds should lead to higher B-H stretching frequencies. Accordingly, the total change in B-H stretching frequencies from the initial to final geometry was computed to be +451 cm^{-1}. In contrast, the overall change in Ge-H asymmetric and symmetric stretches decreased by 136 cm^{-1}, thus the change in B-H stretching frequency is the dominant term (by a factor of three; see Figure 2.14). The summary large positive change in vibrational frequencies for Path **B** leads to an expected k_D of 2.7×10^{-4} s^{-1} (by equation 2.2, $\Sigma\Delta\nu$= +314 cm^{-1}, KIE = 0.82). It should be taken into consideration that the experimental values do have inherent error, and that the rates predicted by computational analysis fall within 3σ of the experimental values for both Paths **A** and **B**. Thus my computational analysis of the KIE is in line with the experimental data and supports decomposition of **6** via an initial bond dissociation process, with a slight preference for Path **B** (starting with Ge-B bond breaking) on the basis of the computed free energies involved.

2.3 Conclusions

This work introduces new NHC•GeH_2•BH_3 donor-acceptor complexes featuring unprecedentedly high Ge content (approaching 40 wt%). It was also shown that $ImMe_2$•GeH_2•BH_3 can deposit nanodimensional films of Ge onto silicon wafers and onto unusual substrates, like glass wool, via a convenient and mild (100 °C) procedure from solution. This procedure requires only standard Schlenk techniques and glassware, and any by-products formed during Ge film deposition can be easily removed by washing

with organic solvent. This is in contrast to pre-existing routes to Ge films that require very high temperatures and/or sophisticated CVD set-ups. Also, four different decomposition pathways were examined for various NHC•EH_2•BH_3 (E = Ge and Sn) complexes, and analysis of the computed Gibbs free energies and kinetic studies point toward initial E-B bond cleavage as the most likely decomposition route, to eventually yield NHC•BH_3, Ge or Sn, and H_2. Future work will involve the application of this mild Ge deposition strategy to nanochemistry (*i.e.*, core-shell nanoparticle synthesis) and modification of the donor-acceptor approach to enable more atom efficient element deposition cycles.

2.4 Experimental procedures

2.4.1 General

All reactions were performed using standard Schlenk techniques under an atmosphere of nitrogen or in a nitrogen-filled glove box (Innovative Technology, Inc.). Solvents were dried using a Grubbs-type solvent purification system manufactured by Innovative Technology, Inc., and stored under an atmosphere of nitrogen prior to use; the only exception was fluorobenzene, which was heated to boiling overnight over calcium hydride, then distilled under nitrogen, degassed via three freeze-pump-thaw cycles, and passed through a column of activated alumina prior to use. $GeCl_4$ was purchased from Strem Chemicals and used as received. Germanium(II) dichloride-dioxane, 2-chloro-1,3-dimethylimidazolinium chloride, methyl iodide, 1-methylimidazole, potassium hydride, Li[BH_4], and Li[BD_4] were purchased from Sigma-Aldrich and used as

received. 4,4′-Difluorobiphenyl was obtained from K&K Laboratories and recrystallized from toluene before use. $Im^iPr_2Me_2$,[16] IPr•GeH_2•BH_3,[7] and $ImMe_2$•BH_3[28] were prepared according to literature procedures.

^1H, ^2H, ^{11}B, $^1H\{^{11}B\}$, and $^{13}C\{^1H\}$ NMR spectra were recorded on a Varian Inova-400 or 500 MHz spectrometer and referenced externally to $SiMe_4$ (^1H, $^{13}C\{^1H\}$), MeOD (^2H), and F_3B•OEt_2 (^{11}B). Elemental analyses were performed by the Analytical and Instrumentation Laboratory at the University of Alberta. Melting points were obtained in sealed glass capillaries under nitrogen using a MelTemp melting point apparatus and are uncorrected. Raman spectroscopy was performed at the Technical University of Munich using a LabRAM HR UV-vis (HORIBA JOBIN YVON) Raman microscope (OLYMPUS BX41) with a SYMPHONY CCD detector and a He–Ne laser (λ = 532 nm). Thermogravimetric analysis (TGA) and differential scanning calorimetry (DSC) were performed by the University of Alberta Analytical and Instrumentation Laboratory, with samples run under a nitrogen atmosphere on a PerkinElmer Pyris 1 TGA/DSC instrument. Scanning electron microscopy (SEM) images were obtained using a Zeiss Sigma 300 VP-FESEM instrument equipped with a secondary electron detector and a Bruker energy-dispersive X-ray (EDX) spectroscopy system operating at 5 kV. X-ray photoelectron spectroscopy data was collected on a Kratos AXIS Ultra using an Al(Mono) source (1486.69 eV). For the high-resolution Ge(3d) spectra, 30 scans were collected with a 20 eV pass energy. CasaXPS (Vamas) software was used to process high-resolution spectra. Spectra were calibrated to the C 1s emission (284.8 eV) arising from adventitious carbon. After calibration, the extrinsic loss structure in the background from

each spectrum was subtracted using a Shirley-type background. The high-resolution Ge(3d) region partner lines had fixed spin-orbit splitting of 0.58 eV. Dynamic light scattering (DLS) was conducted on a Malvern Nanoseries Zetasizer, and the number average was taken as the average particle size reported. Three scans were run on each sample, and standard deviations of size and polydispersity index (PDI) are reported. The powder XRD data were collected at room temperature on a STOE Stadi P diffractometer (Ge(111) monochromator, Cu Kα1 radiation, λ = 1.54056 Å) with a Dectris MYTHEN 1K detector in a Debye–Scherrer geometry; for each measurement, a sample was sealed in a glass capillary (Ø 0.5 mm) under N_2.

2.4.2 Synthetic procedures

Preparation of Im^{i}Pr$_2$Me$_2$•GeCl$_4$ (1): A solution of $GeCl_4$ (0.429 g, 2.00 mmol) in 1 mL of fluorobenzene was added dropwise to a solution of Im^{i}Pr$_2$Me$_2$ (0.361 g, 2.00 mmol)[21] in 10 mL of fluorobenzene. The mixture was stirred for 18 hours to give an orange solution. This solution was concentrated to a volume of *ca.* 1 mL and 2 mL of hexanes was then added. Stirring of the resulting mixture afforded **1** as a light brown precipitate, which was separated from the supernatant and dried (0.740 g, 94 %). Crystals of **1** of suitable quality for X-ray crystallography were grown by cooling a fluorobenzene solution layered with hexanes to -35 °C for one week. ^{1}H NMR (C_6D_6): δ 1.16 (d, 12H, $^3J_{HH}$ = 7.0 Hz, CH(CH_3)$_2$), 1.34 (s, 6H, C=C(CH_3)), 5.96 (sept, 2H, $^3J_{HH}$ = 7.0 Hz, CH(CH$_3$)$_2$). ^{13}C{^{1}H} NMR (C_6D_6): δ 9.8 (C=C(*C*H$_3$)), 20.8 (CH(*C*H$_3$)$_2$), 53.0 (*C*H(CH$_3$)$_2$),

125.5 (C=*C*(CH_3)), 155.7 (N*C*N). Mp: 68 °C (decomp.). Anal. Calc. for $C_{11}H_{20}N_2GeCl_4$: C, 33.47; H, 5.11; N, 7.10. Found: C, 33.69 H, 5.22; N, 6.92 %.

Preparation of crude Im^{i}Pr$_2$Me$_2$•GeH$_2$•BH$_3$ (2): In a glovebox, 8 mL of cold (-35 °C) Et_2O was added to a vial containing **1** (0.080 g, 0.20 mmol) and Li[BH_4] (0.019 g, 0.87 mmol). Evolution of gas was noted immediately, and the reaction mixture was warmed to room temperature and stirred for 3 hours. The volatiles were then removed under vacuum and the product was extracted with three 3 mL aliquots of fluorobenzene; the combined extracts were filtered and the volatiles removed from the filtrate under vacuum to give Im^{i}Pr$_2$Me$_2$•GeH$_2$•BH$_3$ (**2**) as a pale yellow solid (0.041 g, 76 % crude yield). Crystals of suitable quality for X-ray crystallography were grown by cooling a fluorobenzene solution of Im^{i}Pr$_2$Me$_2$•GeH$_2$•BH$_3$ layered with hexanes to -35 °C for 2 days. Bulk purity of only ~80 % was obtained due to the presence of imidazolium salts (*i.e.*, [Im^{i}Pr$_2$Me$_2$H]$^+$) that had similar solubility as **2**. ^{1}H{^{11}B} NMR (C_6D_6): δ 1.03 (d, 12H, $^3J_{HH}$ = 7.0 Hz, CH(C*H*$_3$)$_2$), 1.47 (s, 6H, C=C(C*H*$_3$)), 1.70 (t, 3H, $^3J_{HH}$ = 4.5 Hz, B*H*$_3$), 4.68 (q, 2H, $^3J_{HH}$ = 4.5 Hz, Ge*H*$_2$), 5.15 (sept, 2H, $^3J_{HH}$ = 6.0 Hz, C*H*(CH$_3$)$_2$). ^{13}C{^{1}H} NMR (C_6D_6): δ 9.9 (C=C(*C*H$_3$)), 21.2 (CH(*C*H$_3$)$_2$), 52.7 (*C*H(CH$_3$)$_2$), 126.8 (C=*C*(CH$_3$)), 161.5 (N*C*N). ^{11}B NMR (C_6D_6): δ -38.9 (s, *B*H$_3$).

Preparation of SImMe$_2$•GeCl$_4$ (3): In a variation of a literature procedure,[22] 2-chloro-1,3-dimethylimidazolinium chloride (0.167 g, 1.00 mmol) and Cl_2Ge•dioxane (0.231 g, 0.997 mmol) were suspended in 12 mL of fluorobenzene and this mixture was stirred for 18 hours. The volatiles were removed to afford **3** as a white solid (0.279 g, 89

%). ^{1}H NMR (CD_3CN):[22] δ 3.50 (s, 6H, NCH_3), 3.91 (s, 4H, N(CH_2)$_2$N). ^{13}C{^{1}H} NMR (CD_3CN):[22] δ 36.0 (N*C*H$_3$), 52.4 (N(*C*H$_2$)$_2$N), 172.7 (N*C*N). ^{1}H NMR (C_6D_6): δ 1.95 (s, 4H, N(CH_2)$_2$N), 2.77 (s, 6H, NCH_3).

Reaction of 2-chloro-1,3-dimethylimidazolinium chloride with Li[BH$_4$]: Isolation of the 1,3-dimethyl-1,3-diazolidine *trans*-(bis)borane (4): 2-Chloro-1,3-dimethylimidazolinium chloride (0.204 g, 1.21 mmol) and Li[BH_4] (0.053 g, 2.6 mmol) were combined in 12 mL of Et_2O and the mixture stirred for 18 hours. The volatiles were then removed under vacuum and the resulting white powder was extracted with 10 mL of toluene and filtered through a plug of Celite. Removal of the volatiles from the filtrate gave the known 1,3-dimethyl-1,3-diazolidine *trans*-(bis)borane (**4**) as a white solid (0.137 g, 89 %). ^{1}H{^{11}B} NMR ($CDCl_3$):[23] δ 1.84 (br, 3H, BH_3) 2.94 (s, 4H, N(CH_2)$_2$N), 3.59 (s, 6H, NCH_3), 4.09 (s, 2H, NCH_2N). ^{13}C{^{1}H} NMR ($CDCl_3$): [23] δ 53.5 (N*C*H$_3$), 61.4 (N(*C*H$_2$)$_2$N), 89.0 (N*C*N). ^{11}B NMR ($CDCl_3$): δ -8.1 (q, $^{1}J_{BH}$ = 104 Hz, *B*H$_3$).

Reaction of SIMe$_2$•GeCl$_4$ with Li[BH$_4$]: Alternate preparation of 4: SImMe$_2$•$GeCl_4$ (**3**) (0.238 g, 0.761 mmol) and Li[BH_4] (0.066 g, 2.4 mmol) were combined in a vial (in a glovebox) and 6 mL of Et_2O were then added. The resulting mixture was stirred vigorously for 18 hours and the volatiles were then removed under vacuum. ^{1}H NMR analysis of the crude product in $CDCl_3$ showed no sign of characteristic Ge-H resonances. The resulting brown powder was stirred with 10 mL of toluene and the mixture filtered through a plug of Celite. The volatiles were removed

from the filtrate to yield **4** as a white powder (0.033 g, 52 %). NMR data of **4** matched those from the literature[23] and above.

Preparation of *N,N'*-dimethylimidazolium iodide ([ImMe$_2$H]I):[39] This product is not air-sensitive, but it is extremely hygroscopic. To 150 mL of toluene was added 10.1 mL (0.127 mmol) of 1-methylimidazole followed by 7.9 mL (0.13 mmol) methyl iodide, and the mixture was heated to boiling overnight (under nitrogen). The reaction mixture solidified upon cooling to room temperature and was re-dissolved by adding 100 mL of dry dichloromethane.[40] The product was then precipitated by adding 50 mL of dry hexanes and the resulting pale yellow precipitate of [ImMe$_2$H]I was isolated by filtration and dried under vacuum (27.4 g, 97 %). ^{1}H NMR (D$_2$O):[40] δ 3.92 (s, 6H, NC*H*$_3$), 7.44 (d, 2H, $^4J_{HH}$ = 1.6 Hz, N(C*H*)$_2$N), 8.68 (broad s, 1H, NC(*H*)N). ^{13}C{^{1}H} NMR (D$_2$O): δ 36.9 (N*C*H$_3$), 124.5 (N(*C*H)$_2$N), 137.6 (N*C*(H)N).

Preparation of ImMe$_2$•GeCl$_2$ (5): *N*,*N*′-Dimethylimidazolium iodide (0.912 g, 4.07 mmol) and KH (0.523 g, 13.0 mmol) were suspended in 10 mL of THF and stirred for 4 hours. The suspension was allowed to settle, and the orange solution containing free ImMe$_2$ was filtered into a vial containing Cl$_2$Ge•dioxane (0.944 g, 4.08 mmol) suspended in 2 mL of THF. The remaining ImMe$_2$ in the initial reaction vial was rapidly (< 1 min) extracted with 3 × 2 mL portions of THF, filtered, and the combined filtrates (containing ImMe$_2$) were immediately added to the second reaction vial containing Cl$_2$Ge•dioxane. The reaction mixture was allowed to stir for an additional 5 min before the mixture was concentrated to a volume of *ca.* 6 mL. The resulting solution was cooled

for one day to give **5** as a yellow solid (0.856 g, 87 %). Crystals of **5** that were suitable for X-ray crystallography were obtained by cooling a concentrated solution in THF to -35 °C for one day. ^{1}H NMR (C_6D_6): δ 3.10 (s, 6H, NCH_3), 5.33 (s, 2H, N(CH)$_2$N). ^{13}C{^{1}H} NMR (C_6D_6): δ 36.4 (NCH$_3$), 121.7 (N(CH)$_2$N), 169.3 (NCN). Mp: 85 °C (decomp.). Anal. Calc. for $C_5H_8N_2GeCl_2$: C, 25.06; H, 3.36; N, 11.69. Found: C, 25.21; H, 3.41; N, 11.23 %.

Preparation of ImMe$_2$•GeH$_2$•BH$_3$ (6): ImMe$_2$•GeCl$_2$ (**5**) (0.206 g, 0.860 mmol) was suspended in 2 mL of Et$_2$O. A slurry of Li[BH$_4$] (0.037 g, 1.7 mmol) in 6 mL of Et$_2$O was then added. The resulting mixture was stirred vigorously for 2 hours, and the volatiles were then removed under vacuum. The product was extracted with three 3 mL aliquots of fluorobenzene and the combined extracts were filtered through Celite. Removal of the volatiles from the filtrate under vacuum yielded ImMe$_2$•GeH$_2$•BH$_3$ (**6**) as a white solid (0.109 g, 80 %). Crystals of suitable quality for X-ray crystallography were grown by cooling a fluorobenzene solution layered with hexanes to -35 °C for 24 hours. ^{1}H{^{11}B} NMR (C_6D_6): δ 1.64 (t, 3H, $^{3}J_{HH}$ = 4.5 Hz, BH_3), 2.92 (s, 6H, NCH_3), 4.36 (q, 2H, $^{3}J_{HH}$ = 4.5 Hz, GeH_2), 5.41 (s, 2H, N(CH)$_2$N). ^{13}C{^{1}H} NMR (C_6D_6): δ 36.7 (NCH$_3$), 121.9 (N(CH)$_2$N), 163.7 (NCN - resonance indirectly located with HMBC). ^{11}B NMR (C_6D_6): δ -39.9 (q, $^{1}J_{BH}$ = 98.0 Hz, BH$_3$). Mp: 103-105 °C (decomp.). Anal. Calc. for $C_5H_{13}N_2GeB$: C, 32.53; H, 7.10; N, 15.17. Found: C, 32.93; H, 7.02; N, 14.66 %. IR (ATIR): 1966 cm^{-1} (Ge-H), 2345 cm^{-1} (B-H).

Preparation of $ImMe_2$•GeD_2•BD_3 (6D): $ImMe_2$•$GeCl_2$ (**5**) (0.181 g, 0.755 mmol) was suspended in 5 mL of Et_2O. A slurry of $Li[BD_4]$ (0.043 g, 1.67 mmol) in 5 mL of Et_2O was then added. The resulting mixture was stirred vigorously for 2 hours, and the volatiles were then removed under vacuum. The product was extracted with three 3 mL aliquots of fluorobenzene and the combined extracts were filtered through Celite. Removal of the volatiles from the filtrate under vacuum yielded $ImMe_2$•GeD_2•BD_3 (**6D**) as a white solid (0.119 g, 80 %). Crystals of high purity for kinetic analyses were grown by cooling a concentrated toluene solution of **6D** to -35 °C for 24 hours. ^{1}H NMR (C_6D_6): δ 2.89 (s, 6H, NCH_3), 5.36 (s, 2H, N(CH)$_2$N). ^{11}B NMR (C_6D_6): δ -40.4 (br, BD$_3$). ^{2}H NMR (C_6H_6): δ 1.57 (br, BD_3), 4.35 (s, GeD_2). IR (ATIR): 1434 cm^{-1} (Ge-D), 1765 cm^{-1} (B-D).

Ge film deposition (from solution): In the glovebox, a stock solution was prepared containing 11 mg of $ImMe_2$•GeH_2•BH_3 (**6**) in 14.000 mL of toluene. The solution (4.000 mL) was filtered through glass filter paper and then measured into microwave reaction tubes (obtained from Biotage). Concentration changes, if necessary, occurred via dilution. Substrates were added to the tubes and the tubes were sealed with Teflon caps. The tubes were brought out of the glovebox and placed in an oil bath at 100 °C for 3 or 10 hours, after which the tubes were allowed to cool to room temperature. After being brought into the glovebox, the substrates were removed from solution and rinsed two times with 2 mL portions of benzene. The substrates were then dried under vacuum.

Kinetic Experiments: Decomposition of 6 and 6D: In the glovebox, a stock solution of 4,4′-difluorobiphenyl (4,4′-DFBP) was made by dissolving 82.1 mg in 600 μL of toluene-D_8 (7.19×10^{-2} M). A saturated solution of **6** or **6D** was prepared by stirring 80 mg of compound in 2.000 mL of toluene-D_8 for one hour, and then allowed to settle. 450.0 μL of the clear concentrated **6** or **6D** solution was transferred by micropipette to a J-Young tube, and 40.0 μL of the standard stock solution of 4,4′-DFBP was added, for a total volume of 490.0 μL; the internal standard of 4,4′-DFBP was used to determine the concentration of either **6** or **6D** in solution. A Varian 400 MHz spectrometer was tuned and shimmed for ^{1}H NMR acquisition of the sample at room temperature, and then the sample was removed and the spectrometer temperature was increased to 100 °C. The temperature was calibrated using a standard of ethylene glycol provided by Varian. After re-insertion of the sample and shimming adjustments, a program was set to record ^{1}H spectra every 5 minutes (82 seconds collection, 218 second delay).

2.5 Additional computational data relevant to discussion

2.5.1 Computational methods

The starting geometries for all structures involved in the decomposition of NHC•GeH_2•BH_3 (Scheme 2.4) were obtained from the corresponding X-ray crystallographic data (where possible).[7,10,30] Initial geometries for all compounds involved in ImMe_2•GeH_2•BH_3 and Im•GeH_2•BH_3 decomposition pathways, as well as analogous Sn-containing species, were built from the corresponding optimized structure of

IPr•GeH_2•BH_3 as a starting point. The geometry optimizations, using default convergence criteria, were performed using density functional theory (DFT) with the M06-2X functional.[30] In most computations, the cc-pVDZ basis set[31] was used for all atoms except Sn, where the cc-pVDZ-PP basis set and a corresponding effective core potential was used.[31] For Sn containing compounds, this combination of basis sets will be referred to as cc-pVDZ-(PP). For the largest IPr•GeH_2•BH_3 complex, the 6-311+G(d) basis set[31] was used. Harmonic vibrational analyses were performed at the same level of theory for all optimized stationary points to determine their character (minimum or first-order saddle point) and to acquire the thermochemical data (at 298.15 K). The effect of THF solvent, which was used in the experiment, was also considered using the integral equation formalism polarizable continuum model (IEF-PCM).[41] NBO population analysis[42] on the resulting NHC•GeH_2•BH_3 structures was carried out at the M06-2X/cc-pVDZ (M06-2X/6-311+G(d) for IPr•GeH2•BH3) level of theory.[30,31] The computations were undertaken with Gaussian 09 revision D1 or Gaussian 16 revision B1 software.[43] Raman frequency calculations on bond-stretched species were carried out using density functional theory (DFT) with the B3LYP functional[44] and cc-pVDZ basis set.[31] The desired bond length was frozen and all other bond lengths and angles were allowed to optimize using default convergence criteria.

For all computations and data collected here, full output files are available at: https://doi.org/10.6084/m9.figshare.11962752

2.5.2 Collected outputs and relevant data from computational studies

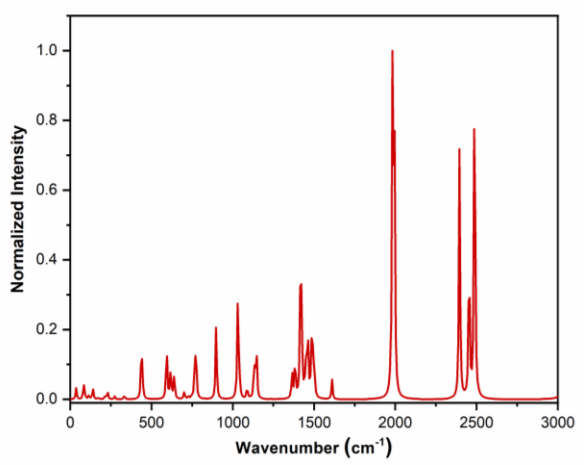

Figure 2.15. Computed Raman spectrum of $ImMe_2$•GeH_2•BH_3, B3LYP/cc-pVDZ. Intensities normalized to maximum peak height. Peak half width at half height set at 4 cm^{-1}.

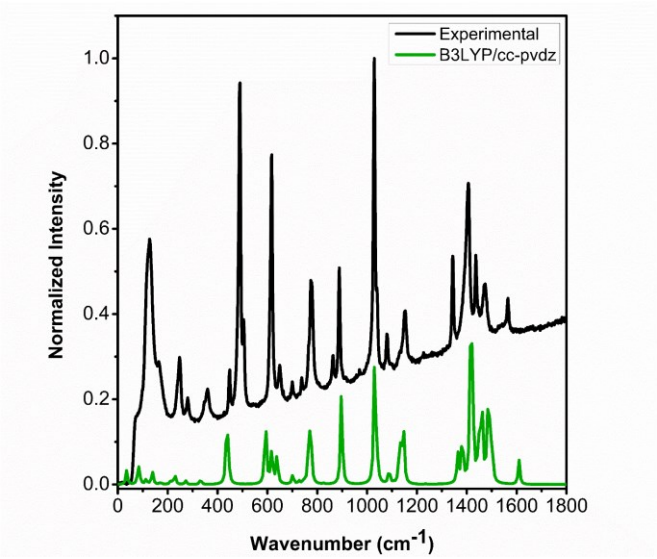

Figure 2.16. Computed (green) and experimental (black) Raman spectra of $ImMe_2$•GeH_2•BH_3, showing excellent agreement between computed and computational spectra. Computational spectrum as per Figure 2.15. Maximum wavenumber plotted is lower than that shown in Figure 2.15 due to extent of experimental data collected.

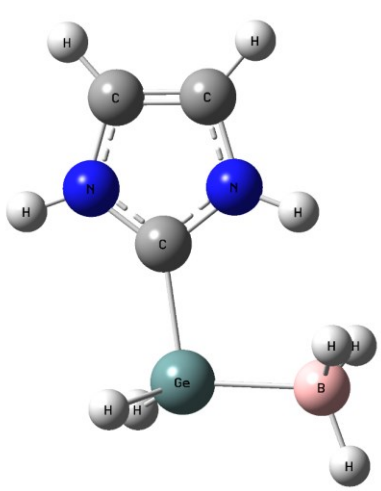

Im•GeH_2•BH_3

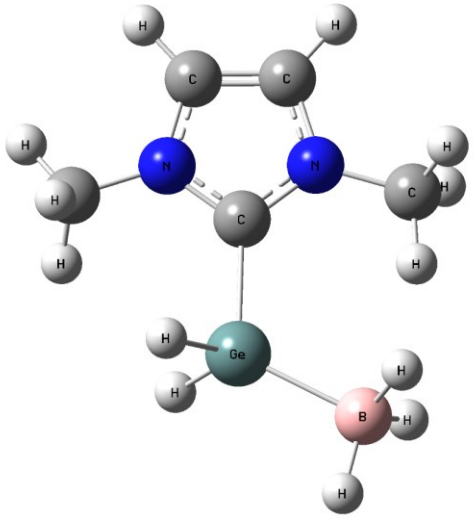

$ImMe_2$•GeH_2•BH_3

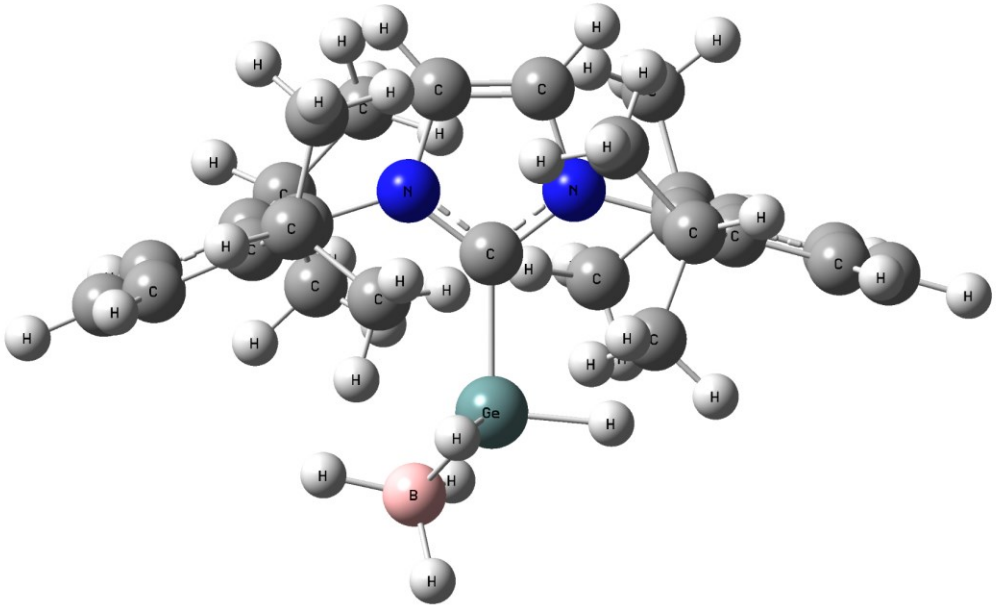

IPr•GeH_2•BH_3

Figure 2.17. Optimized structures of the NHC•GeH_2•BH_3 adducts (NHC = Im, $ImMe_2$ and IPr). Geometries determined at the M06-2X/cc-pVDZ level of theory for $ImMe_2$ and Im-containing adducts and M06-2X/6-311+G(d) for IPr adduct in THF.[30, 31]

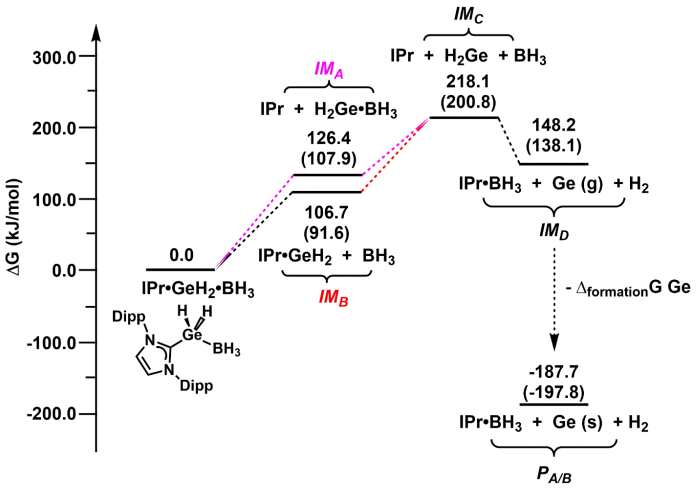

Figure 2.18. Relative energies for decomposition of the IPr•GeH_2•BH_3 adduct via Paths **A** and **B**. Energies determined at the M06-2X/cc-pVDZ level of theory in THF (gas phase results reported in parentheses).[30, 31] Lowest energy states are plotted. in this case, **IM$_C$** contains H_2Ge in the singlet state, and **IM$_D$** is plotted containing Ge(g) (triplet) (see Table 2.3). Gibbs free energy of formation ($\Delta_{formation}G$) for Ge(g) taken as 335.9 kJ/mol.[32]

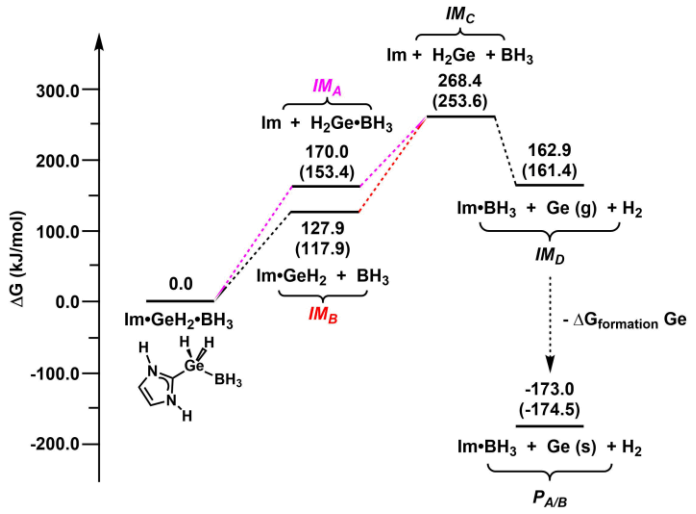

Figure 2.19. Relative energies for decomposition of the Im•GeH_2•BH_3 adduct via Paths **A** and **B**. Energies determined at the M06-2X/cc-pVDZ level of theory in THF (gas phase results reported in parentheses).[30, 31] Lowest energy states are plotted; in this case, **IM$_C$** contains H_2Ge in the singlet state, and **IM$_D$** is plotted containing Ge(g) (triplet) (see Table 2.3). Gibbs free energy of formation ($\Delta_{formation}G$) for Ge(g) taken as 335.9 kJ/mol.[32]

Table 2.3. The relative energies of the NHC•BH_3 + Ge(0) + H_2 products determined at the M06-2X/cc-pVDZ level of theory for $ImMe_2$ and Im-containing adducts and M06-2X/6-311+G(d) for the IPr adduct.[30, 31]

Substitution group	Products	Relative energy (kJ/mol) in the gas phase	Relative energy (kJ/mol) in solvent phase
Im	Im-BH_3 +Ge(singlet) + H_2	281.06	288.16
	Im-BH_3 +Ge(triplet) + H_2	**161.49**	**162.94**
$ImMe_2$	$ImMe_2$-BH_3 +Ge(singlet) + H_2	272.98	285.73
	$ImMe_2$-BH_3 +Ge(triplet) + H_2	**153.41**	**160.51**
IPr	IPr-BH_3 +Ge(singlet) + H_2	252.41	242.99
	IPr-BH_3 +Ge(triplet) + H_2	**138.07**	**148.22**

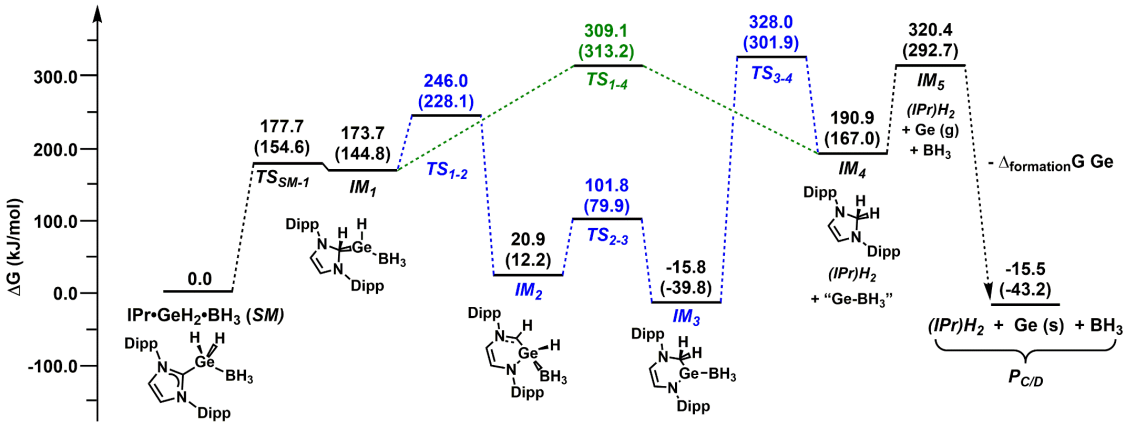

Figure 2.20. Relative energies for decomposition/rearrangement of the IPr•GeH_2•BH_3 adduct via Paths **C** and **D**. Energies determined at the M06-2X/6-311+G(d,p) level of theory in THF (gas phase results reported in parentheses).[30, 31] Lowest energy states are plotted; in this case, $\mathbf{IM_5}$ is plotted containing Ge(g) (triplet) (see Table S6). Gibbs free energy of formation ($\Delta_{formation}G$) for Ge(g) taken as 335.9 kJ/mol.[32]

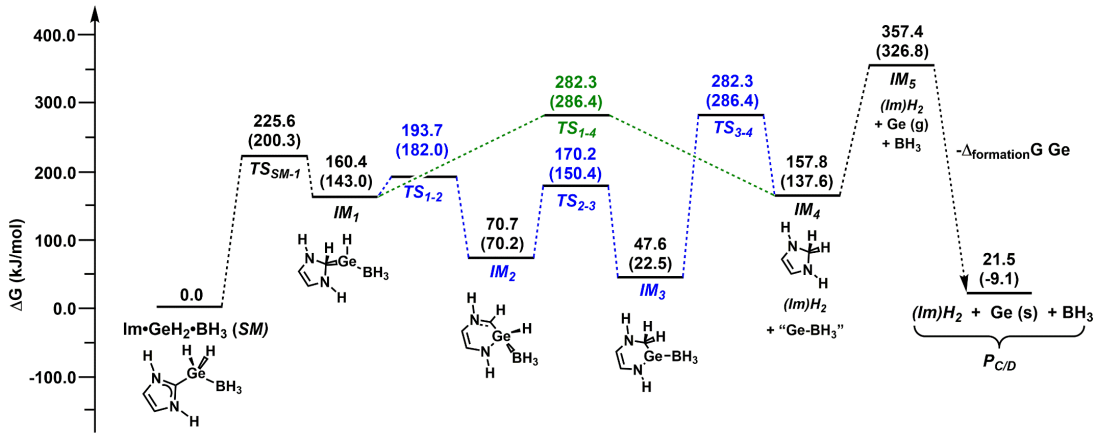

Figure 2.21. Relative energies for decomposition/rearrangement of the Im•GeH_2•BH_3 adduct via Paths **C** and **D**. Energies determined at the M06-2X/cc-pVDZ level of theory in THF (gas phase results reported in parentheses).[30, 31] Lowest energy states are plotted; in this case, IM_5 is plotted containing Ge(g) (triplet) (see Table 2.3). Gibbs free energy of formation ($\Delta_{formation}G$) for Ge(g) taken as 335.9 kJ/mol.[32]

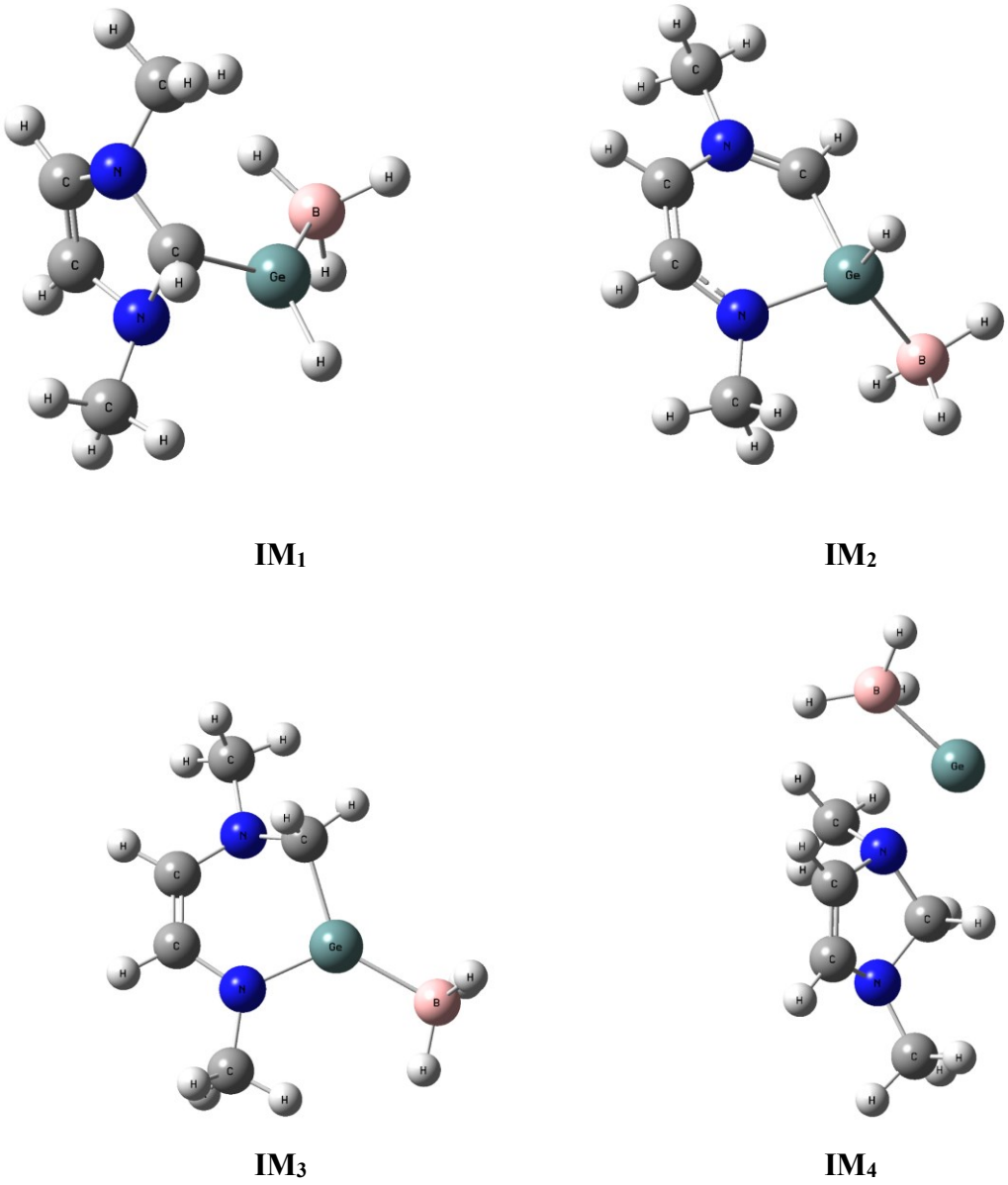

Figure 2.22. Structures of all intermediates and final product of the $ImMe_2$•GeH_2•BH_3 analogue along reaction Paths **C** and **D** as determined at the M06-2X/cc-pVDZ level of theory in THF.[30, 31]

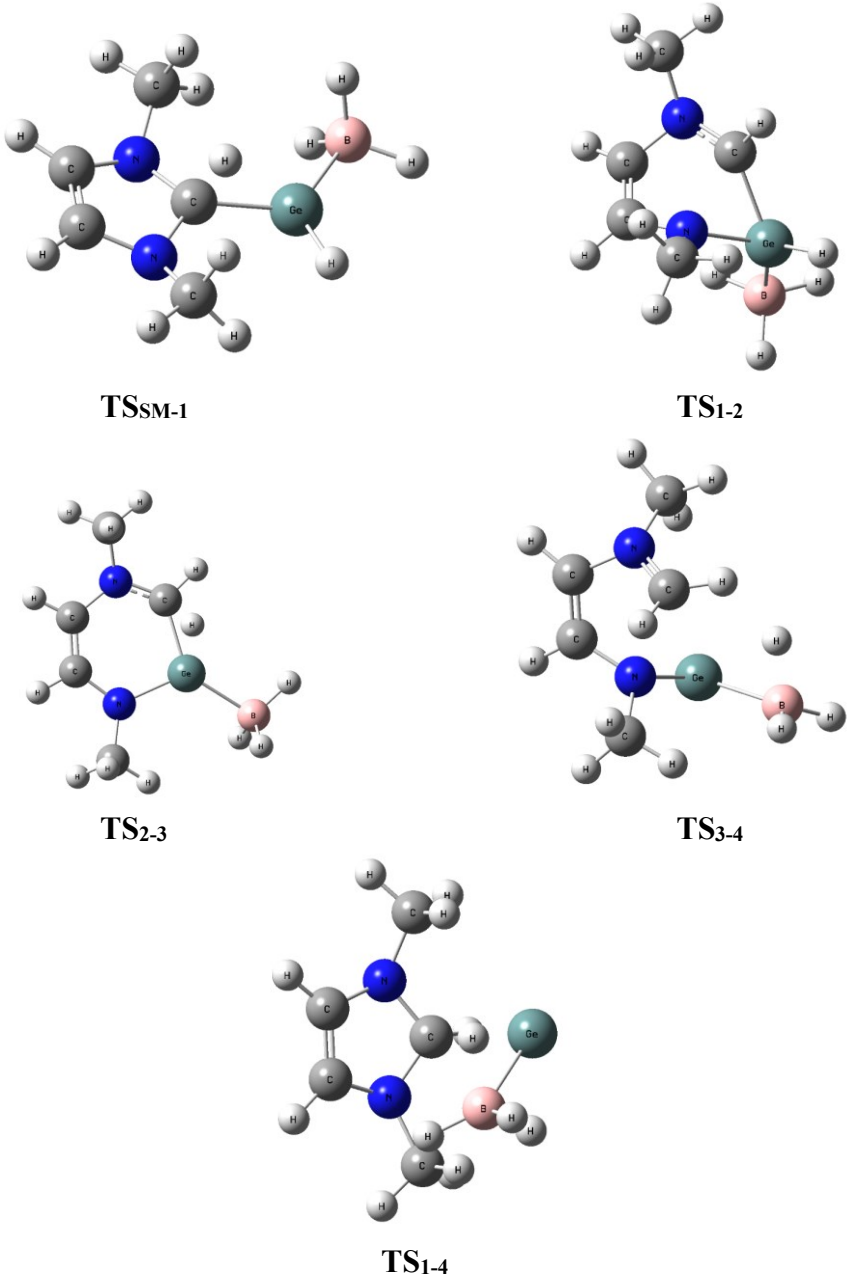

Figure 2.23. Structures of all transition states of the $ImMe_2$•GeH_2•BH_3 analogue along reaction Paths **C** and **D** as determined at the M06-2X/cc-pVDZ level of theory in the gas phase.[30, 31]

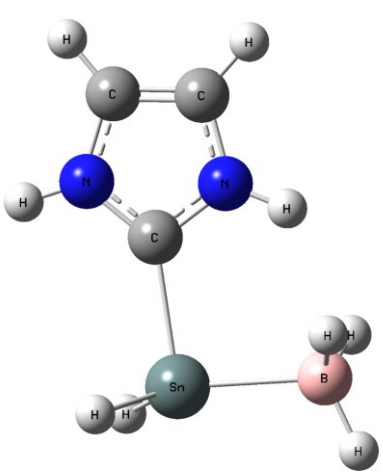

Im•SnH_2•BH_3

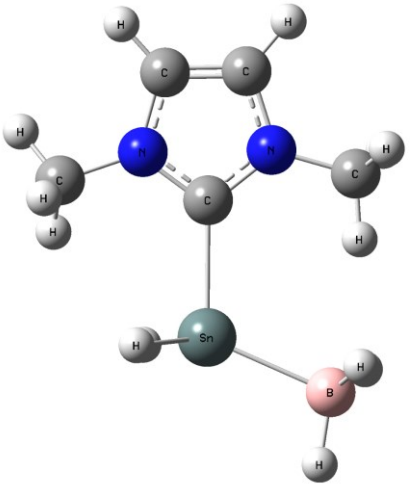

$ImMe_2$•SnH_2•BH_3

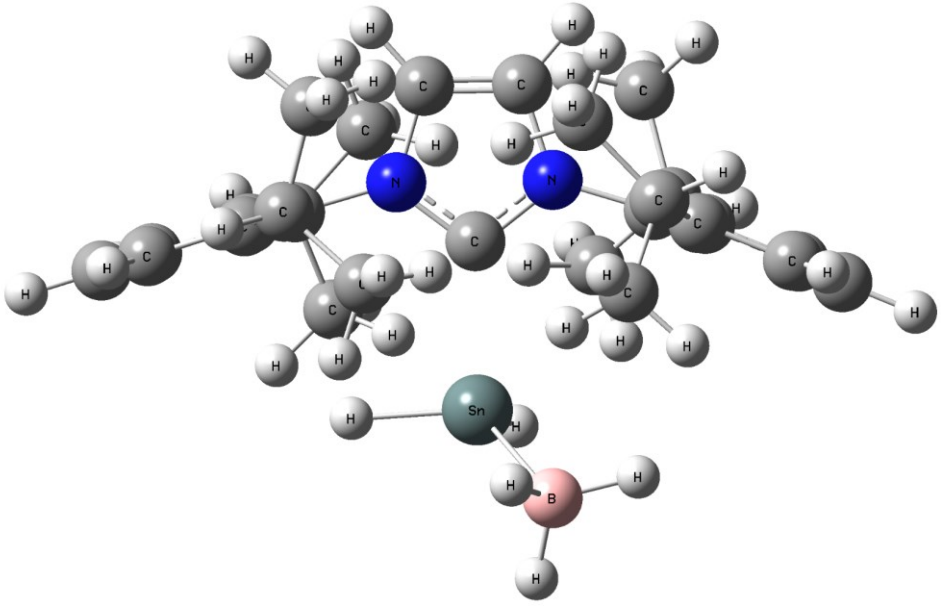

IPr•SnH_2•BH_3

Figure 2.24. Optimized structures of the NHC•SnH_2•BH_3 adducts (NHC = IPr, $ImMe_2$ and Im). Geometries determined at the M06-2X/cc-pVDZ-(PP) level of theory in THF.[30, 31] NBO analysis does not detect the presence of covalent bonding between the C_{NHC}–Sn in the IPr adduct, due to the high polarity of this bond (> 95 % cut-off set by NBO).

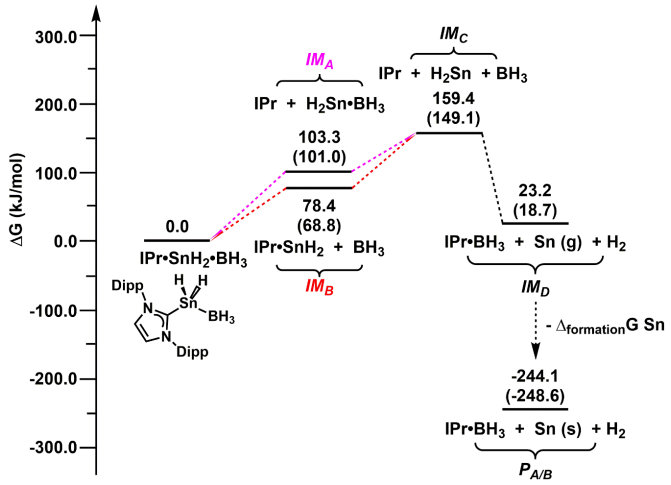

Figure 2.25. Relative energies for decomposition of the IPr•SnH_2•BH_3 adduct via Paths **A** and **B**. Energies determined at the M06-2X/cc-pVDZ-(PP) level of theory in THF (gas phase results reported in parentheses).[30, 31] Lowest energy states are plotted; in this case, **IM$_C$** contains H_2Sn in the singlet state, and IM_D is plotted containing Sn(g) (triplet) (see Table 2.4). Gibbs free energy of formation ($\Delta_{formation}G$) for Sn(g) taken as 267.3 kJ/mol.[32]

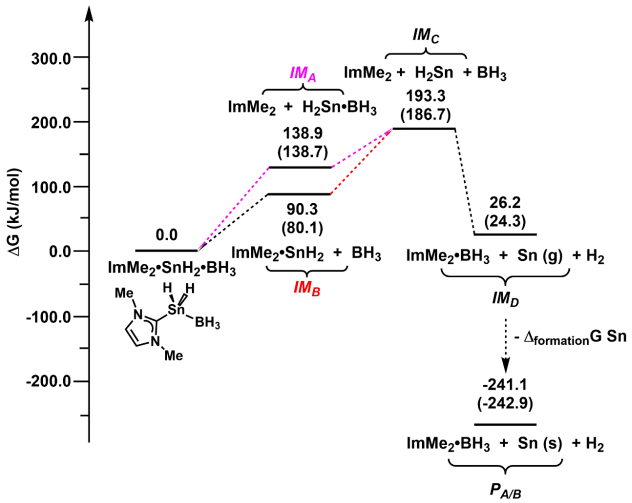

Figure 2.26. Relative energies for decomposition of the ImMe_2•SnH_2•BH_3 adduct via Paths **A** and **B**. Energies determined at the M06-2X/cc-pVDZ-(PP) level of theory in THF (gas phase results reported in parentheses).[30, 31] Lowest energy states are plotted in this case, **IM$_C$** contains H_2Sn in the singlet state, and IM_D is plotted containing $Sn_{(g)}$ (triplet) (see Table 2.4). Gibbs free energy of formation ($\Delta_{formation}G$) for $Sn_{(g)}$ taken as 267.3 kJ/mol.[32]

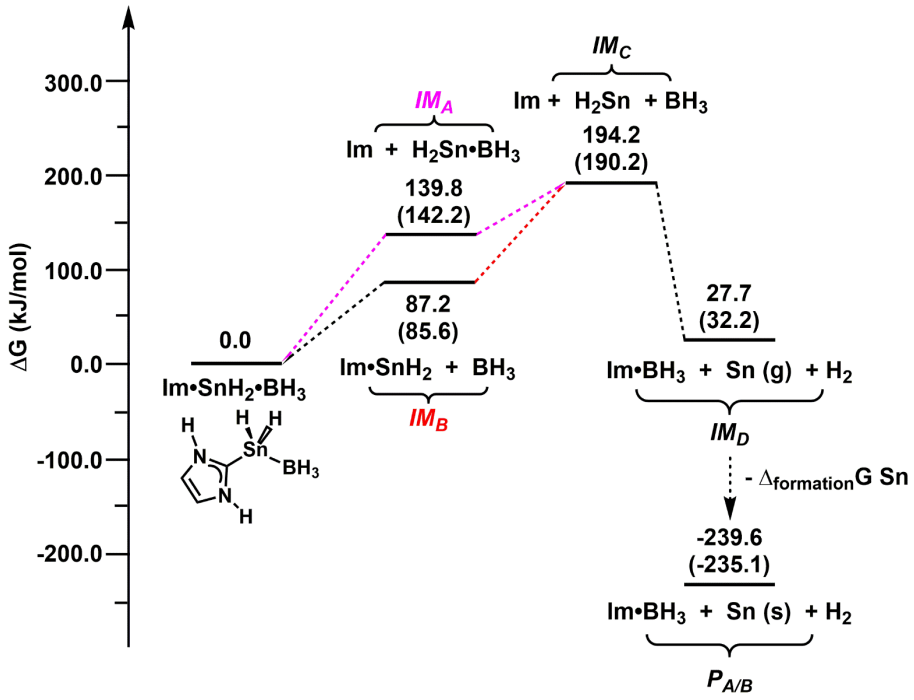

Figure 2.27. Relative energies for decomposition of the Im•SnH_2•BH_3 adduct via Paths **A** and **B**. Energies determined at the M06-2X/cc-pVDZ-(PP) level of theory in THF (gas phase results reported in parentheses).[30, 31] Lowest energy states are plotted; in this case, **IM$_C$** contains H_2Sn in the singlet state, and **IM$_D$** is plotted containing Sn(g) (triplet) (see Table 2.4). Gibbs free energy of formation ($\Delta_{formation}G$) for Sn(g) taken as 267.3 kJ/mol.[32]

Table 2.4. The relative energies of the NHC-BH_3 + Sn(0) + H_2 products determined at the M06-2X/cc-pVDZ-(PP) level of theory.[32]

Substitution group	Products	Relative energy (kJ/mol) in the gas phase	Relative energy (kJ/mol) in the solvent-phase
Im	Im-BH_3 +Sn(singlet) + H_2	151.17	122.66
	Im-BH_3 +Sn(triplet) + H_2	**32.19**	**27.68**
$ImMe_2$	$ImMe_2$-BH_3 +Sn(singlet) + H_2	143.35	121.19
	$ImMe_2$-BH_3 +Sn(triplet) + H_2	**24.38**	**26.21**
IPr	IPr-BH_3 +Sn(singlet) + H_2	137.72	118.16
	IPr-BH_3 +Sn(triplet) + H_2	**118.16**	**23.18**

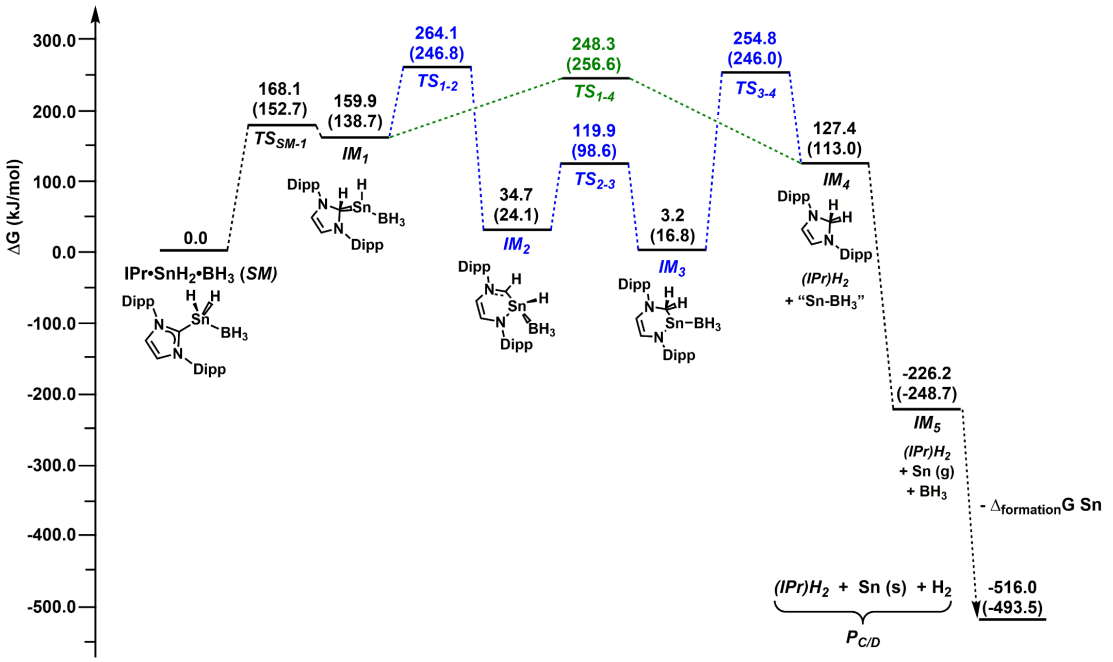

Figure 2.28. Relative energies for decomposition/rearrangement of the IPr•SnH_2•BH_3 adduct via Paths **C** and **D**. Energies determined at the M06-2X/cc-pVDZ-(PP) level of theory in THF (gas phase results reported in parentheses).[30, 31] Lowest energy states are plotted; in this case, **IM5** is plotted containing Sn(g) (triplet) (see Table 2.4). Gibbs free energy of formation ($\Delta_{formation}G$) for Sn(g) taken as 267.3 kJ/mol.[32]

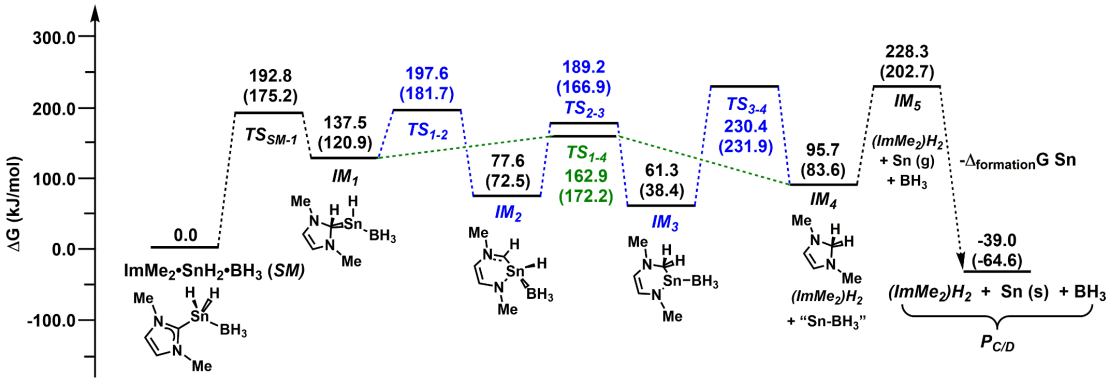

Figure 2.29. Relative energies for decomposition/rearrangement of the $ImMe_2$•SnH_2•BH_3 adduct via Paths **C** and **D**. Energies determined at the M06-2X/cc-pVDZ-(PP) level of theory in THF (gas phase results reported in parentheses).[30, 31] Lowest energy states are plotted; in this case, **IM5** is plotted containing Sn(g) (triplet) (see Table 2.4). Gibbs free energy of formation ($\Delta_{formation}G$) for Sn(g) taken as 267.3 kJ/mol.[32]

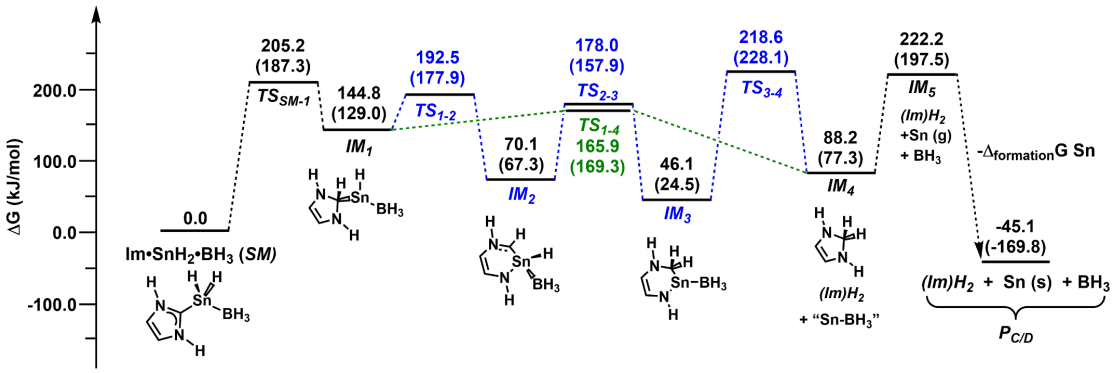

Figure 2.30. Relative energies for decomposition/rearrangement of the Im•SnH_2•BH_3 adduct via Paths **C** and **D**. Energies determined at the M06-2X/cc-pVDZ-(PP) level of theory in THF (gas phase results reported in parentheses).[30, 31] Lowest energy states are plotted in this case, **IM5** is plotted containing Sn(g) (triplet) (See Table 2.4). Gibbs free energy of formation ($\Delta_{formation}G$) for Sn(g) taken as 267.3 kJ/mol.[32]

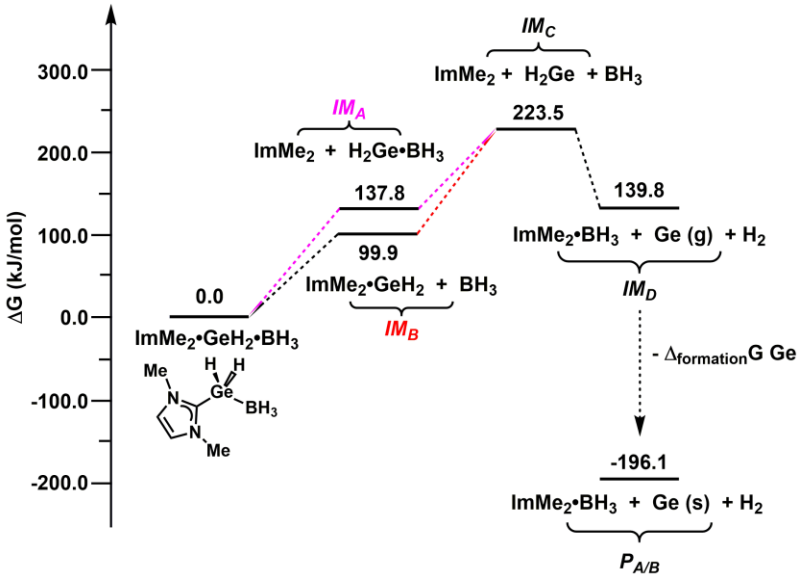

Figure 2.31. Relative energies for decomposition of the $ImMe_2$•GeH_2•BH_3 adduct via Paths **A** and **B** at 100 °C. Energies determined at the M06-2X/cc-pVDZ level of theory.[30, 31] Lowest energy states are plotted; in this case, **IMC** contains H_2Ge in the singlet state, and **IMD** is plotted containing Ge(g) (triplet). Gibbs free energy of formation ($\Delta_{formation}G$) for Ge(g) not available for 100 °C, and is shown as the standard value of 335.9 kJ/mol.[32]

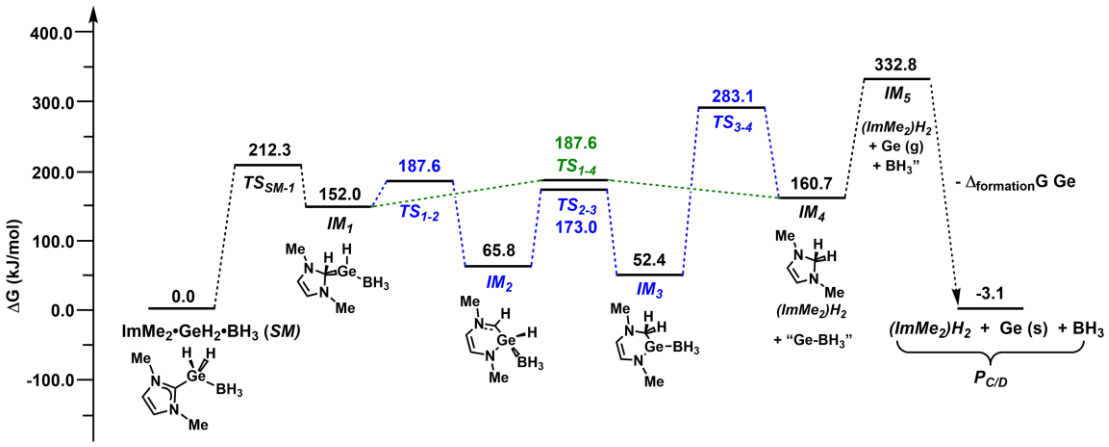

Figure 2.32. Relative energies for decomposition/rearrangement of the $ImMe_2$•GeH_2•BH_3 adduct via Paths **C** and **D** at 100 °C. Energies determined at the M06-2X/cc-pVDZ level of theory in THF.[30, 31] Lowest energy states are plotted; in this case, **IM$_5$** is plotted containing Ge(g) (triplet). Gibbs free energy of formation ($\Delta_{formation}G$) for Ge(g) not available for 100 °C, and is shown as the standard value of 335.9 kJ/mol.[32]

2.6 X-ray crystallographic data

Crystals of appropriate quality for single-crystal X-ray diffraction studies were removed from the mother liquor and immediately covered with a thin layer of hydrocarbon oil (Paratone-N) in a sealed vial for transport to the instrument. A suitable crystal was then selected, attached to a glass fibre, and mounted under a stream of nitrogen in the instrument. All data were collected using a Bruker APEX II CCD detector/D8 diffractometer using Mo/Cu Kα radiation. The data were corrected for absorption through Gaussian integration from indexing of the crystal faces. Structures were solved and refinements were completed using direct methods (SHELXS-97).[45]

Table 2.5. Crystallographic experimental details for $Im^iPr_2Me_2•GeCl_4$ and $Im^iPr_2Me_2•GeH_2•BH_3$.

Compound	$Im^iPr_2Me_2•GeCl_4$ (**1**)	$Im^iPr_2Me_2•GeH_2•BH_3$ (**2**)
formula	$C_{11}H_{20}Cl_4GeN_2$	$C_{11}H_{25}BGeN_2$
formula weight	394.68	268.73
crystal system	monoclinic	orthorhombic
space group	$P2_1/c$ (No. 14)	$Pbca$ (No. 61)
unit cell parameters		
a (Å)	10.8834 (6)	13.9841 (13)
b (Å)	17.6041 (10)	10.6449 (10)
c (Å)	17.5196 (10)	19.1922 (17)
β (°)	92.681 (2)	-
V (Å^3)	3352.9 (3)	2856.9 (5)
Z	8	8
ρ_{calcd} (g cm^{-3})	1.564	1.25
μ (mm^{-1})	8.231	2.119
radiation (λ [Å])	Cu Kα (1.54178) (microfocus source)	Mo Kα (0.71073) (graphite-monochromated)
T (°C)	–100	–100
$2\theta_{max}$ (°)	148.04	56.55
Total data	22879 ($-13 \le h \le 13$, $-21 \le k \le 21$, $-20 \le l \le 21$)	25429 ($-18 \le h \le 18$, $-14 \le k \le 14$, $-25 \le l \le 25$)
Unique data (R_{int})	6768 (0.0479)	3521 (0.0210)
$Data_{obs}$ [$F_o^2 \le 2\sigma(F_o^2)$]	6258	2962
data/restraints/parameters	6768 / 0 / 337	3521 / 0 / 158
final R indices[a]		
R_1 [$F_o^2 \ge 2\sigma(F_o^2)$]	0.0388	0.0261
wR_2 [all data]	0.1081	0.0768
Max/min $\Delta\rho$ (e$^-$ Å^{-3})	1.050 and –0.878	0.591 and –0.323

[a] $R_1 = \Sigma||F_o| - |F_c||/ \Sigma|F_o|$; $wR_2 = [\Sigma\, w(F_o^2 - F_c^2)^2/ \Sigma w(F_o^4)]^{1/2}$

Table 2.6. Crystallographic experimental details for $ImMe_2$•$GeCl_4$ and $ImMe_2$•GeH_2•BH_3.

Compound	$ImMe_2$•$GeCl_4$ (**5**)	$ImMe_2$•GeH_2•BH_3 (**6**)
formula	$C_5H_8Cl_2GeN_2$	$C_5H_{13}BGeN_2$
formula weight	239.62	184.57
crystal system	triclinic	orthorhombic
space group	$P\bar{1}$ (No. 2)	$P2_1/c$ (No. 14)
unit cell parameters		
a (Å)	7.8057(5)	7.4289(5)
b (Å)	12.0002(7)	7.8445(6)
c (Å)	14.9193(9)	15.1553(11)
α	77.0306(7)	-
β (°)	89.8532(7)	98.9943(9)
γ (°)	76.9401(7)	-
V (Å^3)	1324.91(14)	872.33(11)
Z	6	4
ρ_{calcd} (g cm^{-3})	1.802	1.25
μ (mm^{-1})	4.003	3.435
radiation (λ [Å])	Mo Kα (0.71073) (graphite-monochromated)	Mo Kα (0.71073) (graphite-monochromated)
T (°C)	–100	–100
$2\theta_{max}$ (°)	56.36	56.54
Total data	11542 ($-10 \le h \le 10$, $-15 \le k \le 15$, $-19 \le l \le 19$)	7874 ($-9 \le h \le 9$, $-10 \le k \le 10$, $-19 \le l \le 19$)
Unique data (R_{int})	6273 (0.0253)	2127 (0.0217)
$Data_{obs}$ [$F_o^2 \le 2\sigma(F_o^2)$]	4825	1802
data/restraints/parameters	6273 / 0 / 277	3521 / 0 / 158
final R indices[a]		
R_1 [$F_o^2 \ge 2\sigma(F_o^2)$]	0.0342	0.0278
wR_2 [all data]	0.859	0.0751
Max/min $\Delta\rho$ (e$^-$ Å^{-3})	0.727 and –0.428	0.589 and –0.245

[a] $R_1 = \Sigma||F_o| - |F_c||/ \Sigma|F_o|$; $wR_2 = [\Sigma\, w(F_o^2 - F_c^2)^2/ \Sigma w(F_o^4)]^{1/2}$

2.7 References

1. Usually EH_2 species are generated as mixtures with other polyhydrides: (a) J. M. Jasinski, R. Becerra and R. Walsh, *Chem. Rev.*, 1995, **95**, 1203; (b) S. Aldridge and A. J. Downs, *Chem. Rev.*, 2001, **101**, 3305; (c) E. Hirota and H. Ishikawa, *J. Chem. Phys.*, 1999, **110**, 4254; (d) X. Wang and L. Andrews, *J. Am. Chem. Soc.*, 2003, **125**, 6581; (e) N. A. Young, *Coord. Chem. Rev.*, 2013, **257**, 956.
2. (a) H. Jacobsen and T. Ziegler, T. *Inorg. Chem.,* 1996, **35**, 775; (b) Y. Apeloig, R. Pauncz, M. Karni, R. West, W. Steiner and D. Chapman, *Organometallics*, 2003, **22**, 3250 and references therein.
3. (a) J. M. Jasinski and S. M. Gates, *Acc. Chem. Res.*, 1991, **24**, 9; (b) W. Grochala and P. P. Edwards, *Chem. Rev.*, 2004, **104**, 1283; (c) E. Rivard, *Chem. Soc. Rev.*, 2016, **45**, 989.
4. (a) R. R. Schrock, *Acc. Chem. Res.*, 1979, **12**, 98; (b) F. N. Tebbe, G. W. Parshall and D. W. Ovenall, *J. Am. Chem. Soc.*, 1979, **101**, 5074; (c) P. Schwab, M. B. France, J. W. Ziller and R. H. Grubbs, *Angew. Chem., Int. Ed. Engl.*, 1995, **34**, 2039; (d) J. Scott and D. J. Mindiola, *Dalton Trans.*, 2009, 8463.
5. (a) H. von Pechmann, *Ber. Dtsch. Chem. Ges.*, 1894, **27**, 1888; (b) H. Yang, B. Martin and B. Schenkel, *Org. Proc. Res. Develop.*, 2018, **22**, 446–456.
6. For the photo-assisted extrusion of EH_2 units (E = Si and Ge) via cyclobutane and cyclopentene analogues, see: (a) T. J. Barton and N. Tillman, *J. Am. Chem. Soc.*, 1987, **109**, 6711; (b) R. Becerra, S. E. Boganov, M. P. Egorov, O. M. Nefedov and R. Walsh, *Chem. Phys. Lett.*, 1996, **260**, 433; (c) For a computational investigation of this process, see: M.-D. Su, *J. Phys. Chem. A*, 2015, **119**, 8611.

7. K. C. Thimer, S. M. I. Al-Rafia, M. J. Ferguson, R. McDonald and E. Rivard, *Chem. Commun.*, 2009, 7119.

8. E. Rivard, *Dalton Trans.*, 2014, **43**, 8577.

9. For related studies on donor-acceptor stabilization, see: (a) T. J. Marks, *J. Am. Chem. Soc.*, 1971, **93**, 7090; (b) G, Schmid and E. Welz, *Angew. Chem., Int. Ed. Engl.*, 1977, **16**, 785; (c) W. Petz, *Chem. Rev.* 1986, **86**, 1019; (d) A. Vogel, A. Y. Timoshkin and M. Scheer, *Angew. Chem.*, *Int. Ed.*, 2001, **40**, 4409; (e) P. A. Rupar, M. C. Jennings, P. J. Ragogna and K. M. Baines, *Organometallics*, 2007, **26**, 4109; (f) R. S. Ghadwal, R. Azhakar and H. W. Roesky, *Acc. Chem. Res.*, 2013, **46**, 444; (g) A. Jana, V. Huch, H. S. Rzepa and D. Scheschkewitz, *Organometallics*, 2015, **34**, 2130; (h) H. P. Hickox, Y. Wang, Y. Xie, P. Wei, H. F. Schaefer III and G. H. Robinson, *J. Am. Chem. Soc.*, 2016, **138**, 9799; (i) O. Hegen, C. Marquardt, A. Y. Timoshkin and M. Scheer, *Angew. Chem., Int. Ed.*, 2017, **56**, 12783; (j) O. Hegen, J. Bräse, A. Y. Timoshkin and M. Scheer, *Chem. Eur. J.*, 2019, **25**, 485; (k) R. Jambor, J. Tremmel, J. Tydlitát, L. Dostál, A. Ruzicka, X. Deraet, J. Turek and R. Jambor, *Chem. Eur. J.*, 2020, **26**, 6070.

10. (a) S. M. I. Al-Rafia, A. C. Malcolm, S. K. Liew, M. J. Ferguson and E. Rivard, *J. Am. Chem. Soc.*, 2011, **133**, 777; (b) S. M. I. Al-Rafia, A. C. Malcolm, S. K. Liew, M. J. Ferguson, R. McDonald and E. Rivard, *Chem. Commun.*, 2011, **47**, 6987; (c) S. M. I. Al-Rafia, A. C. Malcolm, R. McDonald, M. J. Ferguson and E. Rivard, *Angew. Chem., Int. Ed.*, 2011, **50**, 8354; (d) S. M. I. Al-Rafia, A. C. Malcolm, R. McDonald, M. J. Ferguson and E. Rivard, *Chem. Commun*., 2012, **48**, 1308; (e) S. M. I. Al-Rafia, M. R. Momeni, M. J. Ferguson, R. McDonald, A. Brown and E.

Rivard, *Organometallics*, 2013, **32**, 6658; (f) A. K. Swarnakar, S. M. McDonald, K. C. Deutsch, P. Choi, M. J. Ferguson, R. McDonald and E. Rivard, *Inorg. Chem.* 2014, **53**, 8662.

11. T. K. Purkait, A. K. Swarnakar, G. B. De Los Reyes, F. A. Hegmann, E. Rivard and J. G. C. Veinot, *Nanoscale*, 2015, **7**, 2241.

12. D. D. Vaughn and R. E. Schaak, *Chem. Soc. Rev.* 2013, **42**, 2861.

13. For related examples of Ge nanomaterial formation under harsher (thermal or reducing) conditions, see: (a) K. Tabatabaei, A. L. Holmes, K. A. Newton, E. Muthuswamy, R. Sfadia, S. A. Carter and S. M. Kauzlarich, *Chem. Mater.*, 2019, **31**, 7510; (b) M. J. Kirschenbaum, M. G. Boebinger, M. J. Katz, M. T. McDowell and M. Dasog, *ChemNanoMat*, 2018, **4**, 423; (c) M. Javadi, D. Picard, R. Sinelnikov, M. A. Narreto, F. A. Hegmann and J. G. C. Veinot, *Langmuir*, 2017, **33**, 8757; (d) S. Yoo, C. Yoo, E.-S. Park, W. Kim, Y. K. Lee and C. S. Hwang, *J. Mater. Chem. C*, 2018, **6**, 5025; (e) V. H. Nguyen, A. Dobbie, M. Myronov, D. J. Norris, T. Walther and D. R. Leadley, *Thin Solid Films*, 2012, **520**, 3222; (f) J. C. Malaquias, M. Wu, J. Lin, E. V. C. Robert, J. Sniekers, K. Binnemans, P. J. Dale and J. Fransaer, *Electrochimica Acta*, 2017, **251**, 651.

14. (a) G. D. Frey, J. D. Masuda, B. Donnadieu and G. Bertrand, *Angew. Chem.*, *Int. Ed.*, 2010, **49**, 9444; (b) M. Arrowsmith, M. S. Hill, G. Kociok-Köhn, D. J. MacDougall and M. F. Mahon, *Angew. Chem.*, *Int. Ed.*, 2012, **51**, 2098; (c) D. Schmidt, J. H. J. Berthel, S. Pietsch and U. Radius, *Angew. Chem., Int. Ed.*, 2012, **51**, 8881; (d) S. M. I. Al-Rafia, R. McDonald, M. J. Ferguson and E. Rivard, *Chem. Eur. J.*, 2012, **18**, 13810; (e) T. Wang and D. W. Stephan, *Chem. Eur. J.*, 2014, **20**,

3036; (f) S. Würtemberger-Pietsch, U. Radius and T. M. Marder, *Dalton Trans.*, 2016, **45**, 5880; (g) M. D. Anker, A. L. Colebatch, K. J. Iversen, D. J. D. Wilson, J. L. Dutton, L. García, M. S. Hill, D. J. Liptrot and M. F. Mahon, *Organometallics*, 2017, **36**, 1173; For computational studies, see: (h) M. R. Momeni, E. Rivard and A. Brown, *Organometallics*, 2013, **32**, 6201; (i) K. J. Iversen, D. J. D. Wilson and J. L. Dutton, *Organometallics*, 2013, **32**, 6209.

15. (a) R. Becerra, S. E. Boganov, M. P. Egorov, V. I. Faustov, O. M. Nefedov and R. Walsh, *J. Am. Chem. Soc.,* 1998, **120**, 12657; (b) P. S. Billone, K. Beleznay, C. R. Harrington, L. A. Huck and W. J. Leigh, *J. Am. Chem. Soc.* 2011, **133**, 10523.

16. N. Kuhn and T. Kratz, *Synthesis*, 1993, 561.

17. (a) G. Prabusankar, A. Sathyanarayana, P. Suresh, C. Naga Babu, K. Srinivas, and B. P. Rao Metla, *Coord. Chem. Rev.*, 2014, **269**, 96; (b) V. Nesterov, D. Reiter, P. Bag, P. Frisch, R. Holzner, A. Porzelt and S. Inoue, *Chem. Rev.*, 2018, **118**, 9678.

18. J. P. Coyle, E. R. Sirianni, I. Korobkov, G. P. A. Yap, G. Dey and S. T. Barry, *Organometallics*, 2017, **36**, 2800–2810.

19. S. M. I. Al-Rafia, P. A. Lummis, A. K. Swarnakar, K. C. Deutsch, M. J. Ferguson, R. McDonald and E. Rivard, *Aust. J. Chem.*, 2013, **66***,* 1235.

20. CCDC 1986302-1986305 contain the supplementary crystallographic data for this paper. These data are provided free of charge from The Cambridge Crystallographic Data Centre.

21. P. A. Rupar, V. N. Staroverov, P. J. Ragogna and K. M. Baines, *J. Am. Chem. Soc.*, 2007, **129**, 15138.

22. T. Böttcher, B. S. Bassil and G.-V. Röschenthaler, *Inorg. Chem.*, 2012, **51**, 763.

23. M. Güizado-Rodríguez, A. Ariza-Castolo, G. Merino, A. Vela, H. Noth, V. I. Bakhmutov and R. Contreras, *J. Am. Chem. Soc.*, 2001, **123**, 9144.

24. (a) E. F. Van der Eide, T. Liu, D. M. Camaioni, E. D. Walter and R. M. Bullock, *Organometallics*, 2012, **31**, 1775; (b) A. Doddi, M. Peters and M. Tamm, *Chem. Rev.*, 2019, **119**, 6994.

25. A. J. Ruddy, P. A. Rupar, K. J. Bladek, C. J. Allan, J. C. Avery and K. M. Baines, *Organometallics*, 2010, **29**, 1362.

26. M. M. Bentlohner, M. Waibel, P. Zeller, K. Sarkar, P. Müller-Buschbaum, D. Fattakhova-Rohlfing and T. F. Fässler, *Angew. Chem., Int. Ed.*, 2016, **55**, 2441.

27. J. C. Walton, M. M. Brahmi, L. Fensterbank, E. Lacôte, M. Malacria, Q. Chu, S. Ueng, A. Solovyev and D. P. Curran, *J. Am. Chem. Soc.*, 2010, **132**, 2350.

28. (a) P. J. D. Whiteside, J. A. Chininis and H. K. Hunt, *Coatings*, 2016, **6**, 35; (b) Q. Shi, R. Roux, F. Latourte, F. Hild, D. Loisnard and N. Brynaert, *Ultramicroscopy* 2018, **191**, 18.

29. C. Ratsch and J. A. Venables, *J. Vac. Sci. Tech. A*, 2003, **21**, S96.

30. Y. Zhao and D. Truhlar, *Theor. Chem. Acc.*, 2008, **120**, 215.

31. (a) T. H. Dunning Jr., *J. Chem. Phys.*, 1989, **90**, 1007; (b) A. K. Wilson, D. E. Woon, K. A. Peterson and T. H. Dunning Jr., *J. Chem. Phys.*, 1999, **110**, 7667.

32. D. D. Wagman, W. H. Evans, V. B. Parker, R. H. Schumm, I. Halow, S. M. Bailey, K. L. Churney and R. L. Nuttall, in *Journal of Physical and Chemical Reference Data Vol. 11, Supplement No. 2.* American Chemical Society and American Institute of Physics, Washington, D.C., 1982.

33. S. M. I. Al-Rafia, O. Shynkaruk, S. M. McDonald, S. K. Liew, M. J. Ferguson, R. McDonald, R. H. Herber and E. Rivard, *Inorg. Chem.*, 2013, **52**, 5581.

34. The concentration of **6** was determined by integration of the initial ^{1}H NMR resonances related to 4,4'-difluorobiphenyl as an internal standard.

35. G.-B. Shen, K. Xia, X.-T. Li, J.-L. Li, Y.-H. Fu, L. Yuan and X.-Q. Zhu, *J. Phys. Chem. A*, 2016, **120**, 1779.

36. (a) I. Lee, *Chem. Soc. Rev.*, 1995, **24**, 223; (b) A. Streitwieser, R. H. Jagow, R. C. Fahey and S. Suzuki, *J. Am. Chem. Soc.*, 1958, **80**, 2326.

37. In this analysis/discussion of the change in Ge-H and B-H stretching frequencies, I focused on isolated Ge-H and B-H stretches (three for each bond type) and did not include the impact of coupled Ge-H/B-H modes. When one does consider the impact of such coupled stretches, only modest overall changes in frequency (from Δ5 to Δ20 cm^{-1}) were seen at the various bond elongations investigated; thus, contributions from the coupled modes were ignored.

38. (a) Y. Fujioka, *Nature*, 1929, **124**, 11; (b) K. Venkateswarlu, *Nature*, 1947, **159**, 96; (c) J. Jehlička, H. G. M. Edwards and A. Culka, *Phil. Trans. R. Soc. A*, 2010, **368**, 3109.

39. T. Schaub, M. Backes and U. Radius, *Organometallics*, 2006, **25**, 4196.

40. U. Zoller, *Tetrahedron*, 1988, **44**, 7413.

41. (a) L. A. Curtiss, M. P. McGrath, J.-P. Blaudeau, N. E. Davis, R. C. Binning and L. Radom, *J. Chem. Phys.* 1995, **103**, 6104; (b) R. Krishnan, J. S. Binkley, R. Seeger and J. Pople, *J. Chem. Phys.* 1980, **72**, 650.

42. E. D. Glendening, J. K. Badenhoop, A. E. Reed, J. E. Carpenter, J. A. Bohmann, C. M. Morales and F. Weinhold, NBO 5.9. Theoretical Chemistry Institute, University of Wisconsin, Madison, WI, 2012; http://www.chem.wisc.edu/~nbo5.

43. M. J. Frisch, G. W. Trucks, H. B. Schlegel, G. E. Scuseria, M. A. Robb, J. R. Cheeseman, G. Scalmani, V. Barone, G. A. Petersson, H. Nakatsuji, X. Li, M. Caricato, A. V. Marenich, J. Bloino, B. G. Janesko, R. Gomperts, B. Mennucci, H. P. Hratchian, J.V. Ortiz, A. F. Izmaylov, J. L. Sonnenberg, D. Williams-Young, F. Ding, F. Lipparini, F. Egidi, J. Goings, B. Peng, A. Petrone, T. Henderson, D. Ranasinghe, V. G. Zakrzewski, J. Gao, N. Rega, G. Zheng, W. Liang, M. Hada, M. Ehara, K. Toyota, R. Fukuda, J. Hasegawa, M. Ishida, T. Nakajima, Y. Honda, O. Kitao, H. Nakai, T. Vreven, K. Throssell, J. A. J. Montgomery, J. E. Peralta, F. Ogliaro, M. J. Bearpark, J. J. Heyd, E. N. Brothers, K. N. Kudin, V. N. Staroverov, T. A. Keith, R. Kobayashi, J. Normand, K. Raghavachari, A. P. Rendell, J. C. Burant, S. S. Iyengar, J. Tomasi, M. Cossi, J. M. Millam, M. Klene, C. Adamo, R. Cammi, J. W. Ochterski, R. L. Martin, K. Morokuma, O. Farkas, J. B. Foresman and D. J. Fox, Gaussian 16, Revision B.01, Gaussian, Inc., Wallingford CT.

44. (a) A. D. Becke, *J. Chem. Phys.*, 1993, **98**, 5648; (b) C. Lee, W. Yang and R. G. Parr, *Phys. Rev. B*, 1988, **37**, 785; (c) S. H. Vosko, L. Wilk and M. Nusair, *Can. J. Phys.*, 1980, **58**, 1200; (d) P. J. Stephens, F. J. Devlin, C. F. Chabalowski and M. J. Frisch, *J. Phys. Chem.*, 1994, **98**, 11623.

45. (a) G. M. Sheldrick, *Acta Cryst.*, 2015, **A71**, 3; (b) G. M. Sheldrick, *Acta Cryst.*, 2015, **C71**, 3.

Chapter 3: Access to Metastable $[GeH_2]_n$ Materials via a Molecular "Bottom-up" Approach

3.1 Introduction

Main group element hydrides play a central role in the development of modern chemical vapour and atomic layer deposition (CVD/ALD) strategies,[1] with the use of Group 14 tetrelanes EH_4 (E = Si, Ge and Sn) as volatile element (E) sources being prevalent.[2] Much less is known about the related low oxidation state inorganic methylenes $[EH_2]_n$,[3–5] which can be globally viewed as structural analogues to polyethylene. Poly(dihydrosilylene) $[SiH_2]_n$ has been accessed via the Wurtz-type reduction of I_2SiH_2 with alkali metals, and via the addition of hydrochloric acid to CaSi.[4] A related $[GeH_2]_n$-type material was prepared by Royen and coworkers in 1933 by the addition of acid to CaGe;[5] this product was obtained as an orange solid that decomposed explosively in air when ground. A related hydride-rich product has been obtained from the reaction of Ge(II) dihalides and Li[Et_3BH], and described as "solvochemically activated germanium", although this amorphous material is terminated by both Ge–Cl and Ge–H bonds.[5c] While it is tempting to make a structural link between the latter $[GeH_2]_n$ materials and linear polyethylene, the nature of the reaction of proton sources with the layered ionic material CaGe (*i.e.*, heterogeneous reaction) does not completely rule out the possibility of incomplete hydrogen functionalization at Ge or sample contamination with Ca by-products. Overall, such $[EH_2]_n$ metastable materials are still of great interest as they remain an understudied class of binary element hydride with

possibly novel properties, including substantial σ-electron delocalization modulated via E–E bonding.[6]

The Rivard Group has previously explored the coordination chemistry of inorganic methylenes (SiH_2, GeH_2 and SnH_2) via "donor–acceptor" stabilization protocols.[7] More recently, it has been shown that both complexes of SiH_2 and GeH_2 could be used to release/deposit films of elemental silicon and germanium, respectively, from solution and under mild conditions (<110 °C).[8] The work of Jones, who showed that catalytically active Ge(II) hydrides (LGeH, L = bulky amide group) could be accessed via O^{t}Bu/H exchange,[9] inspired the current "bottom-up" approach to $[GeH_2]_n$ starting from soluble hydride sources and molecular $[Ge(O^tBu)_2]$ (**1**).[10] $[Ge(O^tBu)_2]$ (**1**) is actually a dimeric species in the solid-state with bridging ^{t}BuO groups, $[(^tBuO)Ge(\mu\text{-}O^tBu)_2Ge(O^tBu)]$, but for simplicity it will be drawn as $[Ge(O^tBu)_2]$ (**1**) throughout this Chapter. This Chapter summarizes explorations towards mild preparations of $[GeH_2]_n$ and describes a facile route to thin films of amorphous Ge, examples of hydroboration catalysis, as well as computational details regarding the energetics associated with $[GeH_2]_n$ formation.

3.2 Results and discussion

*3.2.1 Improved route to $[Ge(O^tBu)_2]$ (**1**)*

The route to $[GeH_2]_n$ explored in this Chapter is based on combining the known Ge(II) bis(alkoxide) $[Ge(O^tBu)]_2$ (**1**)[10] with hydride sources to instigate O^{t}Bu/H group exchange at Ge. Somewhat surprisingly, previously known syntheses of **1** were laborious

and involved reacting either germanocene Cp_2Ge ($Cp = C_5H_5^-$)[10] or Veith's germylene $Ge[(N^tBu)_2SiMe_2]$[11] with two equivalents of HO^tBu. Initial attempts to generate **1** more directly via combining the commercially available $Cl_2Ge{\cdot}$dioxane with two equivalents of $K[O^tBu]$ led invariably to the germanide salt, $K[Ge(O^tBu)_3]$.[12] While $K[Ge(O^tBu)_3]$ has been utilized previously,[12b] it lacks a published preparation or crystal structure, which are included in this Chapter for completeness (Figure 3.27). This improved route to **1** started with the intentional synthesis of $K[Ge(O^tBu)_3]$ from $Cl_2Ge{\cdot}$dioxane and three equivalents of $K[O^tBu]$ in THF (95 % isolated yield), followed by addition of an appropriate amount of $Cl_2Ge{\cdot}$dioxane to $K[Ge(O^tBu)_3]$ in benzene to give $[Ge(O^tBu)_2]$ (**1**) as a white solid (94 % isolated yield; Scheme 3.1).[10] As noted previously, $[Ge(O^tBu)_2]$ (**1**) exists as both a monomer and dimer in solution, and this equilibrium was probed with variable temperature NMR (VT-NMR) spectroscopy and is shown in Figure 3.1.

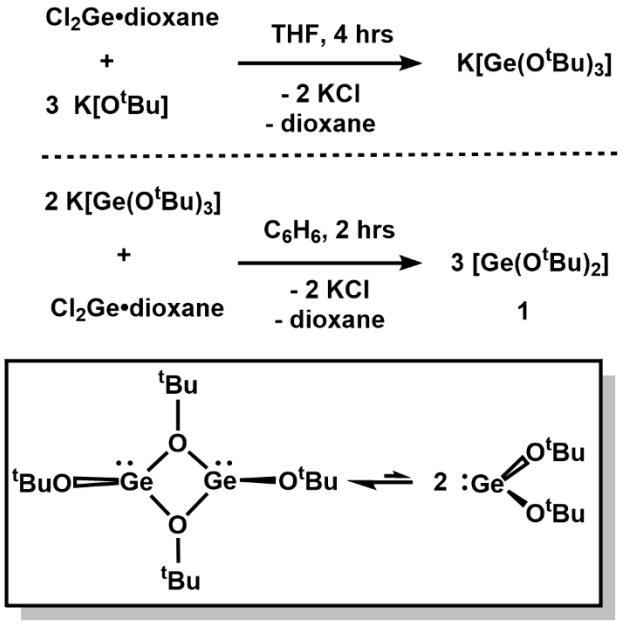

Scheme 3.1. Synthesis of $[Ge(O^tBu)_2]$ (**1**) via a two-step approach.

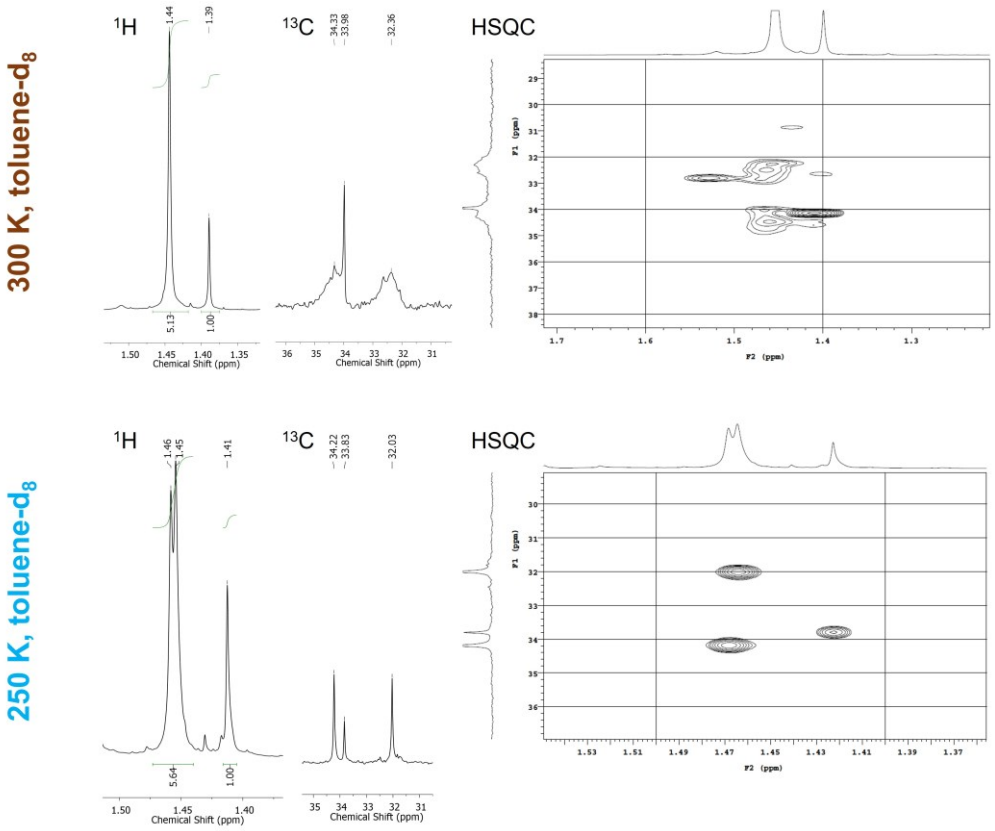

Figure 3.1. VT-NMR and HSQC (heteronuclear single quantum coherence) experiments of [Ge(O^{t}Bu)$_2$] (**1**) in toluene-D$_8$ were conducted. The broad ^{1}H singlet identified as the dimer (1.44 ppm) is resolved into two environments (1.45 and 1.46 ppm, due to [^{t}*Bu*OGe(μ-O^{t}Bu)$_2$GeO^t*Bu*] and [^{t}BuOGe(μ-O^t*Bu*)$_2$GeO^{t}Bu], respectively) at 253 K. These peaks are correlated with HSQC to the broad singlets in the ^{13}C{^{1}H} spectrum, which are also more defined at low temperature. The narrow singlet at 1.39 ppm in ^{1}H spectrum at 300 K is identified as the monomer of the same species; some exchange is noted at low temperatures by the increased relative integration of the dimer-assigned peak. The initial relative integrations between the two species are restored upon return to 300 K.

3.2.2 Hydride metathesis

With a convenient route to [Ge(O^{t}Bu)$_2$] (**1**) in place, hydride metathesis to yield poly(dihydrogermylene) [GeH$_2$]$_n$ was then explored. Treatment of **1** with excess (three equivalents) of pinacolborane, HBpin, in benzene led to the formation of an orange precipitate and a very pale yellow supernatant. Analysis of the supernatant by ^{1}H, ^{11}B and ^{13}C{^{1}H} NMR spectroscopy confirmed that consumption of **1** had transpired (as seen in Figure 3.2), with formation of the expected soluble metathesis product, ^{t}BuOBpin,[13] as summarized in Scheme 3.2. IR spectroscopy on the resulting orange solid (**2a**) confirmed the presence of an intense Ge–H stretching band at 1996 cm^{-1}, which is in the region expected for Ge(II) hydrides.[7–9,14] However, added bands at *ca.* 2970 and 1100–1400 cm^{-1} were observed in this IR spectrum, consistent with C–H and C–C/C–O stretches, indicating the retention of some O^{t}Bu groups. This postulate was supported by elemental analysis (C, H), which was consistent with an approximate molecular formula of [GeH$_{1.64}$(O^{t}Bu)$_{0.36}$]$_n$ for this material (**2a**). Attempts to yield Ge products with higher hydride content by treatment of **1** with excess HBpin (up to 10 equivalents) and longer reaction times (up to two days) at room temperature gave insoluble products with similar composition as **2a**.

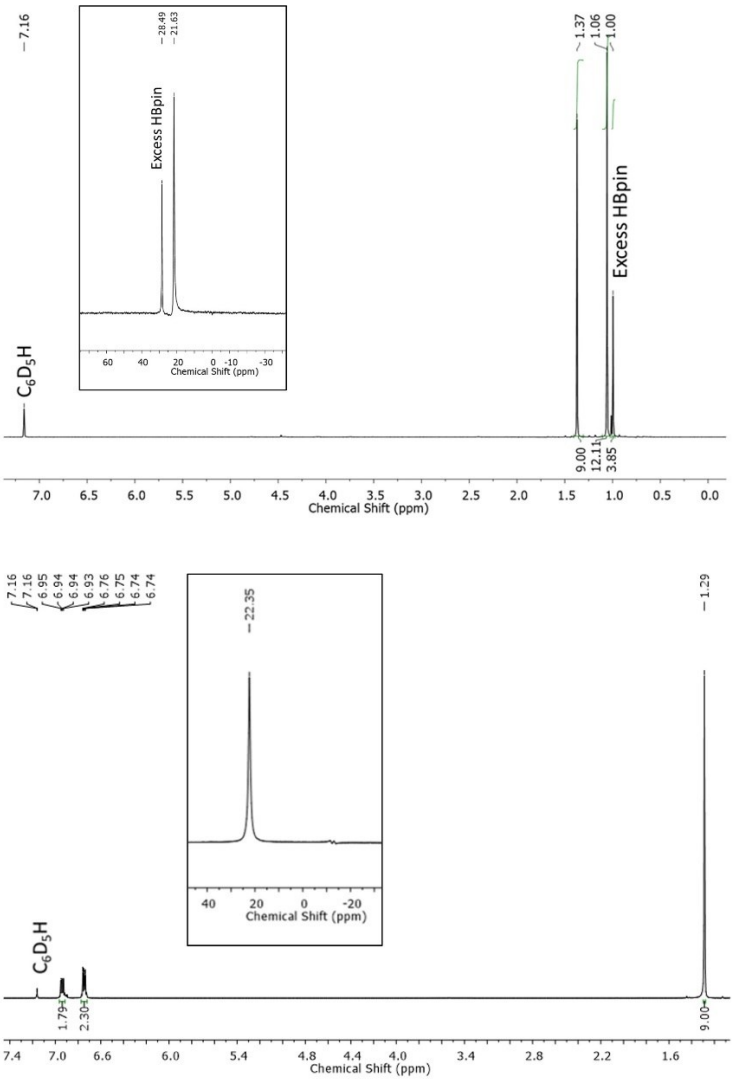

Figure 3.2. ^{1}H and $^{11}B\{^{1}H\}$ (insets) NMR spectra in C_6D_6 of the soluble fraction of the reactions to synthesize **2a** (^{t}BuOBpin,[13] top) and **2b** (^{t}BuOBcat,[15] bottom).

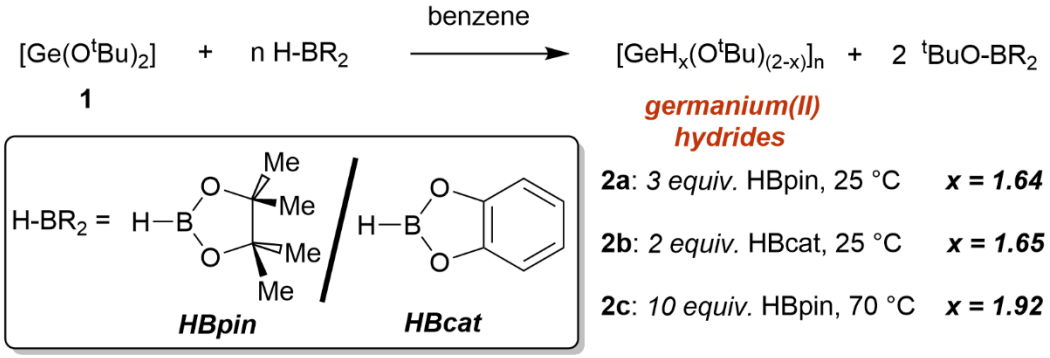

Scheme 3.2. Reaction of $[Ge(O^tBu)_2]$ (**1**) with the hydride sources HBpin and HBcat to yield products with $[GeH_x(O^tBu)_{(2-x)}]_n$ compositions (x = 1.64 to 1.92; **2a**–**2c**). The H and O^tBu content in the products were estimated by elemental analysis (C, H).

In an attempt to fully replace the O^tBu groups in $[Ge(O^tBu)_2]$ (**1**) with hydrides, compound **1** was combined with two equivalents of catecholborane, HBcat, a generally more reactive hydride source than HBpin (Scheme 3.2). This time, a pale yellow precipitate formed (**2b**) and the expected borane by-product $^tBuOBcat$[15] was detected in solution by ^1H, ^{11}B, and $^{13}C\{^1H\}$ NMR spectroscopies (seen in Figure 3.2). While the characterization and degree of substitution in the product **2b** bears striking resemblance to that of **2a**, an in-depth comparison of the two materials was not undertaken; instead, focus was placed on alternate methods to decreasing the $–O^tBu$ content further (see below).

Another attempt to yield pure $[GeH_2]_n$ involved combining **1** with diisobutylaluminum hydride (DIBAL-H) in benzene at 70 °C. In contrast with the abovementioned reactions with HBpin and HBcat, an orange-yellow solution formed with no visible sign of a precipitate. Analysis of the reaction mixture by mass

spectrometry indicated the formation of Al-containing by-products. ^{1}H NMR and ^{13}C{^{1}H} NMR spectroscopy analysis showed the consumption of **1**, with a major set of peaks that have been assigned as $[(^{t}BuO)Al^{i}Bu_2]_2$ and $[^{i}Bu_2Al(\mu\text{-}H)(\mu\text{-}O^{t}Bu)Al^{i}Bu_2]$,[16] the expected products from O^{t}Bu/H exchange with DIBAL-H. Removal of the benzene solvent and addition of pentane led to the precipitation of a deep yellow-orange solid; elemental analysis of this product revealed a high carbon content (%C: 16.73), in line with the retention of ^{t}BuO (and possibly ^{i}Bu) groups. Given the high organic group content in this germanium hydride, no further explorations with DIBAL-H as a hydride source were pursued.

Undaunted by the inability to obtain a pure germanium(II) dihydride product from the abovementioned chemistry, the reaction between $[Ge(O^{t}Bu)_2]$ (**1**) and 10 equivalents of HBpin, was re-investigated but with added heating. Specifically, heating a 10:1 mixture of HBpin and **1** to 70 °C in benzene gave an orange precipitate after 24 hours (Scheme 3.2). The solid-state IR spectrum of this product, **2c**, (Figure 3.3) contained three intense bands at 2014, 810, and 772 cm^{-1}. The IR band at 2014 cm^{-1} can be assigned to Ge–H stretches,[7–9,14] while the lower frequency bands are consistent with GeH_x bending modes.[5b,17] The greatly reduced intensity of IR bands belonging to O^{t}Bu residues in **2c** (Figure 3.3) was also encouraging as it is congruent with a higher degree of O^{t}Bu/H exchange. In this case, elemental analysis (C, H) was used to derive a product formula of $[GeH_{1.92}(O^{t}Bu)_{0.08}]_n$ (**2c**; Scheme 3.2), corresponding to an impressive degree of O^{t}Bu/H substitution on **1** of 96 % (note: two substitution events at each Ge centre are required to afford $[GeH_2]_n$).

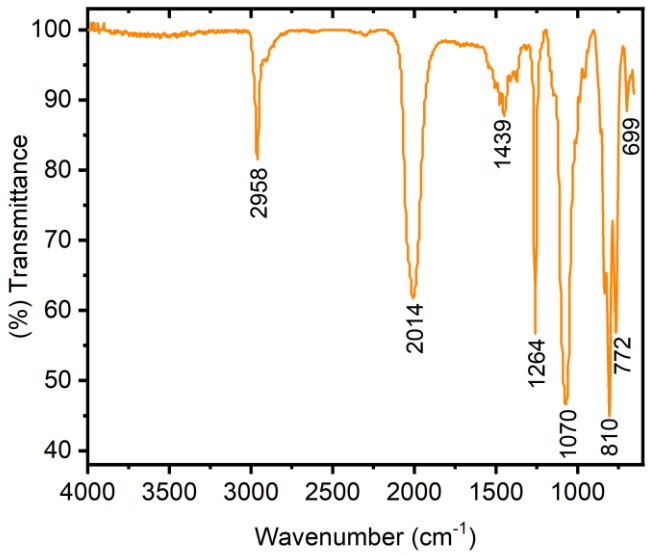

Figure 3.3. FT-IR spectrum of $[GeH_{1.92}(O^tBu)_{0.08}]_n$ (**2c**).

The composition of compound **2c** was analyzed further by XPS (Figure 3.4) and EDX (Figure 3.5b), showing similar atomic content and germanium oxidation state as in a previously reported sample of $[GeH_2]_n$ obtained from the reaction of CaGe with HCl.[5b] Boron was not detected by XPS or EDX, and flame tests versus boron mass% standards determined that **2c** contains less than ca. 0.085 mass% B. Ge(II) hydrides are known to undergo hydride migration to yield mixed oxidation state Ge(I)/Ge(III) environments, thus the proposed branched structures of these $[GeH_2]_n$ materials (in place of linear $[GeH_2]_n$ arrays) is not surprising. The low H content obtained by elemental analysis is likely due to incomplete combustion, and the assignment of **2c** as $[GeH_2]_n$ is evidenced by the similarity of its optoelectronic properties (E_g = 2.5 eV) to known $[GeH_2]_n$

species;[5b] for comparison, the Ge(I) derivatives $[GeH]_n$ have much lower optical band gaps of 1.4 to 1.6 eV,[5d] which is discussed in greater detail below.

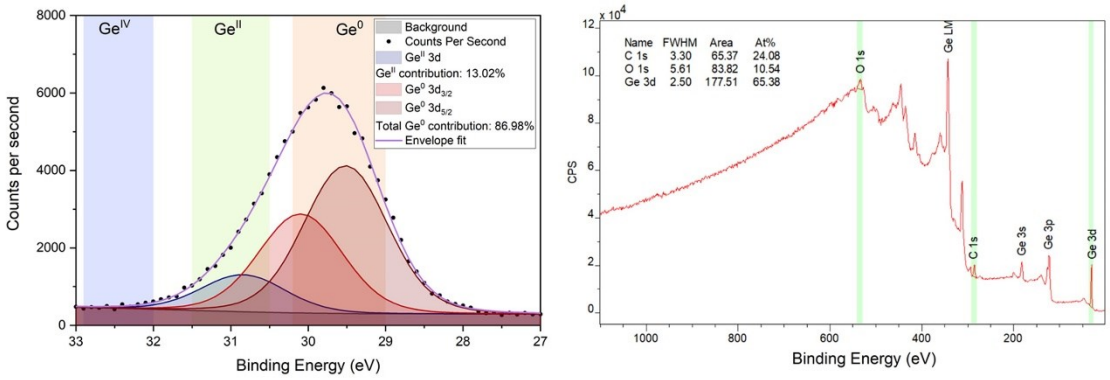

Figure 3.4. High resolution (Ge, 3d, left) and survey (right) XP spectrum of **2c**, referenced to adventitious C 1s (284.8 eV). A strong shoulder next to the Ge 3s peak would be expected if B is present; B 1s energy (Binding energy = 188 eV) overlaps with the edge of the Ge 3s peak (BE = 181 eV). No prominent shoulder is noted, indicating low to no boron incorporation.

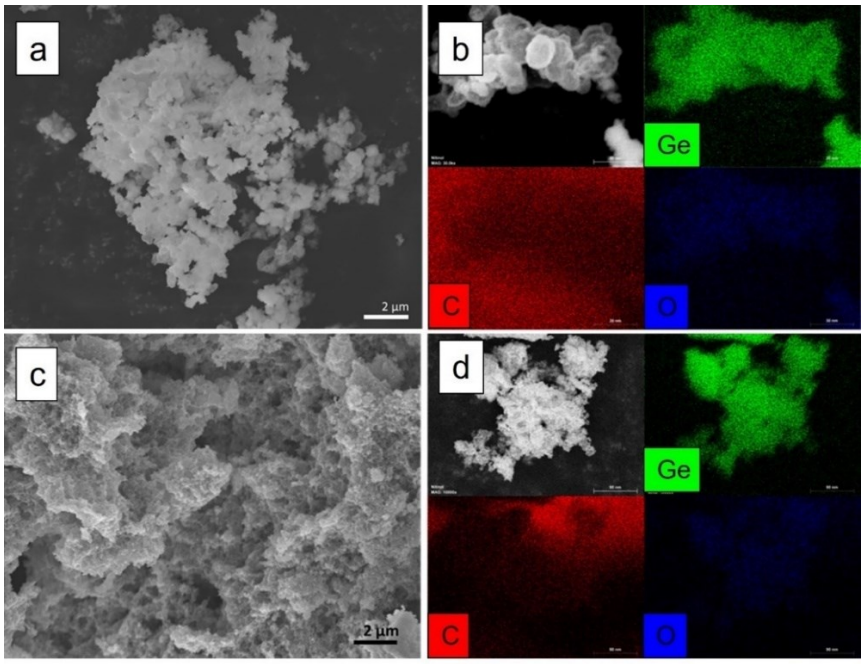

Figure 3.5. (a) SEM secondary electron capture and (b) EDX mapping of **2c** deposited onto carbon tape. (c) SEM secondary electron capture and (d) EDX mapping of **2c** heated to 200 °C for two hours under N_2 and deposited onto carbon tape. Collected at 10 kV.

Analysis of the optical band gap (E_g) in the germanium hydride **2c** was achieved by diffuse reflectance absorption (DRA) spectroscopy, which afforded an estimated E_g value of 2.5 eV (Figure 3.6). Employment of an air-free system was necessary to prevent the decomposition of **2c**. The estimated E_g value in **2c** falls in the range of those found in previously known $[GeH_2]_n$ materials (2.2 to 2.7 eV).[5b] The question relating to the possible structure of **2c** is complicated by the amorphous nature of this solid (see Figure 3.9), and this point will be further discussed when computations on model $[GeH_2]_n$ species are introduced. Heating of **2c** at 200 °C for 2 hours afforded a black solid, which showed a UV-Vis absorption profile that extended up to 800 nm, *ca.* 1.5 eV.

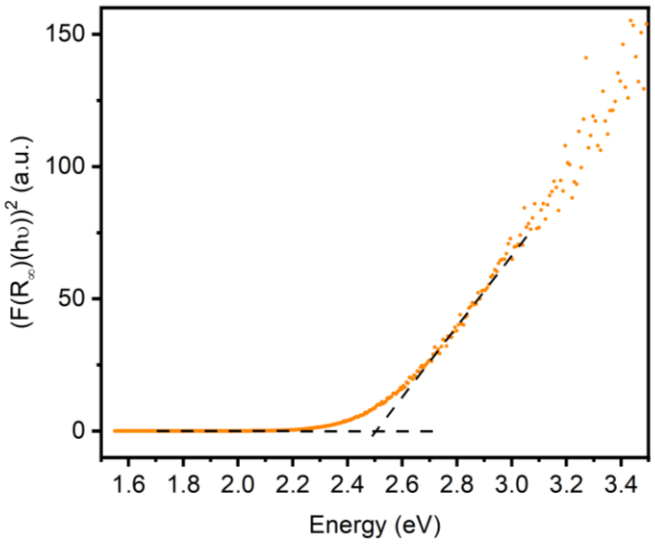

Figure 3.6. Diffuse reflectance absorption plot of $[GeH_{1.92}(O^tBu)_{0.08}]_n$ (**2c**).

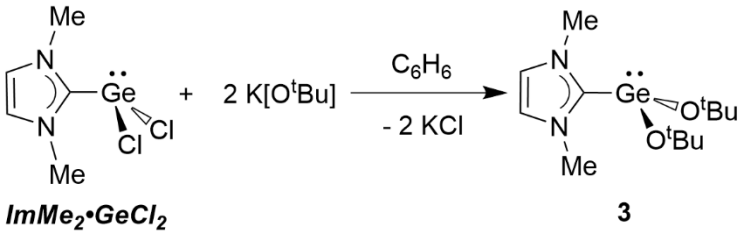

ImMe$_2$•GeCl$_2$ **3** (3.1)

Postulating that an increase in nucleophilicity of the Ge bound O^{t}Bu groups would facilitate O^{t}Bu/H exchange with HBpin, the *N*-heterocyclic carbene complex ImMe$_2$•Ge(O^{t}Bu)$_2$ (**3**) (ImMe$_2$ = [(HCNMe)$_2$C:]) was prepared by combining the known precursor ImMe$_2$•GeCl$_2$ [8a,18] with two equivalents of K[O^{t}Bu] in benzene (76 % yield; equation (3.1)). Yellow crystals of **3** of suitable quality for single-crystal X-ray diffraction were grown from toluene at −35 °C. The resulting structure revealed the presence of a monomeric adduct with the expected trigonal pyramidal geometry at Ge, due to the stereochemically active lone pair at the Ge(II) centre (Figure 3.7). The C1–Ge bond

length in **3** is comparable to the C_{NHC}–Ge distance in the previously reported bis(alkoxy)germylene adduct Im^{i}Pr$_2$Me$_2$•Ge(O^{t}Bu)$_2$ (Im^{i}Pr$_2$Me$_2$ = (MeCN^{i}Pr)$_2$C:),[18b] while a similar trigonal pyramidal geometry can be found about the Ge centre in each complex.

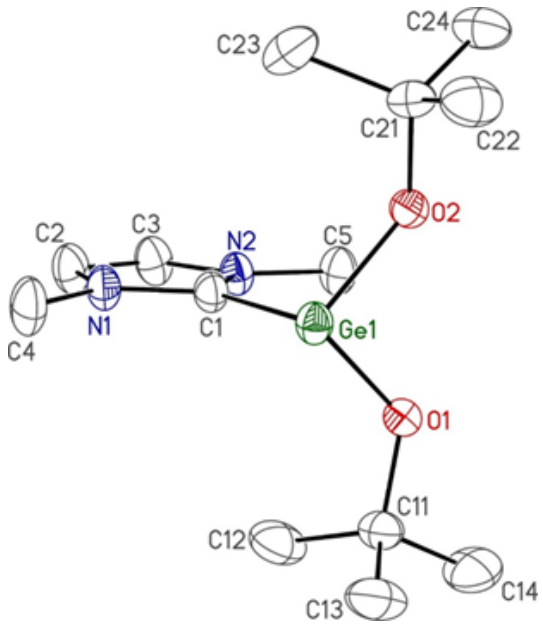

Figure 3.7. ORTEP of one of the two crystallographically independent molecules of ImMe$_2$•Ge(O^{t}Bu)$_2$ (**3**). Thermal ellipsoids are presented at a 30 % probability level, and all hydrogen atoms have been omitted for clarity. Selected bond lengths [Å] and angles [°] with values belonging to the second molecule in the asymmetric unit shown in square brackets: C1–Ge1 2.107(3) [2.113(3)], Ge1–O1 1.8480(19) [1.850 (2)], Ge1–O2 1.8508(19) [1.837(2)]; N1–C1–N2 104.6(2) [104.5(2)], C1–Ge1–O1 120.78(6) [123.57(7)], C1–Ge1–O2 123.23(6) [122.03(7)].

Treatment of **3** with two equivalents of HBpin in benzene gave a red-orange precipitate after 24 hours, which was isolated by filtration and washed with further aliquots of benzene before drying. In contrast to the [GeH$_x$(O^{t}Bu)$_{(2-x)}$]$_n$ materials

previously obtained (**2a** and **2b** in Scheme 3.2), this red-orange solid was very reactive and immediately decomposed exothermically in air, with the copious evolution of smoke. FT-IR analysis indicated that O^{t}Bu/H exchange at Ge in **3** did transpire, however elemental analysis detected substantial N content (%N: 4.7), thus, it appears that some imidazole (carbene) moieties remain as part of this insoluble solid. This synthetic pathway to $[GeH_2]_n$ materials was not pursued further, as **2c** was identified as the most highly H-substituted material, and further investigations were undertaken to better understand its reactivity.

*3.2.3 Reactivity of $[GeH_{1.92}(O^tBu)_{0.08}]_n$ (**2c**)*

While **2c** is insoluble, it was endeavoured to determine whether it could act as a heterogeneous source of GeH_2. First, Bourissou's intramolecular frustrated Lewis pair (FLP), ^{i}Pr$_2$P(C$_6$H$_4$)BCy$_2$ (Cy = cyclohexyl; **PB**),[19] was employed as a trapping agent, as it has been previously shown by the Rivard group to coordinate a GeH_2 unit to give the donor–acceptor complex PB{GeH_2}.[8b] To first identify whether this complex could be employed to trap GeH_2 *in situ*, [Ge(O^{t}Bu)$_2$] (**1**) and two equivalents of HBpin was reacted in THF in the presence of one equivalent of the **PB** ligand (Scheme 3.3). The expected GeH_2 complex PB{GeH_2}[8b] could be identified (see Figure 3.8) in the reaction mixture by ^{11}B and ^{31}P NMR spectroscopy (*ca.* 30 % yield; albeit after 7 days); an insoluble orange precipitate was also observed in this reaction mixture. This result lends support to the hypothesis that **2c** is formed by the oligomerization of GeH_2.

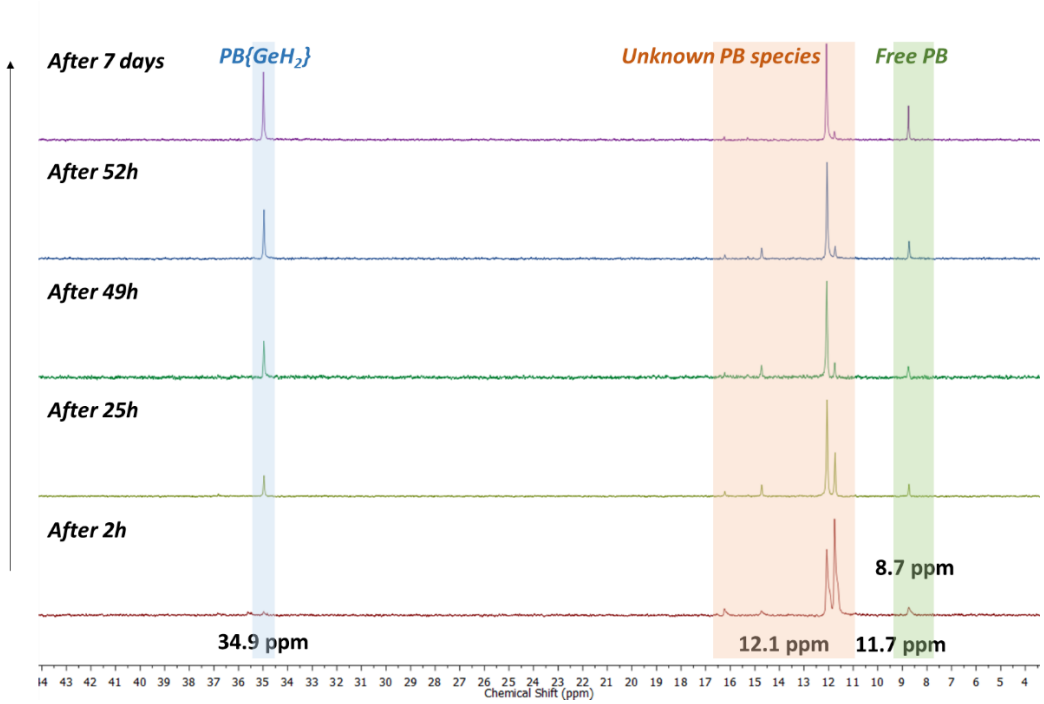

Figure 3.8. $^{31}P\{^{1}H\}$ NMR spectrum of the reaction mixture from $[Ge(O^tBu)_2]$ (**1**) and 2 equivalents of HBpin in the presence of **PB**, showing the gradual production of $PB\{GeH_2\}$[8b] and an unknown **PB**-containing species.

To determine if GeH_2 units could be released from $[GeH_{1.92}(O^tBu)_{0.08}]$ (**2c**), **PB** was added to a slurry of **2c** in C_6D_6 and heated to 60 °C. No $PB\{GeH_2\}$[8b] was detected by NMR spectroscopy. A similar experiment was undertaken with 2,3-dimethylbutadiene as the trapping agent,[20] again without any discernable reaction. These experiments show that **2c** does not act as a heterogenous source of discrete GeH_2 units under mild conditions.

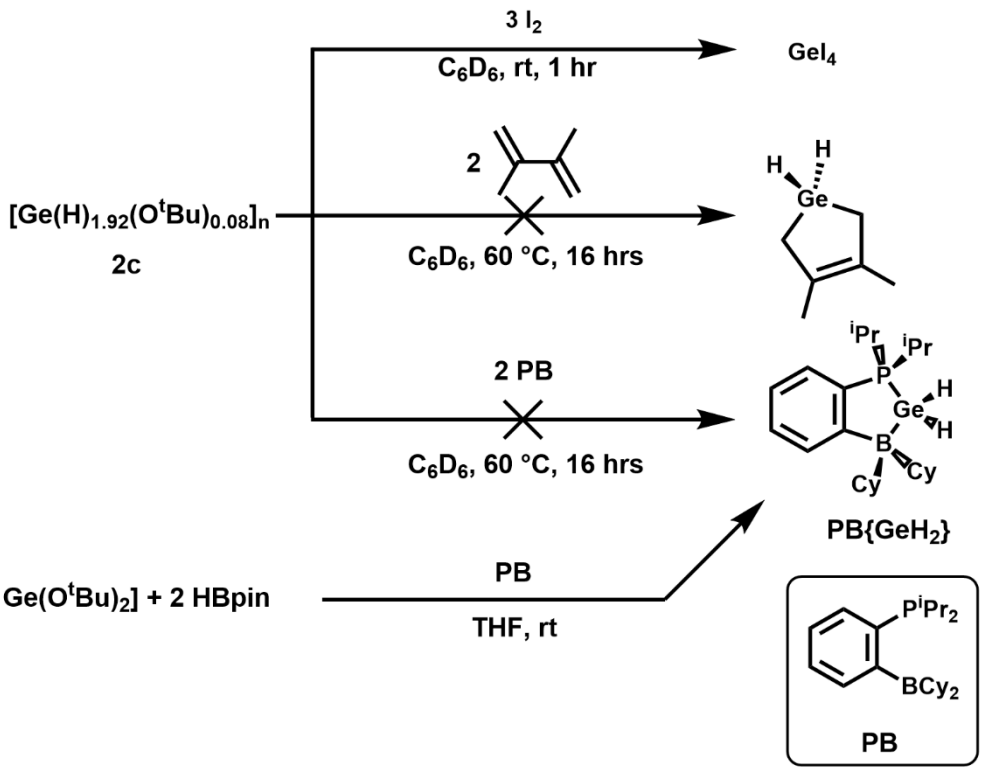

Scheme 3.3. Reactivity of $[GeH_{1.92}(O^tBu)_{0.08}]_n$ **2c**.

Following previous reports of the reaction of $(GeH_x)_n$ materials with halogens,[5d] **2c** was combined with an excess of I_2 at room temperature in C_6H_6, which yielded an orange-yellow solution (Scheme 3.3). After one hour, GeI_4 was recovered as a yellow solid in 87 % yield and identified by powder XRD.[21] This result is encouraging as it demonstrates that **2c** is not entirely unreactive when slurried in organic solvents.

Given the Rivard Group's experience with the use of GeH_2-complexes to form Ge nanoparticles and films upon heating,[7e,8] the use of **2c** as a precursor to elemental Ge (likely) via H_2 loss was explored. Powder XRD of the freshly collected **2c** exhibits broad amorphous reflection patterns whose peaks are consistent with a previous report on bulk

amorphous Ge (Figure 3.9, orange trace).[8a] Heating **2c** under N_2 for 2 hours results in a black granular powder that exhibits new/sharp reflections due to the (111) and (220) reflection planes of α-crystalline Ge,[22] imposed on a broad amorphous pattern (Figure 3.9, black trace).

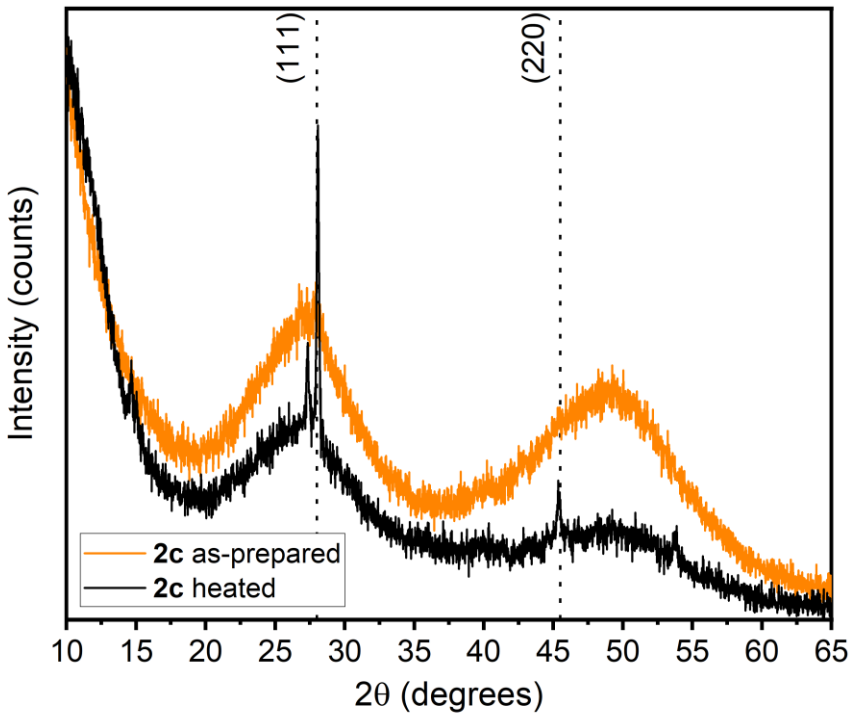

Figure 3.9. Powder XRD of **2c** (orange) and the same precipitate after being heated for 2 hours at 200 °C under N_2 to yield semi-crystalline Ge (black).

While the morphology of **2c** resembles agglomerated particles (200–500 nm in diameter) by secondary electron SEM (Figure 3.5a and b), the heated product appears to have undergone a sintering process whereby individual particles can no longer be

identified (Figure 3.5c and d). To recap, thermal treatment of **2c** appears to lead to the loss of hydrogen and formation of a semicrystalline sample of elemental Ge.

3.2.4 Catalysis studies

Both [Ge(O^{t}Bu)$_2$] (**1**) and the germanium hydride **2c** promote the borylation of aldehydes with HBpin. In the case of **2c**, this transformation appears to be stoichiometric in nature, while only modest turnover frequencies (up to 0.16 h^{-1} at 25 °C) were noted with **1** as a pre-catalyst.

In a pioneering 2014 study,[9,23] the Jones Group showed that bulky low coordinate Ge(II) hydrides, such as L(H)Ge: (L = [N(C$_6$H$_2${C(H)Ph$_2$}$_2$^{i}Pr-2,6,4)(Si^{i}Pr$_3$)]) could be used to promote the very rapid hydroboration of ketones and aldehydes.[9,23] As a result, the abovementioned Ge(II) species [Ge(O^{t}Bu)$_2$] (**1**), [GeH$_{1.92}$(O^{t}Bu)$_{0.08}$]$_n$ (**2c**) and ImMe$_2$•Ge(O^{t}Bu)$_2$ (**3**) were tested for similar catalytic hydroboration chemistry (Scheme 3.4). To begin, a stoichiometric quantity of [Ge(O^{t}Bu)$_2$] (**1**) was added to solutions of various alkene and alkyne substrates and HBpin (1:1:2 molar ratio) in C_6D_6 at room temperature; however, no reaction was found after 48 hours of stirring. Fortunately, **1** was able to act as a hydroboration catalyst towards ketones and aldehydes, with the best result when 10 mol% of [Ge(O^{t}Bu)$_2$] (**1**) was combined with 4-dimethylamino-benzaldehyde and HBpin (two equivalents) at 25 °C in C_6D_6, leading to a conversion of 75 % after 48 hours (80 % after 20 hours at 70 °C), relative to 4,4'-difluorobiphenyl as an ^{1}H NMR internal standard. For comparison, a related pre-catalyst [IPr•GeO^{t}Bu]$^+$ (IPr = [(HCNDipp)$_2$C:]; Dipp = 2,6-^{i}Pr$_2$C$_6$H$_3$) achieved the quantitative hydroborylation of 4-

dimethylaminobenzaldehyde under 6 hours.[23c] Similar conversions (80 % borylation of 4-dimethylaminobenzaldehyde after 48 hours at 25 °C) were found using 10 mol% $ImMe_2$•$Ge(O^tBu)_2$ (**3**) as a pre-catalyst. Notably, mixing the aldehyde with HBpin for 48 hours at 25 °C in C_6D_6 only gave a trace amount (<3 %) of hydroboration product. Surprisingly, the insoluble hydride $[GeH_{1.92}(O^tBu)_{0.08}]_n$ (**2c**) also promoted (at 10 mol% loadings) the hydroboration of 4-$Me_2NC_6H_4C(O)H$, with 22 % conversion noted after 48 hours at 25 °C.

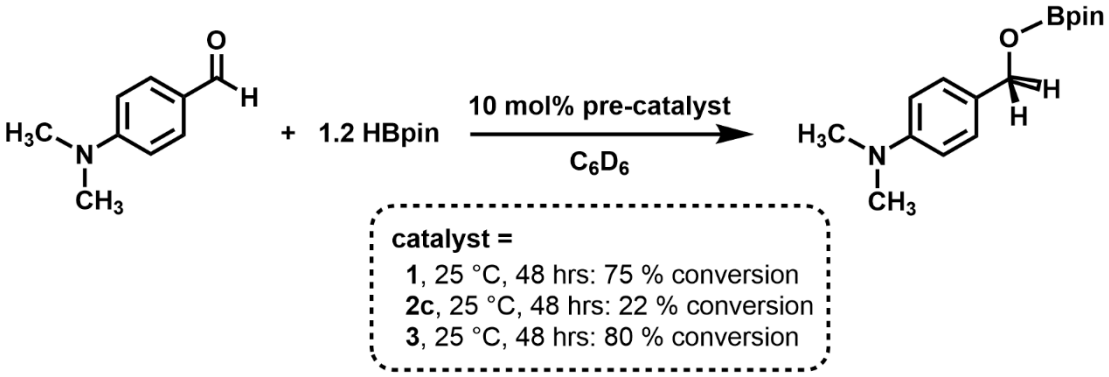

Scheme 3.4. Summary of borylation catalysis promoted by compounds **1**, **2c**, and **3**.

3.2.5 Deposition of thin films of Ge under mild conditions

As part of the quest to push the O^tBu/H substitution at the Ge centre in **1** to an even higher degree of completion, compound **1** was combined with H_3B•SMe_2 (3 equivalents; 2.0 M solution in THF) in toluene. Rather than forming an orange germanium(II) hydride product, the deposition of a mirror of elemental germanium was observed on the glass vial after a total of 5 days at room temperature. *In situ* ^1H and ^{11}B

NMR analyses (Figure 3.10) indicate the formation of $HB(O^tBu)_2$ as a major by-product of this reaction.

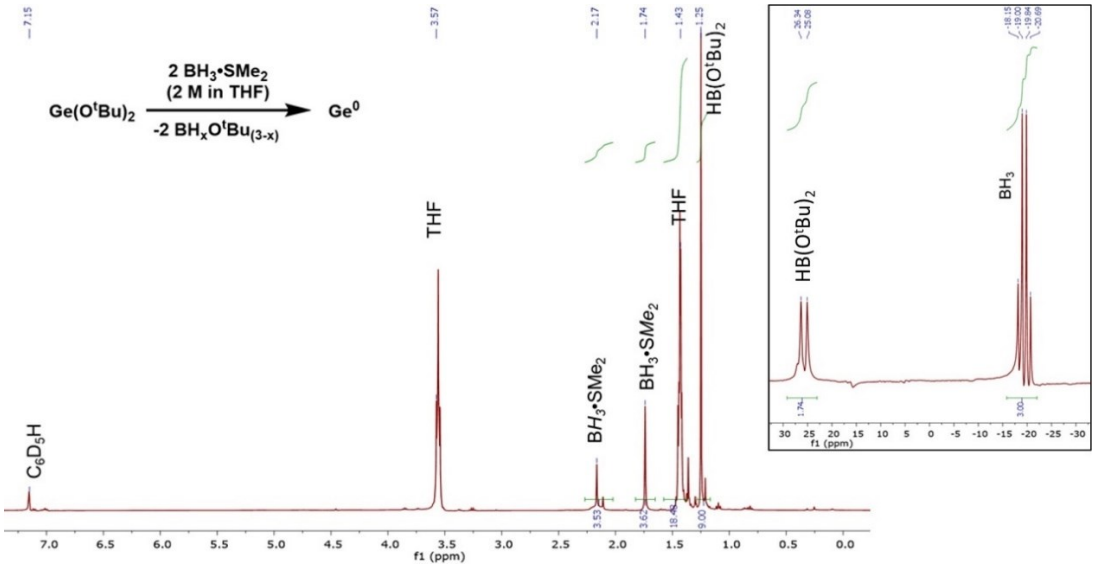

Figure 3.10. *In situ* ^1H NMR and ^{11}B (inset, right) spectrum of the reaction of $[Ge(O^tBu)_2]$ (**1**) with three equivalents of $H_3B{\bullet}SMe_2$ (2.0 M solution in THF) in C_6D_6 after heating for 2 hours at 70 °C.

At higher temperatures (70 °C), Ge mirrors could be deposited on different substrates, including polyethylene terephthalate (PET) (Figure 3.11, bottom left), with reaction times as short as one hour. As shown at the top left of Figure 3.11, the resulting Ge film adopts a lustrous gold-sheen when deposited onto a Si wafer. The optimal condition for Ge deposition involves combining a 0.014 M solution of **1** in toluene with three equivalents of $H_3B{\bullet}SMe_2$ (Figure 3.11), followed by heating at 70 °C for one hour. The thickness of the Ge film can be modified by changing the deposition time: after one hour of reaction Ge films that are 33 ± 5 nm thick were obtained, while 3 hour

depositions yield layers of 62 ± 18 nm (as determined by SEM). As shown in Figure 3.11, larger aggregates of roughly spherical Ge particulates are usually observed on the surface of the films, which could not be completely removed with toluene washes. Lower concentrations of [Ge(O^{t}Bu)$_2$] (**1**) or fewer equivalents of $H_3B{\bullet}SMe_2$ resulted in incomplete Ge coverage of the Si wafer.

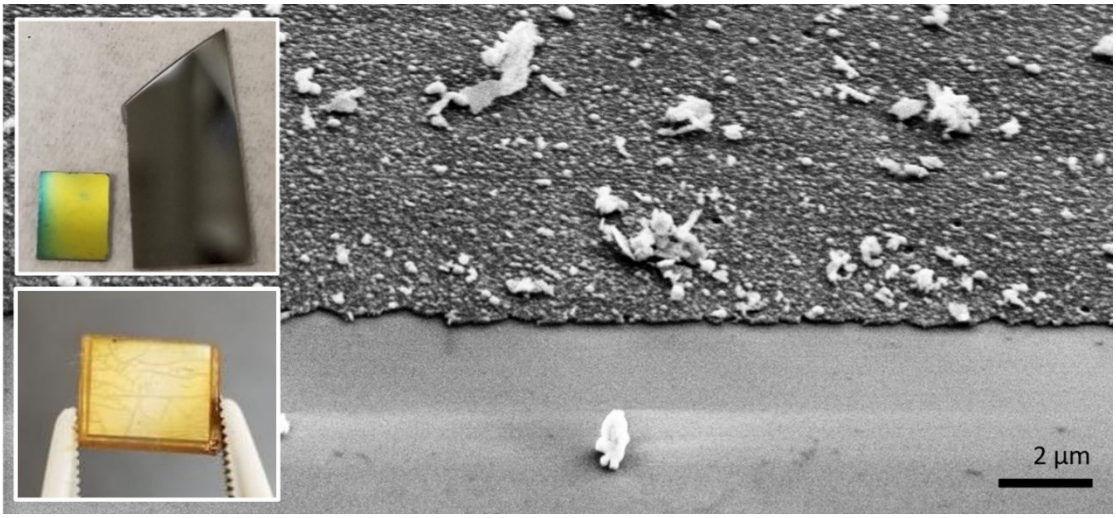

Figure 3.11. SEM of the deposited Ge film from the reaction of [Ge(O^{t}Bu)$_2$] (**1**) (0.014 M in toluene) with $H_3B{\bullet}SMe_2$ (3 equivalents) at 70 °C (3 hours). The bare Si wafer surface is shown in the bottom of the image; the layer was scraped away with a needle. Inset, top: photograph of the gold-coloured mirror coating of Ge (left) next to an unreacted Si wafer substrate (right). Inset, bottom: photograph of gold-coloured coating of Ge on a PET substrate.

While the deposited Ge films were too thin to obtain sufficient signal-to-noise ratios versus the crystalline Si background for Raman and pXRD analyses, the remaining dark red germanium precipitate was collected from the walls of the flask and analyzed.

EDX analysis did not identify the presence of any sulfur in the film (Figure 3.12a and b), however, an XPS spectrum did identify *ca.* 2 atom% S in the collected precipitate, and the binding energy noted (Figure 3.12c and d) was consistent with the presence of organosulfur species, such as surface SMe_2, in place of ionic GeS.

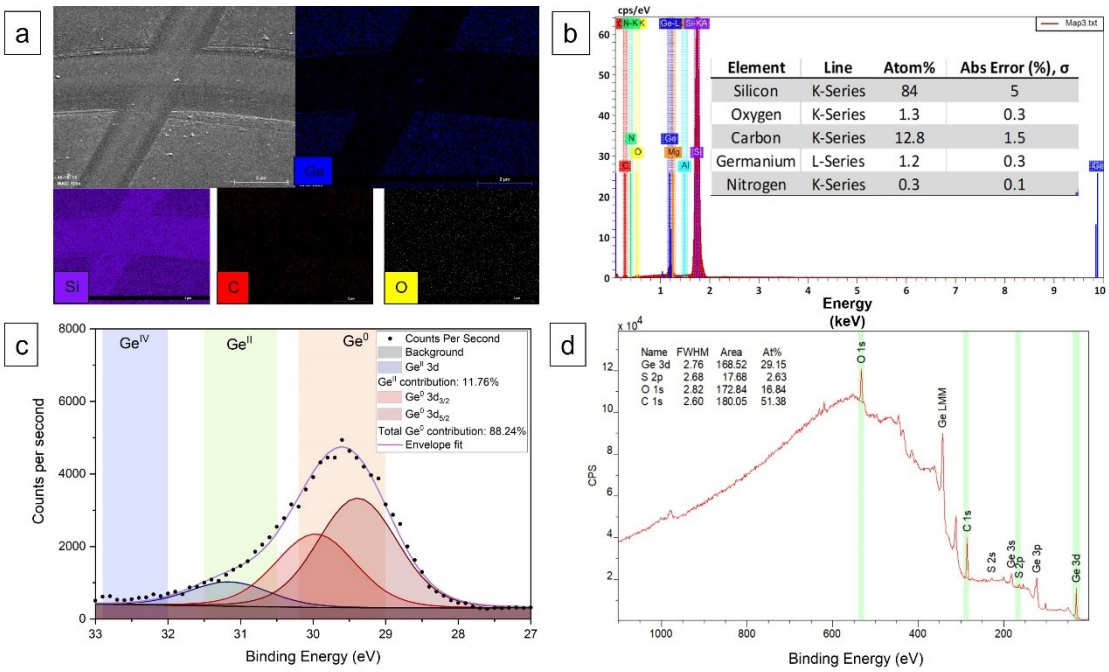

Figure 3.12. (a) EDX element mapping for the Ge film deposited on a Si wafer from combining three equivalents of $H_3B{\bullet}SMe_2$ (2.0 M solution in THF) with a 0.014 M solution of $[Ge(O^tBu)_2]$ (**1**) in 1.5 mL of toluene (heated to 70 °C for 3 hours), producing 62 ± 18 nm thick layers of Ge. Data collected at 5 kV. (b) EDX summary for the element mapping. (c) High resolution (Ge 3d) and (d) survey XP spectrum of precipitate, referenced to adventitious C 1s (284.8 eV). A small quantity of sulfur is detected.

Raman spectroscopy shows the expected Ge–Ge resonance at 290 cm^{-1} for this bulk sample of Ge (Figure 3.13a), while powder X-ray diffraction (pXRD) exhibits a

strong and broad peak that matches the expected (111) reflection of α-crystalline Ge, as well as broad features due to amorphous Ge (Figure 3.13b, red trace). Further crystallinity can be induced by subsequent heating of this bulk precipitate to 200 °C for 2 hours under N_2 (Figure 3.13, black trace) leading to the narrowing of the (111) reflection peak and in line with an increase in crystalline domain size as per the Scherrer equation.[24]

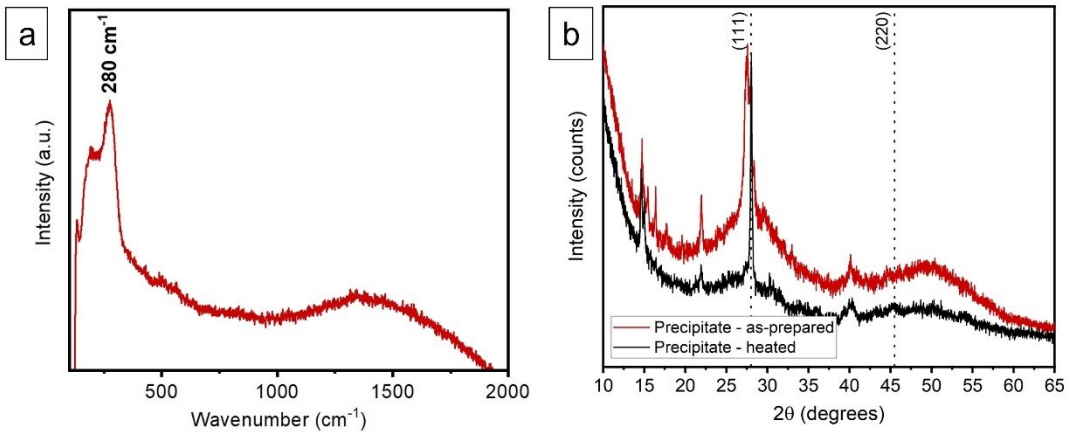

Figure 3.13. (a) Raman spectroscopy of the deposited Ge precipitate (same conditions as described for Figure 3.11) showing the amorphous Ge-Ge stretching frequency at 280 cm^{-1}. (b) Powder XRD of the sample as-prepared (red) and after being heated for 2 hours at 200 °C under N_2 to yield semi-crystalline Ge (black).

The preparation of Ge films by reacting the known monomeric Ge(II) bis(aryloxide) [Ge(OMes*)$_2$] (Mes* = 2,4,6-^{t}Bu$_3$C$_6$H$_2$)[25] with 3 equivalents of $H_3B{\cdot}SMe_2$ in toluene at 70 °C for 3 hours was also attempted. While an orange precipitate did form in the vial, repeating the reaction in the presence of a Si wafer provided poor results, with incomplete surface coverage and high quantities of residual oxygen and carbon, according to energy-dispersive X-ray (EDX) spectroscopy (see Figure 3.14).

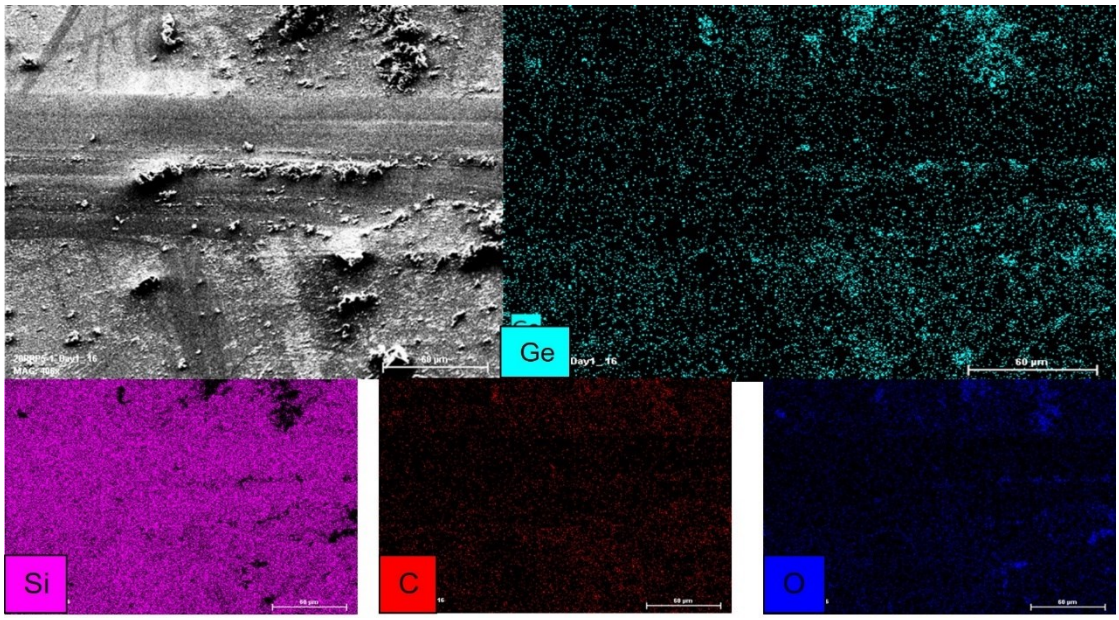

Figure 3.14. SEM backscatter electron image and EDX element mapping for the Ge film deposited from combining three equivalents of $H_3B{\bullet}SMe_2$ (2.0 M solution in THF) with a 0.021 M solution of $[Ge(OMes^*)_2]$ in 1.5 mL of toluene, producing inconsistent surface coverage. Data collected at 5 kV.

*3.2.6 Computed energetics associated with the reaction between [Ge(O^{t}Bu)$_2$] (**1**) and HBpin*

To better understand the energetics associated with $[GeH_2]_n$ information from the reaction of **1** with HBpin, computations at the M06-2X/cc-pVDZ[26] level of theory were undertaken. As expected by the solid-state structure of **1**,[10] the dimeric species $[(^tBuO)Ge(\mu\text{-}O^tBu)_2Ge(O^tBu)]$ is more stable than two equivalents of monomeric $[Ge(O^tBu)_2]$ by 48.6 kJ/mol (or 24.3 kJ/mol per mole of monomeric $[Ge(O^tBu)_2]$, as shown in Figure 3.15). With the exception of the free energy penalty associated with forming monomeric $[Ge(O^tBu)_2]$ from its dimer, the remaining O^tBu/H metathesis steps involving HBpin as a hydride source are exoergic (Figure 3.15). Furthermore, the dimer

[(H)Ge(μ-O^{t}Bu)$_2$Ge(H)] is 42 kJ/mol more stable than the hydride-bridged isomer [(^{t}BuO)Ge(μ-H)$_2$Ge(O^{t}Bu)], therefore only the O^{t}Bu-bridged species is shown in Figure 3.15. Overall these computations show that the reaction of [Ge(O^{t}Bu)$_2$] with 2 equivalents of HBpin to yield 0.5 equivalents of the *trans*-bent germylene dimer $H_2Ge{=}GeH_2$ and 2 equivalents of ^{t}BuOBpin is exoergic by −78.5 kJ/mol. It is expected that added energy will be gained when bulk $[GeH_2]_n$ is formed (*vide infra*) from the oligomerization of extra GeH_2 units. These computations indicate that the path to germanium(II) hydride via free monomeric [Ge(O^{t}Bu)$_2$] (outlined in orange in Figure 3.15) is less energetically viable than the path involving cyclic/dimeric intermediates (Figure 3.15, in green).

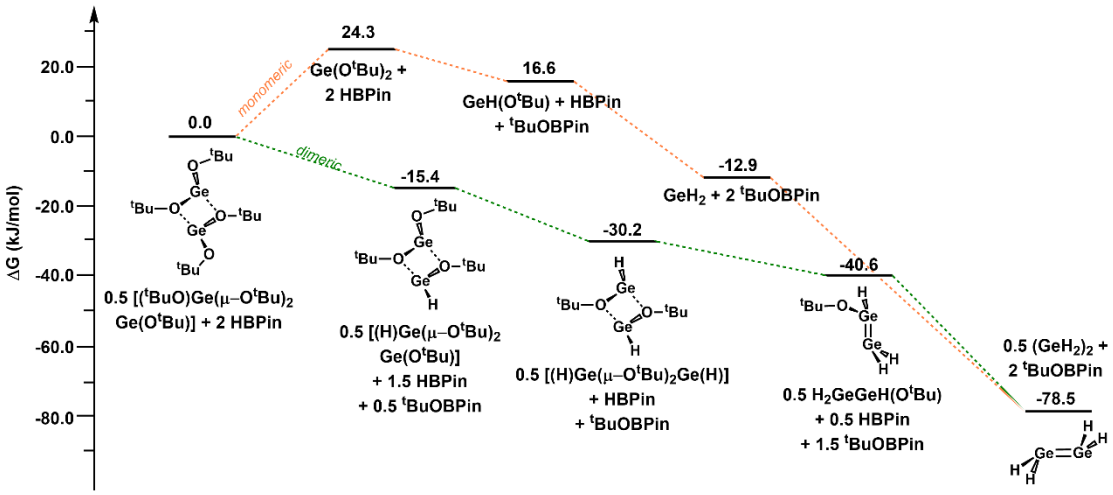

Figure 3.15. Computed reaction pathway for the conversion of dimeric [Ge(O^{t}Bu)$_2$]$_2$ into the $[GeH_2]_2$ dimer (*trans*-bent $H_2Ge{=}GeH_2$) with HBpin; all free energy values are in in kJ/mol. The pathways listed in orange involve the formation of monomeric [Ge(O^{t}Bu)$_2$], while the pathways in green involve Ge heterocycle intermediates.

3.2.7 Computational investigation of $[GeH_2]_n$ oligomers (n = 1–5 and 10)

Prior computational studies have shown that many different isomers of Ge_2H_4 are present on the potential energy surface, all within *ca.* 15 kJ/mol of the planar (D_{2h}) $H_2Ge{=}GeH_2$ isomer; notably, this ethylene-type isomer is not stable and occurs on a first-order saddle point (transition state) between two *trans*-bent isomers.[27] Hence the propensity for hydride migration, such as to form $HGe–GeH_3$ from *trans*-bent $H_2Ge{=}GeH_2$, is much greater for germanium hydrides than for hydrocarbons.[28] Furthermore, the Rivard Group has previously computed the energies of various $(GeCl_2)_n$ oligomers and discovered that branched structures become thermodynamically preferred as the tetrel (Group 14 element) chain becomes longer.[29]

Figure 3.16 summarizes gas phase computations (at the PBE0[30]/cc-pVTZ[26b] level of theory) for various $[GeH_2]_n$ oligomers with n = 1–5. Oligogermanium dihydride structures with two-coordinate Ge(0) centers (*e.g.*, $H_3Ge–Ge–GeH_3$) could not be optimized as energetic minima, preferring instead to adopt either hydride-bridged or hydride-migration products, and have thus been omitted from Figure 3.16. Similarly, the linear $(GeH_2)_3$ structure exists only as a transition state, likely due to the dual electrophilic and nucleophilic nature of this species, leading to its further conversion into the bridging hydride structure shown at the left of Figure 3.16. As can be seen in Figure 3.16, cyclic structures become thermodynamically favoured as the Ge ring size increases, while branched structures are more stable than their corresponding linear $[GeH_2]_n$ forms. As has been previously reported for the analogous oligo(perhydrido)silicon species,[31a] branched structures resulting from hydride migrations are more stable than their linear

counterparts.[31c] These computations indicate that the structure of bulk $[GeH_2]_n$ materials generated in this study (**2a**–**c**), derived from the likely oligomerization of molecular GeH_2 units, are formed by paths wherein hydride migration occurs to yield branched structures.[32]

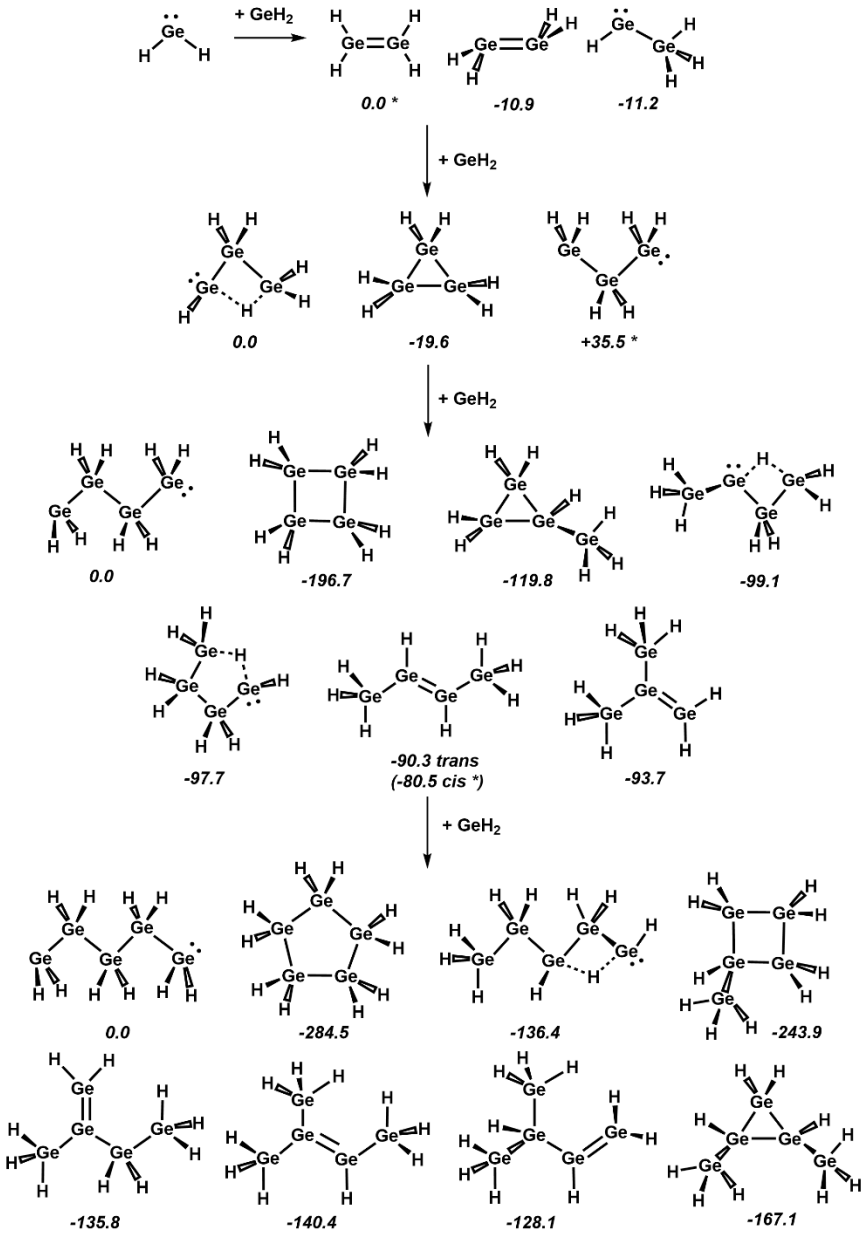

Figure 3.16. Computed relative Gibbs free energies of $[GeH_2]_n$ isomers (n = 1–5) in kJ/mol. Energies marked with an asterisk (*) indicate that the structure optimized at a first-order saddle point (with one imaginary frequency).

To gain more insight into the most likely (dominant) structure of the Ge hydrides **2a**–**2c**, computations were conducted on two different Ge_{10} oligomers: linear H–

$[GeH_2]_{10}$–H (**4**) and an oligomer derived from hydride-migration, H–$[Ge(H)(GeH_3)]_5$–H (**5**) (Figure 3.17). Geometry optimizations were carried out at the PBE0[30]/cc-pVTZ[26b] level, while the energy of the HOMO–LUMO electronic transitions were computed with time-dependent DFT (TD-DFT) at the B3LYP[33]/cc-pVTZ[26b] level of theory. The computed energies of these two isomers are remarkably similar, with the branched system H–$[GeH(GeH_3)]_5$–H (**5**) being lower in energy by only 12 kJ/mol relative to the linear isomer H–$[GeH_2]_{10}$–H (**4**).

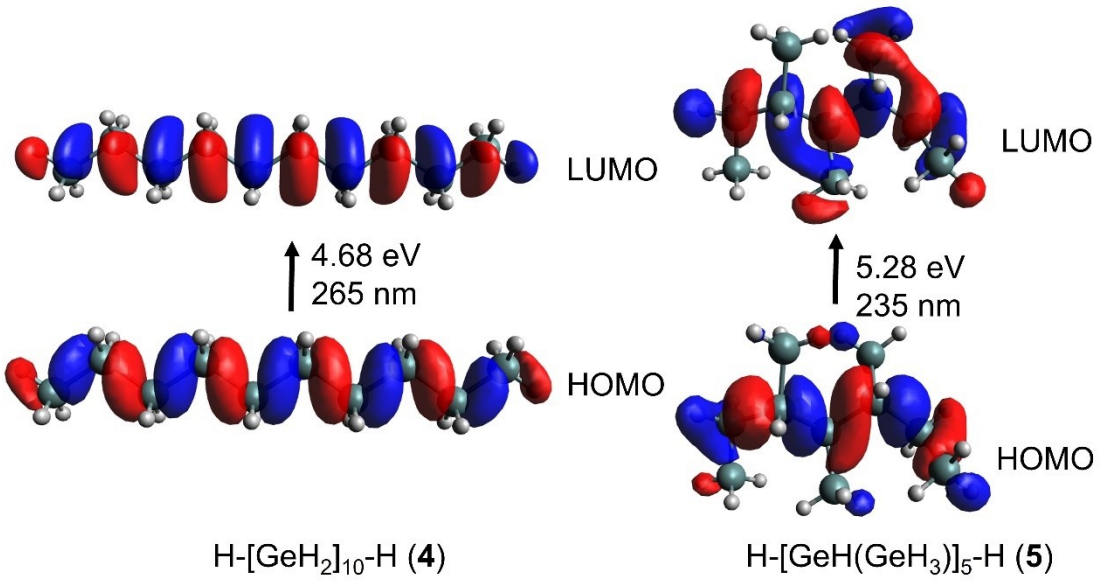

Figure 3.17. HOMO and LUMO orbitals of H–$[GeH_2]_{10}$–H (**4**) and H–$[Ge(H)\{GeH_3\}]_5$–H (**5**) with the structures computed at the PBE0/cc-pVTZ level of theory. The computed energies of the HOMO–LUMO transitions have been determined by time-dependent DFT (TD-DFT) at a B3LYP/cc-pVTZ level of theory.

The computed UV-Vis absorption maxima for each isomer are in the UV region, with λ_{max} values of 265 nm (4.68 eV) and 235 nm (5.28 eV) for the linear (**4**) and branched (**5**) isomers, respectively. The computed transitions are complied in Table 3.1,

and the weighted sum of the transitions are plotted with line broadening applied in Figure 3.18.[34] Thus, the germanium hydride products (**2a**–**c**), which absorb well into the visible region, likely consist of extended chains with more than 10 contiguous Ge atoms present. For comparison, previous computations on linear (zig-zag) $[GeH_2]_n$ led to an approximate band gap of 3.0 eV.[35]

Table 3.1. UV-Vis transitions of the Ge_{10} oligomers, as computed by TD-DFT (B3LYP/cc-pVTZ, structures optimized at the PBE0 /cc-pVTZ level of theory).

Oligomer	#	Contribution	Weight of Contribution	Energy (eV)	Energy (nm)	Oscillator Strength
H-$[GeH_2]_{10}$-H	1	HOMO → LUMO	0.69967	4.6768	265.1	3.3421
H-[GeH $(GeH_3)]_5$-H	1	HOMO → LUMO	0.66941	5.2801	234.81	0.4825
	2	HOMO-1 → LUMO	0.67578	5.3407	232.15	0.0946
	3	HOMO → LUMO+2	0.59827	5.5199	224.61	0.1215
		HOMO-1 → LUMO+2	0.26643			
	4	HOMO-1 → LUMO +2	0.51666	5.7229	216.65	0.1583
		HOMO → LUMO+4	0.2948			
		HOMO-2 → LUMO	0.25739			

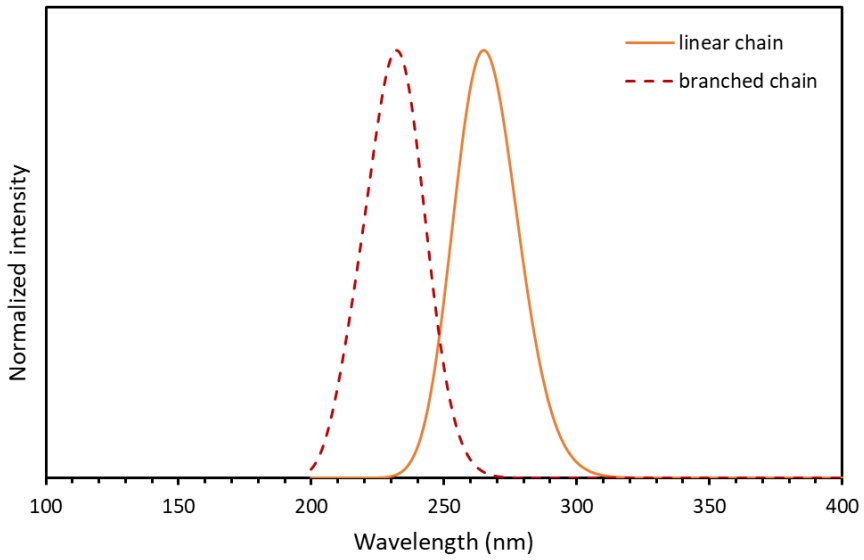

Figure 3.18. Computed UV-Vis absorption spectra of the linear (H-[GeH_2]$_{10}$-H) (**4**, orange solid line) and branched (H-[Ge(H)(GeH_3)]$_5$-H) (**5**, red dashed line) oligomers.

The IR spectra for both the linear and branched $Ge_{10}H_{22}$ isomers **4** and **5** (Table 3.2) were also computed. While the Ge–H stretching frequencies for the GeH, GeH_2, and GeH_3 units all overlap near 2000 cm^{-1}, the fingerprint region provided more distinguishing information. The GeH_2 scissoring motions in the linear isomer **4** were found at 860 cm^{-1}, while unique bending modes belonging to the branched isomer **5** are found at 780 and 692 cm^{-1}, due to –GeH_3 scissoring and ≡Ge–H wagging, respectively. Given the appearance of strong IR absorbances at 772 and 698 cm^{-1} in the solid-state IR spectrum of [$GeH_{1.92}$(O^tBu)$_{0.08}$] (**2c**), and the absence of a peak around 860 cm^{-1} (for a GeH_2 scissoring mode), it suggests that **2c** adopts a predominantly branched structure.

Table 3.2. Computed IR frequencies and assignments for the H-[GeH_2]$_{10}$-H and H-[GeH(GeH_3)]$_5$-H oligomers. Unique frequencies (within 5 cm^{-1}) are highlighted in green. Determined at the PBE0/cc-pVTZ level of theory.

Oligomer	IR Frequency (cm^{-1})	Molecular motion
H-[GeH_2]$_{10}$-H	2147-2143	terminal GeH_3 asym. stretch
	2132-2118	central GeH_2 asym. stretch
	2117-2112	central GeH_2 sym. stretch
	882, 881	terminal GeH_3 scissor
	862-858	central GeH_2 scissor
	791	terminal GeH_3 wag
H-[GeH(GeH_3)]$_5$-H	2148-2133	terminal GeH_3 asym. stretch
	2132-2101	GeH_3 sym. stretch
	2094-2089	Ge-Ge(*H*)-Ge stretch
	874-883	terminal GeH_3 scissor
	801, 785-775	GeH_3 scissor
	692, 697	Ge-Ge(*H*)-Ge wag

3.2.8 Energetics of H/OR exchange: role of the R groups

Following the hypothesis that an increase in nucleophilicity of the Ge-bound –OR groups would facilitate OR/H exchange with HBpin, the energetics associated with HBpin reactions with different $ImMe_2$•$Ge(OR)_2$ species at the M06-2X/cc-pVDZ level[26] were computed. All of the $ImMe_2$•$Ge(OR)_2$ species explored (R = ^{t}Bu, ^{n}Bu, ^{i}Pr, Me, Ph, C_6F_5, and C_6Cl_5) were found to react exoergically with two equivalents of HBpin to make the model complex $ImMe_2$•GeH_2 (Table 3.3). The most exoergic reactions of the series are those involving electron-rich alkoxides, such as $ImMe_2$•$Ge(O^tBu)_2$ ($\triangle_r G$ = −150.7 kJ/mol). Adducts bearing relatively electron withdrawing bis(aryloxide) units showed less favourable $\triangle_r G$ values, with the least exoergic reaction of the series being the reaction

between HBpin and $ImMe_2$•$Ge(OC_6F_5)_2$, with a computed $\Delta_r G$ of −47.9 kJ/mol. Thus, it appears that electron-donating groups at Ge facilitate hydride metathesis with HBpin.

Table 3.3. Gibbs' free energies of reaction ($\Delta_r G$) associated with H/OR group exchange between model $ImMe_2$•$Ge(OR)_2$ adducts and two equivalents of HBpin.

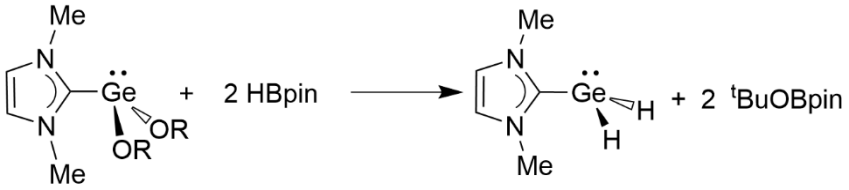

R	Δ_r G (kJ/mol)
^{t}Bu	-150.7
^{n}Bu	-153.9
^{i}Pr	-151.1
Me	-156.6
Ph	-95.2
C_6F_5	-47.9
C_6Cl_5	-54.3

3.3 Conclusions

A mild "bottom-up" synthesis of an isolable analogue of $[GeH_2]_n$ with an estimated composition of $[GeH_{1.92}(O^tBu)_{0.08}]_n$ (**2c**) via H/O^{t}Bu metathesis between [Ge $(O^tBu)_2$] (**1**) and HBpin was presented. Solid-state characterization of **2c** reveals an estimated optical band gap of 2.5 eV, and comparison of the experimental IR data with those of computed models suggest the presence of a highly branched structure. This conclusion is further supported by the computed thermodynamic preference of branched isomers of $[GeH_2]_n$ over linear ones as the number of Ge atoms increase. Furthermore,

heating of **2c** to 200 °C yields semicrystalline Ge, confirming a vastly different reaction paradigm for this germanium hydride material in comparison to its lighter element congener, polyethylene, which does not extrude H_2 upon heating (instead depolymerization into ethylene gas occurs above its ceiling temperature). Combining [$Ge(O^tBu)_2$] (**1**) with the more reactive hydride reagent $H_3B{\bullet}SMe_2$ leads to the deposition of semi-crystalline nanodimensional films of Ge layers at 70 °C. This route represents a very mild and convenient route to germanium films. Future work will involve use of the reported hydride-metathesis strategy to prepare other main group systems, such as those based on tin or mixed elements (*e.g.*, SiGe).

3.4 Experimental procedures

3.4.1 General

All reactions were performed using standard Schlenk techniques under an atmosphere of nitrogen or in a nitrogen-filled glove box (Innovative Technology, Inc.). Solvents were dried using a Grubbs-type solvent purification system manufactured by Innovative Technology, Inc., and stored under an atmosphere of nitrogen prior to use. $Cl_2Ge{\bullet}$dioxane, methyl iodide, potassium *tert*-butoxide, *tert*-butanol, catecholborane (HBcat), $H_3B{\bullet}SMe_2$ (2.0 M solution in THF), diisobutylaluminium hydride (DIBAL-H, 1.0 M solution in hexanes), 2,3-dimethyl-1,3-butadiene and 1-methylimidazole were purchased from Sigma-Aldrich and used as received. 4,4,5,5-Tetramethyl-1,2-dioxaborolane (HBpin) was purchased from Oakwood Chemicals and used as received. 4-Dimethylaminobenzaldehyde was purchased from BDH Chemicals and recrystallized from absolute ethanol prior to use. 4,4'-Difluorobiphenyl was obtained from K&K

Laboratories and recrystallized from toluene before use. $ImMe_2$•$GeCl_2$ ($ImMe_2$ = $(HCNMe)_2C$:),[8a] [$Ge(OMes^*)_2$] (Mes* = 2,4,6-$^tBu_3C_6H_2$),[25] and 1,2-$^iPr_2P(C_6H_4)BCy_2$ (Cy = cyclohexyl) (**PB**),[19] were prepared according to literature procedures. ^1H, $^{11}B/^{11}B\{^1H\}$, $^{13}C\{^1H\}$, and $^{19}F\{^1H\}$ NMR spectra were recorded on a Varian Inova 400 or 500 MHz spectrometer and referenced externally to Me_4Si (^1H, $^{13}C\{^1H\}$), F_3B•OEt_2 ($^{11}B/^{11}B\{^1H\}$) and $CFCl_3$ ($^{19}F\{^1H\}$). Elemental analyses were performed by the Analytical and Instrumentation Laboratory at the University of Alberta. Melting points were obtained in sealed glass capillaries under nitrogen using a MelTemp melting point apparatus and are uncorrected.

3.4.2 Diffusion-ordered spectroscopy (DOSY) experiments

Diffusion-ordered spectroscopy (DOSY) experiments were performed on a 600 MHz Varian/Agilent instrument equipped with a Z-gradient HCN indirect detection probe capable of outputting 72 G/cm of gradient strength. All measurements were carried out non-spinning and at a calibrated temperature of 27.0 °C using the Oneshot45 pulse sequence.[36] For all DOSY experiments, a spectral window of 7.2 kHz was used with a 3 s acquisition time and a 3 s relaxation delay with 4 scans for each gradient increment. Pulse widths and gradient strengths were optimized for each sample. A diffusion delay of 50 ms was used. Fifteen gradient strengths from 2 to 59.5 G/cm were used for the benzene solutions. The spectra were Fourier transformed and baseline corrected prior to discrete processing. Data were fit to a double exponential decay and corrected for non-uniform pulsed field gradients.[37] The diffusion dimension was zero filled to 1024 data

points and the directly detected dimension was zero filled to 256 K data points prior to final DOSY processing. All data were acquired and processed using OpenVNMRJ 2.1A.

3.4.3 Characterization of solid materials

Diffuse reflectance analysis was performed employing a Cary 5000 UV-Vis-NIR spectrophotometer equipped with a DRA-CA-50M diffuse reflectance accessory, a double out-of-plane Littrow monochromator, and a R928 PMT detector. Glass plates were sealed with candelilla wax, a low melting point and low oxygen permeability wax, purchased from amazon.ca (Supplier: "Health & Beauty").

Powder XRD patterns were collected on a Rigaku Ultima IV powder diffractometer equipped with a Co Kα radiation source (Kα1 = 1.78900 Å, Kα2 = 1.79283 Å) operating at 40 kV and 40 mA. A D/Tex Ultra detector was used, with an iron filter to eliminate the Kβ radiation at 1.62083 Å. Samples were placed on zero-background holders. Diffraction data were collected in continuous scan mode between 5 and 90° in 2θ with a step size of 0.0200°.

Scanning electron microscopy (SEM) images were obtained using a Zeiss Sigma 300 VP-FESEM instrument equipped with a secondary electron detector and a Bruker energy-dispersive X-ray (EDX) spectroscopy system operating at 5 kV. Samples were mounted on aluminum stubs with carbon tape.

Raman spectroscopy was performed using a Renishaw's inVia Raman Spectrometer (632 nm or 785 nm, 0.6 mW, 3 × 10 s collection).

Mass spectrometry (EI-MS) was performed by the Mass Spectrometry Facility at the University of Alberta.

X-ray photoelectron spectroscopy (XPS) was conducted on a PHI VersaProbe III at the nanoFAB facility at the University of Alberta operating in energy spectrum mode at 23.17 W. Samples were mounted to the sample holder with double-sided tape and transferred into a portable inert atmosphere antechamber for delivery from the N_2 glovebox into the XPS instrument. The base and operating chamber pressure were maintained at 10^{-7} Pa. A monochromatic Al Kα source (1486.6 eV) was used to irradiate the samples, and the spectra were obtained with an electron take-off angle of 45°. Survey spectra were collected using an elliptical spot with major and minor axis lengths of 2 and 1 mm, respectively, and 280 eV pass energy with a step of 0.1 eV. CasaXPS software (VAMAS) was used to interpret high-resolution spectra. All spectra were internally calibrated to the C 1s emission (284.8 eV).

A flame test was used to determine a threshold for detectible boron content by eye (burns green). Stock solids were created by the grinding of silica gel (no colour by flame test) with boric acid, with known boron mass contents. The solids were burned on a spatula in a propane flame, and the results filmed to check for detectible green in the flame. The lowest threshold for detectable green in the flame was at 0.085 mass% boron.

3.4.4 Synthetic procedures and reactivity studies

K[Ge(O^{t}Bu)$_3$]: To Cl_2Ge•dioxane (0.510 g, 2.20 mmol) in 20 mL of THF was added K[O^{t}Bu] (0.785 g, 7.00 mmol). The reaction mixture was stirred at room temperature for 2 hours and then the mixture was filtered. Removal of the volatiles from the filtrate *in vacuo* afforded K[Ge(O^{t}Bu)$_3$] (0.692 g, 95 %) as a white solid. Crystals of

suitable quality for single-crystal X-ray diffraction were obtained by cooling a saturated toluene solution of K[Ge(O^{t}Bu)$_3$] to –35 °C for 3 days. ^{1}H NMR (C_6D_6, 700 MHz): δ 1.39 (s, 27H, C(C*H*$_3$)$_3$). ^{13}C{^{1}H} NMR (C_6D_6, 700 MHz): δ 69.9 (*C*(CH$_3$)$_3$), 34.7 (C(*C*H$_3$)$_3$). Anal. Calc. for $KC_{12}H_{27}GeO_3$: C, 43.53; H, 8.22. Found: C, 43.33; H, 7.98 %.

[Ge(O^{t}Bu)$_2$] (1): To a solution of K[Ge(O^{t}Bu)$_3$] (0.331 g, 1.00 mmol) in 2 mL of benzene was added Cl_2Ge•dioxane (0.116 g, 0.500 mmol). The reaction mixture was stirred at room temperature for one hour and then the mixture was filtered through a pad of Celite. The volatiles were removed from the filtrate *in vacuo* to give [Ge(O^{t}Bu)$_2$] (**1**) (0.312 g, 94 %) as a white solid. [Ge(O^{t}Bu)$_2$] (**1**) can be recrystallized from a saturated solution of pentane cooled to -35 °C for one week (yield 54 %). ^{1}H NMR (C_6D_6, 500 MHz): δ 1.48 (s, 18H, C(C*H*$_3$)$_3$). ^{13}C{^{1}H} NMR (C_6D_6, 500 MHz): The peak pattern in this NMR spectra indicates the possible presence of both monomer [δ 30.7 (C(*C*H$_3$)$_3$), 74.6 (*C*(CH$_3$)$_3$)] and dimer [^{t}BuOGe(μ-O^{t}Bu)$_2$GeO^{t}Bu]: bridging O^{t}Bu δ 34.4 (C(*C*H$_3$)$_3$), 77.4 (*C*(CH$_3$)$_3$); exocyclic O^{t}Bu δ 32.4 (*C*(CH$_3$)$_3$), 72.2 (C(*C*H$_3$)$_3$). Anal. Calc. for $C_9H_{18}GeO_2$: C, 43.90; H, 8.29. Found: C, 43.73; H, 8.23 %. Diffusion ordered NMR spectroscopy (DOSY) gave a diffusion constant (D) of 10.17(3) m^2/s, equating to a solvodynamic radius of 3.38(1) Å with the literature C_6D_6 viscosity value of 0.6392 Pa•s.[38]

Synthesis of [GeH$_{1.64}$(OtBu)$_{0.36}$]$_n$ (2a) from HBpin: In a nitrogen-filled glove box, 119 μL (0.822 mmol) of HBpin was added to a solution of [Ge(OtBu)$_2$] (**1**) (60.0 mg, 0.274 mmol) in 1 mL of benzene at room temperature. After 2 hours of stirring, an insoluble yellow-orange solid formed. The precipitate was allowed to settle, and the

mother liquor was decanted away. The remaining solid was washed with benzene (4 × 5 mL) and dried under vacuum to give **2a** as a bright yellow-orange solid (15 mg, 55 %; yield based on the formula $[GeH_{1.64}(O^tBu)_{0.36}]_n$). The expected by-product, ^{t}BuOBpin,[13] was identified by ^{1}H, ^{11}B and $^{13}C\{^1H\}$ NMR spectroscopy. IR (ATR): 2970 cm^{-1} (C-H, Ar), 2967 cm^{-1} (C-H), 1996 cm^{-1} (Ge-H), 1134 cm^{-1} (C-O), 835 & 762 cm^{-1} (H-Ge-H). Raman: 2038 cm^{-1} (Ge-H), 289 cm^{-1} (Ge-Ge).

Synthesis of $[GeH_{1.65}(OtBu)_{0.35}]_n$ (2b) from HBcat: In a nitrogen-filled glove box, 43 μL (0.40 mmol) of HBcat was added to a solution of $[Ge(O^tBu)_2]$ (**1**) (40.0 mg, 0.183 mmol) in benzene (1 mL) at room temperature. After the resulting mixture was stirred for 2 hours, the precipitate was allowed to settle and the mother liquor decanted away. The remaining solid was washed with benzene (4 × 5 mL), dried under vacuum to give **2b** as a bright yellow solid (10 mg, 55 %, yield based on the formula $[GeH_{1.65}(O^tBu)_{0.35}]_n$). The expected by-product, ^{t}BuOBcat, was identified by ^{1}H, ^{11}B and $^{13}C\{^1H\}$ NMR spectroscopy.[15] IR (ATR): 3060 cm^{-1} (C-H, Ar), 2956 cm^{-1} (C-H), 2038 cm^{-1} (Ge-H), 1102 cm^{-1} (C-O), 833 & 776 cm^{-1} (H-Ge-H). Raman: 2047 cm^{-1} (Ge-H), 295 cm^{-1} (Ge-Ge). Anal. Calc. for $[GeH_{1.65(}O^tBu)_{0.35}]_n$: C, 16.65; H, 4.78. Found: C, 16.42; H, 2.53 %. Molecular formula calculated based on carbon content.

Synthesis of $[^i Bu_2AlO^tBu]_2$ from DIBAL-H and HO^tBu: Using Schlenk techniques, 318 μL of a 1.0 M solution of DIBAL-H in hexanes (0.16 mmol of dimer $[HAl^iBu_2]_2$) was added dropwise into a Teflon Schlenk flask containing a solution of HO^tBu (23.6 mg, 0.318 mmol) in 1 mL of benzene, at room temperature. After the

resulting mixture was stirred for one hour, the volatiles were removed under vacuum until a white solid remained (36 mg, 53 %). The expected product, $[^{i}Bu_2AlO^{t}Bu]_2$, was identified by ^{1}H and $^{13}C\{^{1}H\}$ NMR spectroscopy. ^{1}H NMR (C_6D_6, 400 MHz): δ 0.26 (d, 8H, $^{3}J_{HH}$ = 6.9 Hz, CH_2), 1.19 (d, 24H, $^{3}J_{HH}$ = 6.5 Hz, CH(CH_3)$_2$), 1.29 (s, 18H, OC(CH_3)$_3$), 2.02-2.09 (m, 4H, CH(CH$_3$)$_2$). $^{13}C\{^{1}H\}$ NMR (C_6D_6, 400 MHz): δ 26.0 (CH_2), 26.3 ($CH(CH_3)_2$), 28.9 (CH(CH_3)$_2$), 31.8 (OC(CH$_3$)$_3$), 74.8 (OC(CH$_3$)$_3$). HR-MS (EI) ($C_{24}H_{54}Al_2O_2$): m/z calc. for ($C_{20}H_{45}Al_2O_2$) 371.30505. Found 371.30522 (Δppm = 0.4).

Attempted Synthesis of $[GeH_2]_n$ from DIBAL-H: In a nitrogen-filled glove box, 402 μL of a 1.0 M solution of DIBAL-H in hexanes (0.40 mmol of monomer $HAl^{i}Bu_2$) was added to a Teflon Schlenk flask containing $[Ge(O^{t}Bu)_2]$ (**1**) (40 mg, 0.18 mmol) dissolved in 2 mL of pentane. The reaction vessel was removed from the glovebox and heated to 70 °C (with stirring) for 2 hours. The product was then isolated inside the glovebox. The slurry was allowed to settle, and the supernatant was decanted. The precipitate was washed with 5 mL of pentane, allowed to settle, and the supernatant decanted; this washing procedure was repeated four times to ensure the removal of all soluble materials. Finally, all volatiles were removed under vacuum until an orange-yellow powder remained (8.8 mg; 49 %, yield based on the formula $[GeH_{1.65}(O^{t}Bu)_{0.35}]_n$) as determined by mass% C from elemental analysis; elemental analysis was not consistent with the formation of $[GeH_2]_n$ as a high C content was detected. The DIBAL-derived side products isolated in the supernatant (volatiles removed by vacuum) were characterized by ^{1}H NMR and $^{13}C\{^{1}H\}$ NMR spectroscopy. IR (ATR) 2873-2929 cm^{-1} (C-H), 1990 cm^{-1} (Ge-H), 1070 cm^{-1} (C-O), 769 and 808 cm^{-1} (H-Ge-H). Raman: 1998

cm^{-1} (Ge-H), 291 cm^{-1} (Ge-Ge). Anal. Calc. for $[GeH_{1.65}(O^tBu)_{0.35}]_n$: C, 16.65; H, 4.78. Found: C, 16.73; H, 4.14 %.

Synthesis of $[GeH_{1.92}(OtBu)_{0.08}]_n$ (2c) from excess HBpin at 70 °C: In a nitrogen-filled glove box, 530 μL (3.65 mmol) of HBpin was added to a solution of $[Ge(O^tBu)_2]$ (**1**) (80.0 mg, 0.365 mmol) in 2 mL of benzene at room temperature. The solution was brought out of the glove box in a Teflon valve-sealed flask and stirred for 16 hours at 70 °C, which afforded a yellow-orange insoluble solid. The precipitate was allowed to settle, and the mother liquor was decanted away. The remaining solid was washed with benzene (4 × 5 mL) and dried under vacuum to give **2c** as a bright yellow-orange solid (20 mg; 68 % yield based on $[GeH_{1.92}(O^tBu)_{0.08}]_n$). The expected by-product, ^{t}BuOBpin, was identified by ^{1}H, ^{11}B and $^{13}C\{^1H\}$ NMR spectroscopies.[13] IR (ATR): 2957 cm^{-1} (C-H), 2013 cm^{-1} (Ge-H), 1069 cm^{-1} (C-O), 772 and 809 cm^{-1} (H-Ge-H). Raman: 2021 cm^{-1} (Ge-H), 292 cm^{-1} (Ge-Ge). Anal. Calc. for $[GeH_{1.92}(O^tBu)_{0.08}]_n$: C, 4.78; H, 3.28 %. Found: C, 4.82; H, 1.96 %. Molecular formula calculated based on carbon content. No green colour was observed in the burning of product **2c**, indicating that the boron incorporation in the solid was less than *ca.* 0.085 mass%.

Synthesis of GeI_4 from $[GeH_{1.92}(OtBu)_{0.08}]_n$ (2c) and I_2: In a nitrogen-filled glove box, a solution of I_2 (0.0948 g, 0.747 mmol) dissolved in 2 mL of C_6D_6 was added to a vial containing 0.020 g (0.25 mmol) of $[GeH_{1.92}(O^tBu)_{0.08}]_n$ (**2c**) at room temperature. The mixture was stirred for one hour resulting in the formation of a dark yellow solution and a dark-purple solid. The reaction mixture was filtered through Celite and the volatiles

were removed from the filtrate to give GeI_4 (yellow solid, 0.126 g, 87 %). Bright orange crystals were grown by sublimation of the yellow solid at room temperature under dynamic vacuum (0.150 mTorr) for 3 hours and identified by pXRD.[21] Mp: 144-146 °C.[39]

Attempted reaction between 2,3-dimethyl-1,3-butadiene and 2c: Under N_2, a solution of 2,3-dimethyl-1,3-butadiene (20.4 mg, 0.248 mmol) in 1 mL of C_6D_6 was added to **2c** (0.010 g, 0.12 mmol) at room temperature. After stirring the mixture at 60 °C for 16 hours, analysis of the reaction mixture by ^{1}H and $^{13}C\{^{1}H\}$ NMR spectroscopy indicated that no reaction transpired.

Attempted reaction between 1,2-$^{i}Pr_2P(C_6H_4)BCy_2$ (PB) and 2c: Under N_2, a solution of **PB** (91.9 mg, 0.248 mmol) in 1 mL of C_6D_6 was added to **2c** (0.010 g, 0.12 mmol) at room temperature. After stirring the mixture at 60 °C for 16 hours, analysis of the reaction mixture by ^{11}B and ^{31}P NMR spectroscopy showed that no reaction had transpired.

***In situ* trapping of GeH_2 with 1,2-$^{i}Pr_2P(C_6H_4)BCy_2$ (PB):** Under N_2, **PB** (0.074 g, 0.20 mmol) and $[Ge(O^{t}Bu)_2]$ (**1**) (0.022 g, 0.10 mmol) were combined in a J-Young NMR tube, *ca.* 0.6 mL of THF and HBpin (0.20 mmol, 38 μL) were then added. The reaction progress was monitored by $^{31}P\{^{1}H\}$ and ^{11}B NMR spectroscopy, which showed the formation of the known germanium(II) dihydride complex PB{GeH_2}[8b] in about 30 % yield, along with unreacted **PB** (*ca.* 20 %)[8b,19] and another unknown product (*ca.* 50 % according to ^{31}P NMR spectroscopy, see Figure 3.8). A duplicate reaction was

conducted in the absence of HBpin, and $^{31}P\{^{1}H\}$ and ^{11}B NMR spectroscopy showed resonances for only the free **PB** species, indicating a lack of coordination between **PB** and [Ge(O^{t}Bu)$_2$] (**1**) under these conditions.

Preparation of ImMe$_2$•Ge(O^{t}Bu)$_2$ (3): To a vial containing ImMe$_2$•GeCl$_2$ (0.423 g, 1.77 mmol) and K[O^{t}Bu] (0.396 g, 3.53 mmol) was added 15 mL of benzene. The mixture was stirred for 18 hours to give a turbid orange coloured mixture. The resulting precipitate was allowed to settle and the supernatant was filtered through Celite to give a yellow filtrate. Removal of the volatiles from the filtrate via freeze-drying under vacuum gave ImMe$_2$•Ge(O^{t}Bu)$_2$ (**3**) as a yellow solid (0.421 g, 76 %). Crystals of suitable quality for single-crystal X-ray crystallography were obtained by cooling a concentrated solution of **3** in toluene to –35 °C for 3 days. ^{1}H NMR (C_6D_6, 500 MHz): δ 1.62 (s, 18H, OC(C*H*$_3$)$_3$), 3.52 (s, 6H, NC*H*$_3$), 5.54 (s, 2H, N(C*H*)$_2$N). $^{13}C\{^{1}H\}$ NMR (C_6D_6, 700 MHz): δ 34.0 (OC(*C*H$_3$)$_3$), 35.8 (N*C*H$_3$), 70.2 (O*C*(CH$_3$)$_3$), 120.5 (N(*C*H)$_2$N). 175.9 (N*C*N). Mp: 83 °C (decomp.). Anal. Calc. for $C_{13}H_{26}GeN_2O_2$: C, 49.57; H, 8.32; N, 8.89. Found: C, 49.59; H, 8.33; N, 8.63 %.

Reaction of ImMe$_2$•Ge(O^{t}Bu)$_2$ (3) with HBpin: To a solution of ImMe$_2$•Ge(O^{t}Bu)$_2$ (0.136 g, 0.432 mmol) in 6 mL of benzene was added HBpin (0.563 mL, 4.32 mmol). The mixture changes rapidly from clear yellow to a yellow-orange slurry. The reaction is heated for 16 hours at 70 °C. The precipitate was allowed to settle and the mother liquor was decanted away. The remaining precipitate was washed three times with benzene (3 × 3 mL) and then dried by vacuum to afford a Ge-H-rich highly air-sensitive

orange-red powder (36 mg) that smokes immediately upon exposure to air. IR (ATR): 2781-2972 cm^{-1} (C-H), 1978 cm^{-1} (Ge-H), 1000-1200 cm^{-1} (N-C), 772 and 809 cm^{-1} (H-Ge-H). Anal. Calc. for $[GeH_2]_n$: H, 2.70. Found: C, 18.62; H, 3.94 %; N, 4.07 %. The elemental analysis indicates an approximate composition of $(ImMe_2)_3Ge_{21}(O^tBu)_4H_{32}$ (C, 19.03; H, 4.38; N, 3.93 %.)

Thermolysis of 2c to form bulk germanium: A sample of **2c** (100 mg) was transferred to a borosilicate glass boat inside an inert atmosphere glove box. Under flowing N_2, the boat was transferred into the tube of a tube furnace (Lindberg 55035), which was pre-heated to 200 °C. The sample was held at 200 °C for two hours under static N_2, and then pushed to the end of the tube (outside the heating element) to cool to room temperature under flowing N_2. When cool, the samples were exposed to air and ground in a mortar and pestle to a fine powder for pXRD analysis. Furthermore, a sample of Ge, made from $[Ge(O^tBu)_2]$ (**1**) and $Me_2S{\bullet}BH_3$, was heated to 200 °C using the abovementioned procedure and analyzed by pXRD afterwards.

3.5 Details of catalysis trials

3.5.1 Stoichiometric hydroboration of carbonyl compounds

In a nitrogen-filled glove box, a mixture of $[Ge(O^tBu)_2]$ (**1**) (0.0219 g, 0.100 mmol) and the carbonyl substrate (0.100 mmol) in C_6D_6 (0.7 mL) was added HBpin (0.0256 g 0.200 mmol), and reacted at room temperature for 8 hours. For screening

reactions, the reaction mixture was monitored by ^{1}H NMR spectroscopy with yield calculated by relative integration to starting materials.

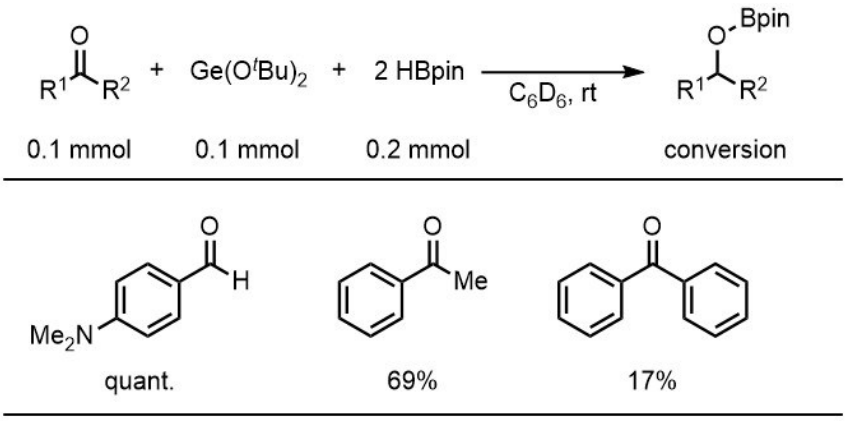

Scheme 3.5. Substrates and reaction conditions for the stoichiometric hydroboration of carbonyl compounds.

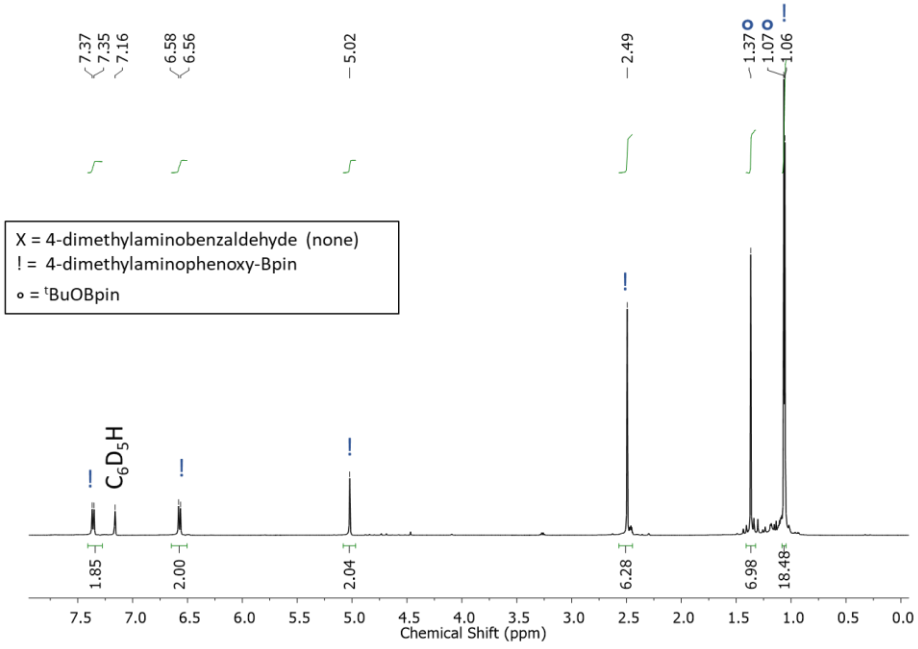

Figure 3.19. ^{1}H NMR spectrum (C_6D_6) of the stoichiometric hydroboration of 4-dimethylaminobenzaldehyde as per Scheme 3.5 with [Ge(O^{t}Bu)$_2$] (**1**) (100 mol%) after 8 hours. No starting material is observed, indicating quantitative conversion.[40]

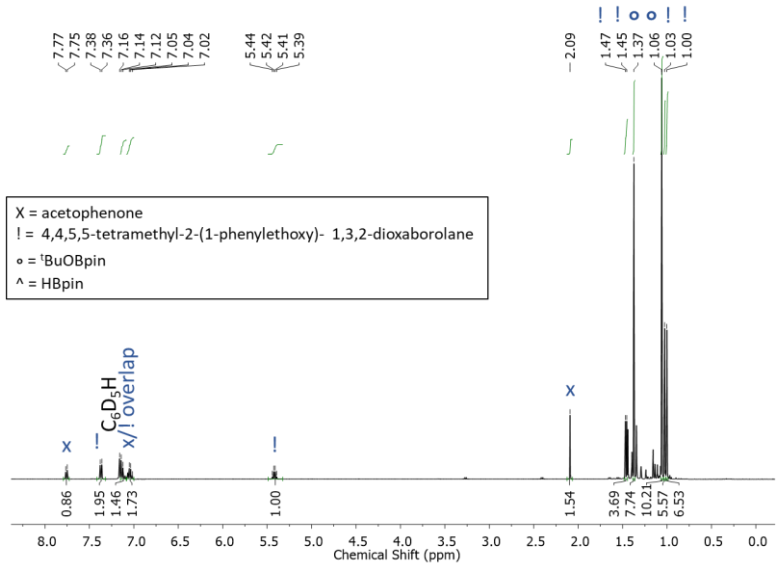

Figure 3.20. ^{1}H NMR spectrum (C_6D_6) of the stoichiometric hydroboration of acetophenone as per Scheme 3.5 with [Ge(O^{t}Bu)$_2$] (**1**) (100 mol%) after 8 hours. Relative integration in the aryl region (7.76 ppm vs. 7.37 ppm) indicates 69 % conversion.[40]

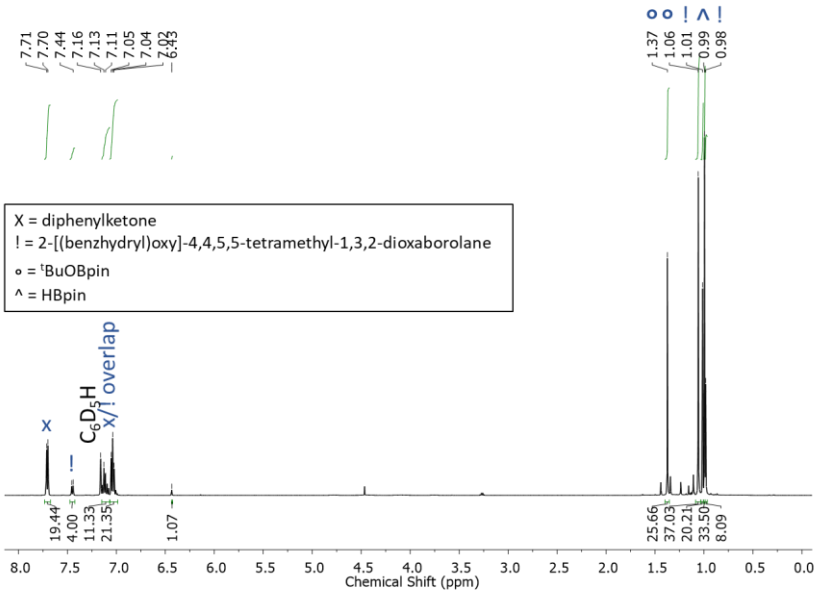

Figure 3.21. ^{1}H NMR spectrum (C_6D_6) of the stoichiometric hydroboration of diphenylketone as per Scheme 3.5 with [Ge(O^{t}Bu)$_2$] (**1**) (100 mol%) after 8 hours. Relative integration in the aryl region (7.70 ppm vs. 7.44 ppm) indicates 17 % conversion.[40]

3.5.2 The catalytic hydroboration of carbonyl compounds

Uncatalyzed hydroboration of 4-dimethylaminobenzaldehyde: In a nitrogen-filled glove box, to a mixture of 4-dimethylaminobenzaldehyde (0.0121 g, 0.0811 mmol) in C_6D_6 (0.600 mL) was added HBpin (0.0125 g, 0.0973 mmol). The reaction mixture was monitored by ^{1}H NMR spectroscopy, with integration relative to an internal standard of 4,4′-difluorobiphenyl (2.0 mg, 0.011 mmol), and the formation of a corresponding hydroborylated product was observed in a 3 % yield after 48 hours.

Catalytic hydroboration of 4-dimethylaminobenzaldehyde promoted by [Ge(O^{t}Bu)$_2$] (1): In a nitrogen-filled glove box, to a mixture of [Ge(O^{t}Bu)$_2$] (**1**) (0.0021 g, 0.010 mmol) and 4-dimethylaminobenzaldehyde (0.0149 g, 0.100 mmol) in C_6D_6 (0.600 mL) was added HBpin (0.0154 g, 0.120 mmol). The reaction mixture was monitored by ^{1}H NMR spectroscopy, with integration relative to an internal standard of 4,4′-difluorobiphenyl (2.9 mg, 0.015 mmol), and the formation of a corresponding hydroborylated product was observed in a 75 % yield after 48 hours.

Catalytic hydroboration of 4-dimethylaminobenzaldehyde promoted by 2c: In a nitrogen-filled glove box, to a mixture of **2c** (0.7 mg, 0.01 mmol) and 4-dimethylaminobenzaldehyde (0.0157 g, 0.100 mmol) in C_6D_6 (0.600 mL) was added HBpin (0.0162 g, 0.126 mmol). 4,4′-Difluorobiphenyl was added as an internal standard (2.1 mg, 0.011 mmol) The reaction mixture was monitored by ^{1}H NMR spectroscopy, with integration relative to an internal standard of 4,4′-difluorobiphenyl (2.1 mg, 0.011

mmol), and formation of the corresponding organoboron hydroborated product was observed in a 22 % yield after 48 hours.

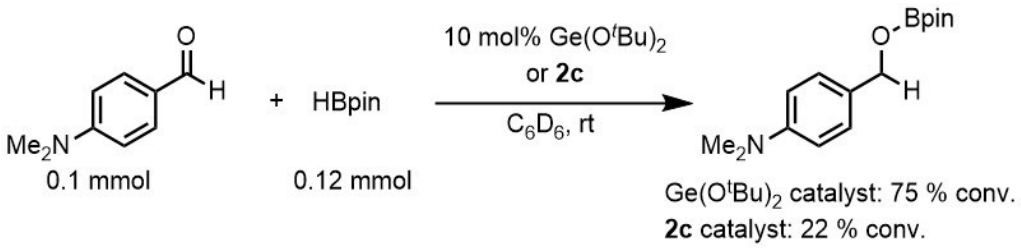

Scheme 3.6. The catalytic hydroboration of 4-dimethylaminobenzaldehyde with either [Ge(O^{t}Bu)$_2$] (**1**) or **2c** as pre-catalysts.

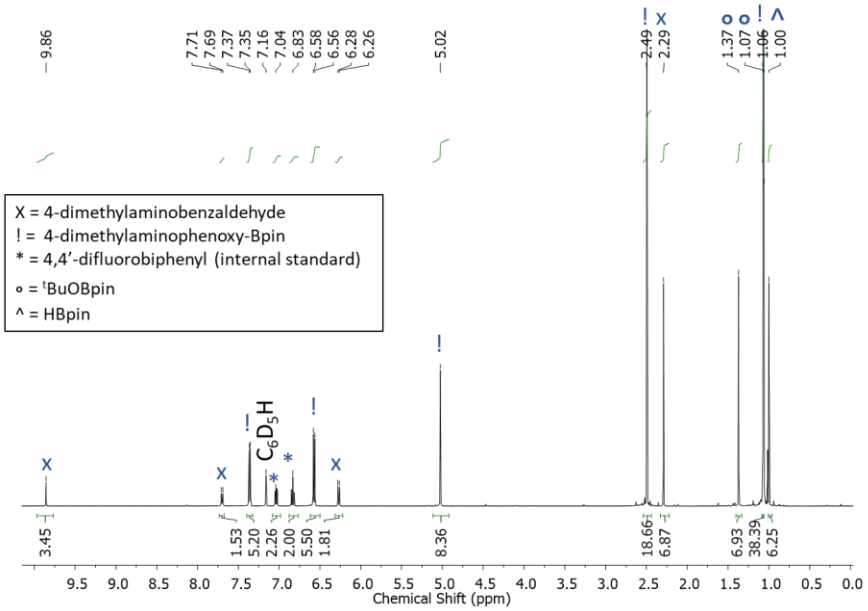

Figure 3.22. ^{1}H NMR spectrum (C$_6$D$_6$) of the catalytic hydroboration of 4-dimethylaminobenzaldehyde as per Scheme 3.6 with [Ge(O^{t}Bu)$_2$] (**1**) (10 mol%) after 48 hours. Integration in the aryl region vs. an internal standard shows 75 % conversion.[40]

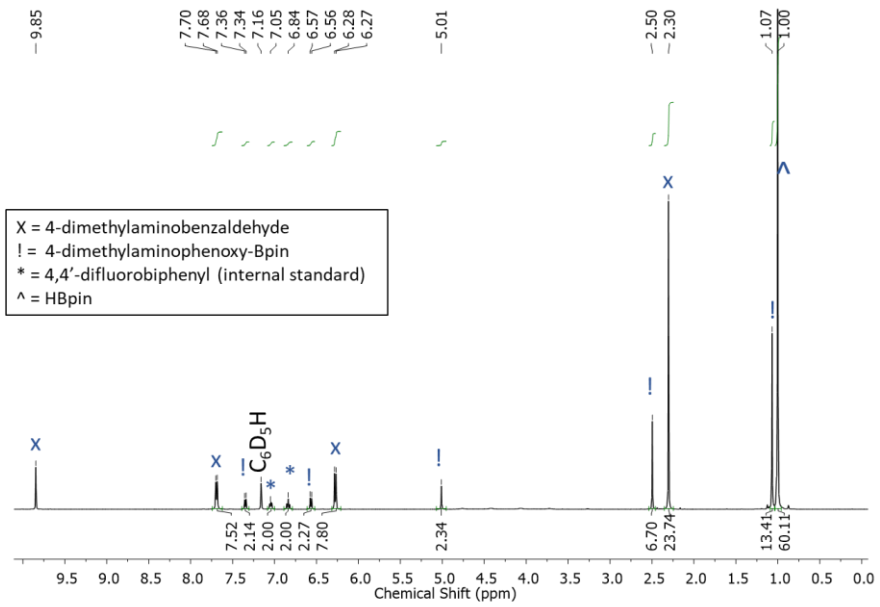

Figure 3.23. ^{1}H NMR spectrum (in C_6D_6) of the catalytic hydroboration of 4-dimethylaminobenzaldehyde as per Scheme 3.6 with 10 mol% of **2c**, after 48 hours. Integration in the aryl region vs. an internal standard shows 22 % conversion.[40]

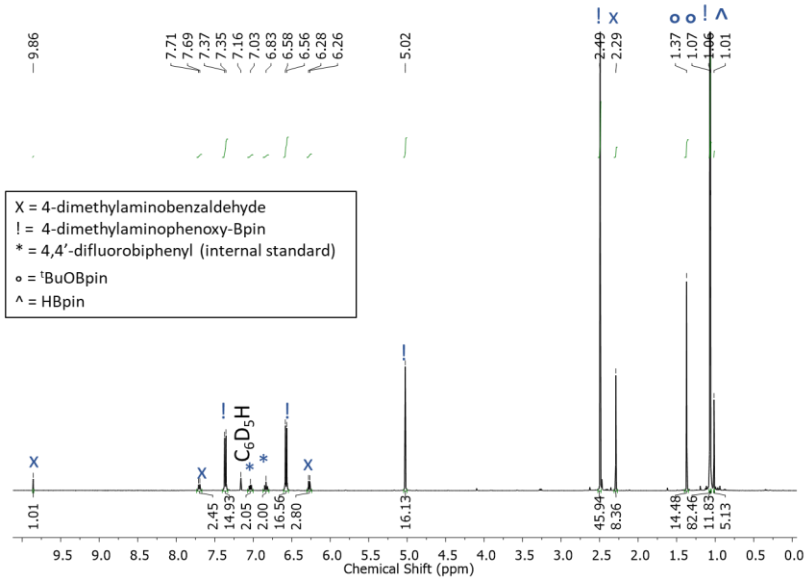

Figure 3.24. ^{1}H NMR spectrum (in C_6D_6) of the catalytic hydroboration of 4-dimethylaminobenzaldehyde as per Scheme 3.6 with 10 mol% of **1**, after 20 hours at 70 °C. Integration in the aryl region vs. an internal standard shows 86 % conversion.[40]

3.5.3 Attempted stoichiometric hydroboration of alkynes

In a nitrogen-filled glove box, to a mixture of [Ge(O^{t}Bu)$_2$] (**1**) (0.0219 g, 0.100 mmol) and alkyne (0.100 mmol) in C_6D_6 (0.7 mL) was added HBpin (0.0256 g 0.200 mmol). The reaction mixture was monitored by ^{1}H NMR spectroscopy, and the formation of a corresponding organoboron compound was NOT observed after 48 hours.

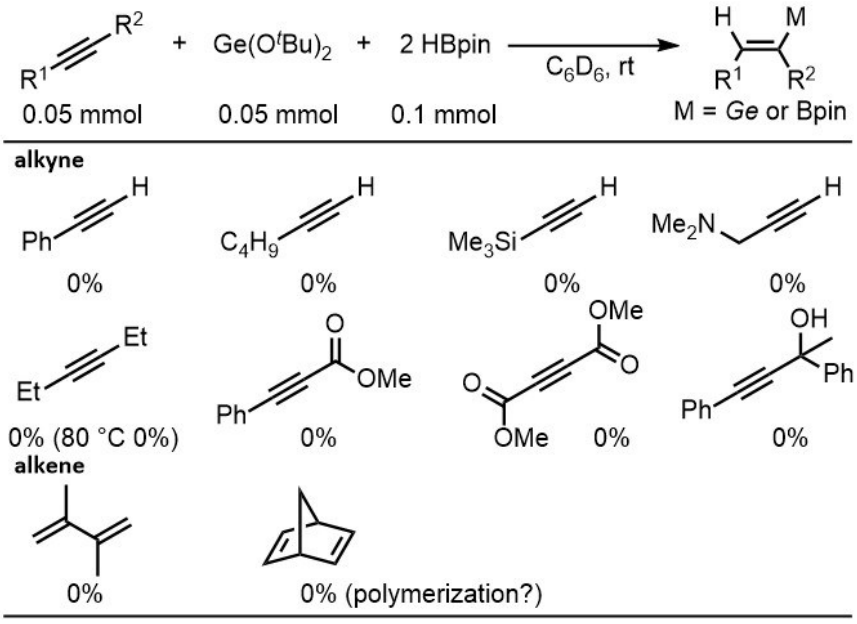

Scheme 3.7. Substrates and reaction conditions for the tested hydroboration of alkynes with [Ge(O^{t}Bu)$_2$] (**1**) as a pre-catalyst.

*3.5.4 Attempted catalytic hydroboration of alkynes with ImMe$_2$•Ge(O^{t}Bu)$_2$ (**3**)*

In a nitrogen-filled glove box, a of ImMe$_2$•Ge(O^{t}Bu)$_2$ (0.0016 g, 0.0051 mmol) and alkyne (0.0500 mmol) in C_6D_6 (0.70 mL) was added HBpin (0.0128 g 0.100 mmol).

The reaction mixture was monitored by ^{1}H NMR spectroscopy, and the formation of a corresponding organoboron compound was NOT observed after 48 hours at room temperature.

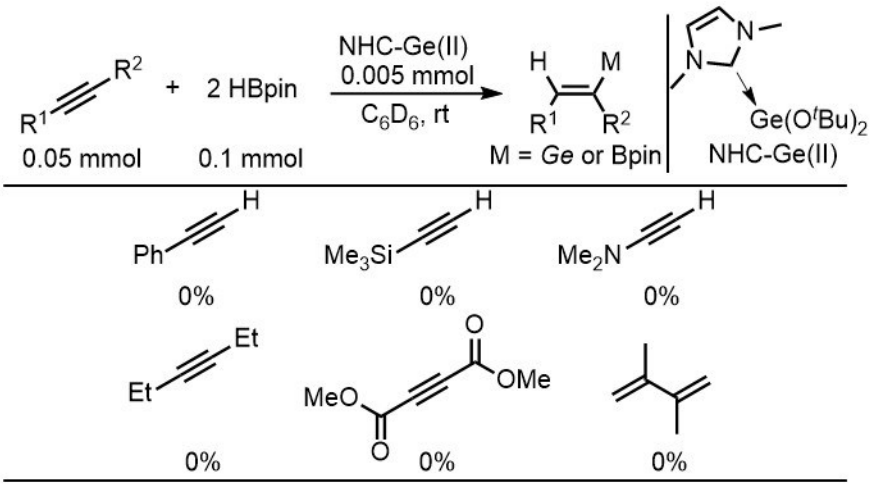

Scheme 3.8. Attempted hydroboration of alkynes with $ImMe_2$•$Ge(O^tBu)_2$ (**3**) as a pre-catalyst.

3.6 Computational methods and additional data

3.6.1 General methods

Computations were performed with the Gaussian16 software.[41] For the computational determination of reaction coordinates for the reaction of $[Ge(O^tBu)_2]$ (**1**) with HBpin and for relative energies of the $ImMe_2$•$Ge(OR)_2$ analogues and geometry optimizations (using default convergence criteria) were performed using density functional theory (DFT) with the M06-2X functional[26a] and the cc-pVTZ basis set.[26b] Harmonic vibrational analyses were performed at the same level of theory for all

optimized stationary points to determine their character (minimum or first-order saddle point) and to acquire the thermochemical data (at 298.15 K).

In keeping with recent computational studies of long-chain Ge species,[42] the geometry optimizations of the oligomerized isomers of $[GeH_2]_n$ (n = 1-5) and the linear H-$(GeH_2)_{10}$-H and branched H-$[GeH(GeH_3)]_5$-H isomers were performed using density functional theory (DFT) with the PBE functional,[30] the cc-pVTZ basis set,[26b] and an empirical dispersion correction GD3BJ.[30] Harmonic vibrational analyses were performed at the same level of theory for all optimized stationary points to determine their character (minimum or first-order saddle point) and to acquire the thermochemical data (at 298.15 K).

Time-dependent density function theory (TD-DFT) computations were carried out on the the linear H-$(GeH_2)_{10}$-H and branched H-$[GeH(GeH_3)]_5$-H isomers using the B3LYP functional[33] and the cc-pVTZ basis set,[26b] with five triplet and 5 singlet excitations resolved. IR and Raman frequency calculations were carried out using density functional theory (DFT) with the B3LYP[33] functional and cc-pVDZ basis set.[26b]

All input (.gjf) and output (.log and .fchk, where applicable) are available online at: 10.6084/m9.figshare.15132588

3.6.2 Collected outputs and relevant data from computational studies

Table 3.4. Relative energies and HOMO/LUMO level tabulations for computed isomers of $[GeH_2]_n$, n = 1-5 (PBE0/cc-pVTZ).

Formula	Free energy relative to chain conformer (kJ/mol)	HOMO (eV)	LUMO (eV)	HOMO/ LUMO gap (eV)
n = 1				
GeH_2 (singlet)	0	6.91	-3.07	3.84
n = 2				
$H_2Ge{=}GeH_2$ planar	0	-5.82	-1.73	4.09
$H_2Ge{=}GeH_2$ *trans*-bent	-10.89	-6.20	-2.46	3.73
$HGe\text{-}GeH_3$	-11.17	-6.65	-3.30	3.34
n=3				
$[GeH_2]_3$ chain	0.00	-5.90	-2.23	3.68
$[GeH_2]_3$ ring	-55.09	-6.74	-0.39	6.34
$H_3Ge\text{-}GeH_2\text{-}GeH$ *	-35.50	-6.30	1.54	7.84
n=4				
$[GeH_2]_4$ chain	0.00	-5.71	-2.86	2.85
$[GeH_2]_4$ ring	-196.74	-7.29	-0.69	6.60
$H_2Ge{=}Ge(GeH_3)_2$ *trans* bent	-93.70	-6.66	-3.27	3.38
$H_3GeGe(H){=}Ge(H)GeH_3$ *cis*	-80.50	-5.76	-1.91	3.84
$H_3GeGe(H){=}Ge(H)GeH_3$ *trans*	-90.30	-6.04	-2.46	3.58
$H_3Ge\text{-}(GeH_2)_2\text{-}GeH$ *	-97.75	-6.18	-2.06	4.13
$H_3Ge\text{-}Ge\text{-}GeH_2\text{-}GeH_3$ *	-99.10	-6.37	1.70	8.07
$H_3Ge(H)Ge$[cyclo-GeH_2-GeH_2]	-119.80	-6.59	-0.68	5.92

Continued on next page

Table 3.4 continued…

Formula	Free energy relative to chain conformer (kJ/mol)	HOMO (eV)	LUMO (eV)	HOMO/ LUMO gap (eV)
n=5				
$[GeH_2]_5$ chain	0.00	-5.35	-3.62	1.73
$[GeH_2]_5$ ring	-284.49	-7.47	-0.66	6.81
H_3Ge-GeH_2-$Ge(GeH_3)$=GeH_2	-135.81	-6.06	-2.56	3.50
H_2Ge=GeH-$GeH(GeH_3)_2$	-128.10	-6.10	-2.54	3.56
H_3Ge-GeH=$Ge(GeH_3)_2$	-140.39	-6.01	-2.47	3.54
H_3Ge-$(GeH_2)_3$-GeH	-136.43	-6.18	-1.57	4.61
[cyclo-$GeH(GeH_3)GeH_2$-$GeH(GeH)_3$]	-167.10	-6.53	-0.84	5.69
[cyclo-$GeH_2GeH_2GeH_2$-$GeH(GeH_3)$]	-243.92	-7.25	-0.82	6.43

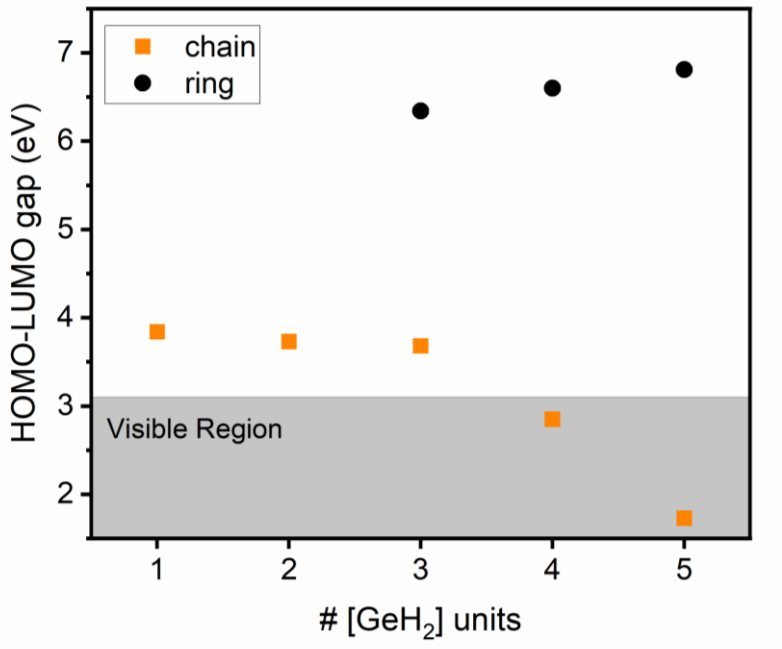

Figure 3.25. HOMO-LUMO band gaps of the chain and ring conformers of $[GeH_2]_n$, where n = 1-5. Determined at the PBE0 /cc-pVTZ level of theory.

3.7 X-ray crystallographic data

Crystals of appropriate quality for single-crystal X-ray diffraction studies were removed from the mother liquor and immediately covered with a thin layer of hydrocarbon oil (Paratone-N) in a sealed vial for transport to the instrument. A suitable crystal was then selected, attached to a glass fibre, and mounted under a stream of nitrogen onto the instrument. All data were collected using a Bruker APEX II CCD detector/D8 diffractometer using Cu Kα radiation. The data were corrected for absorption through Gaussian integration from indexing of the crystal faces. Structures were solved and refinements were completed using direct methods (SHELXT-2014 and SHELXL-2018/3).[43]

Table 3.5. Crystallographic data for K[Ge(O^{t}Bu)$_3$] (CCDC Deposition Number 2094826) and ImMe$_2$•Ge(O^{t}Bu)$_2$ (**3**, CCDC Deposition Number 2094825)

Compound	K[Ge(O^{t}Bu)$_3$]	ImMe$_2$•Ge(O^{t}Bu)$_2$ (**3**)
formula	$C_{12}H_{27}GeKO_3$	$C_{13}H_{26}GeN_2O_2$
formula weight	331.02	314.95
crystal system	orthorhombic	orthorhombic
space group	*P2$_1$2$_1$2$_1$* (No. 19)	*Pbcn* (No. 60)
unit cell parameters		
a (Å)	8.8817(5)	17.4359(6)
b (Å)	10.4187(6)	16.6516(6)
c (Å)	18.1622(10)	24.2090(8)
V (Å^3)	1680.65(16)	7028.7(4)
Z	4	16
ρ_{calcd} (g cm^{-3})	1.308	1.191
μ (mm^{-1})	4.664	2.351
radiation (λ [Å])	Cu Kα (1.54178) (microfocus source)	Cu Kα (1.54178) (microfocus source)
T (°C)	–100	–100
$2\theta_{max}$ (°)	149.20	140.32
Total data	23475 (-11 ≤ *h* ≤ 10, -12 ≤ *k* ≤ 12, -22 ≤ *l* ≤ 22)[a]	70160 (-21 ≤ *h* ≤ 21, -18 ≤ *k* ≤ 20, -29 ≤ *l* ≤ 29)
Unique data (R_{int})	3381 (0.0822)	6690 (0.0593)
Data$_{obs}$ [$F_o^2 \geq 2\sigma(F_o^2)$]	3025	5102
data/restraints/parameters	3381 / 18[b] / 182	6690 / 0 / 329
Flack absolute structure parameter[c]	0.031(14)	
final R indices[d]		
R_1 [$F_o^2 \geq 2\sigma(F_o^2)$]	0.0342	0.0358
wR_2 [all data]	0.0820	0.0992
Max/min $\Delta\rho$ (e$^-$ Å^{-3})	0.272 and –0.400	0.388 and –0.352

[a] Data were collected with the detector set at three different positions. Low-angle (detector 2θ = –33°) data frames were collected using a scan time of 5 s, medium-angle (detector 2θ = 75°) frames using a scan time of 15 s, and high-angle (detector 2θ = 117°) frames using a scan time of 45 s. [b] The rigid-bond restraint (RIGU) was applied to the anisotropic displacement parameters of the carbon atoms of the minor component of the disordered *tert*-butoxy group. [c] The Flack parameter will refine to a value near zero if the structure is in the correct configuration and will refine to a value near one for the inverted configuration.[44] [d] $R_1 = \Sigma||F_o| - |F_c||/\Sigma|F_o|$; $wR_2 = [\Sigma w(F_o^2 - F_c^2)^2/\Sigma w(F_o^4)]^{1/2}$

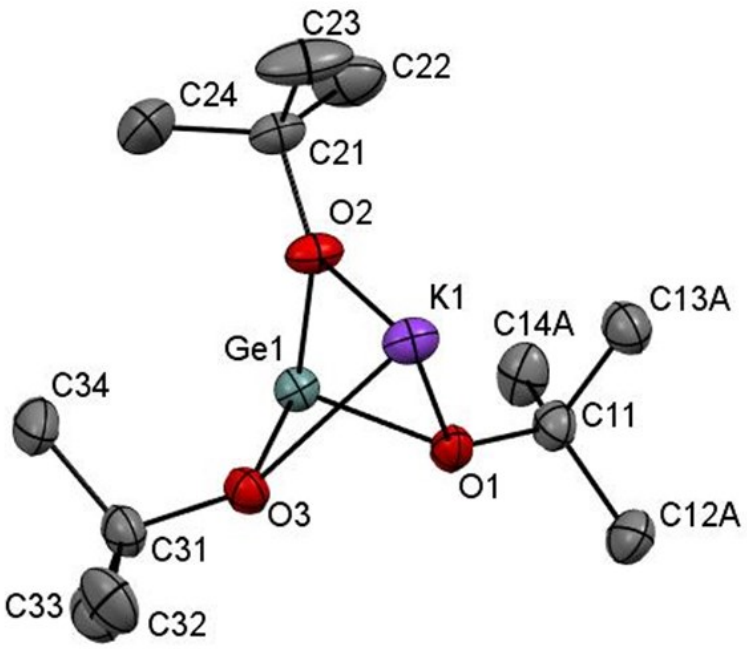

Figure 3.26. ORTEP of K[Ge(O^{t}Bu)$_3$] with thermal ellipsoids presented at a 30 % probability level. All hydrogen atoms have been omitted for clarity. Selected bond lengths [Å] and angles [°]: Ge1-O1 1.883(3), Ge1-O2 1.882(3), Ge1-O3 1.886(3); O1-Ge1-O2 93.54(15), O1-Ge1-O3 84.40(13), O2-Ge1-O3 93.97(14).

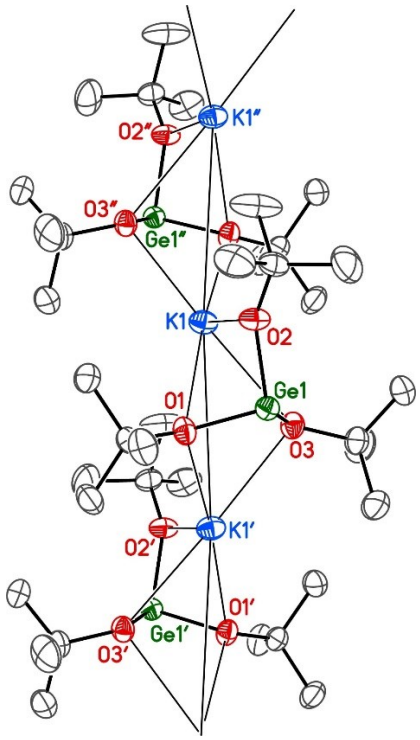

Figure 3.27. View showing the one-dimensional polymeric structure of K[Ge(O^{t}Bu)$_3$]. Hydrogen atoms are not shown for clarity. Primed atoms at x+1/2, $\bar{y}$+1/2, $\bar{z}$+1; double-primed atoms at x–1/2, $\bar{y}$+1/2, $\bar{z}$+1. Thermal ellipsoids are presented at a 30 % probability level. Selected bond lengths [Å] and angles [°]: K1-O1 3.082(4), K1-O1" 2.769(3), K1-O2 2.546(3), K1-O3 3.053(3), K1-O3" 2.875(3); O1-K1-O1" 175.07(6), O3-K1-O3" 176.47(9), O1-K1-O2 57.39(9), O1-K1-O3 48.74(8), O2-K1-O3 58.09(10), Ge1-K1-Ge1" 169.77(3).

3.8 References

1. (a) J. M. Jasinski and S. M. Gates, *Acc. Chem. Res.*, 1991, **24**, 9; (b) J. A. Jegier and W. L. Gladfelter, *Coord. Chem. Rev.*, 2000, **206**, 631; (c) C. E. Knapp and C. J. Carmalt, *Chem. Soc. Rev.*, 2016, **45**, 1036; (d) S. M. George, *Chem. Rev.*, 2010, **110**, 111; (e) K. J. Blakeney, P. D. Martin and C. H. Winter, *Organometallics*, 2020, **39**,

1006; (f) S. C. Buttera, P. Rouf, P. Deminskyi, N. J. O'Brien, H. Pedersen and S. T. Barry, *Inorg. Chem.*, 2021, **60**, 11025.

2. For selected examples, see: (a) W. O. Filtvedt, A. Holt, P. A. Ramachandran and M. C. Melaaen, *Sol. Energy Mater. Sol. Cells*, 2012, **107**, 188; (b) C.-S. Liu, L.-W. Chou, L.-S. Hong and J.-C. Jiang, *J. Am. Chem. Soc.*, 2008, **130**, 5440; (c) C. Xu, R. T. Beeler, G. J. Grzybowski, A. V. G. Chizmeshya, D. J. Smith, J. Menéndez and J. Kouvetakis, *J. Am. Chem. Soc.*, 2012, **134**, 20756.

3. (a) S. Aldridge and A. J. Downs, *Chem. Rev.*, 2001, **101**, 3305; (b) M. M. D. Roy, A. A. Omaña, A. S. S. Wilson, M. S. Hill, S. Aldridge and E. Rivard, *Chem. Rev.*, 2021, **121**, 12784.

4. (a) T. Masuda, Y. Matsuki and T. Shimoda, *Thin Solid Films*, 2012, **520**, 6603; (b) P. John, I. M. Odeh and J. Wood, *J. Chem. Soc., Chem. Commun.*, 1983, 1496; (c) P. Royen and C. Rocktäschel, *Z. Anorg. Allg. Chem.*, 1966, **346**, 279.

5. (a) P. Royen and R. Schwartz, *Z. Anorg. Allg. Chem.*, 1933, **215**, 295; (b) For a recent investigation, see: H. Yu, C. Ni, A. N. Thiessen, Z. Li and J. G. C. Veinot, *ACS Nano*, 2021, **15**, 9368; (c) S. Schlecht, *Angew. Chem., Int. Ed.*, 2002, **41**, 1178; (d) For a related approach to $[GeH]_n$, see: T. Giousis, G. Potsi, A. Kouloumpis, Y. Georgantas, N. Chalmpes, K. Dimos, M.-K. Antoniou, G. Papavassiliou, A. B. Bourlinos, H. J. Kim, V. K. S. Wadi, S. Alhassan, M. Ahmadi, B. J. Kooi, G. Blake, D. M. Balazs, M. A. Loi, D. Gournis and P. Rudolf, *Angew. Chem., Int. Ed.*, 2021, **60**, 360; (e) L. M. Dennis and N. A. Skow, *J. Am. Chem. Soc.*, 1930, **52**, 2369.

6. (a) A. D. Miller and J. Michl, *Chem. Rev.*, 1989, **89**, 1359; (b) C. Krempner, *Polymers*, 2012, **4**, 408.

7. (a) K. C. Thimer, S. M. I. Al-Rafia, M. J. Ferguson, R. McDonald and E. Rivard, *Chem. Commun.*, 2009, 7119; (b) S. M. I. Al-Rafia, A. C. Malcolm, S. K. Liew, M. J. Ferguson and E. Rivard, *J. Am. Chem. Soc.*, 2011, **133**, 777; (c) E. Rivard, *Dalton Trans.*, 2014, **43**, 8577; (d) A. K. Swarnakar, S. M. McDonald, K. C. Deutsch, P. Choi, M. J. Ferguson, R. McDonald and E. Rivard, *Inorg. Chem.*, 2014, **53**, 8662; (e) The use of GeH_2 complexes to yield Ge nanoparticles upon heating has also been described: T. K. Purkait, A. K. Swarnakar, G. B. De Los Reyes, F. A. Hegmann, E. Rivard and J. G. C. Veinot, *Nanoscale*, 2015, **7**, 2241; (f) O Millo, I. Balberg, D. Azulay, T. K. Purkait, A. K. Swarnakar, E. Rivard and J. G. C. Veinot, *J. Phys. Chem. Lett.*, 2015, **6**, 3396.

8. (a) J. Sinclair, G. Dai, R. McDonald, M. J. Ferguson, A. Brown and E. Rivard, *Inorg. Chem.*, 2020, **59**, 10996; (b) A. A. Omaña, R. K. Green, R. Kobayashi, Y. He, E. R. Antoniuk, M. J. Ferguson, Y. Zhou, J. G. C. Veinot, T. Iwamoto, A. Brown and E. Rivard, *Angew. Chem., Int. Ed.*, 2021, **60**, 228.

9. T. J. Hadlington, M. Hermann, G. Frenking and C. Jones, *J. Am. Chem. Soc.*, 2014, **136**, 3028.

10. M. Grenz, E. Hahn, W.-W. du Mont and J. Pickardt, *Angew. Chem., Int. Ed. Engl.*, 1984, **23**, 61.

11. M. Veith, P. Hobein and R. Rösler, *Z. Naturforsch. B*, 1989, **44b**, 1067.

12. (a) M. Veith, J. Hans, L. Stahl, P. May, V. Huch and A. Sebald, *Z. Naturforsch. B*, 1991, **46b**, 403; (b) M. Veith, C. Mathur and V. Huch, *Organometallics*, 1996, **15**, 2858.

13. T. Lui, J. He and Y. Zhang, *Org. Chem. Front.*, 2019, **6**, 2749.

14. L. W. Pineda, V. Jancik, K. Starke, R. B. Oswald and H. W. Roesky, *Angew. Chem., Int. Ed.*, 2006, **45**, 2602.

15. W. Drescher and C. Kleeberg, *Inorg. Chem.*, 2019, **58**, 8215.

16. While ^{t}BuOAl^{i}Bu$_2$ has been reported in the literature, only characterization in solution by ^{27}Al NMR was reported: J. S. Cha, O. O. Kwon and S. Y. Kwon, *Org. Prep. Proc. Int.*, 1996, **28**, 355. As a result, ^{t}BuOAl^{i}Bu$_2$ was prepared from the reaction of HO^{t}Bu and 0.5 equivalents of [(μ-H)Al^{i}Bu$_2$]$_2$ (DIBAL-H) in toluene.

17. (a) S. P. Foster, K.-F. Leung, K. M. Mackay and R. A. Thompson, *Aust. J. Chem.*, 1986, **39**, 1089; (b) J. Jensen, *J. Mol. Struct. (Theochem)*, 2005, **714**, 21; (c) H. Yildirimyan and G. Gattow, *Z. Anorg. Allg. Chem.*, 1985, **521**, 135.

18. For early work on the use of NHCs to stabilize GeR$_2$ units, see: (a) A. J. Arduengo, III, H. V. Rasika Dias, J. C. Calabrese and F. Davidson, *Inorg. Chem.*, 1993, **32**, 1541; (b) P. A. Rupar, M. C. Jennings and K. M. Baines, *Organometallics*, 2008, **27**, 5043; (c) P. A. Rupar, V. N. Staroverov and K. M. Baines, *Organometallics*, 2010, **29**, 4871.

19. S. Bontemps, G. Bouhadir, K. Miqueu and D. Bourrisou, *J. Am. Chem. Soc.*, 2006, **128**, 12056.

20. V. Lemierre, A. Chrostowska, A. Dargelos, P. Baylère, W. J. Leigh and C. R. Harrington, *Appl. Organomet. Chem.*, 2004, **18**, 676.

21. R. Heinemann and P. Schmidt, *Cryst. Growth Des.,* 2020, **20**, 5986.

22. K. Hatano, Y. Asano, Y. Kameda, A. Koshio and F. Kokia, *Mater. Sci. Appl.*, 2017, **8**, 838.

23. (a) M. M. D. Roy, S. Fujimori, M. J. Ferguson, R. McDonald, N. Tokitoh and E. Rivard, *Chem. Eur. J.*, 2018, **24**, 14392; (b) R. Jambor and A. Lycka, *Eur. J. Inorg. Chem.*, 2017, 4887; (c) T. J. Hadlington, C. E. Kefalidis, L. Maron and C. Jones, *ACS Catal.*, 2017, **7**, 1853.

24. (a) P. Scherrer, *Göttinger Nachrichten Math. Phys.*, 1918, **2**, 98; (b) U. Holzwarth and N. Gibson, *Nature Nanotech.*, 2011, **6**, 534.

25. A. Meller and C.-P. Gräbe, *Chem. Ber.*, 1985, **118**, 2020.

26. (a) Y. Zhao and D. Truhlar, *Theor. Chem. Acc.*, 2008, **120**, 215; (b) A. K. Wilson, D. E. Woon, K. A. Peterson and T. H. Dunning Jr., *J. Chem. Phys.*, 1999, **110**, 7667.

27. (a) G. Trinquier, *J. Am. Chem. Soc.*, 1990, **112**, 2130; (b) T. L. Windus and M. S. Gordon, *J. Am. Chem. Soc.*, 1992, **114**, 9559; (c) For computed geometries of E_2X_2 species, see: M. Lein, A. Krapp and G. Frenking, *J. Am. Chem. Soc.*, 2005, **127**, 6290; (d) T. Shimizu and G. Frenking, *Theor. Chem. Acc.*, 2011, **130**, 269.

28. E. Rivard, *Chem. Soc. Rev.*, 2016, **45**, 989.

29. S. M. I. Al-Rafia, M. R. Momeni, R. McDonald, M. J. Ferguson, A. Brown and E. Rivard, *Angew. Chem., Int. Ed.*, 2013, **52**, 6390.

30. J. P. Perdew, K. Burke and M. Ernzerhof, *Phys. Rev. Lett.*, 1996, **77**, 3865.

31. For computational work on oligohydrosilanes, see: (a) K. Takeda, H. Teramae, and N. Matsumoto, *J. Am. Chem. Soc.*, 1986, **8**, 8186; (b) J. R. Damewood Jr. and R. West, *Macromolecules*, 1985, **18**, 159; (c) A. Modelli, D. Jones, L. Favaretto, and G. Distefano, *Organometallics*, 1996, **15**, 380.

32. For readers interested in further analysis of these computations, the full output files are available as part of the Supplementary Information of: J. Sinclair, W. Medroa del Pino, K. Aku-Dominguez, Y. Minami, A. Kiran, M. J. Ferguson, M. Yasuda and E. Rivard, *Dalton Trans.*, 2021, **50**, 17688.

33. (a) A. D. Becke, *J. Chem. Phys.* 1993, **98**, 5648; (b) C. Lee, W. Yang and R. G. Parr, *Phys. Rev. B*, 1988, **37**, 785; (c) S. H. Vosko, L. Wilk and M. Nusair, *Can. J. Phys.*, 1980, **58**, 1200; (d) P. J. Stephens, F. J. Devlin, C. F. Chabalowski and M. J. Frisch, *J. Phys. Chem.*, 1994, **98**, 11623.

34. A line broadening (σ) of 0.000241967 nm^{-1} was applied, according to the method presented on: Creating UV/Visible Plots from the Results of Excited States Calculations. http://gaussian.com/uvvisplot/ [Accessed June 25, 2021].

35. W. Fa and X. C. Zeng, *Chem. Commun.*, 2014, **50**, 9126.

36. (a) M. D. Pelta, G. A. Morris, M. J. Stchedroff and S. J. Hammond, *Magn. Reson. Chem.*, 2002, **40**, S147; (b) A. Botana, J. A. Aguilar, M. Nilsson and G. A. Morris, *J. Magn. Reson.*, 2011, **208**, 270.

37. M. A. Connell, P. J. Bowyer, P. A. Bone, A. L. Davis, A. G. Swanson, M. Nilsson and G. A. Morris, *J. Magn. Reson.*, 2009, **198**, 121.

38. (a) S. Matsuo and T. Makita, *Int. J. Thermophys.*, 1993, **14**, 67; (b) P. Groves, *Polym. Chem.*, 2017, **8**, 6700.

39. A. Laubengayer and P. Brandt, *J. Am. Chem. Soc.*, 1932, **54**, 621.

40. Characteristic ^{1}H NMR of products can be found in: S. Anga, J. Acharya and V. Chandrasekhar, *J. Org. Chem.*, 2021, **86**, 2224.

41. M. J. Frisch, G. W. Trucks, H. B. Schlegel, G. E. Scuseria, M. A. Robb, J. R. Cheeseman, G. Scalmani, V. Barone, G. A. Petersson, H. Nakatsuji, X. Li, M. Caricato, A. V. Marenich, J. Bloino, B. G. Janesko, R. Gomperts, B. Mennucci, H. P. Hratchian, J. V. Ortiz, A. F. Izmaylov, J. L. Sonnenberg, D. Williams-Young, F. Ding, F. Lipparini, F. Egidi, J. Goings, B. Peng, A. Petrone, T. Henderson, D. Ranasinghe, V. G. Zakrzewski, J. Gao, N. Rega, G. Zheng, W. Liang, M. Hada, M. Ehara, K. Toyota, R. Fukuda, J. Hasegawa, M. Ishida, T. Nakajima, Y. Honda, O. Kitao, H. Nakai, T. Vreven, K. Throssell, J. A. J. Montgomery, J. E. Peralta, F. Ogliaro, M. J. Bearpark, J. J. Heyd, E. N. Brothers, K. N. Kudin, V. N. Staroverov, T. A. Keith, R. Kobayashi, J. Normand, K. Raghavachari, A. P. Rendell, J. C. Burant, S. S. Iyengar, J. Tomasi, M. Cossi, J. M. Millam, M. Klene, C. Adamo, R. Cammi, J. W. Ochterski, R. L. Martin, K. Morokuma, O. Farkas, J. B. Foresman and D. J. Fox, Gaussian 16, Revision B.01, Gaussian, Inc., Wallingford CT.

42. (a) S. Harrypersad, L. Liao, A. Khan, R. S. Wylie and D. A. Foucher, *J. Inorg. Organomet. Polym.*, 2015, **25**, 515; (b) W. Fa and X. C. Zeng, *Chem. Commun.*, 2014, **50**, 9126.

43. (a) G. M. Sheldrick, *Acta Cryst.*, 2015, **A71**, 3; (b) G. M. Sheldrick, *Acta Cryst.*, 2015, **C71**, 3.

44. (a) H. D. Flack, *Acta Crystallogr.*, 1983, **A39**, 876; (b) H. D. Flack and G. Bernardinelli, *Acta Crystallogr.*, 1999, **A55**, 908; (c) H. D. Flack and G. Bernardinelli, *J. Appl. Cryst.*, 2000, **33**, 1143.

Chapter 4: Molecular Precursors for Room Temperature Elemental Tin Deposition

4.1 Introduction

In comparison to the lighter Group 14 elements, the element-hydrogen bonds in tin hydrides are weaker[1] and more thermally sensitive.[2] This sensitivity can be troublesome when attempting to isolate molecular tin(II) hydrides, which necessitates the use of bulky anionic co-ligands[3] or strong Lewis acid-base pairs (*i.e.*, donor-acceptor stabilization)[4] to isolate them. Given the prior success of E-H bond formation from the reaction of $[Ge(O^tBu)_2]$ with hydridic boranes for elemental Ge layer deposition at mild temperatures,[5] an investigation of the tin analogue $[Sn(O^tBu)_2]_2$ for the same purpose was undertaken. While thin films of Ge(0) were able to be deposited at 70 °C using H/O^tBu exchange,[5] it was expected that the formation and decomposition of the intermediate tin hydrides could occur at lower temperatures, offering an even milder method for the deposition of tin metal from solution.

The parent Sn(IV) hydride, SnH_4, can be used to deposit nanoscale layers of metallic tin,[2] however physical vapour deposition (*e.g.*, sputtering) is used more commonly to form crystalline layers of Sn in device manufacturing.[6] Tin deposition from SnH_4 can be applied to the production of indium tin oxide (ITO),[7] the transparent electrode used in many solar cells and organic light-emitting diodes. Aerosol-assisted chemical vapour deposition (AACVD) is also used to produce ITO, where In(III)

precursors are dissolved in polar solvents in the presence of 5 mol% of tin precursors (*e.g.*, $SnCl_2$•2 H_2O or $Sn(acac)_2Br_2$, acac = acetylacetonate) to deposit crystalline films of ITO at 500 °C.[8]

$Sn(OR)_2$ (R = Me or Et) are commonly used precursors for organotin chemistry[9] and molecular tin alkoxides have been previously obtained through a number of synthetic pathways. $Sn(OR)_2$ (R = Me or Et) can be further functionalized by *trans*-alcoholysis with larger primary and secondary alcohols to install these larger functional groups on the tin centre.[10] This general ligand exchange approach has been leveraged to produce tin(II) precursors for SnO deposition from tin alkoxides,[9,11] however tin(II) alkoxides have not been investigated as precursors for the deposition of pure tin metal.

4.2 Results and discussion

*4.2.1 Improved synthesis of $[Sn(O^tBu)_2]_2$ (**1**)*

Similar to the $[Ge(O^tBu)_2]$ discussed previously in this Thesis, published syntheses for $[Sn(O^tBu)_2]_2$ (**1**) proceeded through Veith's stannylene $Sn[(N^tBu)_2SiMe_2]$[12] and subsequent reactions with two equivalents of *tert*-butyl alcohol (see Scheme 4.1, reactions (i)-(ii)).[12,13] The improved route to $[Sn(O^tBu)_2]_2$ (**1**) presented here mirrors the synthesis of $[Ge(O^tBu)_2]$ in Chapter 3, where two sequential salt-elimination reactions are required. First, the addition of three equivalents of $K[O^tBu]$ to $SnCl_2$ in THF at –35 °C produced the $K[Sn(O^tBu)_3]$ as a white solid (78 % isolated yield, Scheme 4.1(iv)). Subsequently, $[Sn(O^tBu)_2]_2$ (**1**) was obtained by the reaction of two equivalents

$K[Sn(O^tBu)_3]$ with $SnCl_2$ in toluene/THF at –35 °C, forming $[Sn(O^tBu)_2]_2$ (**1**) in quantitative yield (Scheme 4.1(v)). This tin(II) alkoxide has been reported to be a dimer in both the solid and solution states, and shows only a broad singlet at 1.45 ppm in the ^1H NMR spectrum (in C_6D_6 at room temperature).[13a]

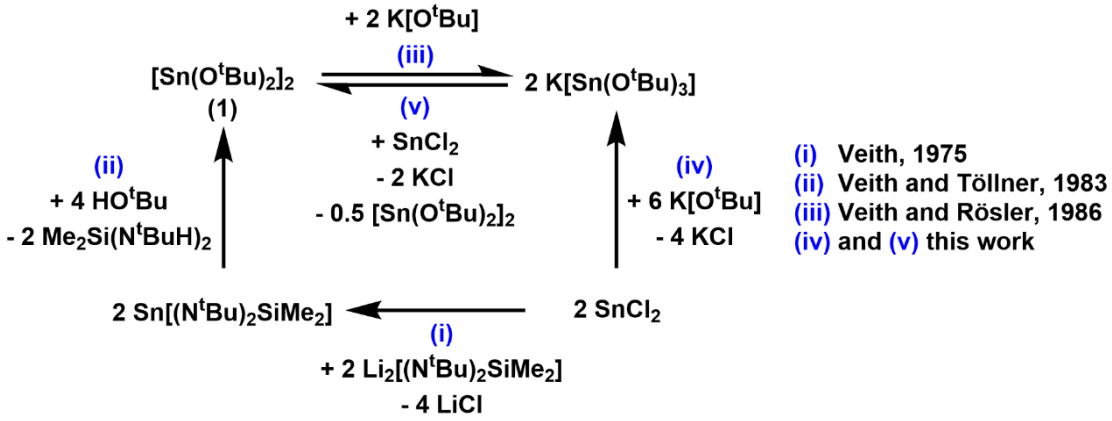

Scheme 4.1. Summary of previously reported synthetic steps to obtain $[Sn(O^tBu)_2]_2$ (**1**) (i-iii) and the improved synthesis reported here (iv and v).

$K[Sn(O^tBu)_3]$ has been previously synthesized (see Scheme 4.1, reaction (iii)), along with the Li, Na, Rb and Cs salts,[13b] at lower yields and via a more indirect series of reactions (analogous to Scheme 4.1(i-iii)). In the improved direct synthesis from $SnCl_2$ and $K[O^tBu]$, the resulting $K[Sn(O^tBu)_3]$ is purified by extraction into toluene, or can be crystallized from a saturated solution of THF as the THF solvate $\{K[Sn(O^tBu)_3]\}_2$•2 THF. The previously reported single-crystal X-ray structure for $K[Sn(O^tBu)_3]$ contains infinite linear coordination via $K^+\cdots O^tBu$ contacts, as is known for the germanium analogue $K[Ge(O^tBu)_3]$.[5] The coordination of THF to the K^+ cations in $K[Sn(O^tBu)_3]$ affords discrete dimers in the solid-state. As expected, the three-coordinate Sn(II) centres

in $\{K[Sn(O^tBu)_3]\}_2$•2 THF adopt pyramidalized geometries, due to the presence of a thermochemically active lone pair.

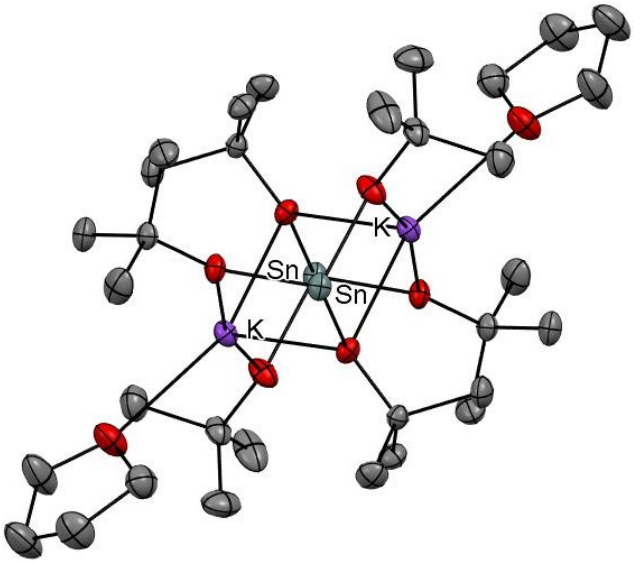

Figure 4.1. ORTEP of $\{K[Sn(O^tBu)_3]\}_2$•2 THF. Thermal ellipsoids plotted at a 30 % probability level. Selected bond lengths [Å] and angles [°]: Sn1-O1 2.074(1), Sn1-O2 2.066(1), Sn1-O3 2.0892(8), K1-O1 2.6816(9), K1-O2 2.6633(9), K1-O3 2.704(1), K1-O4 2.766(2); O1-Sn1-O2 92.90(4), O2-Sn1-O3 83.65(4), O1-Sn1-O3 88.46(4).

4.2.2 An N-heterocyclic carbene (NHC) complex of $Sn(O^tBu)_2$

The association of an *N*-heterocyclic carbene to a $Sn(O^tBu)_2$ moeity could be used to tune the reactivity and volatility of the tin precursor by disrupting strong Sn-O interactions in the solid-state dimer of $[Sn(O^tBu)_2]_2$ (**1**), and stabilize partially substituted NHC-Sn(H)O^{t}Bu intermediates. Following established literature procedures,[14,15] the free carbene $ImMe_2$ ($ImMe_2$ = [(HCNMe)$_2$C:]) was produced *in situ* and combined with tin(II) dichloride in a THF/toluene solution (4:1) to produce $ImMe_2$•$SnCl_2$ (**2**) (Scheme 4.2).

Crystals of **2** were obtained from a concentrated THF solution and the crystallographically determined bond lengths and angles about the Sn centre in this complex are consistent with previously reported NHC•$SnCl_2$ species;[14] specifically, the bond angles at Sn approach 90°, suggesting a high degree of s-character within the non-bonding lone pair at Sn.

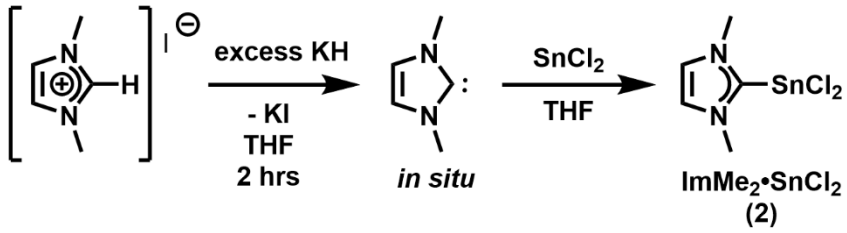

Scheme 4.2. Synthesis of $ImMe_2$•$SnCl_2$ (**2**).

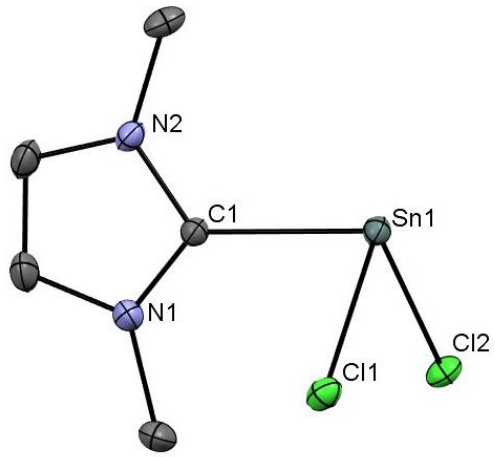

Figure 4.2. ORTEP of $ImMe_2$•$SnCl_2$ (**2**). Thermal ellipsoids plotted at 30 % probability level. Select bond lengths [Å] and angles [°]: C1-Sn1 2.298(2), Sn1-Cl1 2.5287(5), Sn1-Cl2 2.5287(5); C1-Sn1-Cl1 89.39(5), C1-Sn1-Cl2 91.83(5), Cl1-Sn1-Cl2 90.23(2).

Subsequent reaction of **2** with two equivalents of K[O^{t}Bu] in Et_2O produced the target complex $ImMe_2$•$Sn(O^tBu)_2$ (**3**) via the elimination of KCl. The optimized reaction conditions (see Scheme 4.3) involved the dropwise addition of a slurry of K[O^{t}Bu] to a suspension of $ImMe_2$•$SnCl_2$ (**2**) (both in diethyl ether cooled to -35 °C) afforded the yellow solid $ImMe_2$•$Sn(O^tBu)_2$ (**3**) after work-up. This product was characterized by ^{1}H and $^{13}C\{^1H\}$ NMR spectroscopy. Further investigation will be undertaken to determine whether complex **3** has the requisite thermal properties for atomic layer deposition (ALD), such as a lower volatilization temperature compared to **1**. In an effort to obtain **3** through fewer synthetic steps, *N,N*'-dimethylimidazolium iodide ($[ImMe_2H]I$)[15] was combined with $K[Sn(O^tBu)_3]$ and heated to 70 °C, with the goal of product formation via the elimination of *tert*-butyl alcohol and KI (Scheme 4.3). Unfortunately, ^{1}H and $^{13}C\{^1H\}$ NMR spectroscopy indicated that another undesired carbene-containing product was formed, likely $[ImMe_2H][Sn(O^tBu)_3]$ following the elimination of KI.

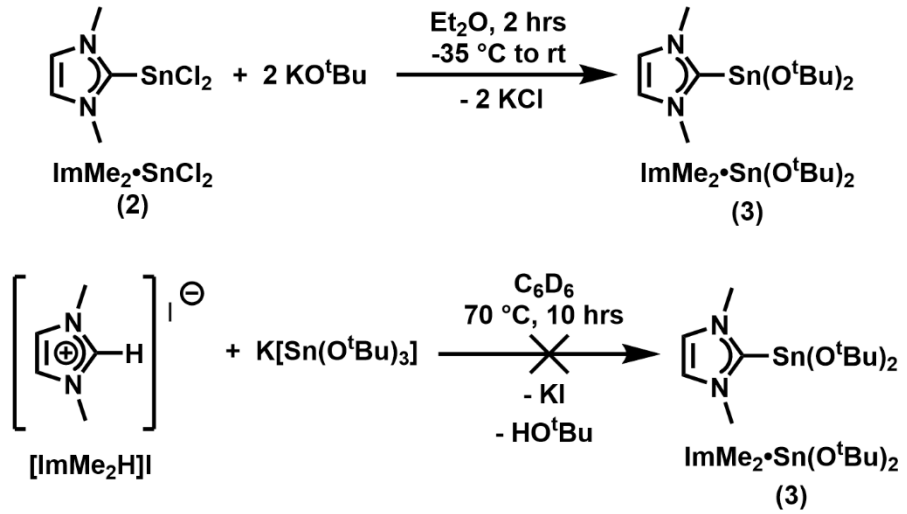

Scheme 4.3. Reaction to produce $ImMe_2•Sn(O^tBu)_2$ (**3**) (top) and unsuccessful attempt to produce **3** from combining *N,N*'-dimethylimidazolium iodide ($[ImMe_2H]I$)[15] with $K[Sn(O^tBu)_3]$.

*4.2.3 Tin(0) deposition from $[Sn(O^tBu)_2]_2$ (**1**), $ImMe_2•Sn(O^tBu)_2$ (**3**), and $Sn[N(SiMe_3)_2]_2$ (**4**)*

Given the thermal instability of many tin(II) hydrides,[2] it is expected that should these species form in solution, they will undergo rapid dehydrogenation to deposit Sn(0), liberating H_2 in the process. The germanium analogue of compound **1**, **[**$Ge(O^tBu)_2$], has been shown previously to react with excess HBpin (pinacolborane) to produce the hydride-rich solid $[GeH_{1.92}(O^tBu)_{0.08}]_n$, where two O^tBu/H exchanges would have to occur at each Ge centre to produce the heavy polyethylene analogue $[GeH_2]_n$.[5] Heating $[GeH_{1.92}(O^tBu)_{0.08}]_n$ to above 200 °C, or mixing $[Ge(O^tBu)_2]$ with a more reactive hydride source ($Me_2S•BH_3$) at 70 °C yielded elemental Ge.[5] Given this established reactivity in the lighter Group 14 analogue, $[Sn(O^tBu)_2]_2$ (**1**) and $ImMe_2•Sn(O^tBu)_2$ (**3**) were reacted with HBpin in C_6D_6 (Scheme 4.4). In both reactions, a dark grey precipitate was formed

immediately and ^{1}H and ^{11}B NMR spectroscopy indicated the presence of the expected ^{t}BuOBpin by-product[16] in solution (Figure 4.3). In the reaction of **3** with 2 equivalents of HBpin, multiple NHC-containing products were formed, including likely a dihydroaminal [$(HCNMe_2)CH_2$], based on the two peaks in the ^{1}H NMR spectrum in the 5.5-5.7 ppm region, where similar signals and profiles have been reported for larger $(NHC)H_2$ derivatives.[4]

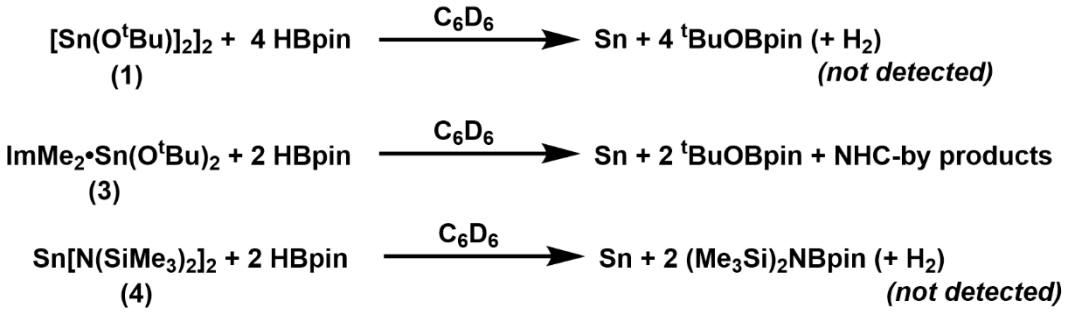

Scheme 4.4. Reaction of **1** and **3** with the hydride source HBpin to release Sn(0).

In addition to depositing tin from the precursors synthesized in this Thesis, the commercially available liquid $Sn[N(SiMe_3)_2]_2$ (**4**) was also reacted with HBpin. The reaction of this Sn precursor with hydride sources is largely unreported, however $Sn[N(SiMe_3)_2]_2$ has previously been used for the solvothermal synthesis of Pb/Te/Sn nanoparticles.[17] Interestingly, the final stage of the Pb/Te/Sn nanocrystal synthesis reported by Jiang *et al.* included the addition of $Li[HBEt_3]$ (in the presence of Me_3SiCl), reportedly to remove the organic ligands from all metal precursors.[17] Indeed, ^{1}H NMR spectral analysis of the soluble by-products of the reaction between $Sn[N(SiMe_3)_2]_2$ (**4**) and two equivalents of HBpin at room temperature (Scheme 4.4) show only the expected

$(Me_3Si)_2NBpin$ by-product.[18] No sign of ^tBuOH was found by NMR spectroscopy (Figure 4.3) in any of the deposition reactions outlined in Scheme 4.4. While this by-product may be formed by reductive elimination from a $SnO^tBu(H)$ intermediate, any alcohol formed could be rapidly consumed by a subsequent reaction with HBpin in solution to form H_2 and $^tBuOBpin$ (confirmed by an NMR-scale reaction between HBpin and ^tBuOH, *vide infra*). Subsequent reactivity studies with alternative hydride sources or low-temperature experiments could be pursued to better understand the mechanism of Sn(0) formation, in conjunction with computational analysis of the reaction pathway.

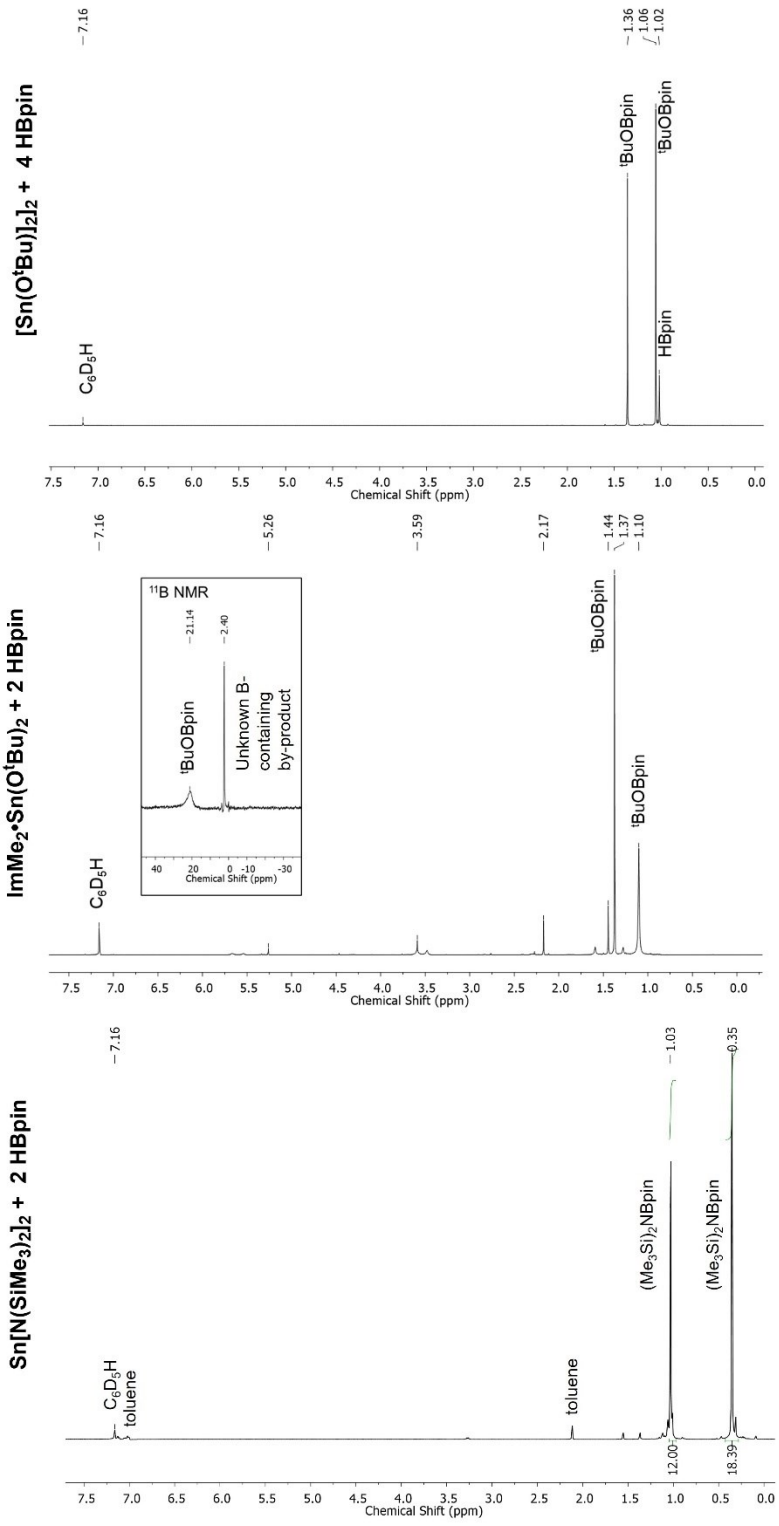

Figure 4.3. ^{1}H NMR spectra of reaction by-products (primarily ^{t}BuOBpin[16] and $(Me_3Si)_2NBpin$[18]) from the reactions depicted in Scheme 4.4, each conducted in C_6D_6.

Powder X-ray diffraction (pXRD) analysis of the grey precipitate obtained from the reaction of $[Sn(O^tBu)_2]_2$ (**1**) with HBpin was conducted to determine the identity and crystallinity of the solid. The product was rinsed two times with 2 mL of toluene, the solvent decanted away, and the remaining volatiles removed by vacuum. The obtained Sn powder showed strong crystalline reflections aligning with the published diffraction pattern of tin.[19] The precipitate collected from the reaction of $Sn[N(SiMe_3)_2]_2$ (**4**) and two equivalents of HBpin at room temperature (Scheme 4.4) produced a crystalline Sn product of similar quality (Figure 4.4). Thus, both $[Sn(O^tBu)_2]_2$ and $Sn[N(SiMe_3)_2]_2$ are promising candidates for solution deposition of crystalline Sn at room temperature.

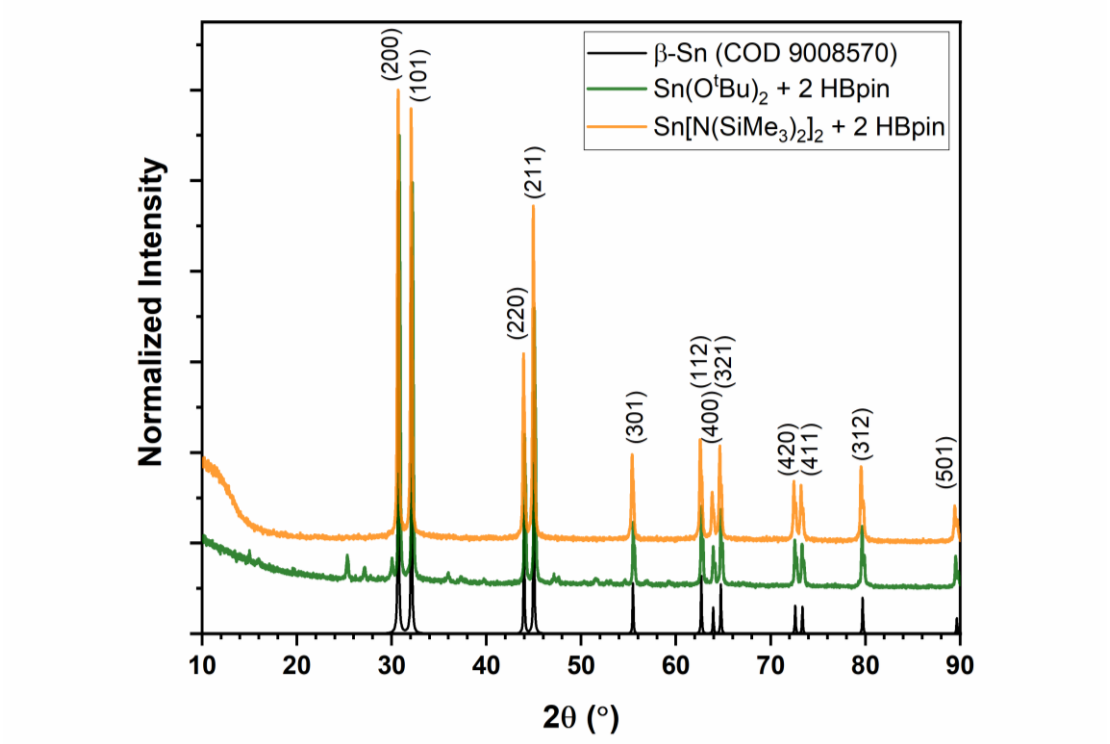

Figure 4.4. pXRD analysis of the β-Sn precipitate[19] deposited from the reaction of $[Sn(O^tBu)_2]_2$ (**1**) and $Sn[N(SiMe_3)_2]_2$ (**4**) with HBpin.

4.3 Conclusions

An improved method is presented for the preparation of the tin(II) alkoxide $[Sn(O^tBu)_2]_2$ (**1**),[14,15] and two new NHC-supported tin species, $ImMe_2•SnCl_2$ (**2**) and $ImMe_2•Sn(O^tBu)_2$ (**3**), were also synthesized. The Sn(II) complexes **1** and **4** were reacted with HBpin to induce O^tBu/H exchange at the Sn centres at room temperature, resulting in the formation of Sn metal with remarkable crystallinity. While tin depositions onto substrates have yet to be explored, the crystallinity of the Sn metal obtained from a room temperature reaction is promising for future applications in device manufacturing.[6-8] This reaction method is also desirable as the resulting by-products (*i.e.*, $^tBuOBpin$, $(Me_3Si)_2NBpin$, H_2) are highly soluble and/or volatile substances which can easily be removed through washing or by vacuum.

4.4 Experimental procedures

4.4.1 General

All reactions were performed using standard Schlenk techniques under an atmosphere of nitrogen or in a nitrogen-filled glove box (Innovative Technology, Inc.). Solvents were dried using a Grubbs-type solvent purification system manufactured by Innovative Technology, Inc., and stored under an atmosphere of nitrogen prior to use. $SnCl_2$, methyl iodide, potassium *tert*-butoxide, *tert*-butanol, and 1-methylimidazole were purchased from Sigma-Aldrich and used as received. $Sn[N(SiMe_3)_2]_2$ (**4**) was purchased

from Gelest Inc. and used as received. 4,4,5,5-Tetramethyl-1,2-dioxaborolane (HBpin) was purchased from Oakwood Chemicals and used as received. ^{1}H, $^{11}B/^{11}B\{^{1}H\}$, $^{13}C\{^{1}H\}$, and ^{119}Sn NMR spectra were recorded on a Varian Inova 400 or 500 MHz spectrometer and referenced externally to Me_4Si (^{1}H, $^{13}C\{^{1}H\}$), $F_3B{\bullet}OEt_2$ ($^{11}B/^{11}B\{^{1}H\}$) and $SnMe_4$ ($^{119}Sn\{^{1}H\}$). Elemental analyses were performed by the Analytical and Instrumentation Laboratory at the University of Alberta. Melting points were obtained in sealed glass capillaries under nitrogen using a MelTemp melting point apparatus and are uncorrected.

4.4.2 Characterization of solid materials

Powder XRD patterns were collected on a Rigaku Ultima IV powder diffractometer equipped with a Co Kα radiation source (Kα1 = 1.78900 Å, Kα2 = 1.79283 Å) operating at 40 kV and 40 mA. A D/Tex Ultra detector was used, with an iron filter to eliminate the Kβ radiation at 1.62083 Å. Approximately 5 mg of sample was placed on zero-background silicon holders and mounted in the instrument. Diffraction data were collected in continuous scan mode between 5 and 90° in 2θ with a step size of 0.0200°.

4.4.3 Synthetic procedures and reactivity

Preparation of K[Sn(O^{t}Bu)$_3$]: To $SnCl_2$ (4.416 g, 23.29 mmol) in 50 mL of THF at -78 °C was added a solution of K[O^{t}Bu] (7.840 g, 69.87 mmol) in 50 mL THF at the same temperature. The reaction mixture was stirred and warmed gradually to room

temperature for 10 hours and then volatiles were removed by vacuum. 2 × 100 mL of Et_2O was added to the flask, and the suspension was filtered through a pad of Celite to collect the supernatant. Removal of the volatiles from the filtrate *in vacuo* afforded $K[Sn(O^tBu)_3]$ (5.156 g, 68 %) as a white solid. Crystals of the $K[Sn(O^tBu)_3]$•2 THF of suitable quality for single-crystal X-ray diffraction were obtained by cooling a saturated THF solution of $K[Sn(O^tBu)_3]$ to -35 °C for 3 days. Data for $K[Sn(O^tBu)_3]$: ^{1}H NMR (C_6D_6): δ 1.39 (s, 27H, C(C*H*$_3$)$_3$).[13a] ^{13}C{^{1}H} NMR (C_6D_6): δ 69.6 (*C*(CH$_3$)$_3$), 35.7 (C(*C*H$_3$)$_3$). ^{119}Sn{^{1}H} NMR (C_6D_6): δ -250.0. Anal. Calc. for $KC_{12}H_{27}SnO_3$: C, 38.22; H, 7.22. Found: C, 38.09; H, 6.96 %.

Preparation of $[Sn(O^tBu)_2]_2$ (1): A solution of $SnCl_2$ (0.0664 g, 0.350 mmol in 5 mL THF at -35 °C) was added dropwise to a stirring slurry of $K[Sn(O^tBu)_3]$ (0.264 g, 0.701 mmol) in 10 mL of cold toluene (-35 °C). The reaction mixture was stirred and warmed to room temperature for 2 hours, after which the volatiles were removed. The solid was extracted with 2 × 10 mL of hexanes, and the combined extracts were filtered through Celite. The volatiles were removed from the filtrate by vacuum to give **1** as a white solid (0.279 g, 78 %). ^{1}H NMR (C_6D_6): δ 1.45 (broad s, 36H, OC(C*H*$_3$)$_3$).[13b] ^{13}C{^{1}H} NMR (C_6D_6): δ 31.9 (OC(*C*H$_3$)$_3$), 73.3 (O*C*(CH$_3$)$_3$). ^{119}Sn{^{1}H} NMR (C_6D_6, 500 MHz): δ -350.0.

Preparation of $ImMe_2$•$SnCl_2$ (2): In a variation of a literature procedure,[15] N,N-dimethylimidazolium iodide (0.293 g, 1.31 mmol) and KH (0.250 g, 6.23 mmol) were suspended in 10 mL of THF and stirred for 4 hrs. The precipitate was allowed to settle,

and the orange solution containing free $ImMe_2$ was filtered into a vial containing $SnCl_2$ (0.248 g, 1.31 mmol) suspended in 4 mL of THF. The reaction mixture was allowed to proceed for 15 minutes. The volatiles were then removed from the reaction mixture to give a white solid (0.856 g, 87 %). Crystals suitable for X-ray crystallography were obtained by cooling a concentrated solution in THF to -35 °C for one day. ^{1}H NMR ($CDCl_3$): δ 4.17 (s, 6H, NC*H*$_3$), 7.06 (s, 2H, N(C*H*)$_2$N). ^{13}C{^{1}H} NMR ($CDCl_3$): δ 37.9 (N*C*H$_3$), 123.0 (N(*C*H)$_2$N), 187.5 (N*C*N). ^{119}Sn NMR ($CDCl_3$, 500 MHz): δ -600.3. Mp: 165 °C (decomp.). Anal. Calc. for $C_5H_8N_2SnCl_2$: C, 21.02; H, 2.82; N, 9.80. Found: C, 21.19; H, 2.83; N, 9.42 %.

Preparation of $ImMe_2$•Sn(O^{t}Bu)$_2$ (3): A suspension of KO^{t}Bu (0.095 g, 0.85 mmol) in 3 mL Et_2O was added dropwise to a stirring solution of **1** (0.121 g, 0.423 mol) in 5 mL of Et_2O. The reaction mixture was stirred for 2 hours, after which it was allowed to settle, and the mother liquor was filtered through Celite. The remaining solid was re-suspended in toluene (10 mL) and stirred for 10 minutes to extract additional product. The extract was filtered through Celite, added to the first extraction, and the volatiles were removed under vacuum to give **3** as a yellow solid (0.088 g, 58 %). ^{1}H NMR (C_6D_6): δ 1.64 (s, 18H, C(C*H*$_3$)$_3$), 3.48 (s, 6H, NC*H*$_3$), 5.62 (s, 2H, N(C*H*)$_2$N). ^{13}C{^{1}H} NMR (C_6D_6): δ 35.5 (OC(*C*H$_3$)), 36.4 (N*C*H$_3$), 70.2 (O*C*(CH$_3$)), 120.9 (N(*C*H)$_2$N). ^{119}Sn{^{1}H} NMR (C_6D_6, 500 MHz): δ -600.4. Mp: 123 °C.

Deposition of Sn(0) from precursors (1), (3), and Sn[N(SiMe$_3$)$_2$]$_2$ (4) : For NMR-scale reactions, solutions of each precursor in C_6D_6 (~10 mg in 500 µL) were

preprared and loaded into J-Young tubes. The appropriate equivalents of HBpin (as per Scheme 4.4) were added by micropipette, and NMR spectra were collected. For larger-scale reactions for collection of Sn precipitate, 0.100 M solutions of the precursor in toluene were prepared at room temperature, followed by the addition of the appropriate amount of HBpin (as per Scheme 4.4). For all reactions, immediate darkening of the reaction mixture occurred upon HBpin addition. In the case of precursors **1** and $Sn[N(SiMe_3)_2]_2$ (**4**), the reaction formed dark grey precipitate within 3 minutes, and Sn mirrors were visible on the inside surface of the vials after 1 hour. The volatiles were removed from the reaction mixture under vacuum. The dark grey precipitates were washed with 3 mL dry toluene, allowed to settle, and the supernatant decanted away. The solids were dried by vacuum and submitted for further analysis.

Preparation of ^{t}BuOBpin: To a J-Young NMR tube containing 20.0 μL (0.153 mmol) HBpin in 600 μL C_6D_6 was added 7.3 μL (0.077 mmol) of HO^{t}Bu. This experiment was conducted only to confirm reactivity, and NMR spectra were collected within 10 minutes of the start of the reaction. The only product formed was ^{t}BuOBpin**.** ^{1}H NMR (C_6D_6): δ 1.05 (s, 12H, OC(CH_3)$_3$), 1.35 (s, 9H, O-[C(CH_3)$_2$]$_2$-O). ^{11}B NMR (C_6D_6): δ 21.7.[16]

4.5 X-ray crystallographic data

Crystals of appropriate quality for single-crystal X-ray diffraction studies were removed from the mother liquor and immediately covered with a thin layer of hydrocarbon oil (Paratone-N) in a sealed vial for transport to the diffractometer. A suitable crystal was then selected, attached to a glass fibre, and mounted under a stream of nitrogen onto the instrument. All data were collected using a Bruker APEX II CCD detector/D8 diffractometer using Cu Kα radiation. The data were corrected for absorption through Gaussian integration from indexing of the crystal faces. Structures were solved and refinements were completed using direct methods (SHELXT-2014 and SHELXL-2018/3).[20]

Table 4.1. Crystallographic data for K[Sn(O^{t}Bu)$_3$]•2 THF and ImMe$_2$•SnCl$_2$ (**2**).

Compound	K[Sn(O^{t}Bu)$_3$]•2 THF	ImMe$_2$•SnCl$_2$ (**2**)
formula	$C_{32}H_{70}K_2O_8Sn_2$	$C_5H_8SnN_2Cl_2$
formula weight	898.46	285.72
crystal system	triclinic	monoclinic
space group	$P\bar{1}$ (No. 2)	$P2_1/n$ (No. 14)
unit cell parameters		
a (Å)	10.1877(7)	7.6355(2)
b (Å)	10.8255(7)	8.8033(3)
c (Å)	99.6840(9)	13.9001(4)
α (°)	99.6840(9)	-
β (°)	113.7973(8)	92.7393(8)
γ (°)	96.7925(9)	-
V (Å^3)	1078.17(12)	933.26(5)
Z	1	4
ρ_{calcd} (g cm^{-3})	1.384	2.034
μ (mm^{-1})	1.390	26.52
radiation (λ [Å])	Mo Kα (0.71073) (microfocus source)	Cu Kα (1.54178) (microfocus source)
T (°C)	–100	–100
$2\theta_{max}$ (°)	66.53	148.08
Total data	41251 (-15 ≤ h ≤ 15, -16 ≤ k ≤ 16, -16 ≤ l ≤ 16)	35591 (-9 ≤ h ≤ 9, -9 ≤k ≤ 10, -17 ≤ l ≤ 17)
Unique data (R_{int})	7951 (0.0173)	1876 (0.0296)
Data$_{obs}$ [$F_o^2 \geq 2\sigma(F_o^2)$]	7288	1828
data/restraints/parameters	7915 / 55[b] /252	1876 / 0 / 93
final R indices[a]		
R_1 [$F_o^2 \geq 2\sigma(F_o^2)$]	0.0227	0.0186
wR_2 [all data]	0.0592	0.0482
Max/min $\Delta\rho$ (e$^-$ Å^{-3})	0.774 and –0.431	0.291 and –1.093

[a] $R_1 = \Sigma||F_o| - |F_c||/\Sigma|F_o|$; $wR_2 = [\Sigma w(F_o^2 - F_c^2)^2/\Sigma w(F_o^4)]^{1/2}$ [b] The minor component of the "whole-molecule" disorder was restrained to have approximately the same geometry as that of the major orientation by use of the *SHELXL* **SAME** instruction. The atoms of the minor component were refined with a common isotropic displacement parameter.

4.6 References

1. (a) E. Rivard, *Chem. Soc. Rev.*, 2016, **45**, 989; (b) M. M. D. Roy, A. A. Omaña, A. S. S. Wilson, M. S. Hill, S. Aldridge and E. Rivard, *Chem. Rev.*, 2021, **121**, 12784.
2. (a) V. H. Nguyen, A. Dobbie, M. Myronov, D. J. Norris, T. Walther and D. R. Leadley, *Thin Solid Films,* 2012, **520**, 3222; (b) R. Venkatasubramanian, R. T. Pickett and M. L. Timmons, *J. Appl. Phys.*, **1989**, *66*, 5662.
3. (a) B. E. Eichler and P. P. Power, *J. Am. Chem. Soc.*, 2000, **122**, 8785; (b) L. W. Pineda, V. Jancik, K. Starke, R. B. Oswald and H. W. Roesky, *Angew. Chem., Int. Ed.*, 2006, **45**, 2602.
4. S. M. I. Al-Rafia, A. C. Malcolm, S. K. Liew, M. J. Ferguson and E. Rivard, *J. Am. Chem. Soc.*, 2011, **133**, 777.
5. J. Sinclair, W. Medroa del Pino, K. Aku-Dominguez, Y. Minami, A. Kiran, M. J. Ferguson, M. Yasuda and E. Rivard, *Dalton Trans.*, 2021, **50**, 17688.
6. C. G. Granqvist, *Appl. Phys. A*, 1993, **57**, 19.
7. C. E. Knapp and C. J. Carmalt, *Chem. Soc. Rev.*, 2016, **45**, 1036.
8. M. Takeuchi and K. Maki, *Jpn. J. Appl. Phys.*, 2007, **46**, 7852.
9. A. Suzuki and K. Maki, *Chem. Vap. Dep.*, 2006, **12**, 608.
10. (a) N. Hollingsworth, G. Kociok-Köhn, K. C. Molloy and A. L. Sudlow, *Dalton Trans.*, 2010, **39**, 5446; (b) N. Hollingsworth, G. A. Horley, M. Mazhar, M. F. Mahon, K. C. Molloy, P. W. Haycock, C. P. Myers and G. Critchlow, *Appl. Organometal. Chem.*, 2006, **20**, 687; (c) W. Ikuko and K. Ichiro, *Chem. Lett.*, 1972, **1**, 325.
11. J. D. Parish, M. W. Snook and A. L. Johnson, *Dalton Trans.*, 2021, **50**, 13902.

12. M. Veith, *Angew. Chem. Int. Ed. Engl.*, 1975, **4**, 263.

13. (a) M. Veith and F. Töllner, *J. Organomet. Chem.*, 1983, 219; (b) M. Veith and R. Rösler, *Z. Natutforch.*, 1986, **41b**, 1071.

14. (a) K. C. Thimer, S. M. I . Al-Rafia, M. J. Ferguson, R. McDonald and E. Rivard, *Chem. Commun.*, 2009, 7119; (b) N. Kuhn, T. Kratz, D. Bläser and R. Boese, *Chem. Ber.*, 1995, **128**, 245; (b) B. Bantu, G. M. Pawar, U. Decker, K. Wurst, A. M. Schmidt and M. R. Buchmeiser, *Chem. Eur. J.*, 2009, **15**, 3103.

15. J. Sinclair, G. Dai, R. McDonald, M. J. Ferguson, A. Brown and E. Rivard, *Inorg. Chem.*, 2020, **59**, 10996.

16. T. Lui, J. He and Y. Zhang, *Org. Chem. Front.*, 2019, **6**, 2749.

17. W. Jiang, Z.-L. Yang, D. Weng, J.-W. W, Y.-F. Lu, M.-J. Zhang and Z.-Z. Yang, *Chin. Chem. Lett.*, 2014, **25**, 849.

18. Z. Huang, S. Wang, X. Zhu, Q. Yuan, Y. Wei, S. Zhou and X. Mu, *Inorg. Chem.*, 2018, **57**, 15069.

19. (a) R. W. G. Wyckoff, *Crystal Structures Vol. 1*, Interscience Publishers, New York, 1963; (b) S. Grazulis, D. Chateigner, R. T. Downs, A. T. Yokochi, M. Quiros, L. Lutterotti, E. Manakova, J. Butkus, P. Moeck and A. Le Bail, *J. Appl. Cryst.*, 2009, **42**, 726; (c) M. Alf, D. Gultrkin and H. Akbulut, *Acta Phys. Pol. A*, 2013, **123**, 323.

20. (a) G. M. Sheldrick, *Acta Cryst.*, 2015, **A71**, 3; (b) G. M. Sheldrick, *Acta Cryst.*, 2015, **C71**, 3.

Chapter 5: Summary and Future Work

5.1 Cursory review and proposed research directions

In Chapter 2, a germanium dihydride moiety was stabilized in a Lewis acid-base push-pull system with an *N*-heterocyclic carbene (NHC) and BH_3 to form $ImMe_2$•GeH_2•BH_3 ($ImMe_2$, $(HCNMe)_2C$:). $ImMe_2$•GeH_2•BH_3 has a high wt% Ge (39 %), and can deposit nanoscale layers of amorphous germanium onto silicon substrates upon heating to 70 °C in solution. The mechanism of this decomposition was revealed by experimental and computational studies to proceed through direct cleavage of the C_{NHC}–Ge and Ge–B bonds (*vide supra*, Chapter 2).

Although computational analysis revealed that the Ge–B bond in $ImMe_2$•GeH_2•BH_3 likely breaks prior to the C_{NHC}–Ge during thermal decomposition, experimental kinetic studies were unable to confirm this conclusion. The deuterated analogue, $ImMe_2$•GeD_2•BD_3 was prepared from the reaction of $ImMe_2$•$GeCl_2$ and $Li[BD_4]$ for kinetic experiments, however, the secondary inverse kinetic isotope effect observed could not be deconvoluted into contributions from C_{NHC}–Ge vs. Ge–B bond breakage, due to the H/D substitution occurring at both the Ge and B centres.[1] The decomposition rates (k) of the $ImMe_2$•GeH_2•BH_3 and $ImMe_2$•GeD_2•BD_3 could be compared to that of the $ImMe_2$•GeH_2•BD_3. Pathway **B** (preliminary Ge–B bond breakage) could be proven by showing that $k(ImMe_2$•GeD_2•$BD_3)$ = $k(ImMe_2$•GeH_2•$BD_3)$ and $k(ImMe_2$•GeH_2•$BH_3)$ = $k(ImMe_2$•GeD_2•$BH_3)$.[1] Given that the planarization of $B(H/D)_3$ was shown to be the driving force in this decomposition

pathway, only the deuteration of the boron centre should have an impact on the decomposition rate of the complex.

$ImMe_2•GeH_2•BD_3$ could be synthesized by the reaction of $ImMe_2•GeCl_2$ with BD_3 (as $THF•BD_3$ or $Me_2S•BD_3$) to give $ImMe_2•GeCl_2•BD_3$, followed by a reaction with the hydride source $Na[HBEt_3]$ or $Li[HBEt_3]$. Given the stronger Lewis basicity of BH_3 relative to BEt_3,[2] this reaction should yield $ImMe_2•GeH_2•BD_3$ (Scheme 5.1) without replacement of the BD_3 by the BEt_3 released during the second synthetic step. The oppositely substituted $ImMe_2•GeD_2•BH_3$ could be obtained by the coordination of BH_3 (introduced as $THF•BH_3$ or $Me_2S•BH_3$) to $ImMe_2•GeCl_2$ to form $ImMe_2•GeCl_2•BH_3$,[3] followed by mixing with $Na[HBEt_3]$ or $Li[DBEt_3]$, forming $ImMe_2•GeD_2•BH_3$.

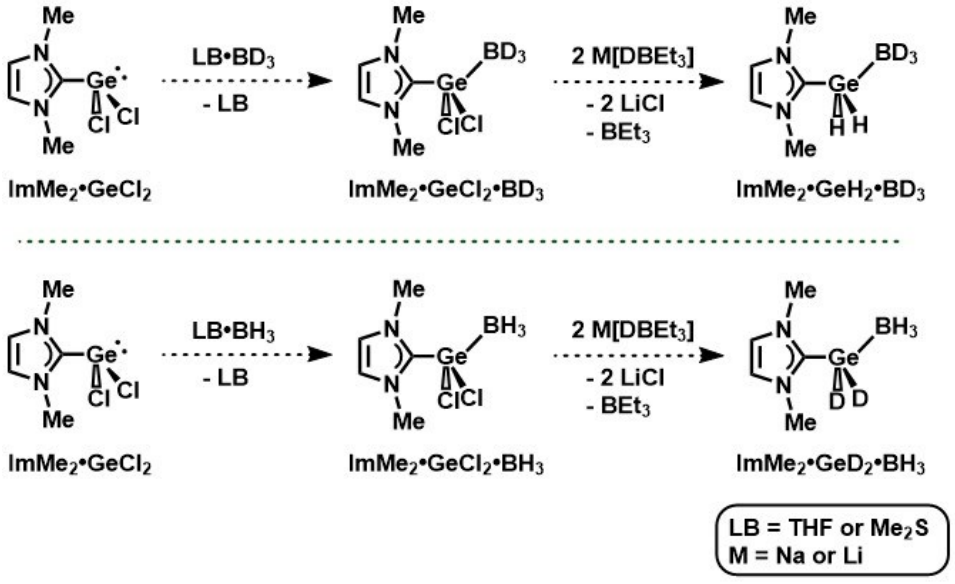

Scheme 5.1. Reaction scheme for the selective deuteration of $ImMe_2•GeH_2•BD_3$ and $ImMe_2•GeD_2•BH_3$. LB = THF or SMe_2.

Chapter 3 discussed the improved synthesis of [Ge(O^{t}Bu)$_2$] and its subsequent applications in the synthesis of oligogermanes (namely, the most substituted species [GeH$_{1.92}$(O^{t}Bu)$_{0.08}$]$_n$) and to applications in germanium film deposition via reactions with various hydride sources. An NHC-supported system was also investigated, with experimental studies on ImMe$_2$•Ge(O^{t}Bu)$_2$ conducted and larger alkoxide analogues investigated computationally. These NHC•Ge(OR)$_2$ complexes were generally determined to be incompatible with oligogermane synthesis or germanium deposition due to their incomplete conversion to [GeH$_2$] upon reaction with hydride sources.

In the course of exploring ImMe$_2$•GeR$_2$ species for the work recounted in Chapter 3, two monosubstituted halogermanium adducts were also produced: ImMe$_2$•GeCl(O^{t}Bu) (Scheme 5.2) and Im^{i}Pr$_2$Me$_2$•GeCl$_3$^{t}Bu. ImMe$_2$•GeCl(O^{t}Bu) was prepared from combining K[O^{t}Bu] and ImMe$_2$•GeCl$_2$,[4,5] and the free carbene Im^{i}Pr$_2$Me$_2$ (Im^{i}Pr$_2$Me$_2$ = (MeCN^{i}Pr)$_2$C:) can be reacted directly with the commercially available ^{t}BuGeCl$_3$ to give Im^{i}Pr$_2$Me$_2$•GeCl$_3$^{t}Bu. While these complexes were not further explored for reactivity and deposition in the context of Chapter 3, they are interesting molecules for further study. For example, the stoichiometric reaction of ImMe$_2$•GeCl(O^{t}Bu) with a Li[BH$_4$] may result in a metastable ImMe$_2$•GeH(O^{t}Bu)•BH$_3$, which could undergo reductive elimination of HO^{t}Bu, either immediately or upon gentle heating.[6] This decomposition chemistry may deposit elemental Ge and release free NHC,[4] or form small NHC-substituted Ge clusters (Scheme 5.2). Ge$_3$ clusters are predicted to be stable with NHC coordination, based on computational work conducted by Frenking, Merino and coworkers,[7] and NHC-Cu Ge clusters (*e.g.*, IPrCu{η^3-Ge$_9$R$_3$}, IPr = ([(HCNDipp)$_2$C:,

Dipp = 2,6-$^{i}Pr_2C_6H_3$, R = $Si(SiMe_3)_3$ or $Si^{i}Pr_3$)[8] have been studied extensively in the Fässler Group at Technische Universität München for fundamental study and applications in germanium deposition.[8] NHC•GeCl(OR) species with more sterically hindered alkoxide functionalization could be generated following the same synthetic procedure shown in Scheme 5.2. These bulky alkoxides could act as protecting groups to generate more thermally stable NHC•GeH(OR) for tunable deposition via thermally induced reductive elimination or reaction with a stoichiometric hydride following the method outlined in Chapter 3. Thermally tunable deposition may be advantageous for tailoring deposition rates, crystallinity, or substrate interactions. A protected $[NHC•Ge(OR)]^{+}$ cation could also be generated; similar species are known to act as catalysts for hydroboration.[9] Similar reactivity could be induced from the $Im^{i}Pr_2Me_2•GeCl_3{}^{t}Bu$, with the ^{t}Bu acting as a protecting group for the instillation of hydrides or other functionalities (Scheme 5.3); it is expected that reductive elimination form the Ge centre would occur in subsequent reactions[6] to relieve the steric bulk present at the five-coordinate Ge in this molecule. It may also be possible to use a $Im^{i}Pr_2Me_2•Ge^{t}Bu(H)•LA$ as a starting material for the formation of soluble $[^{t}BuGe]_n$ clusters (investigated previously as conductive films)[10] or substituted oligomers $[GeH_x{}^{t}Bu_y]_n$ via the elimination of $Im^{i}Pr_2Me_2•$ LA and H_2 (Scheme 5.3).

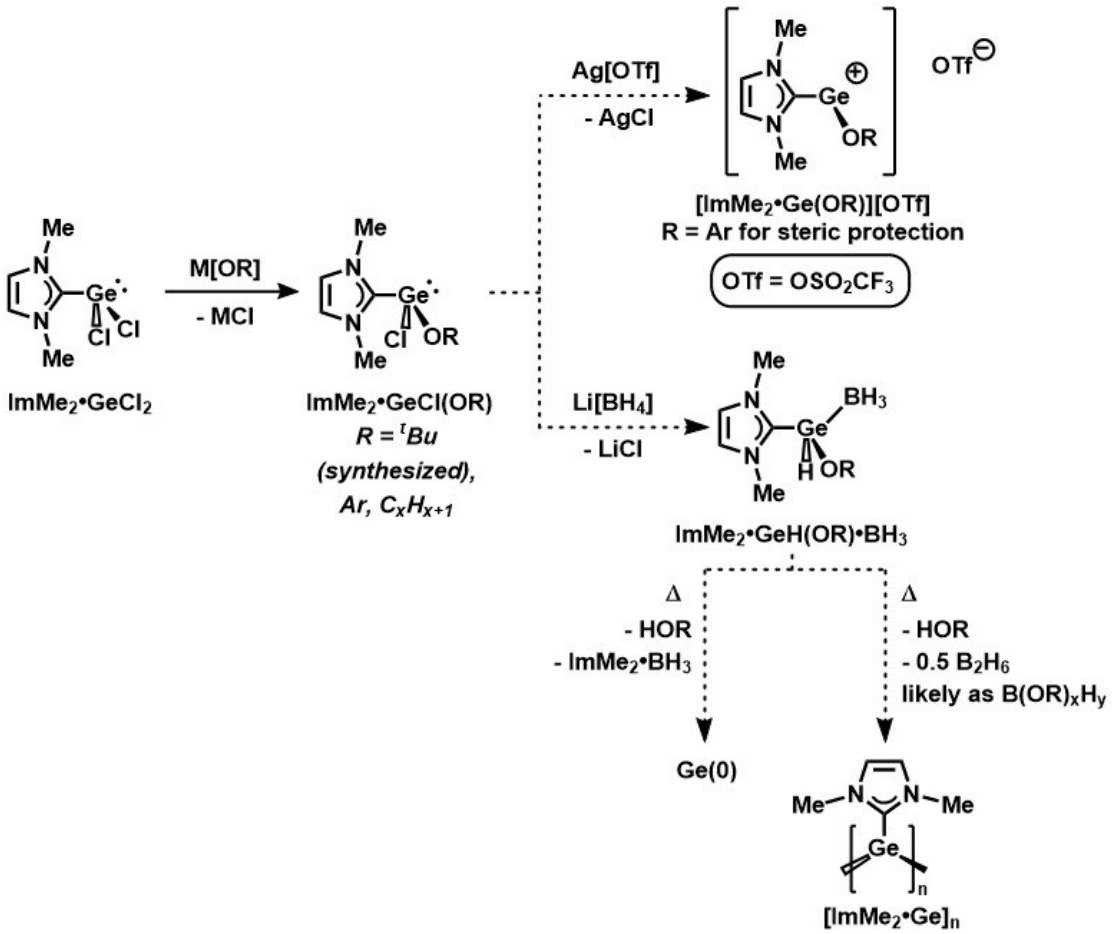

Scheme 5.2. Synthesis and proposed reactions of $ImMe_2$•GeCl(O^{t}Bu).

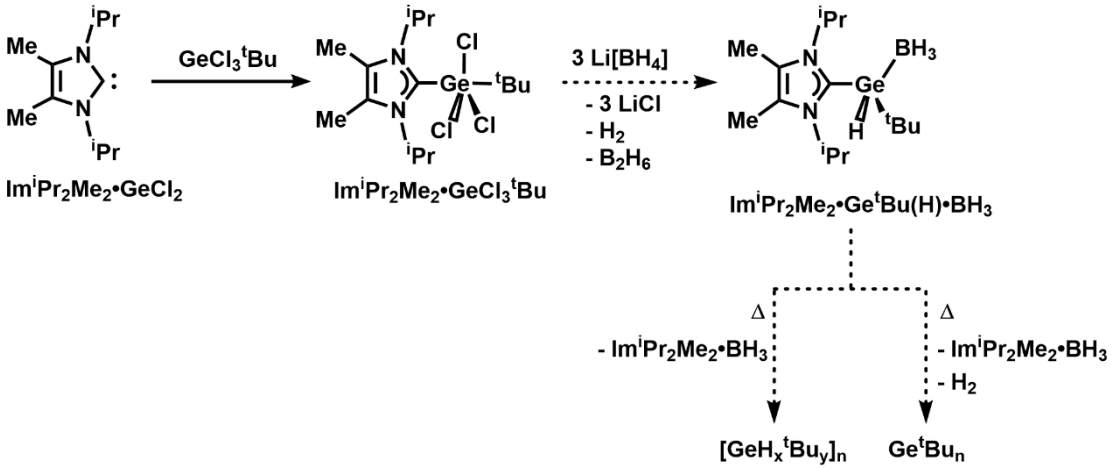

Scheme 5.3. Synthesis and proposed reactions of Im $^{i}Pr_2Me_2$•$GeCl_3{}^{t}Bu$.

The common theme throughout Chapters 2 through 4 is the application of molecular precursors to the deposition of Group 14 elements. Detailed in this Thesis are several experiments involving film deposition in solution onto smooth surfaces. One advantage of solution-based deposition methods is the facilitation of conformal deposition onto porous or textured surfaces. For example, a brief collaboration with Yingjie (Jay) He of the Veinot group at the University of Alberta showed that $ImMe_2$•GeH_2•BH_3 could be used to deposit germanium throughout a graphene aerogel (Figure 5.1). This procedure created a high-surface area porous germanium scaffold, which was tested as an anode material in Li-batteries in collaboration with Jasper Woodard in the Buriak group. Germanium is of interest as a battery electrode material due to its high relative capacity compared to carbon/graphene, the current industrial standard (1420 mA/h vs 370 mA/h, respectively),[11] however swelling and cracking of the germanium materials cause high failure rates, which is why structured porous materials are under investigation.[11] Unfortunately, the germanium-decorated graphene aerogel

performed worse than the isolated amorphous Ge precipitate from a thermal decomposition of $ImMe_2$•GeH_2•BH_3 alone. Though this particular scaffold/Ge pairing did not show the immediate desired improvement to battery performance, the concept of Ge deposition onto structured or textured materials remains plausible for other applications such as non-crystalline substrates, for example other high-surface area battery materials, optical fibres, and flexible substrates. Low temperature depositions are of particular interest to applications with thermally sensitive substrates like plastics or organic coatings.[12] A similar procedure could be applied with the $Ge(O^tBu)_2$ and hydride source pairs used in Chapter 3, or the analogous $[Sn(O^tBu)_2]_2$ system explored in Chapter 4. In addition, since $[Ge(O^tBu)_2]$ and $[Sn(O^tBu)_2]_2$ both react rapidly with hydride sources to deposit elemental layers, they could be combined in solution to produce mixed Ge/Sn films of controllable composition. The different reaction rates of these compounds to the hydride sources would have to be considered and explored when optimizing solution deposition for the Group 14 mixed-element films, but these films could have a wide range of applications as semiconductors in transistors and other devices.[13]

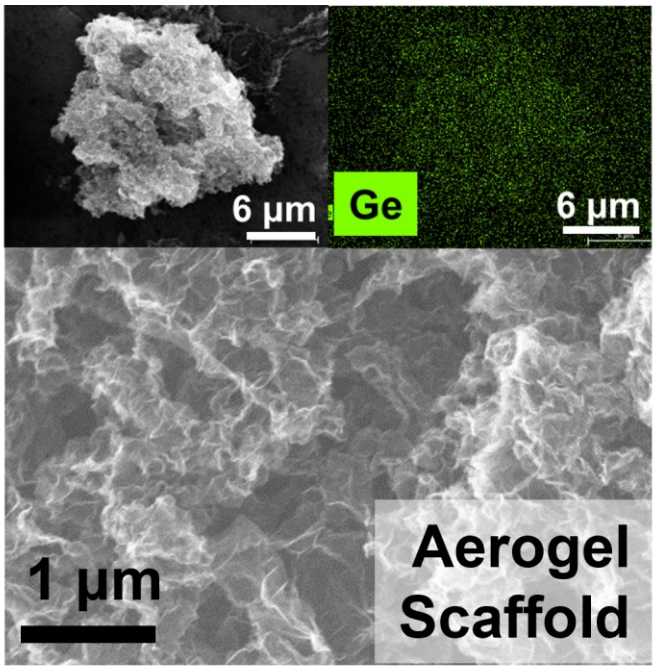

Figure 5.1. Secondary electron micrographs (top left, bottom) of a graphene aerogel containing deposited Ge(0) (energy dispersive X-ray spectroscopy Ge mapping shown top right). Ge was deposited by heating the aerogel in a toluene solution of $ImMe_2$•GeH_2•BH_3 (~5×10^{-3} M, 100 °C, 3 hours).

Collaborations are ongoing in the Rivard Group with the Emslie Group at McMaster University to further explore the application of the Group 14 complexes presented in this Thesis to atomic layer deposition (ALD). Complexes must be assessed for volatility and thermal stability. Although it was determined that [$Ge(OMes^*)_2$] (Mes* = 2,4,6-$^tBu_3C_6H_2$) was inappropriate for germanium deposition at the temperatures explored in Chapter 3, this and other Group 14 *bis*-alkoxides may prove more suitable for lower pressure, higher temperature reactivity. In addition, $Ge(OR)_2$ can be tested for its reactivity with *bis*(trimethylsilyl)telluride in solution and in ALD reactors as a precursor

for GeTe formation (Scheme 5.4),[14] a crucial component of GeSeTe semiconducting materials for phase-change random access memory devices.[15]

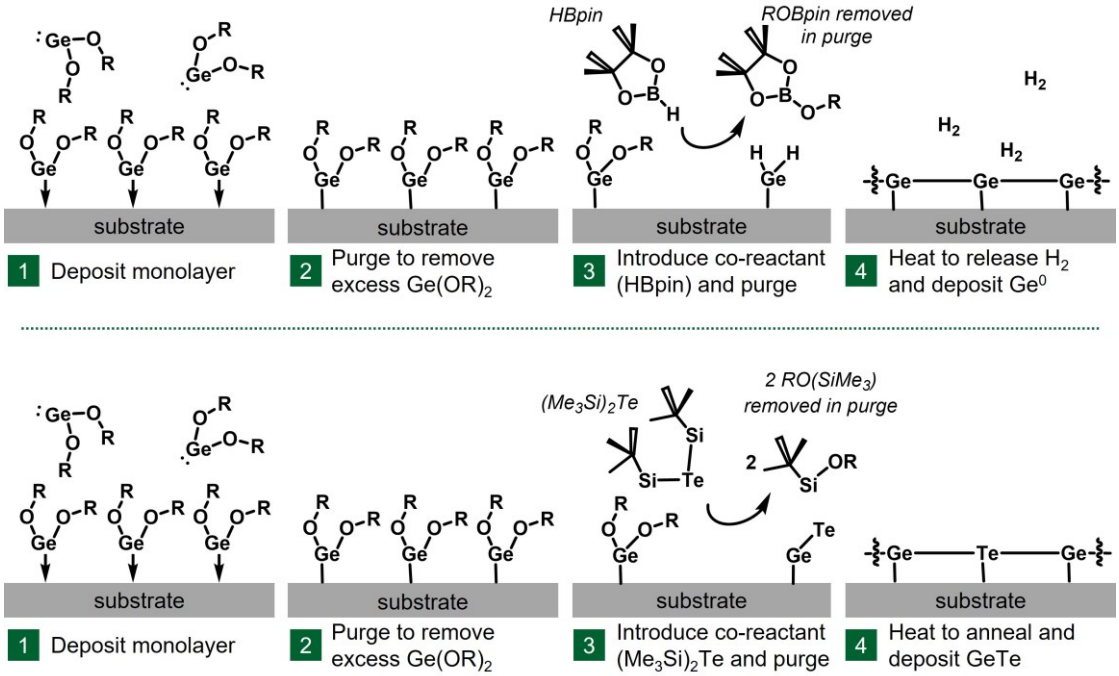

Scheme 5.4. Applications of $Ge(OR)_2$ for the growth of Ge and GeTe layers in an ALD reactor.

5.2 References

1. (a) G.-B. Shen, K. Xia, X.-T. Li, J.-L. Li, Y.-H. Fu, L. Yuan and X.-Q. Zhu, *J. Phys. Chem. A*, 2016, **120**, 1779; (b) I. Lee, *Chem. Soc. Rev.*, 1995, **24**, 223; (c) A. Streitwieser, R. H. Jagow, R. C. Fahey and S. Suzuki, *J. Am. Chem. Soc.*, 1958, **80**, 2326.

2. S. M. I. Al-Rafia, A. C. Malcolm, R. McDonald, M. J. Ferguson and E. Rivard, *Chem. Commun*., 2012, **48**, 1308.

3. (a) K. C. Thimer, S. M. I. Al-Rafia, M. J. Ferguson, R. McDonald and E. Rivard, *Chem. Commun*., 2009, 7119; (b) S. M. I. Al-Rafia, A. C. Malcolm, S. K. Liew, M. J. Ferguson and E. Rivard, *J. Am. Chem. Soc*., 2011, **133**, 777.

4. J. Sinclair, G. Dai, R. McDonald, M. J. Ferguson, A. Brown and E. Rivard, *Inorg. Chem*., 2020, **59**, 10996.

5. (a) P. A. Rupar, M. C. Jennings and K. M. Baines, *Organometallics*, 2008, **27**, 5043; (b) A. C. Filippou, O. Chernov, B. Blom, K. W. Stumpf and G. Schnakenburg, *Chem. Eur. J*., 2010, **16**, 2866.

6. T. Chu and G. I. Nikinov, *Chem. Rev*., 2018, **118**, 3608.

7. S. Pan, R. Saha, E. Osorio, P. K. Chattaraj, G. Frenking and G. Merino, *Chem. Eur. J*., 2017, **23**, 7463.

8. (a) F. S. Geitner, M. A. Giebel, A. Pöthig and T. F. Fässler, *Molecules*, 2017, **22**, 1204; (b) L. J. Schiegerl, M. Melaimi, D. R. Tolentino, W. Klein, G. Bertrand and T. F. Fässler, *Inorg. Chem*., 2019, **58**, 3256.

9. M. M. D. Roy, S. Fujimori, M. J. Ferguson, R. McDonald, N. Tokitoh and E. Rivard, *Chem. Eur. J*., 2018, **24**, 14392.

10. (a) A. Watanabe, M. Unno, F. Hojo and T. Miwa, *J. Mater. Sci. Lett*., 2001, **20**, 491; (b) A. Watanabe, M. Unno, F. Hojo and T. Miwa, *Chem. Lett*., 2001, **30**, 1092.

11. (a) U. Kasavajjula, C. Weng and A. J. Appleby, *J. Power Sources*, 2007, **163**, 1003; (b) X. Xiao, X. Li, S. Zheng, J. Shao, H. Xue and H. Pang, *Adv. Mat. Interfaces*, 2017, **4**, 1600798.

12. C. E. Knapp and C. J. Carmalt, *Chem. Soc. Rev.*, 2016, **45**, 1036.

13. S. Gupta, X. Gong, R. Zhang, Y.-C. Yeo, S. Takagi and K. C. Saraswat, *MRS Bull.*, 2014, **39**, 678.

14. (a) K. Knapas, T. Hatanpää, M. Ritala and M. Leskelä, *Chem. Mater.*, 2010, **22**, 1386; (b) V. Pore, T. Hatanpää, M. Ritala and M. Leskelä, *J. Am. Chem. Soc.*, 2009, **131**, 3478; (c) M. Ritala, V. Pore, T. Hatanpää, M. Heikkilä, M. Leskelä, K. Mizohata, A. Schrott, S. Raoux and S. M. Rossnagel, *Microelectron. Eng.*, 2009, **86**, 1946; (d) T. Sarnet, V. Pore, T. Hatanpää, M. Ritala, M. Leskelä, A. Schrott, Y. Zhu, S. Raoux and H.-Y. Cheng, *J. Electrochem. Soc.*, 2011, **158**, D694.

15. (a) T. Eom, T. Gwon, S. Yoo, B. J. Choi, M.-S. Kim, I. Buchanan, M. Xiao and C. S. Hwang, *Chem. Mater.*, 2014, **26**, 1583; (b) T. Eom, S. Choi, B. J. Choi, M. H. Lee, T. Gwon, S. H. Rha, W. Lee, M.-S. Kim, M. Xiao, I. Buchanan, D.-Y. Cho and C. S. Hwang, *Chem. Mater.*, 2012, **24**, 2099; (c) S. Yoo, C. Yoo, E.-S. Park, W. Kim, Y. K. Lee and C. S. Hwang, *J. Mater. Chem. C*, 2018, **6**, 5025.

Complete Bibliography

Chapter 1: Introduction

1. E. Rivard, *Chem. Soc. Rev.*, 2016, **45**, 989.
2. M. M. D. Roy, A. A. Omaña, A. S. S. Wilson, M. S. Hill, S. Aldridge and E. Rivard, *Chem. Rev.*, 2021, **121**, 12784.
3. D. Ugur, A. J. Storm, R. Verberk, J. C. Brouwer and W. G. Sloof, *Appl. Surf. Sci.*, 2014, **288**, 673.
4. C.-J. Chem, M. H. Back and R. A. Back, *Can. J. Chem.*, **1976**, *54*, 3175.
5. (a) W. Simmler, in *Ullman's Encyclopedia of Industrial Chemistry*, Wiley-VCH Verlag GmbH & Co. KGaA, Weinheim, 7th edn., vol. 32, 2012; (b) W. O. Filtvedt, A. Holt, P. A. Ramachandran and M. C. Melaaen, *Sol. Energy Mater. Sol. Cells*, 2012, **107**, 188 and references therein.
6. (a) V. H. Nguyen, A. Dobbie, M. Myronov, D. J. Norris, T. Walther and D. R. Leadley, *Thin Solid Films,* 2012, **520**, 3222; (b) R. Venkatasubramanian, R. T. Pickett and M. L. Timmons, *J. Appl. Phys.*, **1989**, *66*, 5662.
7. (a) J. M. Jasinski and S. M. Gates, *Acc. Chem. Res.*, 1991, **24**, 9; (b) W. L. M. Weerts, M. H. J. M. de Croon and G. B. Marin, *J. Electrochem. Soc.*, 1998, **145**, 1318; (c) J. Dzarnoski, H. E. O'Neal and M. A. Ring, *J. Am. Chem. Soc.*, 1981, **103**, 5740 and references therein.
8. Y. Apeloig, R. Pauncz, M. Karni, R. West, W. Steiner and D. Chapman, *Organometallics*, 2003, **22**, 3250 and references therein.

9. D. F. Shriver, M. Weller, T. Overton, J. Rourke and F. Armstrong, *Inorganic Chemistry*, W. H. Freemen and Co., New York, 6th edn, 2014, p. 301.

10. P. P. Power, *J. Chem. Soc., Dalton Trans.*, 1998, 2939.

11. (a) X. Wang and L. Andrews, *J. Am. Chem. Soc.*, 2003, **125**, 6581; (b) S. Aldridge and A. J. Downs, *Chem. Rev.*, 2001, **101**, 3305; (c) E. Hirota and H. Ishikawa, *J. Chem. Phys.*, 1999, **110**, 4254; (d) X. Wang, L. Andrews and G. P. Kushto, *J. Phys. Chem. A*, 2002, **106**, 5809; (e) P. S. Billone, K. Beleznay, C. R. Harrington, L. A. Huck, and W. J. Leigh, *J. Am. Chem. Soc.*, 2011, **133**, 10523.

12. E. Rivard, *Dalton Trans.*, 2014, **43**, 8577.

13. (a) A. Haaland, *Angew. Chem., Int. Ed. Engl.*, 1989, **28**, 992; (b) D. Himmel, I. Krossing and A. Schnepf, *Angew. Chem., Int. Ed.*, 2014, **53**, 370.

14. (a) W. Petz, *Chem. Rev.*, 1986, **86**, 1019; (b) M. S. Holt, W. L. Wilson and J. H. Nelson, *Chem. Rev.*, 1989, **89**, 11.

15. (a) T. J. Marks and A. R. Newman, *J. Am. Chem. Soc.*, 1973, **95**, 769; (b) G. W. Grynkewich, B. Y. K. Ho, T. J. Marks, D. J. Tomaja and J. J. Zuckerman, *Inorg. Chem.*, 1973, **12**, 2522.

16. (a) P. A. Rupar, V. N. Staroverov, P. J. Ragogna and K. M. Baines, *J. Am. Chem. Soc.*, 2007, 129. 15138; (b) M. J. Ward, P. A. Rupar, M. W. Murphy, Y.-M. Yiu, K. M. Baines and T. K. Sham, *Chem. Commun.*, 2010, **46**, 7016; (c) P. A. Rupar, M. C. Jennings and K. M. Baines, *Organometallics*, 2008, **27**, 5043; (d) P. A. Rupar, V. N. Staroverov and K. M. Baines, *Science*, 2008, **322**, 1360; (e) P. A. Rupar, M. C. Jennings, P. J. Ragogna and K. M. Baines, *Organometallics*, 2007, **26**, 4109.

17. (a) U. Vogel, A. Y. Timoshkin and M. Scheer, *Angew. Chem., Int. Ed.*, 2001, **40**, 4409; (b) M. Bodensteiner, U. Vogel, A. Y. Timoshkin and M. Scheer, *Angew. Chem., Int. Ed.*, 2009, **48**, 4629; (c) M. Bodensteiner, A. Y. Timoshkin, E. V. Peresypkina, U. Vogel and M. Scheer, *Chem. Eur. J.*, 2013, **19**, 957; (d) C. Marquardt, A. Adolf, A. Stauber, M. Bodensteiner, A. V. Virovets, A. Y. Timoshkin and M. Scheer, *Chem. Eur. J.*, 2013, **19**, 11887; (e) C. Marquardt, C. Thoms, A. Stauber, G. Balázs, M. Bodensteiner and M. Scheer, *Angew. Chem., Int. Ed.*, 2014, **53**, 3727.

18. A. J. Arduengo III, R. L. Harlow and M. Kline, *J. Am. Chem. Soc.*, 1991, **113**, 361.

19. V. Nesterov, D. Reiter, P. Bag, P. Frisch, R. Holzner, A. Porzelt and S. Inoue, *Chem. Rev.*, 2018, **118**, 9678.

20. (a) D. J. Nelson and S. P. Nolan, *N-Heterocyclic Carbenes*, Wiley-VCH Verlag GmbH & Co. KGaA, New York, 2014, pp. 1−24; (b) D. J. Nelson and S. P. Nolan, *Chem. Soc. Rev.* 2013, **42**, 6723; (c) J. P Moerdyk and C. W. Bielawski, *Contemporary Carbene Chemistry*, John Wiley & Sons, Inc., New York, 2013, pp. 40−74; (d) G. Bertrand, *Reactive Intermediate Chemistry*; John Wiley & Sons, Inc., New York, 2005, pp. 329−373; (e) M. C. Jahnke and F. E. Hahn, *N-Heterocyclic Carbenes: From Laboratory Curiosities to Efficient Synthetic Tools*, The Royal Society of Chemistry, UK, 2017, pp. 1−45.

21. (a) C. D. Martin, M. Soleilhavoup and G. Bertrand, *Chem. Sci.*, 2013, **4**, 3020; (b) K. C. Mondal, S. Roy and H. W. Roesky, *Chem. Soc. Rev.*, 2016, **45**, 1080.

22. (a) M. W. Lui, C. Merten, M. J. Ferguson, R. McDonald, Y. Xu and E. Rivard, *Inorg. Chem.*, 2015, **54**, 2040; (b) H. W. Wanzlick, *Angew. Chem., Int. Ed. Engl.*,

1962, **1**, 75; (c) H. W. Wanzlick, and H. J. Schönherr, *Angew. Chem., Int. Ed. Engl.,* 1968, **7**, 141; (d) H. W. Wanzlick, B. Lachmann and E. Schikora, *Chem. Ber.*, 1965, **98**, 3170.

23. G. Prabusankar, A. Sathyanarayana, P. Suresh, C. N. Babu, K. Srinivas and B. P. R Metla, *Coord. Chem. Rev.*, 2014, **269**, 96.

24. K. C. Thimer, S. M. I. Al-Rafia, M. J. Ferguson, R. McDonald and E. Rivard, *Chem. Commun.*, 2009, 7119.

25. A. Sidiropoulos, C. Jones, A. Stasch, S. Klein and G. Frenking, *Angew. Chem., Int. Ed.*, 2009, **48**, 9701.

26. A. J. Ruddy, P. A. Rupar, K. J. Bladek, C. J. Allan, J. C. Avery and K. M. Baines, *Organometallics*, 2010, **29**, 1362.

27. A. C. Filippou, O. Chernov, B. Blom, K. W. Stumpf and G. Schnakenburg, *Chem. Eur. J.*, 2010, **16**, 2866.

28. S. M. I. Al-Rafia, R. McDonald, M. J. Ferguson and E. Rivard, *Chem. Eur. J.*, 2012, **18**, 13810.

29. M. Y. Abrahim, Y. Wang, Y. Xie, P. Wei, H. F. Schaefer III, P. v. R. Schleyer and G. H. Robinson, *J. Am. Chem. Soc.*, 2011, **133**, 8874.

30. S. M. I. Al-Rafia, A. C. Malcolm, S. K. Liew, M. J. Ferguson and E. Rivard, *J. Am. Chem. Soc.*, 2011, **133**, 777.

31. S. M. I. Al-Rafia, A. C. Malcolm, R. McDonald, M. J. Ferguson and E. Rivard, *Chem. Commun*., 2012, **48**, 1308.

32. R. S. Ghadwal, H. W. Roesky, S. Merkel, J. Henn and D. Stalke, *Angew. Chem., Int. Ed.*, 2009, **48**, 5683.

33. (a) H. J. Bestmann and O. Kratzer, *Chem. Ber.*, 1963, **96**, 1899; (b) H. J. Bestmann, K. Sühs and T. Röder, *Angew. Chem., Int. Ed. Engl.*, 1981, **20**, 1038; (c) I. V. Borisova, N. N. Zemlyansky, V. K. Belsky, N. D. Kolosova, A. N. Sobolev, Y. N. Luzikov, Y. A. Ustynyuk and I. P. Beletskaya, *J. Chem. Soc., Chem. Commun.*, 1982, 1090; (d) H. J. Bestmann, T. Röder and K. Sühs, *Chem. Ber.*, 1988, **121**, 1509; (e) F. Breitsameter, H.-P. Schrödel, A. Schmidpeter, H. Nöth and S. Rojas-Lima, *Z. Anorg. Allg. Chem.*, 1999, **625**, 1293.

34. A. K. Swarnakar, S. M. McDonald, K. C. Deutsch, P. Choi, M. J. Ferguson, R. McDonald and E. Rivard, *Inorg. Chem.*, 2014, **53**, 8662.

35. T. K. Purkait, A. K. Swarnakar, G. B. De Los Reyes, F. A. Hegmann, E. Rivard and J. G. C. Veinot, *Nanoscale*, 2015, **7**, 2241.

36. For a review on nanoscale colloidal germanium, see: D. D. Vaughn II and R. E. Schaak, *Chem. Soc. Rev.*, 2013, **42**, 2861 and references therein.

37. (a) S. Prabakar, A. Shiohara, S. Hanada, K. Fujioka, K. Yamamoto and R. D. Tilley, *Chem. Mater.*, 2010, **22**, 482; (b) N. Shirahata, D. Hirakawa, Y. Masuda and Y. Sakka, *Langmuir*, 2013, **29**, 7401.

38. K. I. Lesczyńska, P. Deglmann, C. Präsang, V. Huch, M. Zimmer, D. Schweinfurth and D. Scheschkewitz, *Dalton. Trans.*, 2020, **49**, 13218.

39. D. Lutters, C. Severin, M. Schmidtmann and T. Müller, *J. Am. Chem. Soc.*, 2016, **138**, 6061.

40. C. P. Sindlinger, W. Grahneis, F. S. W. Archer and L. Wesemann, *Chem. Eur. J.*, 2016, **22**, 7554.

41. T. J. Haddlington, B. Schwartze, E. I. Izgorodina and C. Jones, *Chem. Commun.*, 2015, **51**, 6854.

42. S. Kahn, P. P. Samuel, R. Michel, J. M. Deiterich, R. Mata, J. P. Demers, A. Lange, H. W. Roesky and D. Stalke, *Chem. Commun.*, 2012, **48**, 4890.

43. S. E. Koponen, P. G. Gordon and S. T. Barry, *Polyhedron*, 2016, **108**, 59.

44. D. J. H. Emslie, P. Chadha and J. S. Price, *Coord. Chem. Rev.*, 2013, **257**, 3282.

45. A. C. Jones and M. L. Hitchman, *Chemical Vapour Deposition: Precursors Processes and Applications*, RSC Publishing, Cambridge, 2009.

46. A. E. Van Arkel and J. H. De Boer, *Z. Anorg, Allg. Chem.*, 1925, **148**, 345.

47. J. S. De Lodyguine, U. S. Patent 575, 002, 1893.

48. For some examples of ALD precursors see: (a) H. Kim, *J. Vac. Sci. Technol., B*, 2003, **21**, 2231; (b) F. Zaera, *J. Phys. Chem. Lett.*, 2012, **3**, 1301; (c) N. Bahlawane, K. Kohse Höeinghaus, P. A. Premkumar and D. Lenoble, *Chem. Sci.*, 2012, **3**, 929; (d) M. Knez, K. Nielsch and L. Niinistö, *Adv. Mater.*, 2007, **19**, 3425; (e) S. M. George, *Chem. Rev.*, 2010, **110**, 111; (f) H. Kim, H.-B.-R. Lee and W.-J. Maeng, *Thin Solid Films*, 2009, **517**, 2563; (g) F. Zaera, *J. Mater. Chem.*, 2008, **18**, 3521; (h) R. L. Puurunen, *J. Appl. Phys.*, 2005, **97**, 121301; (i) M. Leskelä and M. Ritala, *Angew. Chem., Int. Ed.*, 2003, **42**, 5548.

49. C. E. Knapp and C. J. Carmalt, *Chem. Soc. Rev.*, 2016, **45**, 1036.

50. G. Hodes, *Chemical Solution Deposition of Semiconductor Films*, CRC Press, New York, 2002.

51. (a) C. Puscher. *Dingl. J.*, 1869, **190**, 421; (b) J. Emerson-Reynolds. *J. Chem. Soc.*, 1884, **45**, 162.

52. B. Vidjayacoumar, D. J. H. Emslie, J. M. Blackwell, S. B. Clendenning and J. F. Britten, *Chem. Mater.*, 2010, **22**, 4854.

53. A. Vidjayacoumar, V. Ramalingam, D. J. H. Emslie, J. M. Blackwell and S. B. Clendenning, *ECS Trans.*, 2012, **50**, 53.

54. A. Ludviksson, R. Zhang, C. T. Campbell and K. Griffiths, *Surf. Sci.*, 1994, **313**, 64, and references therein.

55. P. J. Pallister, S. C. Buttera and S. T. Barry, *J. Phys. Chem. C*, 2014, **118**, 1618.

56. G. Shang, M. J. Hampden-Smith and E. N. Duelser, *Chem. Commun.*, 1996, 1733.

57. H. Sun, X. Qin and F. Zaera, *J. Phys. Chem. Lett.*, 2012, **17**, 2523.

58. J. P. Coyle, W. H. Monillas, G. P. A. Yap and S. T. Barry, *Inorg. Chem.*, 2008, **47**, 683.

59. (a) J. Bardeen, B. H. Walter and Bell Telephone Lab Inc, U. S. Patent 2524035A, 1948; (b) H. F. Mataré and H. Welker, U.S. Patent 2673948A, 1948.

60. P. A. Gargini, in *Nanoelectronics: Materials, Devices, Applications*, eds. R. Puers, L. Baldi, M. van de Voorde and S. E. van Nooten, Wiley-VCH Verlag GmbH & Co. KGaA, Weinheim, 1st edn, 2012, ch. 1, pp. 3-54.

61. H.-J. Mussig and J. Dabrowski, *Silicon Surfaces and Formation of Interfaces*, World Scientific Publishing Company, London, 2000.

62. (a) T. Eom, T. Gwon, S. Yoo, B. J. Choi, M.-S. Kim, I. Buchanan, M. Xiao and C. S. Hwang, *Chem. Mater.*, 2014, **26**, 1583; (b) T. Eom, S. Choi, B. J. Choi, M. H. Lee, T. Gwon, S. H. Rha, W. Lee, M.-S. Kim, M. Xiao, I. Buchanan, D.-Y.Cho and C. S. Hwang, *Chem. Mater.*, 2012, **24**, 2099; (c) S. Yoo, C. Yoo, E.-S. Park, W. Kim, Y. K. Lee and C. S. Hwang, *J. Mater. Chem. C*, 2018, **6**, 5025.

63. (a) K. Knapas, T. Hatanpää, M. Ritala and M. Leskelä, *Chem. Mater.*, 2010, **22**, 1386; (b) V. Pore, T. Hatanpää, M. Ritala and M. Leskelä, *J. Am. Chem. Soc.*, 2009, **131**, 3478; (c) M. Ritala, V. Pore, T. Hatanpää, M. Heikkilä, M. Leskelä, K. Mizohata, A. Schrott, S. Raoux and S. M. Rossnagel, *Microelectron. Eng.*, 2009, **86**, 1946; (d) T. Sarnet, V. Pore, T. Hatanpää, M. Ritala, M. Leskelä, A. Schrott, Y. Zhu, S. Raoux and H.-Y. Cheng, *J. Electrochem. Soc.* 2011, **158**, D694.

64. W. Hunks, P. S. Chen, T. Chen, M. Stender, G. T. Stauf, L. Maylott, C. Xu and J. F. Roeder *Mater. Res. Soc. Symp. Proc.*, 2008, vol. 1071, Materials Research Society.

65. G. Wang, M. Kolahdouz, J. Luo, C. Qin, S. Gu, Z. Kong, X. Yin, W. Xiong, X. Zhao, J. Liu, T. Yang, J. Li, H. Yin, H. Zhu, W. Wang, C. Zhao, T. Ye and H. H. Radamson, *J. Mater. Sci. Mater. Electron.*, 2020, **31**, 26.

66. T. David, J.-N. Aqua, K. Liu, L. Favre, A. Ronda, M. Abbarchi, J.-B. Claude and I. Berbezier, *Sci. Rep.*, 2018, **8**, 289.

67. S. Gupta, X. Gong, R. Zhang, Y.-C. Yeo, S. Takagi and K. C. Saraswat, *MRS Bull.*, 2014, **39**, 678.

68. Z. Xia, H. Song, M. Kim, M. Zhou, T.-H. Chang, D. Liu, X. Yin, K. Xiong, H. Mi, X. Wang, F. Xia, Z. Yu, Z. (J.) Ma and Q. Gan, *Sci. Adv.*, 2017, **3**, e1602783.

69. (a) K.-T. Lee, S. Seo, J. Y. Lee and L. J. Guo, *Adv. Mater.*, 2014, **26**, 6324; (b) K.-T. Lee, S. Seo, J. Y. Lee and L. J. Guo, *Appl. Phys. Lett.*, 2014, **104**, 231112.

70. (a) V. Steenhoff, M. Theuring, M. Vehse, K. von Maydell and C. Agert, *Adv. Opt. Mater.*, 2015, **3**, 182; (b) D. O. Sigle, L. Zhang, S. Ithurria, B. Dubertret and J. J. Baumberg, *J. Phys. Chem. Lett.*, 2016, **6**, 1099; (c) Y. Xin, L. Wu, L. Ge, C. Han, Y. Li and S. Fang, *J. Mater. Chem. A*, 2015, **3**, 8659.

71. For a review, see: (a) R. Mülhaupt, *Angew. Chem., Int. Ed.*, 2004, **43**, 1054; (b) H. Staudinger, *Ber. Dtsch. Chem. Ges.*, 1924, **57**, 1203; (c) Original reports of polyethylene termed it as polymethylene: H. von Pechmann, *Ber. Dtsch. Chem. Ges.*, 1899, **31**, 2640.

72. (a) K. Ziegler, E. Holzkamp, H. Breil and H. Martin, *Angew. Chem.*, 1955, **67**, 426; (b) G. Natta, *Makromol. Chem.*, 1960, **35**, 94; (c) S. D. Ittel, L. K. Johnson and M. Brookhart, *Chem. Rev.*, 2000, **100**, 1169; (d) F. di Lena and K. Matyjaszewski, *Prog. Polym. Sci.*, 2010, **35**, 959.

73. (a) G. Grzybowski, A. V. G. Chizmeshya, C. Senaratne, J. Menendez and J. Kouvetakis, *J. Mater. Chem. C*, 2013, **1**, 5223; (b) F. Fehér and I. Fischer, *Z. Anorg. Allg. Chem.*, 1976, **421**, 9; (c) A. F. Clifford and G. R. Zeilenga, *Inorg. Chem.*, 1969, **8**, 1789; (d) S. D. Gokhale, J. E. Drake and W. L. Jolly, *J. Inorg. Nucl. Chem.*, 1965, **27**, 1911; (e) M. Akhtar, *Synth. React. Inorg. Met.-Org. Chem.*, 1986, **16**, 729; (f) Photolysis has also been used to generate higher silane oligomers: G. G. A. Perkins and F. W. Lampe, *J. Am. Chem. Soc.*, 1980, **102**, 3764; (g) G. Olbrich, P. Potzinger, B. Reimann and R. Walsh, *Organometallics*, 1984, **3**, 1267.

74. (a) J. Ma and S. Inagaki, *J. Am. Chem. Soc.*, 2001, **123**, 1193; (b) For the relative stability of branched and linear $(GeCl_2)_x$ oligomers, see: S. M. I. Al-Rafia, M. R. Momeni, R. McDonald, M. J. Ferguson, A. Brown and E. Rivard, *Angew. Chem., Int. Ed.*, 2013, **52**, 6390.

75. W. A. Eger, A. Genest and N. Rösch, *Chem. Eur. J.*, 2012, **18**, 9106.

76. (a) J. R. Damewood Jr. and R. West, *Macromolecules*, 1985, **18**, 159; (b) K. Takeda, K. Shiraishi and N. Matsumoto, *J. Am. Chem. Soc.*, 1990, **112**, 5043.

77. (a) C.-A. Wurtz, *Chim. Phys.*, 1855, **44**, 275; (b) A. D. Craig and A. G. MacDiarmid, *J. Inorg. Nucl. Chem.*, 1962, **24**, 161.

78. (a) A. Stock and C. Somieski, *Ber. Dtsch. Chem. Ges.*, 1916, **49**, 111; (b) F. Fehér, H. Baier, B. Enders, M. Krancher, J. Laakmann, F. J. Ocklenburg and D. Skrodski, *Z. Anorg. Allg. Chem.*, 1985, **530**, 191; (c) C. J. Ritter, WO 2012/021634 A2, **2012**; (d) W. C. Johnson and S. Isenberg, *J. Am. Chem. Soc.*, 1935, **57**, 1349; (e) P. L. Timms and C. S. G. Phillips, *Inorg. Chem.*, 1964, **3**, 606.

79. (a) T. Masuda, Y. Matsuki and T. Shimoda, *Thin Solid Films*, 2012, **520**, 6603; (b) P. John, I. M. Odeh and J. Wood, *J. Chem. Soc., Chem. Commun.*, 1983, 1496.

80. T. Shimoda, Y. Matsuki, M. Furusawa, T. Aoki, I. Yudasaka, H. Tanaka, H. Iwasawa, D. Wang, M. Miyasaka and Y. Takeuchi, *Nature*, 2006, **440**, 783.

81. (a) P. Royen and R. Schwartz, *Z. Anorg. Allg. Chem.*, 1933, **215**, 295; (b) L. M. Dennis and N. A. Skow, *J. Am. Chem. Soc.*, 1930, **52**, 2369; (c) For a related approach to $[GeH]_n$, see: T. Giousis, G. Potsi, A. Kouloumpis, K. Spyrou, Y. Georgantas, N. Chalmpes, K. Dimos, M.-K. Antoniou, G. Papavassiliou, A. B. Bourlinos, H. J. Kim, V. K. S. Wadi, S. Alhassan, M. Ahmadi, B. J. Kooi, G. Blake, D. M. Balazs, M. A. Loi, D. Gournis and P. Rudolf, *Angew. Chem., Int. Ed.*, 2021, **60**, 360.

82. P. Royen and C. Rocktäschel, *Z. Anorg. Allg. Chem.*, 1966, **346**, 279.

83. H. Yu, C. Ni, A. N. Thiessen, Z. Li and J. G. C. Veinot, *ACS Nano*, 2021, **15**, 9368.

Chapter 2: Insight into the Decomposition Mechanism of Donor-Acceptor Complexes of EH_2 (E = Ge and Sn) and Access to Germanium Thin Films from Solution

1. Usually EH_2 species are generated as mixtures with other polyhydrides: (a) J. M. Jasinski, R. Becerra and R. Walsh, *Chem. Rev.*, 1995, **95**, 1203; (b) S. Aldridge and A. J. Downs, *Chem. Rev.*, 2001, **101**, 3305; (c) E. Hirota and H. Ishikawa, *J. Chem. Phys.*, 1999, **110**, 4254; (d) X. Wang and L. Andrews, *J. Am. Chem. Soc.*, 2003, **125**, 6581; (e) N. A. Young, *Coord. Chem. Rev.*, 2013, **257**, 956.
2. (a) H. Jacobsen and T. Ziegler, T. *Inorg. Chem.,* 1996, **35**, 775; (b) Y. Apeloig, R. Pauncz, M. Karni, R. West, W. Steiner and D. Chapman, *Organometallics*, 2003, **22**, 3250 and references therein.
3. (a) J. M. Jasinski and S. M. Gates, *Acc. Chem. Res.*, 1991, **24**, 9; (b) W. Grochala and P. P. Edwards, *Chem. Rev.*, 2004, **104**, 1283; (c) E. Rivard, *Chem. Soc. Rev.*, 2016, **45**, 989.
4. (a) R. R. Schrock, *Acc. Chem. Res.*, 1979, **12**, 98; (b) F. N. Tebbe, G. W. Parshall and D. W. Ovenall, *J. Am. Chem. Soc.*, 1979, **101**, 5074; (c) P. Schwab, M. B. France, J. W. Ziller and R. H. Grubbs, *Angew. Chem., Int. Ed. Engl.*, 1995, **34**, 2039; (d) J. Scott and D. J. Mindiola, *Dalton Trans.*, 2009, 8463.
5. (a) H. von Pechmann, *Ber. Dtsch. Chem. Ges.*, 1894, **27**, 1888; (b) H. Yang, B. Martin and B. Schenkel, *Org. Proc. Res. Develop.*, 2018, **22**, 446–456.
6. For the photo-assisted extrusion of EH_2 units (E = Si and Ge) via cyclobutane and cyclopentene analogues, see: (a) T. J. Barton and N. Tillman, *J. Am. Chem. Soc.*, 1987, **109**, 6711; (b) R. Becerra, S. E. Boganov, M. P. Egorov, O. M.

Nefedov and R. Walsh, *Chem. Phys. Lett.*, 1996, **260**, 433; (c) For a computational investigation of this process, see: M.-D. Su, *J. Phys. Chem. A*, 2015, **119**, 8611.

7. K. C. Thimer, S. M. I. Al-Rafia, M. J. Ferguson, R. McDonald and E. Rivard, *Chem. Commun.*, 2009, 7119.

8. E. Rivard, *Dalton Trans.*, 2014, **43**, 8577.

9. For related studies on donor-acceptor stabilization, see: (a) T. J. Marks, *J. Am. Chem. Soc.*, 1971, **93**, 7090; (b) G, Schmid and E. Welz, *Angew. Chem., Int. Ed. Engl.*, 1977, **16**, 785; (c) W. Petz, *Chem. Rev.* 1986, **86**, 1019; (d) A. Vogel, A. Y. Timoshkin and M. Scheer, *Angew. Chem.*, *Int. Ed.*, 2001, **40**, 4409; (e) P. A. Rupar, M. C. Jennings, P. J. Ragogna and K. M. Baines, *Organometallics*, 2007, **26**, 4109; (f) R. S. Ghadwal, R. Azhakar and H. W. Roesky, *Acc. Chem. Res.*, 2013, **46**, 444; (g) A. Jana, V. Huch, H. S. Rzepa and D. Scheschkewitz, *Organometallics*, 2015, **34**, 2130; (h) H. P. Hickox, Y. Wang, Y. Xie, P. Wei, H. F. Schaefer III and G. H. Robinson, *J. Am. Chem. Soc.*, 2016, **138**, 9799; (i) O. Hegen, C. Marquardt, A. Y. Timoshkin and M. Scheer, *Angew. Chem., Int. Ed.*, 2017, **56**, 12783; (j) O. Hegen, J. Bräse, A. Y. Timoshkin and M. Scheer, *Chem. Eur. J.*, 2019, **25**, 485; (k) R. Jambor, J. Tremmel, J. Tydlitát, L. Dostál, A. Ruzicka, X. Deraet, J. Turek and R. Jambor, *Chem. Eur. J.*, 2020, **26**, 6070.

10. (a) S. M. I. Al-Rafia, A. C. Malcolm, S. K. Liew, M. J. Ferguson and E. Rivard, *J. Am. Chem. Soc.*, 2011, **133**, 777; (b) S. M. I. Al-Rafia, A. C. Malcolm, S. K. Liew, M. J. Ferguson, R. McDonald and E. Rivard, *Chem. Commun.*, 2011, **47**, 6987; (c) S. M. I. Al-Rafia, A. C. Malcolm, R. McDonald, M. J. Ferguson and E. Rivard, *Angew. Chem., Int. Ed.*, 2011, **50**, 8354; (d) S. M. I. Al-Rafia, A. C. Malcolm, R.

McDonald, M. J. Ferguson and E. Rivard, *Chem. Commun*., 2012, **48**, 1308; (e) S. M. I. Al-Rafia, M. R. Momeni, M. J. Ferguson, R. McDonald, A. Brown and E. Rivard, *Organometallics*, 2013, **32**, 6658; (f) A. K. Swarnakar, S. M. McDonald, K. C. Deutsch, P. Choi, M. J. Ferguson, R. McDonald and E. Rivard, *Inorg. Chem.* 2014, **53**, 8662.

11. T. K. Purkait, A. K. Swarnakar, G. B. De Los Reyes, F. A. Hegmann, E. Rivard and J. G. C. Veinot, *Nanoscale*, 2015, **7**, 2241.

12. D. D. Vaughn and R. E. Schaak, *Chem. Soc. Rev.* 2013, **42**, 2861.

13. For related examples of Ge nanomaterial formation under harsher (thermal or reducing) conditions, see: (a) K. Tabatabaei, A. L. Holmes, K. A. Newton, E. Muthuswamy, R. Sfadia, S. A. Carter and S. M. Kauzlarich, *Chem. Mater.*, 2019, **31**, 7510; (b) M. J. Kirschenbaum, M. G. Boebinger, M. J. Katz, M. T. McDowell and M. Dasog, *ChemNanoMat*, 2018, **4**, 423; (c) M. Javadi, D. Picard, R. Sinelnikov, M. A. Narreto, F. A. Hegmann and J. G. C. Veinot, *Langmuir*, 2017, **33**, 8757; (d) S. Yoo, C. Yoo, E.-S. Park, W. Kim, Y. K. Lee and C. S. Hwang, *J. Mater. Chem. C*, 2018, **6**, 5025; (e) V. H. Nguyen, A. Dobbie, M. Myronov, D. J. Norris, T. Walther and D. R. Leadley, *Thin Solid Films*, 2012, **520**, 3222; (f) J. C. Malaquias, M. Wu, J. Lin, E. V. C. Robert, J. Sniekers, K. Binnemans, P. J. Dale and J. Fransaer, *Electrochimica Acta*, 2017, **251**, 651.

14. (a) G. D. Frey, J. D. Masuda, B. Donnadieu and G. Bertrand, *Angew. Chem.*, *Int. Ed.*, 2010, **49**, 9444; (b) M. Arrowsmith, M. S. Hill, G. Kociok-Köhn, D. J. MacDougall and M. F. Mahon, *Angew. Chem.*, *Int. Ed.*, 2012, **51**, 2098; (c) D. Schmidt, J. H. J. Berthel, S. Pietsch and U. Radius, *Angew. Chem., Int. Ed.*, 2012,

51, 8881; (d) S. M. I. Al-Rafia, R. McDonald, M. J. Ferguson and E. Rivard, *Chem. Eur. J.*, 2012, **18**, 13810; (e) T. Wang and D. W. Stephan, *Chem. Eur. J.*, 2014, **20**, 3036; (f) S. Würtemberger-Pietsch, U. Radius and T. M. Marder, *Dalton Trans.*, 2016, **45**, 5880; (g) M. D. Anker, A. L. Colebatch, K. J. Iversen, D. J. D. Wilson, J. L. Dutton, L. García, M. S. Hill, D. J. Liptrot and M. F. Mahon, *Organometallics*, 2017, **36**, 1173; For computational studies, see: (h) M. R. Momeni, E. Rivard and A. Brown, *Organometallics*, 2013, **32**, 6201; (i) K. J. Iversen, D. J. D. Wilson and J. L. Dutton, *Organometallics*, 2013, **32**, 6209.

15. (a) R. Becerra, S. E. Boganov, M. P. Egorov, V. I. Faustov, O. M. Nefedov and R. Walsh, *J. Am. Chem. Soc.,* 1998, **120**, 12657; (b) P. S. Billone, K. Beleznay, C. R. Harrington, L. A. Huck and W. J. Leigh, *J. Am. Chem. Soc.* 2011, **133**, 10523.

16. N. Kuhn and T. Kratz, *Synthesis*, 1993, 561.

17. (a) G. Prabusankar, A. Sathyanarayana, P. Suresh, C. Naga Babu, K. Srinivas, and B. P. Rao Metla, *Coord. Chem. Rev.*, 2014, **269**, 96; (b) V. Nesterov, D. Reiter, P. Bag, P. Frisch, R. Holzner, A. Porzelt and S. Inoue, *Chem. Rev.*, 2018, **118**, 9678.

18. J. P. Coyle, E. R. Sirianni, I. Korobkov, G. P. A. Yap, G. Dey and S. T. Barry, *Organometallics*, 2017, **36**, 2800–2810.

19. S. M. I. Al-Rafia, P. A. Lummis, A. K. Swarnakar, K. C. Deutsch, M. J. Ferguson, R. McDonald and E. Rivard, *Aust. J. Chem.*, 2013, **66***,* 1235.

20. CCDC 1986302-1986305 contain the supplementary crystallographic data for this paper. These data are provided free of charge from The Cambridge Crystallographic Data Centre.

21. P. A. Rupar, V. N. Staroverov, P. J. Ragogna and K. M. Baines, *J. Am. Chem. Soc.*, 2007, **129**, 15138.

22. T. Böttcher, B. S. Bassil and G.-V. Röschenthaler, *Inorg. Chem.*, 2012, **51**, 763.

23. M. Güizado-Rodríguez, A. Ariza-Castolo, G. Merino, A. Vela, H. Noth, V. I. Bakhmutov and R. Contreras, *J. Am. Chem. Soc.*, 2001, **123**, 9144.

24. (a) E. F. Van der Eide, T. Liu, D. M. Camaioni, E. D. Walter and R. M. Bullock, *Organometallics*, 2012, **31**, 1775; (b) A. Doddi, M. Peters and M. Tamm, *Chem. Rev.*, 2019, **119**, 6994.

25. A. J. Ruddy, P. A. Rupar, K. J. Bladek, C. J. Allan, J. C. Avery and K. M. Baines, *Organometallics*, 2010, **29**, 1362.

26. M. M. Bentlohner, M. Waibel, P. Zeller, K. Sarkar, P. Müller-Buschbaum, D. Fattakhova-Rohlfing and T. F. Fässler, *Angew. Chem., Int. Ed.*, 2016, **55**, 2441.

27. J. C. Walton, M. M. Brahmi, L. Fensterbank, E. Lacôte, M. Malacria, Q. Chu, S. Ueng, A. Solovyev and D. P. Curran, *J. Am. Chem. Soc.*, 2010, **132**, 2350.

28. (a) P. J. D. Whiteside, J. A. Chininis and H. K. Hunt, *Coatings*, 2016, **6**, 35; (b) Q. Shi, R. Roux, F. Latourte, F. Hild, D. Loisnard and N. Brynaert, *Ultramicroscopy* 2018, **191**, 18.

29. C. Ratsch and J. A. Venables, *J. Vac. Sci. Tech. A*, 2003, **21**, S96.

30. Y. Zhao and D. Truhlar, *Theor. Chem. Acc.*, 2008, **120**, 215.

31. (a) T. H. Dunning Jr., *J. Chem. Phys.*, 1989, **90**, 1007; (b) A. K. Wilson, D. E. Woon, K. A. Peterson and T. H. Dunning Jr., *J. Chem. Phys.*, 1999, **110**, 7667.

32. D. D. Wagman, W. H. Evans, V. B. Parker, R. H. Schumm, I. Halow, S. M. Bailey, K. L. Churney and R. L. Nuttall, in *Journal of Physical and Chemical Reference*

Data Vol. 11, Supplement No. 2. American Chemical Society and American Institute of Physics, Washington, D.C., 1982.

33. S. M. I. Al-Rafia, O. Shynkaruk, S. M. McDonald, S. K. Liew, M. J. Ferguson, R. McDonald, R. H. Herber and E. Rivard, *Inorg. Chem.*, 2013, **52**, 5581.

34. The concentration of **6** was determined by integration of the initial ^{1}H NMR resonances related to 4,4'-difluorobiphenyl as an internal standard.

35. G.-B. Shen, K. Xia, X.-T. Li, J.-L. Li, Y.-H. Fu, L. Yuan and X.-Q. Zhu, *J. Phys. Chem. A*, 2016, **120**, 1779.

36. (a) I. Lee, *Chem. Soc. Rev.*, 1995, **24**, 223; (b) A. Streitwieser, R. H. Jagow, R. C. Fahey and S. Suzuki, *J. Am. Chem. Soc.*, 1958, **80**, 2326.

37. In this analysis/discussion of the change in Ge-H and B-H stretching frequencies, I focused on isolated Ge-H and B-H stretches (three for each bond type) and did not include the impact of coupled Ge-H/B-H modes. When one does consider the impact of such coupled stretches, only modest overall changes in frequency (from Δ5 to Δ20 cm^{-1}) were seen at the various bond elongations investigated; thus, contributions from the coupled modes were ignored.

38. (a) Y. Fujioka, *Nature*, 1929, **124**, 11; (b) K. Venkateswarlu, *Nature*, 1947, **159**, 96; (c) J. Jehlička, H. G. M. Edwards and A. Culka, *Phil. Trans. R. Soc. A*, 2010, **368**, 3109.

39. T. Schaub, M. Backes and U. Radius, *Organometallics*, 2006, **25**, 4196.

40. U. Zoller, *Tetrahedron*, 1988, **44**, 7413.

41. (a) L. A. Curtiss, M. P. McGrath, J.-P. Blaudeau, N. E. Davis, R. C. Binning and L. Radom, *J. Chem. Phys.* 1995, **103**, 6104; (b) R. Krishnan, J. S. Binkley, R. Seeger and J. Pople, *J. Chem. Phys.* 1980, **72**, 650.

42. E. D. Glendening, J. K. Badenhoop, A. E. Reed, J. E. Carpenter, J. A. Bohmann, C. M. Morales and F. Weinhold, NBO 5.9. Theoretical Chemistry Institute, University of Wisconsin, Madison, WI, 2012; http://www.chem.wisc.edu/~nbo5.

43. M. J. Frisch, G. W. Trucks, H. B. Schlegel, G. E. Scuseria, M. A. Robb, J. R. Cheeseman, G. Scalmani, V. Barone, G. A. Petersson, H. Nakatsuji, X. Li, M. Caricato, A. V. Marenich, J. Bloino, B. G. Janesko, R. Gomperts, B. Mennucci, H. P. Hratchian, J.V. Ortiz, A. F. Izmaylov, J. L. Sonnenberg, D. Williams-Young, F. Ding, F. Lipparini, F. Egidi, J. Goings, B. Peng, A. Petrone, T. Henderson, D. Ranasinghe, V. G. Zakrzewski, J. Gao, N. Rega, G. Zheng, W. Liang, M. Hada, M. Ehara, K. Toyota, R. Fukuda, J. Hasegawa, M. Ishida, T. Nakajima, Y. Honda, O. Kitao, H. Nakai, T. Vreven, K. Throssell, J. A. J. Montgomery, J. E. Peralta, F. Ogliaro, M. J. Bearpark, J. J. Heyd, E. N. Brothers, K. N. Kudin, V. N. Staroverov, T. A. Keith, R. Kobayashi, J. Normand, K. Raghavachari, A. P. Rendell, J. C. Burant, S. S. Iyengar, J. Tomasi, M. Cossi, J. M. Millam, M. Klene, C. Adamo, R. Cammi, J. W. Ochterski, R. L. Martin, K. Morokuma, O. Farkas, J. B. Foresman and D. J. Fox, Gaussian 16, Revision B.01, Gaussian, Inc., Wallingford CT.

44. (a) A. D. Becke, *J. Chem. Phys.*, 1993, **98**, 5648; (b) C. Lee, W. Yang and R. G. Parr, *Phys. Rev. B*, 1988, **37**, 785; (c) S. H. Vosko, L. Wilk and M. Nusair, *Can. J.*

Phys., 1980, **58**, 1200; (d) P. J. Stephens, F. J. Devlin, C. F. Chabalowski and M. J. Frisch, *J. Phys. Chem.*, 1994, **98**, 11623.

45. (a) G. M. Sheldrick, *Acta Cryst.*, 2015, **A71**, 3; (b) G. M. Sheldrick, *Acta Cryst.*, 2015, **C71**, 3.

Chapter 3: Access to Metastable $[GeH_2]_n$ Materials via a Molecular "Bottom-up" Approach

1. (a) J. M. Jasinski and S. M. Gates, *Acc. Chem. Res.*, 1991, **24**, 9; (b) J. A. Jegier and W. L. Gladfelter, *Coord. Chem. Rev.*, 2000, **206**, 631; (c) C. E. Knapp and C. J. Carmalt, *Chem. Soc. Rev.*, 2016, **45**, 1036; (d) S. M. George, *Chem. Rev.*, 2010, **110**, 111; (e) K. J. Blakeney, P. D. Martin and C. H. Winter, *Organometallics*, 2020, **39**, 1006; (f) S. C. Buttera, P. Rouf, P. Deminskyi, N. J. O'Brien, H. Pedersen and S. T. Barry, *Inorg. Chem.*, 2021, **60**, 11025.

2. For selected examples, see: (a) W. O. Filtvedt, A. Holt, P. A. Ramachandran and M. C. Melaaen, *Sol. Energy Mater. Sol. Cells*, 2012, **107**, 188; (b) C.-S. Liu, L.-W. Chou, L.-S. Hong and J.-C. Jiang, *J. Am. Chem. Soc.*, 2008, **130**, 5440; (c) C. Xu, R. T. Beeler, G. J. Grzybowski, A. V. G. Chizmeshya, D. J. Smith, J. Menéndez and J. Kouvetakis, *J. Am. Chem. Soc.*, 2012, **134**, 20756.

3. (a) S. Aldridge and A. J. Downs, *Chem. Rev.*, 2001, **101**, 3305; (b) M. M. D. Roy, A. A. Omaña, A. S. S. Wilson, M. S. Hill, S. Aldridge and E. Rivard, *Chem. Rev.*, 2021, **121**, 12784.

4. (a) T. Masuda, Y. Matsuki and T. Shimoda, *Thin Solid Films*, 2012, **520**, 6603; (b) P. John, I. M. Odeh and J. Wood, *J. Chem. Soc., Chem. Commun.*, 1983, 1496; (c) P. Royen and C. Rocktäschel, *Z. Anorg. Allg. Chem.*, 1966, **346**, 279.

5. (a) P. Royen and R. Schwartz, *Z. Anorg. Allg. Chem.*, 1933, **215**, 295; (b) For a recent investigation, see: H. Yu, C. Ni, A. N. Thiessen, Z. Li and J. G. C. Veinot, *ACS Nano*, 2021, **15**, 9368; (c) S. Schlecht, *Angew. Chem., Int. Ed.*, 2002, **41**, 1178; (d) For a related approach to $[GeH]_n$, see: T. Giousis, G. Potsi, A. Kouloumpis, Y. Georgantas, N. Chalmpes, K. Dimos, M.-K. Antoniou, G. Papavassiliou, A. B. Bourlinos, H. J. Kim, V. K. S. Wadi, S. Alhassan, M. Ahmadi, B. J. Kooi, G. Blake, D. M. Balazs, M. A. Loi, D. Gournis and P. Rudolf, *Angew. Chem., Int. Ed.*, 2021, **60**, 360; (e) L. M. Dennis and N. A. Skow, *J. Am. Chem. Soc.*, 1930, **52**, 2369.

6. (a) A. D. Miller and J. Michl, *Chem. Rev.*, 1989, **89**, 1359; (b) C. Krempner, *Polymers*, 2012, **4**, 408.

7. (a) K. C. Thimer, S. M. I. Al-Rafia, M. J. Ferguson, R. McDonald and E. Rivard, *Chem. Commun.*, 2009, 7119; (b) S. M. I. Al-Rafia, A. C. Malcolm, S. K. Liew, M. J. Ferguson and E. Rivard, *J. Am. Chem. Soc.*, 2011, **133**, 777; (c) E. Rivard, *Dalton Trans.*, 2014, **43**, 8577; (d) A. K. Swarnakar, S. M. McDonald, K. C. Deutsch, P. Choi, M. J. Ferguson, R. McDonald and E. Rivard, *Inorg. Chem.*, 2014, **53**, 8662; (e) The use of GeH_2 complexes to yield Ge nanoparticles upon heating has also been described: T. K. Purkait, A. K. Swarnakar, G. B. De Los Reyes, F. A. Hegmann, E. Rivard and J. G. C. Veinot, *Nanoscale*, 2015, **7**, 2241; (f) O Millo, I. Balberg, D. Azulay, T. K. Purkait, A. K. Swarnakar, E. Rivard and J. G. C. Veinot, *J. Phys. Chem. Lett.*, 2015, **6**, 3396.

8. (a) J. Sinclair, G. Dai, R. McDonald, M. J. Ferguson, A. Brown and E. Rivard, *Inorg. Chem.*, 2020, **59**, 10996; (b) A. A. Omaña, R. K. Green, R. Kobayashi, Y. He, E. R. Antoniuk, M. J. Ferguson, Y. Zhou, J. G. C. Veinot, T. Iwamoto, A. Brown and E. Rivard, *Angew. Chem., Int. Ed.*, 2021, **60**, 228.

9. T. J. Hadlington, M. Hermann, G. Frenking and C. Jones, *J. Am. Chem. Soc.*, 2014, **136**, 3028.

10. M. Grenz, E. Hahn, W.-W. du Mont and J. Pickardt, *Angew. Chem., Int. Ed. Engl.*, 1984, **23**, 61.

11. M. Veith, P. Hobein and R. Rösler, *Z. Naturforsch. B*, 1989, **44b**, 1067.

12. (a) M. Veith, J. Hans, L. Stahl, P. May, V. Huch and A. Sebald, *Z. Naturforsch. B*, 1991, **46b**, 403; (b) M. Veith, C. Mathur and V. Huch, *Organometallics*, 1996, **15**, 2858.

13. T. Lui, J. He and Y. Zhang, *Org. Chem. Front.*, 2019, **6**, 2749.

14. L. W. Pineda, V. Jancik, K. Starke, R. B. Oswald and H. W. Roesky, *Angew. Chem., Int. Ed.*, 2006, **45**, 2602.

15. W. Drescher and C. Kleeberg, *Inorg. Chem.*, 2019, **58**, 8215.

16. While ^{t}BuOAl^{i}Bu$_2$ has been reported in the literature, only characterization in solution by ^{27}Al NMR was reported: J. S. Cha, O. O. Kwon and S. Y. Kwon, *Org. Prep. Proc. Int.*, 1996, **28**, 355. As a result, ^{t}BuOAl^{i}Bu$_2$ was prepared from the reaction of HO^{t}Bu and 0.5 equivalents of [(μ-H)Al^{i}Bu$_2$]$_2$ (DIBAL-H) in toluene.

17. (a) S. P. Foster, K.-F. Leung, K. M. Mackay and R. A. Thompson, *Aust. J. Chem.*, 1986, **39**, 1089; (b) J. Jensen, *J. Mol. Struct. (Theochem)*, 2005, **714**, 21; (c) H. Yildirimyan and G. Gattow, *Z. Anorg. Allg. Chem.*, 1985, **521**, 135.

18. For early work on the use of NHCs to stabilize GeR_2 units, see: (a) A. J. Arduengo, III, H. V. Rasika Dias, J. C. Calabrese and F. Davidson, *Inorg. Chem.*, 1993, **32**, 1541; (b) P. A. Rupar, M. C. Jennings and K. M. Baines, *Organometallics*, 2008, **27**, 5043; (c) P. A. Rupar, V. N. Staroverov and K. M. Baines, *Organometallics*, 2010, **29**, 4871.

19. S. Bontemps, G. Bouhadir, K. Miqueu and D. Bourrisou, *J. Am. Chem. Soc.*, 2006, **128**, 12056.

20. V. Lemierre, A. Chrostowska, A. Dargelos, P. Baylère, W. J. Leigh and C. R. Harrington, *Appl. Organomet. Chem.*, 2004, **18**, 676.

21. R. Heinemann and P. Schmidt, *Cryst. Growth Des.,* 2020, **20**, 5986.

22. K. Hatano, Y. Asano, Y. Kameda, A. Koshio and F. Kokia, *Mater. Sci. Appl.*, 2017, **8**, 838.

23. (a) M. M. D. Roy, S. Fujimori, M. J. Ferguson, R. McDonald, N. Tokitoh and E. Rivard, *Chem. Eur. J.*, 2018, **24**, 14392; (b) R. Jambor and A. Lycka, *Eur. J. Inorg. Chem.*, 2017, 4887; (c) T. J. Hadlington, C. E. Kefalidis, L. Maron and C. Jones, *ACS Catal.*, 2017, **7**, 1853.

24. (a) P. Scherrer, *Göttinger Nachrichten Math. Phys.*, 1918, **2**, 98; (b) U. Holzwarth and N. Gibson, *Nature Nanotech.*, 2011, **6**, 534.

25. A. Meller and C.-P. Gräbe, *Chem. Ber.*, 1985, **118**, 2020.

26. (a) Y. Zhao and D. Truhlar, *Theor. Chem. Acc.*, 2008, **120**, 215; (b) A. K. Wilson, D. E. Woon, K. A. Peterson and T. H. Dunning Jr., *J. Chem. Phys.*, 1999, **110**, 7667.

27. (a) G. Trinquier, *J. Am. Chem. Soc.*, 1990, **112**, 2130; (b) T. L. Windus and M. S. Gordon, *J. Am. Chem. Soc.*, 1992, **114**, 9559; (c) For computed geometries of E_2X_2 species, see: M. Lein, A. Krapp and G. Frenking, *J. Am. Chem. Soc.*, 2005, **127**, 6290; (d) T. Shimizu and G. Frenking, *Theor. Chem. Acc.*, 2011, **130**, 269.

28. E. Rivard, *Chem. Soc. Rev.*, 2016, **45**, 989.

29. S. M. I. Al-Rafia, M. R. Momeni, R. McDonald, M. J. Ferguson, A. Brown and E. Rivard, *Angew. Chem., Int. Ed.*, 2013, **52**, 6390.

30. J. P. Perdew, K. Burke and M. Ernzerhof, *Phys. Rev. Lett.*, 1996, **77**, 3865.

31. For computational work on oligohydrosilanes, see: (a) K. Takeda, H. Teramae, and N. Matsumoto, *J. Am. Chem. Soc.*, 1986, **8**, 8186; (b) J. R. Damewood Jr. and R. West, *Macromolecules*, 1985, **18**, 159; (c) A. Modelli, D. Jones, L. Favaretto, and G. Distefano, *Organometallics*, 1996, **15**, 380.

32. For readers interested in further analysis of these computations, the full output files are available as part of the Supplementary Information of: J. Sinclair, W. Medroa del Pino, K. Aku-Dominguez, Y. Minami, A. Kiran, M. J. Ferguson, M. Yasuda and E. Rivard, *Dalton Trans.*, 2021, **50**, 17688.

33. (a) A. D. Becke, *J. Chem. Phys.* 1993, **98**, 5648; (b) C. Lee, W. Yang and R. G. Parr, *Phys. Rev. B*, 1988, **37**, 785; (c) S. H. Vosko, L. Wilk and M. Nusair, *Can. J. Phys.*, 1980, **58**, 1200; (d) P. J. Stephens, F. J. Devlin, C. F. Chabalowski and M. J. Frisch, *J. Phys. Chem.*, 1994, **98**, 11623.

34. A line broadening (σ) of 0.000241967 nm^{-1} was applied, according to the method presented on: Creating UV/Visible Plots from the Results of Excited States Calculations. http://gaussian.com/uvvisplot/ [Accessed June 25, 2021].

35. W. Fa and X. C. Zeng, *Chem. Commun.*, 2014, **50**, 9126.

36. (a) M. D. Pelta, G. A. Morris, M. J. Stchedroff and S. J. Hammond, *Magn. Reson. Chem.*, 2002, **40**, S147; (b) A. Botana, J. A. Aguilar, M. Nilsson and G. A. Morris, *J. Magn. Reson.*, 2011, **208**, 270.

37. M. A. Connell, P. J. Bowyer, P. A. Bone, A. L. Davis, A. G. Swanson, M. Nilsson and G. A. Morris, *J. Magn. Reson.*, 2009, **198**, 121.

38. (a) S. Matsuo and T. Makita, *Int. J. Thermophys.*, 1993, **14**, 67; (b) P. Groves, *Polym. Chem.*, 2017, **8**, 6700.

39. A. Laubengayer and P. Brandt, *J. Am. Chem. Soc.*, 1932, **54**, 621.

40. Characteristic ^{1}H NMR of products can be found in: S. Anga, J. Acharya and V. Chandrasekhar, *J. Org. Chem.*, 2021, **86**, 2224.

41. M. J. Frisch, G. W. Trucks, H. B. Schlegel, G. E. Scuseria, M. A. Robb, J. R. Cheeseman, G. Scalmani, V. Barone, G. A. Petersson, H. Nakatsuji, X. Li, M. Caricato, A. V. Marenich, J. Bloino, B. G. Janesko, R. Gomperts, B. Mennucci, H. P. Hratchian, J. V. Ortiz, A. F. Izmaylov, J. L. Sonnenberg, D. Williams-Young, F. Ding, F. Lipparini, F. Egidi, J. Goings, B. Peng, A. Petrone, T. Henderson, D. Ranasinghe, V. G. Zakrzewski, J. Gao, N. Rega, G. Zheng, W. Liang, M. Hada, M. Ehara, K. Toyota, R. Fukuda, J. Hasegawa, M. Ishida, T. Nakajima, Y. Honda, O. Kitao, H. Nakai, T. Vreven, K. Throssell, J. A. J. Montgomery, J. E. Peralta, F. Ogliaro, M. J. Bearpark, J. J. Heyd, E. N. Brothers, K. N. Kudin, V. N. Staroverov, T. A. Keith, R. Kobayashi, J. Normand, K. Raghavachari, A. P. Rendell, J. C. Burant, S. S. Iyengar, J. Tomasi, M. Cossi, J. M. Millam, M. Klene, C. Adamo, R. Cammi, J. W. Ochterski, R. L. Martin, K. Morokuma, O. Farkas, J.

B. Foresman and D. J. Fox, Gaussian 16, Revision B.01, Gaussian, Inc., Wallingford CT.

42. (a) S. Harrypersad, L. Liao, A. Khan, R. S. Wylie and D. A. Foucher, *J. Inorg. Organomet. Polym.*, 2015, **25**, 515; (b) W. Fa and X. C. Zeng, *Chem. Commun.*, 2014, **50**, 9126.

43. (a) G. M. Sheldrick, *Acta Cryst.*, 2015, **A71**, 3; (b) G. M. Sheldrick, *Acta Cryst.*, 2015, **C71**, 3.

44. (a) H. D. Flack, *Acta Crystallogr.*, 1983, **A39**, 876; (b) H. D. Flack and G. Bernardinelli, *Acta Crystallogr.*, 1999, **A55**, 908; (c) H. D. Flack and G. Bernardinelli, *J. Appl. Cryst.*, 2000, **33**, 1143.

Chapter 4: Molecular Precursors for Room Temperature Elemental Tin Deposition

1. (a) E. Rivard, *Chem. Soc. Rev.*, 2016, **45**, 989; (b) M. M. D. Roy, A. A. Omaña, A. S. S. Wilson, M. S. Hill, S. Aldridge and E. Rivard, *Chem. Rev.*, 2021, **121**, 12784.

2. (a) V. H. Nguyen, A. Dobbie, M. Myronov, D. J. Norris, T. Walther and D. R. Leadley, *Thin Solid Films,* 2012, **520**, 3222; (b) R. Venkatasubramanian, R. T. Pickett and M. L. Timmons, *J. Appl. Phys.*, **1989**, *66*, 5662.

3. (a) B. E. Eichler and P. P. Power, *J. Am. Chem. Soc.*, 2000, **122**, 8785; (b) L. W. Pineda, V. Jancik, K. Starke, R. B. Oswald and H. W. Roesky, *Angew. Chem., Int. Ed.*, 2006, **45**, 2602.

4. S. M. I. Al-Rafia, A. C. Malcolm, S. K. Liew, M. J. Ferguson and E. Rivard, *J. Am. Chem. Soc.*, 2011, **133**, 777.

5. J. Sinclair, W. Medroa del Pino, K. Aku-Dominguez, Y. Minami, A. Kiran, M. J. Ferguson, M. Yasuda and E. Rivard, *Dalton Trans.*, 2021, **50**, 17688.

6. C. G. Granqvist, *Appl. Phys. A*, 1993, **57**, 19.

7. C. E. Knapp and C. J. Carmalt, *Chem. Soc. Rev.*, 2016, **45**, 1036.

8. M. Takeuchi and K. Maki, *Jpn. J. Appl. Phys.*, 2007, **46**, 7852.

9. A. Suzuki and K. Maki, *Chem. Vap. Dep.*, 2006, **12**, 608.

10. (a) N. Hollingsworth, G. Kociok-Köhn, K. C. Molloy and A. L. Sudlow, *Dalton Trans.*, 2010, **39**, 5446; (b) N. Hollingsworth, G. A. Horley, M. Mazhar, M. F. Mahon, K. C. Molloy, P. W. Haycock, C. P. Myers and G. Critchlow, *Appl. Organometal. Chem.*, 2006, **20**, 687; (c) W. Ikuko and K. Ichiro, *Chem. Lett.*, 1972, **1**, 325.

11. J. D. Parish, M. W. Snook and A. L. Johnson, *Dalton Trans.*, 2021, **50**, 13902.

12. M. Veith, *Angew. Chem. Int. Ed. Engl.*, 1975, **4**, 263.

13. (a) M. Veith and F. Töllner, *J. Organomet. Chem.*, 1983, 219; (b) M. Veith and R. Rösler, *Z. Natutforch.*, 1986, **41b**, 1071.

14. (a) K. C. Thimer, S. M. I . Al-Rafia, M. J. Ferguson, R. McDonald and E. Rivard, *Chem. Commun.*, 2009, 7119; (b) N. Kuhn, T. Kratz, D. Bläser and R. Boese, *Chem. Ber.*, 1995, **128**, 245; (b) B. Bantu, G. M. Pawar, U. Decker, K. Wurst, A. M. Schmidt and M. R. Buchmeiser, *Chem. Eur. J.*, 2009, **15**, 3103.

15. J. Sinclair, G. Dai, R. McDonald, M. J. Ferguson, A. Brown and E. Rivard, *Inorg. Chem.*, 2020, **59**, 10996.

16. T. Lui, J. He and Y. Zhang, *Org. Chem. Front.*, 2019, **6**, 2749.

17. W. Jiang, Z.-L. Yang, D. Weng, J.-W. W, Y.-F. Lu, M.-J. Zhang and Z.-Z. Yang, *Chin. Chem. Lett.*, 2014, **25**, 849.

18. Z. Huang, S. Wang, X. Zhu, Q. Yuan, Y. Wei, S. Zhou and X. Mu, *Inorg. Chem.*, 2018, **57**, 15069.

19. (a) R. W. G. Wyckoff, *Crystal Structures Vol. 1*, Interscience Publishers, New York, 1963; (b) S. Grazulis, D. Chateigner, R. T. Downs, A. T. Yokochi, M. Quiros, L. Lutterotti, E. Manakova, J. Butkus, P. Moeck and A. Le Bail, *J. Appl. Cryst.*, 2009, **42**, 726; (c) M. Alf, D. Gultrkin and H. Akbulut, *Acta Phys. Pol. A*, 2013, **123**, 323.

20. (a) G. M. Sheldrick, *Acta Cryst.*, 2015, **A71**, 3; (b) G. M. Sheldrick, *Acta Cryst.*, 2015, **C71**, 3.

Chapter 6: Summary and Future Work

1. (a) G.-B. Shen, K. Xia, X.-T. Li, J.-L. Li, Y.-H. Fu, L. Yuan and X.-Q. Zhu, *J. Phys. Chem. A*, 2016, **120**, 1779; (b) I. Lee, *Chem. Soc. Rev.*, 1995, **24**, 223; (c) A. Streitwieser, R. H. Jagow, R. C. Fahey and S. Suzuki, *J. Am. Chem. Soc.*, 1958, **80**, 2326.

2. S. M. I. Al-Rafia, A. C. Malcolm, R. McDonald, M. J. Ferguson and E. Rivard, *Chem. Commun*., 2012, **48**, 1308.

3. (a) K. C. Thimer, S. M. I. Al-Rafia, M. J. Ferguson, R. McDonald and E. Rivard, *Chem. Commun.*, 2009, 7119; (b) S. M. I. Al-Rafia, A. C. Malcolm, S. K. Liew, M. J. Ferguson and E. Rivard, *J. Am. Chem. Soc.*, 2011, **133**, 777.

4. J. Sinclair, G. Dai, R. McDonald, M. J. Ferguson, A. Brown and E. Rivard, *Inorg. Chem.*, 2020, **59**, 10996.

5. (a) P. A. Rupar, M. C. Jennings and K. M. Baines, *Organometallics*, 2008, **27**, 5043; (b) A. C. Filippou, O. Chernov, B. Blom, K. W. Stumpf and G. Schnakenburg, *Chem. Eur. J.*, 2010, **16**, 2866.

6. T. Chu and G. I. Nikinov, *Chem. Rev.*, 2018, **118**, 3608.

7. S. Pan, R. Saha, E. Osorio, P. K. Chattaraj, G. Frenking and G. Merino, *Chem. Eur. J.*, 2017, **23**, 7463.

8. (a) F. S. Geitner, M. A. Giebel, A. Pöthig and T. F. Fässler, *Molecules*, 2017, **22**, 1204; (b) L. J. Schiegerl, M. Melaimi, D. R. Tolentino, W. Klein, G. Bertrand and T. F. Fässler, *Inorg. Chem.*, 2019, **58**, 3256.

9. M. M. D. Roy, S. Fujimori, M. J. Ferguson, R. McDonald, N. Tokitoh and E. Rivard, *Chem. Eur. J.*, 2018, **24**, 14392.

10. (a) A. Watanabe, M. Unno, F. Hojo and T. Miwa, *J. Mater. Sci. Lett.*, 2001, **20**, 491; (b) A. Watanabe, M. Unno, F. Hojo and T. Miwa, *Chem. Lett.*, 2001, **30**, 1092.

11. (a) U. Kasavajjula, C. Weng and A. J. Appleby, *J. Power Sources*, 2007, **163**, 1003; (b) X. Xiao, X. Li, S. Zheng, J. Shao, H. Xue and H. Pang, *Adv. Mat. Interfaces*, 2017, **4**, 1600798.

12. C. E. Knapp and C. J. Carmalt, *Chem. Soc. Rev.*, 2016, **45**, 1036.

13. S. Gupta, X. Gong, R. Zhang, Y.-C. Yeo, S. Takagi and K. C. Saraswat, *MRS Bull.*, 2014, **39**, 678.

14. (a) K. Knapas, T. Hatanpää, M. Ritala and M. Leskelä, *Chem. Mater.*, 2010, **22**, 1386; (b) V. Pore, T. Hatanpää, M. Ritala and M. Leskelä, *J. Am. Chem. Soc.*, 2009, **131**, 3478; (c) M. Ritala, V. Pore, T. Hatanpää, M. Heikkilä, M. Leskelä, K. Mizohata, A. Schrott, S. Raoux and S. M. Rossnagel, *Microelectron. Eng.*, 2009, **86**,

1946; (d) T. Sarnet, V. Pore, T. Hatanpää, M. Ritala, M. Leskelä, A. Schrott, Y. Zhu, S. Raoux and H.-Y. Cheng, *J. Electrochem. Soc.*, 2011, **158**, D694.

15. (a) T. Eom, T. Gwon, S. Yoo, B. J. Choi, M.-S. Kim, I. Buchanan, M. Xiao and C. S. Hwang, *Chem. Mater.*, 2014, **26**, 1583; (b) T. Eom, S. Choi, B. J. Choi, M. H. Lee, T. Gwon, S. H. Rha, W. Lee, M.-S. Kim, M. Xiao, I. Buchanan, D.-Y. Cho and C. S. Hwang, *Chem. Mater.*, 2012, **24**, 2099; (c) S. Yoo, C. Yoo, E.-S. Park, W. Kim, Y. K. Lee and C. S. Hwang, *J. Mater. Chem. C*, 2018, **6**, 5025.

Appendix: Starting Grassroots Initiatives to Foster Equity, Diversity, and Inclusivity in the Chemistry Department at the University of Alberta

1. N. Etkin, M. A. Armour, T. Franz-Odendaal, G. Rayner-Canham, M. Rayner-Canham, H. A. Al-Abadleh and K. Jones, *Making Chemistry Inclusive*, Hayden-McNeil, Plymouth, 2016.
2. Women in Scholarship, Engineering, Science, and Technology, ualberta.ca/services/wisest/index.html, (accessed November 2020).
3. WiSER, wiseredmonton.ca, (accessed November 2020).
4. Faculty of Science Diversity Report, https://www.ualberta.ca/science/about-us/contours/2016-fall-contours/2016/october/faculty-of-sciencediversity-report.html, (accessed November 2020).
5. Canadian Association of University Teachers, CAUT Almanac of Post-Secondary Education in Canada, 2014, https://www.caut.ca/docs/defaultsource/almanac/almanac_2013-2014_print_finalE20A5E5CA0EA6529968D1CAF.pdf?sfvrsn=2, (accessed 15 July 2020).

6. M. M. Ferreira, *Int. J. Sci. Educ.*, 2003, **25**, 969.

7. National Science Foundation, Women, Minorities, and Persons with Disabilities in Science and Engineering, 2019, https://ncses.nsf.gov/pubs/nsf19304/digest, (accessed November 2020).

8. Royal Society of Chemistry, Diversity Landscape of the Chemical Sciences, 2018, https://www.rsc.org/globalassets/02-about-us/our-strategy/inclusion-diversity/cm-044-17_a4-diversity-landscape-of-the-chemical-sciencesreport_web-2.pdf, (accessed November 2020).

9. Royal Society of Chemistry. Exploring the Workplace for LGBTQ+ Physical Scientists, 2019, https://www.rsc.org/globalassets/04-campaigningoutreach/campaigning/lgbt-report/lgbt-report_web.pdf, (accessed July 2020).

10. Pride in STEM. LGBTSTEM Day 2019 Press Release, https://prideinstem.org/lgbtstem-day-2019-press-release, (accessed July 2020).

11. International Union of Pure and Applied Chemistry, IUPAC100 Global Women's Breakfast. https://iupac.org/100/global-breakfast/, (accessed November 2020).

12. Canadians Working for Inclusivity in Chemical Sciences, Engineering, and Technology, www.cwicnetwork.ca, (accessed November 2020).

13. University of Alberta Chemistry Department, Chemistry Lecture Series https://www.ualberta.ca/chemistry/news-and-events/lectureseries/index.html, (accessed November 2020).

14. J. Stockard, J. Greene, G. Richmond and P. J. Lewis, *Chem. Educ.*, 2018, **95**, 1492.

15. J. Stockard, J. Greene, J. P. J. Lewis and G. J. Richmond, *Women Minor. Scien. Eng.*, 2008, **14**, 1.

16. J. Stockard, J. Greene, P. J. Lewis and G. Richmond, in *Mentoring strategies to facilitate the advancement of women faculty*, ed. K. K. Karukstis, B. L. Gourley, M. Rossi and L. L. Wright, American Chemical Society, Washington D.C., 2010, ch. 10, pp. 153–163.

17. K. TallBear, *Native American DNA - Tribal Belonging and the False Promise of Genetic Science*, University of Minnesota Press, Minneapolis, 2013.

18. K. Tallbear, *Kalfou*, 2019, **6**, 24.

19. Natural Science and Engineering Research Council. Women in Science and Engineering in Canada, 2017, https://www.nserc-crsng.gc.ca/_doc/Reports-Rapports/WISE2017_e.pdf, (accessed July 2020).

20. A. A. Eaton, J. F. Saunders, R. K. Jacobson and K. West, K. *Sex Roles*, 2020, **82**, 127.

21. A. W. Woolley, C. F. Chabris, A. Pentland, N. Hashmi and T. W. Malone, *Science*, 2010, **330**, 686.

22. R. B. Freeman and W. Huang, *Nature*, 2014, **513**, 305.

23. S. S. Levine, E. P. Apfelbaum, M. Bernard, V. L. Bartelt, E. J. Zajac and D. Stark, *Proc. Natl. Acad. Sci. USA,* 2014, **111**, 18524.

24. American Chemical Society. ACS Salary Report 2015. https://acs.org/content/acs/en/careers/salaries/surveys/salary-report-2015.html, (accessed July 2020).

25. Working towards Inclusivity in Chemistry Toronto, http://croftw.chem.utoronto.ca/wp/womeninchemto/, (accessed November 2020).

26. USask Women in Chemistry, https://usask-wic.com/, (accessed November 2020).

27. University of Alberta Department of Chemistry EDI Committee, Our Commitment to Equity, Diversity, and Inclusion, 2020, https://www.ualberta.ca/chemistry/news-and-events/news/2020/august/edi_post.html, (accessed November 2020).

28. M. F. Jimenez, T. M. Laverty, S. P. Bombaci, K. Wilkins, D. E. Bennett, and L. Pejchar, *Nat. Ecol. Evol.,* 2019, **3**, 1030.

Appendix: Starting Grassroots Initiatives to Foster Equity, Diversity, and Inclusivity in the University of Alberta Department of Chemistry

I. Motivations

Less than four decades ago, there were zero women faculty and about 70 % of the student body was male in the Department of Chemistry at the University of Alberta.[1] After Dr. Margaret-Ann Armour joined the Department, she spearheaded the formation of the Women in Scholarship, Engineering, Science, and Technology[2] (WISEST) organization in 1982 to increase the number of female students in the Faculty of Science. Currently, WISEST is focused on increasing engagement of high school students from underrepresented groups to consider careers in science by hosting summer research opportunities. With WISEST focused on introducing young women to science, Women in Science, Engineering and Research[3] (WiSER) promotes the retention and advancement of women in the STEM workforce. As Associate Dean of Diversity in the Faculty of Science at the University of Alberta, Dr. Armour directed Project Catalyst, a committee formed in 2005 that is aimed at understanding hiring biases towards female candidates (family life assumptions, technical skill assessments) and overcoming the structural barriers (maternity leave, timeline to tenure, lack of mentorship) to increase the appointment and retainment of women in the Faculty of Science. Even after 11 years of work, the overall percentage of female faculty has only increased to a total of 15 % at the University of Alberta.[4]

Although steps have been taken to rectify gender disparity in chemistry, such as the initiatives outlined above, only 28 % of assistant professors in chemistry departments throughout Canada are women and significantly less (10 %) are full professors.[5] These numbers are also reflected at the University of Alberta, where faculty and staff are disproportionate in their representation compared with the student body. The lack of mentorship and representation levy a heavy burden on graduate students, who may be first generation academics, far from their support networks, or struggle to find their place in the chemistry community for other reasons.[6] This is reflected in the disproportionate attrition of underrepresented individuals at the juncture between graduate school and post-graduate careers in science.[7,8]

Many of the equity-focused groups at the University of Alberta target the recruitment of high school students into the sciences (WISEST) or those who are entering or are already in the workforce as career scientists (Project Catalyst, WISER). Although these projects focus on STEM-wide issues, a group serving a small subsection of STEM may be able to enact changes much more quickly at the department level. In the spring of 2017, the University of Alberta's Women in Chemistry initiative was founded to bridge this gap and provide support to underrepresented groups in the trainee stages of their careers in chemistry.

The drive behind the foundation of this group was varied, with each graduate student bringing different perspectives based on past experiences. Many members recounted instances of discrimination, implicit bias, microaggressions, gaslighting,

imposter syndrome, and sexual harassment. These experiences fuelled the desire to create a more inclusive environment where diversity is celebrated and equity is fought for. The group, led by a graduate student executive team with support from a Faculty Advisor and occasional undergraduate student volunteers, has a vision of engaging the Department of Chemistry in a cultural shift towards the active retention of underrepresented groups in chemistry.

Since its initiation, the group has grown, both in terms of membership and in addressing the needs of graduate student peers. Recognizing that this group should serve all persons in the community, and after a series of discussions and departmental feedback, the name was officially changed to University of Alberta Working for Inclusivity in Chemistry (UAWIC) to better reflect the true nature of its membership. The UAWIC group set out to build an equitable, diverse, and inclusive environment through the following goals:

1. To build community among members of the Chemistry Department by breaking down the barriers between hierarchical academic roles, allowing for a greater understanding amongst groups (faculty, students, staff) to develop. The sharing of lived experiences can allow for open discussion and will help department members gain insight to other perspectives in chemistry.
2. To retain the diverse graduate student population in chemistry by giving graduate students tools and training to enrich their career development, with a specific focus on highlighting diverse scientists and career paths. UAWIC hopes to provide the space for individuals to be supported in their pursuit of science at

the graduate level and to place the inclusion of historically excluded groups at the forefront.

The events and initiatives described below were organized to execute the vision of creating a more inclusive environment at the University of Alberta. They are presented here to act as a template for further action and support for equity, diversity, and inclusion (EDI) initiatives. Broadly, these events can be operated with limited budgets by leveraging departmental connections with alumni, local industry, and government.

II. Goal 1: community building

II.i Department-wide community building: Visibility and food

Most of the social events organized by UAWIC utilize food as a way to bring people together. World Food Day invites all members of the department to contribute food to a potluck-style lunch and gives people the opportunity to share some of their culture. This event has been particularly successful in accommodating people with food restrictions, as participants are asked to indicate the name and ingredients of their dish. Pi Day is another potluck event where department members contribute both sweet and savory pies for others to enjoy. The event spans the entire department, as chairpersons, administrative staff, professors, and others volunteer to be pie'd in the face. The event helps break down the hierarchy of the department, as graduate students pie faculty, service staff pie administrators, and undergraduates pie their lab teaching assistants. These events facilitate community building and equality through shared experience and good food, which in turn supports the first goal.

II.ii Visible allyship

As the scope of UAWIC expanded, the group wanted to outwardly show its support for different intersectional identities within both EDI and STEM. Visibility of allyship is one major area that has been identified to help make workspaces in the physical sciences more welcoming to underrepresented groups.[9] Flying a rainbow flag or posting Black Lives Matter signs, for example, can promote more inclusive spaces and increase visibility of allies. Additionally, these symbols can generate conversation and can help one locate safe spaces to talk about issues they may be facing. In an attempt to increase visibility of allyship at conferences, a set of enamel pins were designed that people can wear to signify that they are potential allies. Current pins advocate for Women in Chemistry, diversity, and support for those who have invisible identities, (*i.e.*, members of the LGBTQ+ community or people with disabilities). These pins, seen in Figure A.1, also serve as ongoing fundraising for the group and have been sold internationally for chemists to identify themselves as allies at work and conferences.

In an effort to engage the entire department in visibility initiatives, UAWIC participated in the international LGBTQ+ in STEM day[10] through a door decorating contest. Research groups in the Chemistry Department volunteered to decorate their door, and UAWIC hosted a tour to view all the participating doors. Approximately 30% of the research groups in the department participated, and many of the door decorations were left up for months after the fact to serve as visibility for those who are allies to the LGBTQ+ community (Figure A.1, top, right, and bottom).

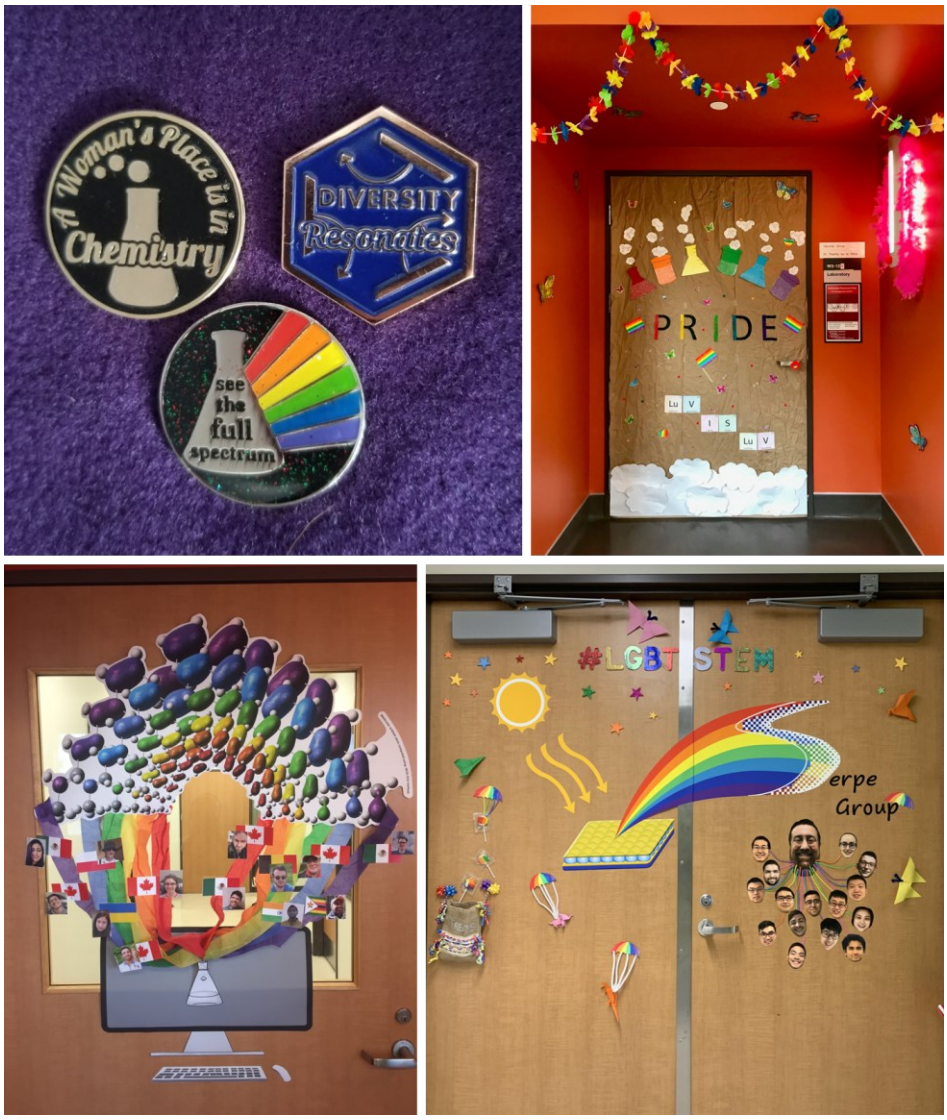

Figure A.1. Examples of visible allyship. Top left, enamel pins. Door decorating contest participants: top right, Harynuk group; bottom right, Brown and Klobukowski Groups; bottom left, Serpe Group.

The LGBTQ+ in STEM event and the IUPAC Global Women's Breakfast[11] are two events that, though hosted internationally, UAWIC is able to participate in locally. These events bring together communities around the world to learn from each other.

The global recognition of groups working on diversity and inclusion issues is important for the ongoing success of groups like UAWIC, as they allow the sharing of event ideas and prevent burnout via mutual support. These events act to highlight diverse chemists internationally, as well as within the department, and aid in creating an inclusive environment that will have a lasting effect on the community, supporting the ongoing goals of UAWIC.

II.iii Peer-to-peer community building: meet and greets

As a fledgling group, UAWIC sought to highlight diverse chemists who visited the department to give research seminars. UAWIC offers to host visiting speakers who identify as members of underrepresented groups in chemistry or who follow non-traditional careers in a casual coffee hour open to the entire department. Being an informal activity, these hours give students and postdocs time to ask questions about careers, barriers to advancement in chemistry, and work–life balance in a safe setting. Given the gender disparity and profound lack of diversity in faculty membership across Canada,[5] these events allow access to a larger pool of representative academics and professionals. The mentorship by these visiting speakers, however brief, provided invaluable insight into work environments and challenges upon the completion of graduate school. This event series regularly draws groups of 10–15 attendees. Although this represents only 5 % of the graduate student body, theseattendees represented different groups with different interests, depending on the speaker. For example, new female professors tended to draw postdoctoral researchers and graduate students

interested in pursuing academia, whereas pharmacological industry representatives drew an entirely different cohort of student attendees. Together, the reach for these events would be approximately 25 % of the total graduate student population. The meet and greet hours function within the framework of both of the goals by facilitating conversation and connections among individuals with similar interests and highlighting diverse scientists in the wider chemistry community.

III. Goal 2: retention of diverse graduate student chemists

Multiple factors can affect the desire of a student to continue in academia and pursue advanced careers in chemistry, and the group strived to give graduate students tools to navigate their chosen career path. UAWIC provides professional development tools through workshops (LOGIC, Highlighting Diverse Career Paths) and also trains students in potential barriers they or their colleagues may face along the way (LOGIC, Margaret-Ann Armour Lecture Series, Diversity in STEMinars).

III.i Leaders overcoming gender inequality in chemistry retreat

In 2018, UAWIC organized the 2nd annual Leaders Overcoming Gender Inequality in Chemistry (LOGIC) retreat. This event began in 2017 as an initiative hosted by the graduate student members of the Women in Chemistry (now known as Working towards Inclusivity in Chemistry) Group at the University of Toronto. The inaugural event was inspired by the Puget Sound Women Chemists retreat and was held as a

satellite event to the Canadian Chemistry Conference and Exhibition (CCCE) to reach a wider audience of Canadian chemists. LOGIC includes seminars, workshops, panel discussions, and networking sessions focused on a central theme. In past years, themes have included "Becoming a Confident Chemist and Future Leader" (Toronto, 2017) and "Paving a Path to a Career in Chemistry" (Edmonton, 2018). These retreats focused on building professional development skills for graduate students and early career researchers and providing resources for identifying mentors and sponsors for your career path. In 2019 and 2020, the themes were "Women Leading and Excelling" (Quebec, 2019) and "Beyond the Visible Spectrum" (Winnipeg/Virtual, 2020) where the focus was predominantly on educating and training individuals on EDI topics. This retreat is based on learning uncomfortable topics in an environment that encourages questions and discussion. Mentorships often begin within LOGIC, as some attendees are new to these topics and how they relate to STEM, whereas others are highly educated in EDI issues and can help guide beginners.

The breakdown of attendee statistics, collected by the respective organizing committee of that year, over the last four years can be seen in Fig. 2. Graduate students make up the majority of the attendee roster with an average of 53 %. The remaining half is distributed among postdoctoral researchers, academics (assistant professors, associate professors, full professors, technicians), industry, and government chemists. Since the first LOGIC retreat, the number of participants has increased, with a major increase in 2020 due to the retreat being moved online and the alleviation of registration fees. Additionally, the breakdown of attendee gender for LOGIC shows that there is a much

greater number of female attendees than any other gender. This may be due to the original scope of the conference (women in chemistry), and UAWIC is working to incorporate components in the future that will bring people of all genders to the discussion.

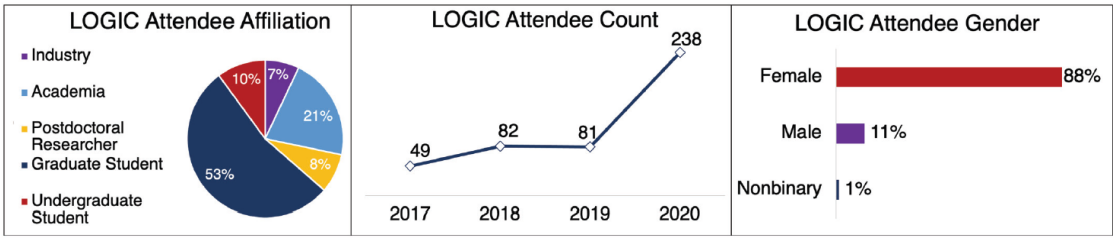

Figure A.2. Attendee statistics based on data over four years of the LOGIC retreat. Left: attendee affiliation averaged over data from 2017 to 2020. Middle: growth in annual number of attendees. Right: self-reported attendee gender (female, male, nonbinary) percentages averaged over data from 2017 to 2020.

Anonymous feedback from previous LOGIC retreats provides insight to the most valuable aspects of the conference as identified by attendees. Participants explained that they left the conference feeling invigorated and inspired to tackle EDI challenges:

> *"It was important and empowering to learn about what issues women in science face when heading into the workforce as PIs or in other chemistry related fields, and I feel more prepared heading into the next stage in my career being aware of these issues. I will be proactive in fighting for equity in my place of work, and have been inspired by so many amazing women who have already paved their way in their respective fields."* (participant 1)
>
> and

"Pursue what you love to do nomatter what barriers or challenges you encounter, and don't be afraid to seek out mentors and colleagues in the chemistry community for support." (participant 2)

Feedback also showed that attendees learned about aspects of intersectionality and how to better support underrepresented groups in STEM:

"Being a white woman is not ideal in science, but it's a helluva lot more privileged than being a woman of colour, and I need to recognize that advantage as such, and make sure that I work to increase diversity of all its forms, and not just women. That is important." (participant 3)

and

"It gave me tools and language to express myself and help me become a more effective and active ally." (participant 4)

Attendees have reported that bringing these discussions to their own department would be valuable and would like to set up avenues for dissemination of EDI topics:

"You've inspired me to encourage students in my department to come together and discuss equity, diversity and inclusion since as it stands, we do not have any such organization or platform for these conversations." (participant 5)

and

"I think all Department Heads should be attending as it really opens one's eyes to the challenges faced by so many." (participant 6)

LOGIC 2020 was adjusted to a virtual format due to COVID-19 restrictions. The online platform boosted attendee numbers three-fold from the previous year, and since travel and accommodations were no longer required, there were a large number of international registrants from countries like USA, Australia, England, Belgium, Scotland, and Switzerland. Additionally, this allowed us to offer more inclusive and flexible programming such as pre-recorded and close-captioned seminars. Discussions on the Slack platform allowed attendees to be part of the conference without excluding those with career or caretaking commitments or language barriers.

Over time, LOGIC has evolved into a community-driven event organized by an overarching network, Canadians Working for Inclusivity in Chemical Sciences, Engineering, and Technology[12] (CWIC). Representatives from other inclusivity groups across Canada are now involved and a community is built through working towards a common goal.

III.ii Margaret-Ann Armour Lecture Series

In honour of Dr. Margaret-Ann Armour's contribution to scientific research and advancement of diversity at the University of Alberta, UAWIC established the annual student-invited Margaret-Ann Armour Lecture Series in 2019.[13] This lecture series showcases that chemists can be both outstanding in their research and promote diversity and inclusion within chemistry.

Potential speakers for this series are short-listed by the graduate student members of the UAWIC executive, and an anonymous voting ballot is electronically sent to all graduate students and postdoctoral fellows in the department for final selection. The UAWIC Co-Chairs will reach out to the chosen speaker and invite them to visit the University of Alberta campus for a two-part lecture series. One of the lectures will be a research presentation, and the second lecture will be dedicated to showcasing the career path and personal involvement of the visitor in EDI initiatives. Once they have accepted, members of the UAWIC executive team will begin planning and executing all aspects of the speaker's visit, from flights to accommodations to meals to campus room and projector booking to advertising. To ensure both students and faculty have a chance to meet the speaker, UAWIC arranges for a student pizza lunch open to all graduate students and postdoctoral fellows, a dinner with the entire executive team, as well as individual one-on-one faculty meetings between the visitor and professors of the Chemistry Department. An endeavour of this type does require significant planning, and the process is begun, initiated by the student vote, about a year in advance of the anticipated visit. Furthermore, to successfully deliver this lecture series as a free event to all members of the university community interested in attending, UAWIC actively fundraises through the year by hosting food-centered events, promoting pin sales, and writing grants for additional support.

The inaugural speaker was Dr. Geraldine Richmond, Professor of Chemistry at the University of Oregon and founder of COACh (Committee On the Advancement of Women Chemists), an organization focusing on increasing the presence of women in

science by providing resources on building successful careers.[14–16] Dr. Richmond spoke about her research on nanoemulsions, as well as highlighting the importance of groups such as COACh. The invited speaker for 2020 was Dr. Molly Shoichet, Professor of Chemistry at the University of Toronto, who spoke to us about her work on developing hydrogels and her career path. Department members were exposed to strong role models that excel both in research and embracing diversity. Meeting leaders that exemplify the goals is a valuable network building opportunity that has been well received by the department (on average 65 attendees). This seminar series highlights EDI work as crucial to the success of science, rather than a pursuit external to it. The speakers are lifelong champions for inclusivity in their own communities and provide valuable insights into what still needs to be done in this area.

III.iii Diversity in STEMinars

The Diversity in STEMinar lecture series was founded in 2019 to bring more diverse perspectives into the Chemistry Department and foster discussion on topics outside of the expertise of the UAWIC executive committee. The focus is on identifying local speakers with research interests under the STEM umbrella but who also make diversity and inclusivity a focus in their career. The first speaker, Dr. Kim TallBear, addressed the colonial past and present of science, in particular in genomic and biological studies.[17,18] For the second STEMinar, UAWIC leveraged a mandatory professional development program within the Faculty of Graduate Studies and Research at the University of Alberta to increase attendance and broaden the pool of attendees to the

entire Faculty of Science. Reaching over 80 students, faculty, and staff, Dr. Lisa Willis discussed the statistics of diverse representation in STEM academia,[19] the fallacy of improvement in this area,[20] and the benefits to problem solving and creative idea production that result from assembling diverse teams.[21–23] These seminars will continue to operate as a way to educate the community on the intersections of diversity and scientific research and highlight local scientists who are experts and passionate about this work. This broad education on the status of EDI movements in STEM supports both of the goals by fostering discussion within the department and highlighting areas in which improvements can be made in support for underrepresented groups during their time at the University of Alberta.

III.iv Highlighting diverse career paths

Chemistry-degree holders pursue a vast range of career trajectories after graduation[24] and exposure to non-academic jobs is extremely limited in university settings. UAWIC regularly uses its network of professional chemists to showcase possible chemistry career opportunities available through panel discussions. Speakers include individuals from all walks of life, ranging from government scientists, to process chemists, to scientific editors. Attendees engaged in discussions about navigating a career in chemistry and were exposed to different employment opportunities available to them. These events are specifically tailored to support the second goal. By including a diverse range of speakers, open discussion, and sharing experiences, UAWIC equips attendees with in-depth knowledge of what to expect when entering the chemistry workforce.

IV. Canadian women in chemical sciences network

Through many of these events, UAWIC executive member met other graduate students and groups working on EDI issues in chemistry. In collaboration with the University of Toronto Working for Inclusivity in Chemistry[25] and the University of Saskatchewan Women in Chemistry[26] groups, the CWIC Network was formed. This team is focused on providing guidance and resources to up and coming CWIC chapters across Canada, as well as creating a network for these chapters to share resources and experiences with each other. Since 2018, the number of affiliated groups has grown from three to thirteen. The CWIC Network is affiliated with the Chemical Institute of Canada (CIC) as a member resource group and is the first of its kind in the Canadian chemistry community. CWIC shares similar goals to the UAWIC group but has a far greater reach into the academic and industrial spheres. For example, CWIC organized an EDI symposium at the 102nd Canadian Chemistry Conference and Exhibition (postponed to 2021 due to the COVID-19 pandemic) focused on allyship in the Canadian chemistry community.

V. Conclusions and future perspectives

As EDI initiatives grow in size and number in the international community, UAWIC has worked to be at the forefront of the movement within graduate chemistry communities in Canada. Due to the mentorship and sponsorship of Dr. Margaret-Ann Armour during the inception of the group, noticeable changes within the Department of Chemistry have been made. Professional development activities such as career panels, the

LOGIC conference, and seminars (Margaret-Ann Armour Lecture Series, Diversity in STEMinar series) provide attendees with the tools to navigate academic and industrial systems and identify inequities so they can be addressed. Visibility through social events, door decorating initiatives, and lapel pins have helped to identify allies in the community and help those of all backgrounds and identities to feel welcome. Looking forward, UAWIC aims to continue advocacy efforts within the University of Alberta. The Department of Chemistry has recently formed an EDI Committee, on which a graduate student representative from UAWIC is present. The prerogatives of the Departmental EDI Committee[27] are heavily based on the EDI components of NSERC funding applications, upon which UAWIC was previously consulted. Involvement in these higher level departmental committees allows for direct input on policy development, resource allocation, and other crucial, concrete changes to the social and professional environment at the university. Connections within the CWIC Network will also enable a continued push for the re-examination of systemic bias and inequitable practices in the wider Canadian chemistry community. The LOGIC conferences, as well as the hosting of EDI sessions within the CCCE conferences, will enable the ongoing support and growth of these initiatives and continue to promote diversity and inclusion in the Canadian chemistry community through visibility and education. However, as UAWIC is a local group serving the community of underrepresented minorities in chemistry at the University of Alberta, the primary focus will continue to be the development of a positive and inclusive environment that strives for equity and diversity. I hope Dr. Armour would be proud.

The aims of UAWIC will continue to evolve as new individuals become part of the executive team and share their stories and perspectives. UAWIC has flourished due to its varied membership, representing diverse identities and experiences of those who wish to join us. It is vital to acknowledge that, although each group is working towards the same goals of inclusion and diversity, the ways in which these initiatives manifest in each department and in each group may be different.

As a last thought, I encourage everyone to take a stand and be part of the conversation around equity, diversity, and inclusion in STEM, but especially those who are not part of underrepresented or marginalized groups, as they tend to disproportionately carry most diversity initiatives.[28] Take responsibility to educate yourself and others about systemic racism and biases that are ingrained in academia and Canadian culture and help to improve the quality of life and safety of others who may be less privileged.

VI. References

1. N. Etkin, M. A. Armour, T. Franz-Odendaal, G. Rayner-Canham, M. Rayner-Canham, H. A. Al-Abadleh and K. Jones, *Making Chemistry Inclusive*, Hayden-McNeil, Plymouth, 2016.
2. Women in Scholarship, Engineering, Science, and Technology, ualberta.ca/services/wisest/index.html, (accessed November 2020).
3. WiSER, wiseredmonton.ca, (accessed November 2020).

4. Faculty of Science Diversity Report, https://www.ualberta.ca/science/about-us/contours/2016-fall-contours/2016/october/faculty-of-sciencediversity-report.html, (accessed November 2020).
5. Canadian Association of University Teachers, CAUT Almanac of Post-Secondary Education in Canada, 2014, https://www.caut.ca/docs/defaultsource/almanac/almanac_2013-2014_print_finalE20A5E5CA0EA6529968D1CAF.pdf?sfvrsn=2, (accessed 15 July 2020).
6. M. M. Ferreira, *Int. J. Sci. Educ.*, 2003, **25**, 969.
7. National Science Foundation, Women, Minorities, and Persons with Disabilities in Science and Engineering, 2019, https://ncses.nsf.gov/pubs/nsf19304/digest, (accessed November 2020).
8. Royal Society of Chemistry, Diversity Landscape of the Chemical Sciences, 2018, https://www.rsc.org/globalassets/02-about-us/our-strategy/inclusion-diversity/cm-044-17_a4-diversity-landscape-of-the-chemical-sciencesreport_web-2.pdf, (accessed November 2020).
9. Royal Society of Chemistry. Exploring the Workplace for LGBTQ+ Physical Scientists, 2019, https://www.rsc.org/globalassets/04-campaigningoutreach/campaigning/lgbt-report/lgbt-report_web.pdf, (accessed July 2020).
10. Pride in STEM. LGBTSTEM Day 2019 Press Release, https://prideinstem.org/lgbtstem-day-2019-press-release, (accessed July 2020).
11. International Union of Pure and Applied Chemistry, IUPAC100 Global Women's Breakfast. https://iupac.org/100/global-breakfast/, (accessed November 2020).

12. Canadians Working for Inclusivity in Chemical Sciences, Engineering, and Technology, www.cwicnetwork.ca, (accessed November 2020).

13. University of Alberta Chemistry Department, Chemistry Lecture Series https://www.ualberta.ca/chemistry/news-and-events/lectureseries/index.html, (accessed November 2020).

14. J. Stockard, J. Greene, G. Richmond and P. J. Lewis, *Chem. Educ.*, 2018, **95**, 1492.

15. J. Stockard, J. Greene, J. P. J. Lewis and G. J. Richmond, *Women Minor. Scien. Eng.*, 2008, **14**, 1.

16. J. Stockard, J. Greene, P. J. Lewis and G. Richmond, in *Mentoring strategies to facilitate the advancement of women faculty*, ed. K. K. Karukstis, B. L. Gourley, M. Rossi and L. L. Wright, American Chemical Society, Washington D.C., 2010, ch. 10, pp. 153–163.

17. K. TallBear, *Native American DNA - Tribal Belonging and the False Promise of Genetic Science*, University of Minnesota Press, Minneapolis, 2013.

18. K. Tallbear, *Kalfou*, 2019, **6**, 24.

19. Natural Science and Engineering Research Council. Women in Science and Engineering in Canada, 2017, https://www.nserc-crsng.gc.ca/_doc/Reports-Rapports/WISE2017_e.pdf, (accessed July 2020).

20. A. A. Eaton, J. F. Saunders, R. K. Jacobson and K. West, K. *Sex Roles*, 2020, **82**, 127.

21. A. W. Woolley, C. F. Chabris, A. Pentland, N. Hashmi and T. W. Malone, *Science*, 2010, **330**, 686.

22. R. B. Freeman and W. Huang, *Nature*, 2014, **513**, 305.

23. S. S. Levine, E. P. Apfelbaum, M. Bernard, V. L. Bartelt, E. J. Zajac and D. Stark, *Proc. Natl. Acad. Sci. USA,* 2014, **111**, 18524.

24. American Chemical Society. ACS Salary Report 2015. https://acs.org/content/acs/en/careers/salaries/surveys/salary-report-2015.html, (accessed July 2020).

25. Working towards Inclusivity in Chemistry Toronto, http://croftw.chem.utoronto.ca/wp/womeninchemto/, (accessed November 2020).

26. USask Women in Chemistry, https://usask-wic.com/, (accessed November 2020).

27. University of Alberta Department of Chemistry EDI Committee, Our Commitment to Equity, Diversity, and Inclusion, 2020, https://www.ualberta.ca/chemistry/news-and-events/news/2020/august/edi_post.html, (accessed November 2020).

28. M. F. Jimenez, T. M. Laverty, S. P. Bombaci, K. Wilkins, D. E. Bennett, and L. Pejchar, *Nat. Ecol. Evol.,* 2019, **3**, 1030.